Mathematical Modelling of Pattern Formation in Developmental Biology

Gordon S. Hunt

Submitted for the degree of
Doctor of Philosophy

Heriot-Watt University

Department of Mathematics,
School of Mathematical and Computer Sciences.

October 2013

Abstract

The transformation from a single cell to the adult form is one of the remarkable wonders of nature. However, the fundamental mechanisms and interactions involved in this metamorphic change still remain elusive. Due to the complexity of the process, researchers have attempted to exploit simpler systems and, in particular, have focussed on the emergence of varied and spectacular patterns in nature. A number of mathematical models have been proposed to study this problem with one of the most well studied and prominent being the novel concept provided by A.M. Turing in 1952. Turing's simple yet elegant idea consisted of a system of interacting chemicals that reacted and diffused such that, under certain conditions, spatial patterns can arise from near homogeneity. However, the implicit assumption that cells respond to respective chemical levels, differentiating accordingly, is an oversimplification and may not capture the true extent of the biology. Here, we propose mathematical models that explicitly introduce cell dynamics into pattern formation mechanisms. The models presented are formulated based on Turing's classical mechanism and are used to gain insight into the significance and impact that cells may have in biological phenomena. The first part of this work considers cell differentiation and incorporates two conceptually different cell commitment processes: asymmetric precursor differentiation and precursor specification. A variety of possible feedback mechanisms are considered with the results of direct activator upregulation suggesting a relaxation of the two species Turing Instability requirement of long range inhibition, short range activation. Moreover, the results also suggest that the type of feedback mechanism should be considered to explain observed biological results. In a separate model, cell signalling is investigated using a discrete mathematical model that is derived from Turing's classical continuous framework. Within this, two types of cell signalling are considered, namely autocrine and juxtacrine signalling, with both showing the attainability of a variety of wavelength patterns that are illustrated and explainable through individual cell activity levels of receptor, ligand and inhibitor. Together with the full system, a reduced two species system is investigated that permits a direct comparison to the classical activator-inhibitor model and the results produce pattern formation in systems considering both one and two diffusible species together with an autocrine and/or juxtacrine signalling mechanism. Formulating the model in this way shows a greater applicability to biology with fundamental cell signalling and the interactions involved in Turing type patterning described using clear and concise variables.

Acknowledgements

Firstly, I would like to thank my supervisor, Dr Kevin Painter, for all his help and guidance throughout. Many thanks for giving your time so generously. Our discussions were invaluable and the meetings with Denis, Kirsty and Jeanette at the Roslin Institute were particularly insightful. I thank them too for allowing me to gain a biologist's perspective. Finally, a big thank you to my family and fiancée Amy for all the support they have provided during my studies and the interest they have taken in this work. I acknowledge the Engineering and Physical Sciences Research Council for providing funding for this work.

Contents

Chapter 1

Background

1.1 Introduction

The development of an embryo to a fully formed organism is clearly a remarkable and extremely robust event. The question of how this occurs is at the heart of developmental biology research and has been a key area of interest originating from the days of the Greek philosopher Aristotle (384-322 BC). In asking the thought provoking question of how an embryo is formed Aristotle sparked the controversy that was the preformation/epigenesis debate. It was believed that either an organism is formed from an enlargement of an already fully differentiated fertilised egg (preformation) or, similarly to what is known now, forms from successive differentiation of cells and unfolding of an organism to produce the developed form (epigenesis). Although Aristotle supported the epigenesis argument, [1], little was known to prove his claim. Unbeknown to people at this time, a much greater advancement in scientific techniques was required to resolve this issue and it was not until the last century with the understanding of deoxyribonucleic acid (DNA) and genetics that this debate was finally decided.

The twentieth century advancement in molecular biology has rejuvenated research into developmental biology with studies into the mechanisms that give rise to the growth, form and structure of an embryo to its fully formed state. At the same time, a variety of theoretical models have been hypothesised to explain the underlying molecular and mechanical interactions that give rise to patterning, [2]. The merging between theory and application promises signficant hope in uncovering the interactions involved not only in morphogenesis, but also the basic mechanisms involved in tissue organisation, homeostasis, repair and disease of the adult organism.

1.2 Biological Pattern Formation and Morphogenesis

Throughout the natural world we see varied and spectacular patterning in chemical, physical and biological systems and much research has been undertaken to determine the initiation and nature of the events in which patterned sequences and repeated units exist. Examples include: the Belousov-Zhabotinsky chemical reaction, where a reaction occurs due to the oxidisation of malonic acid by bromate ions, [3]; electrical impulses in electrophysiology, [4]; spatial population dynamics exhibited by a predator-prey type system in ecology [2]; morphogenesis of leaf vascular [5], [6]; patterning observed in the growth of bacteria such as *Eschirichia-coli*, [7], and also pigmentation patterning in a number of systems, [2] (see Fig. 1.1).

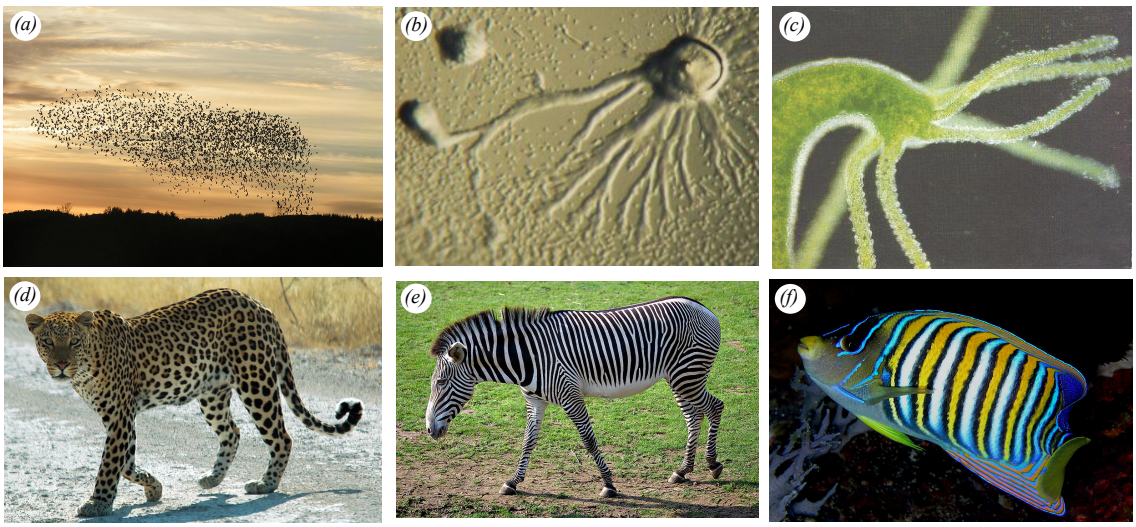

Figure 1.1: Examples of varied patterning throughout nature: (a) bird flock behaviour, (b) aggregation of dictyostelium discoidum, (c) hydra tentacle formation, (d) leopard pigmentation, (e) zebra stripes, (f) angelfish pomancathus pigmentation. These originate from applications in both biology and ecology and involve pattern formation on different scales. Pictures are taken from
(a) `http://en.wikipedia.org/wiki/File:Fugle_%C3%B8rns%C3%B8_073.jpg`,
(b) `http://en.wikipedia.org/wiki/File:Dictyostelium_Aggregation.JPG`,
(c) `http://dickeywiki.pbworks.com/w/page/26480220/Hydra%20@%20Home`,
(d) `http://en.wikipedia.org/wiki/File:Namibie_Etosha_Leopard_01edit.jpg`, (e) `http://en.wikipedia.org/wiki/File:Equus_grevyi_%28aka%29.jpg`,
(f) `http://en.wikipedia.org/wiki/File:Angelfish_Nick_Hobgood.jpg`.

Although our knowledge of embryogenesis has increased greatly over the past thirty or so years there appears to be much more to learn from this intriguing topic. Research into developmental biology has provided significant gain into the unanswered questions arising within this field with some of the earliest work suggesting the presence of substances within systems that regulate pattern formation, [8], [9]. In particular, Turing considered chemicals within this context which he termed morphogens. Here, he assumed that the evolution of the morphogens could account for morphogenesis, providing the chemical blueprint for a cell population. However, Wolpert provided a conceptual definition of a morphogen when he proposed the French Flag Model which attempted to describe cellular differentiation of a mass of cells that commit to three distinct types, denoted by blue, white and red, Fig. 1.2. Using this framework, a prepatterned morphogen gradient provides the positional information which cells can interpret and, depending on particular threshold levels, differentiate accordingly, [10].

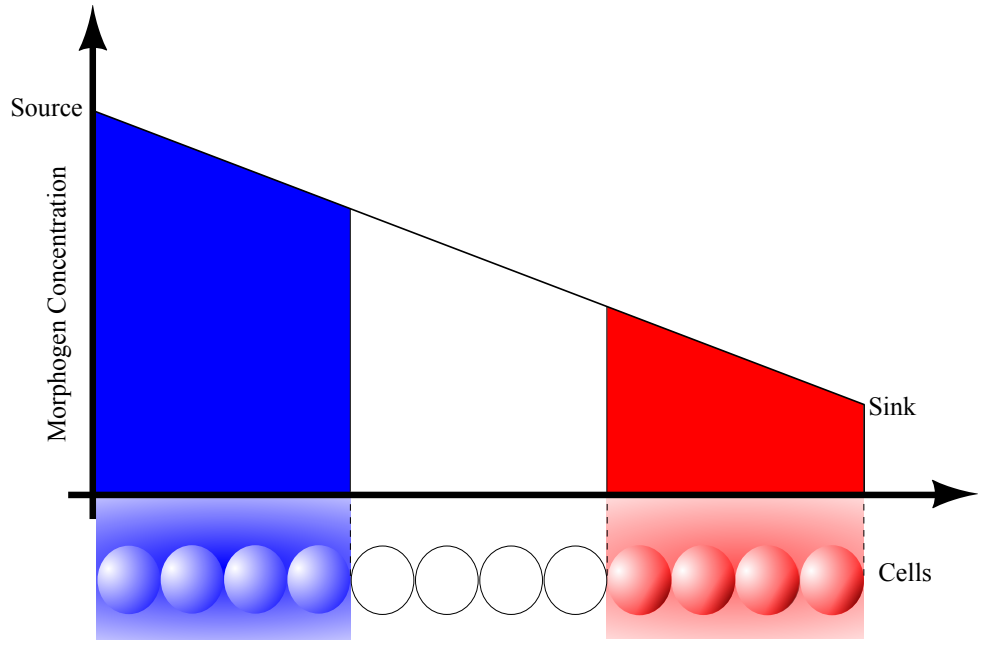

Figure 1.2: Schematic illustrating the french flag model which provides a conceptual definition of a morphogen. Proposed by Wolpert, [10], cells interpret positional information via a morphogen gradient. From this, cells become committed to three distinct types denoted by blue, white and red.

The model preceeded the discovery of the first morphogen known as bicoid. The German biologist Christiane Nüsslein-Volhard in the 1970s discovered this whilst at-

tempting to identify morphogens involved in the development of the model organism drosophila melanogaster. Nowadays many new morphogens have been discovered by biologists working on various organisms in developmental biology. Some of these include Fibroblast Growth Factors (FGF), Bone Morphogenetic Proteins (BMP), Ectodyplasmic Reticulum (EDAR), Hedgehog (HH), Wingless/Integrated (WNT) and Dickkopf (DKK) (see [11–18] for evidence within applications). These signalling molecules regulate development and it is suggested that these provide the necessary cues and information to govern cellular fate. A prime example is the segmentation of the Drosophila embryo where segmented gene expression arises from a maternally inherited pre-pattern, [19].

Throughout early development organisms appear to follow a particular pattern but after gastrulation this patterning appears to break down producing the diverse structures observed in different organisms. However, this early phenomena produces a mechanism that researchers are keen to exploit and a number of mathematical approaches have been proposed.

1.2.1 Reaction-Diffusion and Turing Models

Reaction-diffusion models have been employed in biological applications to describe a variety of systems, [2]. In doing so, they focus on the physical variables attributed to biological processes across both space and timescales. These types of models are often formulated based on the conservation of mass within a system. More specifically, let V be a volume bounded by an arbitrarily closed surface S and then the rate of change of the physical variables will depend on the flux (net movement) and the net production i.e. the sources/sinks due to the creation/loss of matter. Mathematically this becomes,

$$\frac{\partial}{\partial t}\int_V \mathbf{u} dv = -\int_S \mathbf{J}\cdot\mathbf{ds} + \int_V \mathbf{F}(\cdot)dv, \tag{1.1}$$

where $\mathbf{u}$ denotes the vector of physical variables, $\mathbf{J}$ is the flux and $\mathbf{F}(\cdot)$ incorporates the net production. By using the divergence theorem ($\int_S \mathbf{J}\cdot\mathbf{ds} = \int_V \nabla\cdot\mathbf{J}dv$) we obtain,

$$\int_V \left(\frac{\partial \mathbf{u}}{\partial t} + \nabla\cdot\mathbf{J} - \mathbf{F}(\cdot)\right) dv = 0, \tag{1.2}$$

and since V is arbitrary the integrand must be zero. Therefore, the conservation equation for $\mathbf{u}$ becomes,

$$\frac{\partial \mathbf{u}}{\partial t} = -\nabla\cdot\mathbf{J} + \mathbf{F}(\cdot). \tag{1.3}$$

Using this form, we can model a variety of different biological movement with the most common involving the incorporation of Fickian diffusion, [20] ($\mathbf{J} = -D\nabla\mathbf{u}$):

$$\frac{\partial \mathbf{u}}{\partial t} = D\nabla^2\mathbf{u} + \mathbf{F}(\cdot), \tag{1.4}$$

where $\mathbf{u}(\mathbf{r}, t)$ is a vector of variables at position $\mathbf{r}$ and time t, D is a matrix of diffusion coefficients and $\mathbf{F}(\cdot)$ incorporates the reaction properties.

One of the most notable theories using reaction-diffusion systems is found in the work of A.M. Turing. In his 1952 seminal paper Alan Turing proposed a model to account for the symmetry breaking phenomena initiating morphogenesis, [9]. In doing so, he used a system of reaction diffusion equations and showed that, under certain conditions, spatial patterns in chemical concentrations can arise from near homogeneity. This novel and counter intuitive concept proposes that diffusion may be the destabalising factor from which patterns can form and is aptly named Diffusion-Driven Instability (DDI) or Turing Instability.

Let $\mathbf{u}(\mathbf{r}, t)$ in (1.4) denote a vector of m chemicals that react and diffuse throughout a domain, denoted $\Omega \in \mathbf{R}^n$, enclosed by a boundary, $\partial\Omega$, such that we have a system following Turing's general form. The full system is defined with initial conditions $\mathbf{u}(\mathbf{r}, 0) = \mathbf{u}_0$ in Ω and boundary conditions on $\partial\Omega$. The initial conditions are often set to be a small random perturbation of the steady state and typically zero flux boundary conditions are commonly employed to emulate the impermeability of chemicals across the domain.

The positive homogeneous steady state of (1.4) is given by $\mathbf{u}_s$, satisfying $\mathbf{F}(\mathbf{u}_s) = 0$. Linearising about the homogeneous steady state using $\mathbf{u} = \mathbf{u}_s + \hat{\mathbf{u}}$, where $\hat{\mathbf{u}}$ is a vector of small perturbations, gives the linearised system

$$\hat{\mathbf{u}}_t = D\nabla^2\hat{\mathbf{u}} + J^*\hat{\mathbf{u}}, \tag{1.5}$$

where D is a diagonal matrix of diffusion coefficients and J^* is the Jacobian evaluated at the steady state:

$$D = \begin{pmatrix} D_1 & 0 & \dots & 0 \\ 0 & D_2 & \dots & 0 \\ \vdots & \vdots & \ddots & \vdots \\ 0 & 0 & \dots & D_m \end{pmatrix}, \quad J^* = \begin{pmatrix} \frac{\partial F_1}{\partial u_1} & \cdots & \frac{\partial F_1}{\partial u_m} \\ \vdots & \ddots & \vdots \\ \frac{\partial F_m}{\partial u_1} & \cdots & \frac{\partial F_m}{\partial u_m} \end{pmatrix}\Bigg|_{\mathbf{u}_s}. \tag{1.6}$$

Solving the system according to zero-flux boundary conditions, we define the time-independent solution to the spatial eigenvalue problem as $\mathbf{U}$ such that

$$\nabla^2\mathbf{U} + k^2\mathbf{U} = 0, \quad \mathbf{n}\cdot\nabla\mathbf{U} = 0 \quad \text{on} \quad \partial\Omega. \tag{1.7}$$

Considering the one dimensional domain $x \in [0\ a]$, solutions arise of the form

$$\mathbf{U} \propto cos(\frac{n\pi x}{a}), \tag{1.8}$$

where n is an integer. These satisfy the zero-flux boundary conditions and wavelike patterns arise with eigenvalue $k = \frac{n\pi}{a}$, now being considered as the wavenumber. In this way, the wavenumber relates to the wavelength of the pattern by $\omega = \frac{2\pi}{k}$. Now seek solutions to the linearised problem of the form

$$\hat{\mathbf{u}} = \sum_k c_k e^{\lambda t} \mathbf{U}_k, \tag{1.9}$$

where each eigenfunction $\mathbf{U}_k$ corresponds to the wavenumber k, c_k are constants determined by a Fourier expansion of the initial conditions and λ is the temporal growth rate. Substituting the solution into (1.5) leads to the requirement for nontrivial solutions,

$$\left|J^* - \lambda I - Dk^2\right| = 0, \tag{1.10}$$

where J^* is the matrix of partial derivatives at the steady state, I is the identity matrix and D is the diagonal matrix of diffusion coefficients. The expansion of this leads to an m^{th} order characteristic polynomial which consists of solutions, $\lambda_i(k^2)$, $i = 1, ..., m$, that have dependence on the wavenumber, k. From this, a Turing instability occurs if, in the absence of any spatial terms, $Re(\lambda_i(k^2 = 0)) < 0$ for all i and for some $k^2 \neq 0$ the solutions have positive real part for some i, $Re(\lambda_i(k^2 \neq 0)) > 0$.

Therefore, by fixing the value of all parameters except one, which we define the bifurcation parameter d, we can observe a Turing bifurcation when this passes through a critical value, d_c, Fig. 1.3(a). Assuming the steady state is stable to a spatially uniform perturbation, we consider plots of the maximum $Re(\lambda_i(k^2 \neq 0)) > 0$ for some i, i.e. the dispersion relation. When $d < d_c$ there is no diffusion-driven instability and the wavenumbers are stable but for $d = d_c$ we are at the point of instability. Therefore, for $d > d_c$ there is a bounded set of linearly unstable wavenumbers, satisfying $k_1^2 < k^2 < k_2^2$, where admissible wavenumbers within the range can grow exponentially to produce pattern formation of Turing type. These patterns, in the absence of any external disturbances, will result in peaks and troughs of chemical concentrations. Provided there is a bounded set of linearly unstable wavenumbers with an admissible wavenumber the peaks and troughs will also exhibit equal wavelengths across the domain, known as a characteristic wavelength (see Fig. 1.3(b)).

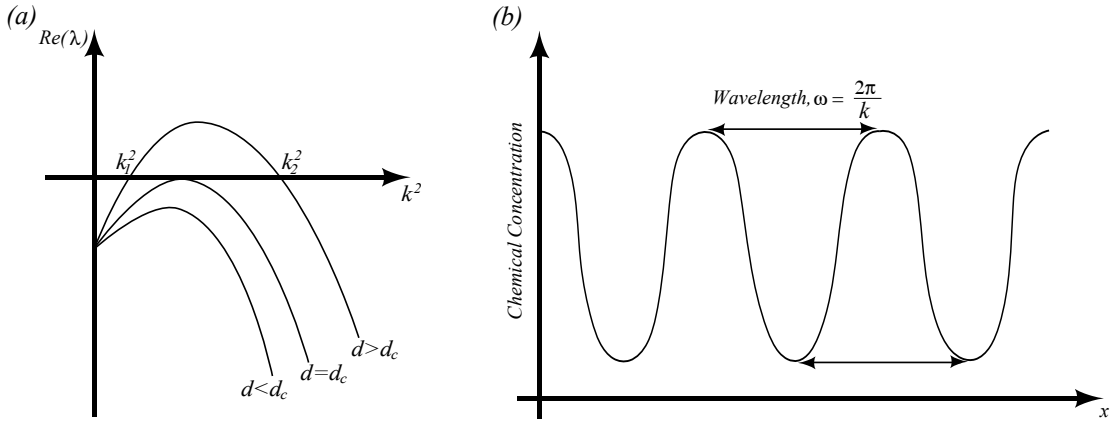

Figure 1.3: Illustrations of (a) plots of the dispersion relation for varying bifurcation parameter, d. When $d < d_c$ a Turing instability cannot occur but as d passes through d_c ($d > d_c$) there is a Turing bifurcation. With this, there is a bounded set of linearly unstable wavenumbers, satisfying $k_1^2 < k^2 < k_2^2$, which has $Re(\lambda(k^2 \neq 0)) > 0$. Admissible wavenumbers lying within this range can lead to pattern formation of Turing type and, due to the bounded unstable wavenumbers, the peaks and troughs of the pattern will exhibit equal wavelengths across the domain. A schematic of a one dimensional pattern, where x denotes the spatial variable, can be seen in (b). A double sided arrow indicates the wavelength of the pattern with the relationship between the wavelength and wavenumber shown i.e. $\omega = \frac{2\pi}{k}$. This wavelength is consistent across the domain and is known as the characteristic wavelength.

The simplest system for which this can occur consists of two chemical species:

$$\frac{\partial A}{\partial t} = D_A \nabla^2 A + F(A, B), \tag{1.11}$$

$$\frac{\partial B}{\partial t} = D_B \nabla^2 B + G(A, B), \tag{1.12}$$

where $A(\mathbf{r}, t)$, $B(\mathbf{r}, t)$ are the concentrations of two chemicals at spatial position $\mathbf{r}$ and time t, D_A, D_B are positive diffusion coefficients of the chemicals and $F(A, B)$, $G(A, B)$ incorporate the biochemical reactions and interactions between A and B. The full system is defined with initial conditions $A(\mathbf{r}, 0) = A_0$, $B(\mathbf{r}, 0) = B_0$ in Ω and boundary conditions on $\partial\Omega$.

Using the framework discussed above, a standard linear stability analysis about the assumed positive uniform steady state, $(A_s,\ B_s)$, (i.e. $F(A_s, B_s) = G(A_s, B_s) = 0$), will provide the (DDI) conditions on the parameters for which Turing patterns can arise. In particular, we look for the homogeneous steady state to be (i) stable to a homogeneous perturbation ($Re(\lambda(k^2 = 0)) < 0$) and (ii) unstable to an inhomogeneous perturbation such that at least one eigenvalue has $Re(\lambda(k^2 \neq 0)) > 0$, [21]. Imposing these conditions, the general DDI conditions for a two species system such as the one

above, (1.11)-(1.12), are given by

$$tr(J^*) = F_A + G_B < 0, \tag{1.13}$$

$$\det(J^*) = F_A G_B - F_B G_A > 0, \tag{1.14}$$

$$D_B F_A + D_A G_B > 0, \tag{1.15}$$

$$(D_B F_A + D_A G_B)^2 - 4 D_A D_B \det J^* > 0, \tag{1.16}$$

where F_A, F_B, G_A, G_B are the partial derivatives evaluated at the steady state and the Jacobian, J^*, is given by

$$J^* = \begin{pmatrix} F_A & F_B \\ G_A & G_B \end{pmatrix}_{(A_s, B_s)}. \tag{1.17}$$

For full details of the analysis see Murray, [2]. The chemicals $A(\mathbf{r}, t)$, $B(\mathbf{r}, t)$ are often termed the activator and inhibitor respectively. In this way, it is assumed that the activator acts to upregulate the system whereas the inhibitor suppresses activity. Together with the required conditions for DDI to exist, (1.13)-(1.16), the analysis shows that the simplest two species system requires the inhibitor to diffuse faster than the activator ($D_B > D_A$ in (1.11)-(1.12)). This concept of long range inhibition, short range activation, [22], allows the activator to grow locally while the inhibitor suppresses its activity at distant sites.

Under these restrictions, simulations of the model will lead to spontaneously generated peaks and troughs in chemical concentrations. These resulting spatially heterogeneous patterns are typically assumed to provide the positional information, [10], to which a uniform cell population can interpret and differentiate according to arbitrary threshold levels.

Turing Systems in Action

Turing firstly investigated a model consisting of linear kinetics and continued by discussing more complicated and realistic nonlinear reactions and domains. In doing so, he suggested possible biological applications that may adhere to this theory such as gastrulation, whorled leaves and hydra tentacle formation, [9]. However, it was not until the 1990s that this theory was observed experimentally. The long range inhibition, short range activation requirement initially prevented some of the scientific community from considering Turing's idea as a plausible mechanism for pattern formation and development. However the CIMA reaction provided a plausible application for the theory, [23]. Within this chemical system starch, originally being used

as an indicator, binds to iodide effectively reducing the diffusive capabilities of the activator in the system and enhancing the notion of short range activation, long range inhibition required for the application of Turing theory.

Even before this, however, a number of mathematical studies were undertaken using Turing models. For example, Gierer and Meinhardt proposed a Turing model to account for hydra tentacle formation, [22], and, although it is now thought to be unlikely, Kauffman *et al* proposed a Turing model to explain Drosophila segmentation in 1978, [24]. However, since the emergence of experimental agreement, provided by the CIMA reaction, Turing models have been used to attempt to explain an abundance of applications including animal & fish pigmentation patterns, [25], [26], [27], mollusc shell patterns, [28], skin appendage formation such as hair follicle and feather bud patterning, [18], [29], [30], [31], [32] and skeletal & limb bud morphogenesis, [33]. In particular, a greater understanding of the molecular interactions of these systems has led to proposed Turing systems that appear to match experimental predictions, [18], [32], [27], providing evidence that Turing systems may sufficiently explain certain types of biological pattern formation.

Limitations of Turing Theory

Research using Turing type models has resulted in the formulation of models that are capable of replicating a variety of patterns in 2D, from spots to stripes, [34], [32]. Selection of parameter values and the precise form of the kinetics within these models is key in observing particular simulated patterns, [27, 35–37]. As a result, we can infer that parameter fitting is vitally important in determining the nature of resultant patterns. However, the restriction that Turing type models impose on parameter selection is an issue and perhaps a limitation of using the theory. Undertaking the DDI analysis produces a region of parameter space where Turing patterns exist. Although this gives some indication of possible parameter values it also restricts our choice. Further to this, in the simplest two species models, restriction in the diffusive capabilities of the two chemicals (long range inhibition, short range activation) may provide further limitations in the use of these types of models to explain biological systems.

However, a main drawback of using the simplest models within biological contexts is the absence of any explicit consideration of cells. Within this framework, the typical assumption of cell differentiation above a certain threshold level may represent a naive approach to modelling pattern formation. Cell processes are fundamental in any biological process and determining their significance in pattern formation will be key to understanding the precise mechanisms that may be regulating and maintaining biological phenomena.

1.2.2 Reaction Kinetics

The form of the kinetics can be a determining factor of the resulting simulated pattern, and the exact nature of these will clearly depend on the biological application. Two general forms for the reaction kinetics consist of pure and cross systems, [21], and the schematic in Fig. 1.4 shows the different properties of these two systems.

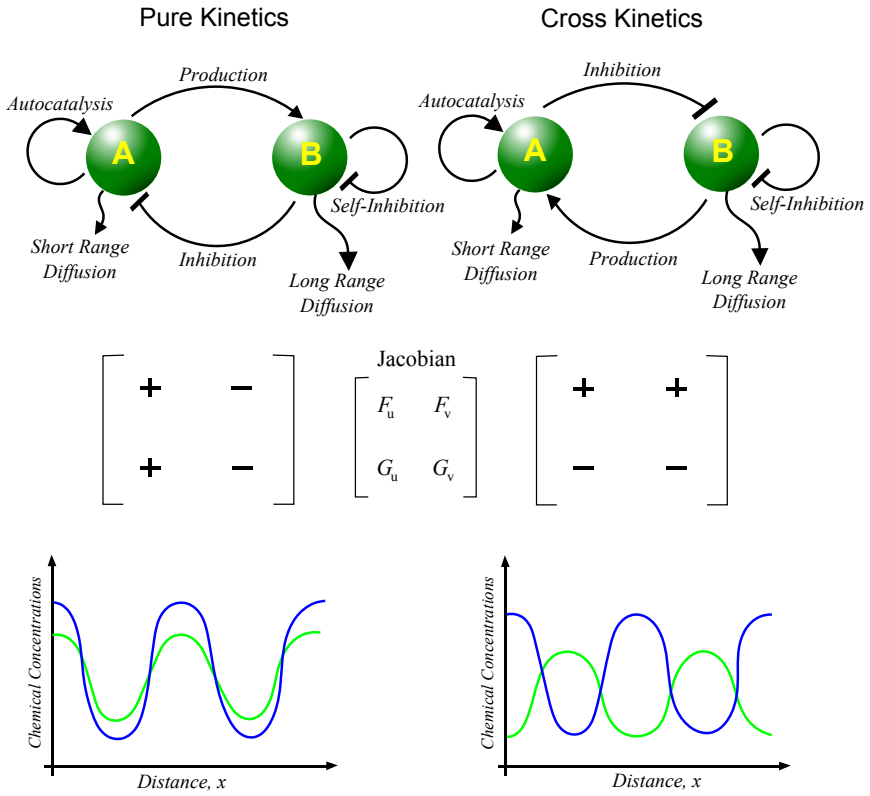

Figure 1.4: A schematic diagram illustrating the differences between the two types of Turing models: pure and cross kinetics. On comparison, kinetics that adhere to the above interactions will lead to simulations that exhibit in-phase and out-of-phase peaks and troughs in chemical concentrations for pure and cross systems respectively.

Within pure type systems, an activator, A, stimulates the production of itself via autocatalysis while being supressed by an inhibitor, B. The activator also promotes the production of inhibitor. Similarly, cross type systems consider the autocatalysis of the activator, A, but now incorporates suppression of the 'inhibitor', B. Furthermore, the 'inhibitor' upregulates activator within the system and, as a result, it may be more appropriate to consider the inhibitors role as facilitating reactions. For example, these cross systems have often been referred to as activator-substrate depletion models, [38],

where the inhibitor is assumed to be used as an activating factor, [39].

The structure of the Jacobian matrix and typical illustrations of one dimensional model simulations show the intrinsic differences in the two models, Fig. 1.4. Pure and cross type kinetics respectively result in 'in-phase' and 'out-of-phase' peaks and troughs in chemical concentrations. This means that with pure type kinetics when activator concentrations are high, inhibitor concentrations are at a peak also. On the contrary, with cross type kinetics when activator concentrations are high, inhibitor levels are at a trough. These resultant evolutions show the significance of the reaction kinetic choice when modelling specific biological situations.

A number of kinetic schemes exist to study pattern formation in reaction-diffusion theory, [4]. As discussed previously, the CIMA reaction provided a plausible application of Turing's theory when starch was added to the system. This has been used as the basis for a model proposed by Lengyel and Epstein, [40]. Moreover, the reaction between oxygen and uric acid in the presence of the enzyme uricase was used for the basis of the Thomas kinetics, [41]. Although these two have been proposed based on specific applications, hypothetical reactions have also been considered (see for example the Brusselator reaction, [42]). For illustration, we provide two other well studied cases that can be classified as pure and cross kinetic systems. In particular, we look at the Gierer-Meinhardt, [22], and Schnakenberg, [43], kinetics.

Gierer-Meinhardt

The Gierer-Meinhardt kinetics proposed in 1972, [22], have become a classic scheme in the study of pattern formation. The model follows a pure activator-inhibitor framework (Fig. 1.4) and can take different forms depending on model requirements. However, one specific form that was proposed in the original paper considers the following:

$$\frac{\partial A}{\partial t} = k_1 + \frac{k_2 A^2}{(k_3 + A^2)B} - k_4 A + D_A \nabla^2 A, \tag{1.18}$$

$$\frac{\partial B}{\partial t} = k_5 + k_6 A^2 - k_7 B + D_B \nabla^2 B, \tag{1.19}$$

where A, B represent the activator and inhibitor respectively, k_i, $i = 1, .., 7$ are positive rate constants and D_A, D_B are the diffusion coefficients. Specifically, the activator and inhibitor have basal rates, k_1, k_5, activator simulates its own production (autocatalysis) with saturation effects whilst being suppressed by the inhibitor, $\frac{k_2 A^2}{(k_3+A^2)B}$, activator promotes the production of inhibitor, $k_3 A^2$, and both chemicals degrade linearly, $-k_4 A$, $-k_7 B$. The model given above, and modifications to this, have been widely applied and studied in biological situations and, under certain conditions, has been successful in forming various patterned solutions from stripes to spots, [44], [39], [32]. However, a simplified version of this system can be considered

that retains some of the biologically relevant details whilst also being analytically tractable:

$$\frac{\partial A}{\partial t} = k_2 \frac{A^2}{B} - k_4 A + D_A \nabla^2 A, \tag{1.20}$$

$$\frac{\partial B}{\partial t} = k_6 A^2 - k_7 B + D_B \nabla^2 B. \tag{1.21}$$

Here, the variables and coefficients remain unchanged but the activator no longer undergoes saturation. Moreover, the basal rates are assumed to be negligible. Using the nondimensionalisation $u = \frac{k_6}{k_2} A$, $v = \frac{k_6 k_7}{k_2^2} B$, $\mathbf{r}^* = \frac{k_7}{D_A}\mathbf{r}$, $t^* = k_7 t$, $\alpha = \frac{k_4}{k_7}$, $d = \frac{D_B}{D_A}$, the model becomes,

$$\frac{\partial u}{\partial t^*} = \frac{u^2}{v} - \alpha u + \nabla^2 u, \tag{1.22}$$

$$\frac{\partial v}{\partial t^*} = u^2 - v + d\nabla^2 v, \tag{1.23}$$

where u, v are the activator and inhibitor and α, d are positive parameters. As a consequence of the linear stability analysis we will require, together with the appropriate DDI conditions, $d > 1$ such that $D_B > D_A$ (long range inhibition, short range activation). In this case, the DDI conditions become

$$0 < \alpha < 1, \tag{1.24}$$

$$d\alpha - 1 > 0, \tag{1.25}$$

$$(d\alpha - 1)^2 - 4d\alpha > 0. \tag{1.26}$$

These conditions delimit the region where DDI is possible and parameters chosen within this range will lead to spatial pattern formation of Turing type (see Fig. 1.5(a),(b)(i)).

Schnakenberg

The Schnakenberg kinetics, [43], follows a cross activator-inhibitor framework (Fig. 1.4) and is derived using specific rate reactions:

$$X \underset{k_3}{\overset{k_1}{\rightleftharpoons}} A, \quad Y \overset{k_4}{\to} B, \quad 2A + B \overset{k_2}{\to} 3A.$$

By using the Law of Mass Action, the model becomes

$$\frac{\partial A}{\partial t} = k_1 + k_2 A^2 B - k_3 A + D_A \nabla^2 A, \tag{1.27}$$

$$\frac{\partial B}{\partial t} = k_4 - k_2 A^2 B + D_B \nabla^2 B, \tag{1.28}$$

where A, B represent the activator and inhibitor respectively, k_i, $i = 1, .., 4$ are positive rate constants and D_A, D_B are the diffusion coefficients. In this case we consider constant basal rates, k_1, k_4, production of the activator via facilitation from 'inhibitor', $k_2 A^2 B$, and decay of activator, $-k_3 A$. The sink term in the inhibitor evolution equation, $-k_2 A^2 B$, corresponds to the continual utilisation of inhibitor during activator upregulation. Using the nondimensionalisation $u = \left(\frac{k_2}{k_3}\right)^{\frac{1}{2}} A$, $v = \left(\frac{k_2}{k_3}\right)^{\frac{1}{2}} B$, $\mathbf{r}^* = \frac{k_3}{D_A}\mathbf{r}$, $t^* = k_3 t$, $\delta = \frac{k_1}{k_3}\left(\frac{k_2}{k_3}\right)^{\frac{1}{2}}$, $\rho = \frac{k_4}{k_3}\left(\frac{k_2}{k_3}\right)^{\frac{1}{2}}$, $d = \frac{D_B}{D_A}$, the model becomes,

$$\frac{\partial u}{\partial t^*} = \delta + u^2 v - u + \nabla^2 u, \tag{1.29}$$

$$\frac{\partial v}{\partial t^*} = \rho - u^2 v + d\nabla^2 v, \tag{1.30}$$

where u, v are the activator and inhibitor and ρ, δ, d are positive parameters. Once again, the nondimensionalisation leads to $d = \frac{D_B}{D_A}$ and we will require, together with the appropriate DDI conditions, $d > 1$ for pattern formation (long range inhibition, short range activation). Here, the DDI conditions become

$$\rho - \delta - (\delta + \rho)^3 < 0, \tag{1.31}$$

$$\delta + \rho > 0, \tag{1.32}$$

$$d(\rho - \delta) - (\delta + \rho)^3 > 0, \tag{1.33}$$

$$\left(d(\rho - \delta) - (\delta + \rho)^3\right)^2 - 4d(\rho + \delta)^4 > 0. \tag{1.34}$$

Similarly, the region where DDI is possible and the simulations for a specific parameter set showing pattern formation of Turing type can be seen in Fig. 1.5(a),(b)(ii). In this case, there are out-of-phase peaks and troughs in activator/inhibitor concentrations.

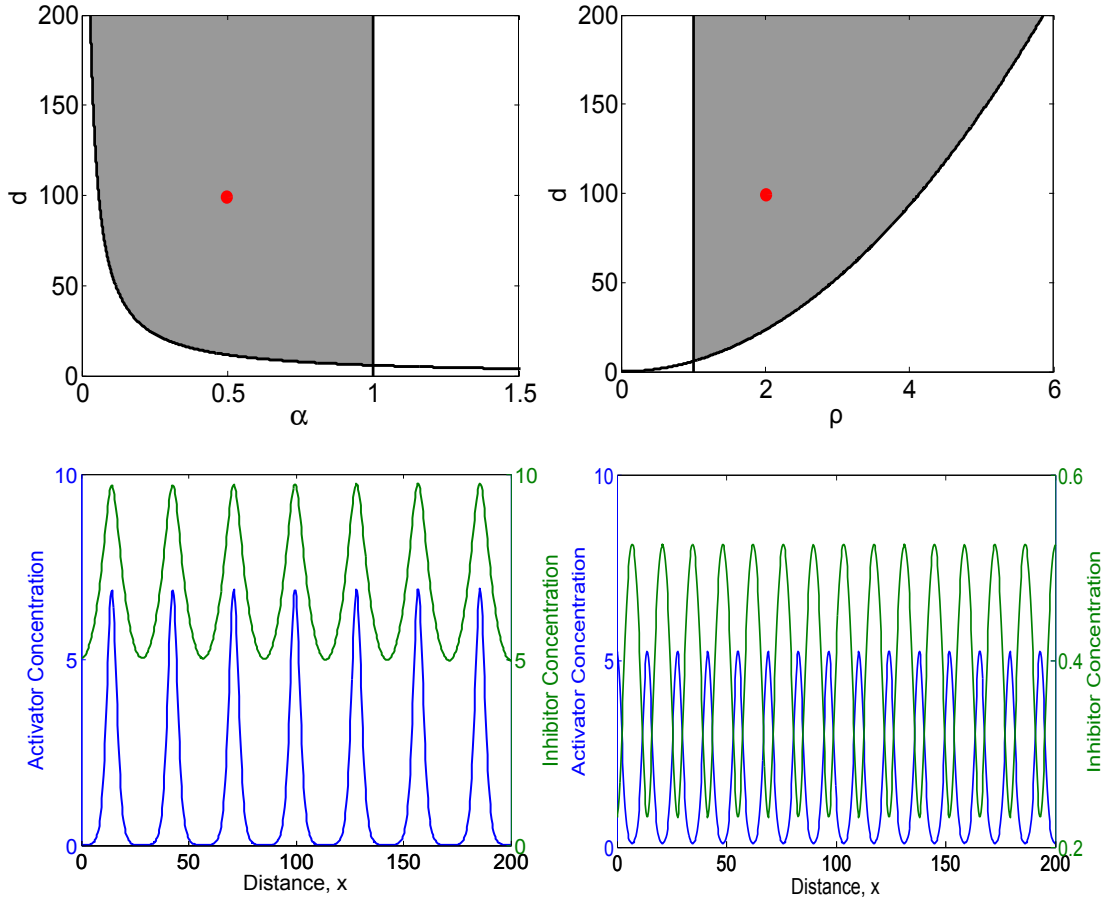

(a) Pure: Gierer-Meinhardt Kinetics

(b) Cross: Schnakenberg Kinetics

Figure 1.5: Plots of the (a) parameter space and (b) model simulations for the two types of Turing model: (i) Pure Gierer-Meinhardt kinetics and (ii) Cross Schnakenberg kinetics. The grey region indicates the possible $\alpha - d$ in the pure case and $\rho - d$ parameter values in the cross case, that will produce pattern formation. In the simulations the parameters were chosen to be $\alpha = 0.5$, $\delta = 0$, $\rho = 2$ and $d = 100$ indicated in the parameter space plots by the red dot. The initial conditions were given as a 2% random perturbation to the homogeneous steady state and the boundary conditions are zero-flux. The simulations were produced using MATLAB's in-built PDE solver, *pdepe*, with relative and absolute tolerance levels at 10^{-6}.

1.2.3 Cell Based Models

Mechanical Models

In contrast to Turing theory, mechanical models focus on the simultaneous aggregation and differentiation of cells. In doing so, they consider the interactions and mechanical forces between the cells and the surrounding environment, [45]. One well studied and commonly used mechanical model in mathematical biology is known as a chemotaxis model. With this, it is proposed that cells respond to chemicals within the environment and move up or down concentration gradients by detecting the chemical gradient. Competition between the directed movement and diffusion is key within this model, with chemotaxis the destabilising factor from which cell aggregations and patterns arise. A general model encompassing these assumptions is given by

$$\frac{\partial n}{\partial t} = \nabla \cdot (D_n \nabla n - \chi(m) n \nabla m) + F(n, m), \tag{1.35}$$

$$\frac{\partial m}{\partial t} = D_m \nabla^2 m + G(n, m). \tag{1.36}$$

Here $n(\mathbf{r}, t)$ and $m(\mathbf{r}, t)$ are the density of cells and concentration of chemoattractants respectively at position $\mathbf{r}$ and time t, D_n, D_m are the diffusion coefficients, χ is the chemoattractant sensitivity and F and G incorporate the reactions involving m and n. Within this generalised system we model the possibility of cells moving up concentration gradients and thus being attracted to high levels of chemical concentrations. The response of cells down a concentration gradient would constitute chemorepulsion.

Cell-chemotaxis models were first introduced in the work of Keller and Segel in 1970, [46]. For an explanation of the Keller-Segel model and extensions to this see [47] and references therein. Following Keller and Segel's work, these types of models have been employed to describe bacterial motion and patterns. In particular the cellular slime mold Dictyostelium discoideum has been extensively studied and shown to exhibit chemotactic behaviour through the secretion and subsequent attraction of cyclic adenosine monophosphate (cAMP), [48]. Further to this, a variety of patterns in populations including Dictyostelium and *Eschirichia-coli* have been successfully replicated using mathematics, [7], [49], [34]. In the context of developmental biology, chemotaxis models have been used to describe a number of biological systems including fish & snake pigmentation patterns, [50], [51], [34] and references therein, feather bud patterning, [52], and primitive streak formation in gastrulation, [53], among others.

Chemotaxis is not the only plausible mechanism for cell movement however. For example, cells may move in response to a gradient of adhesion (haptotaxis), light (phyllotaxis), magnetic fields (galvanotaxis), amongst others. With the incorporation of these and other physical laws of mechanics more complicated models can be for-

mulated. In the 1980's Oster and Murray pioneered work into models incorporating contractile forces exerted by cells on each other and their surroundings in mesenchymal morphogenesis, [54], [45]. In doing so, they proposed that a model formulated using mechanical laws could be sufficient to describe chondrogenesis in limb bud development. Moreover, they provided a framework for further study. Since then there has been much success seen in the application of such a model to biological situations such as wound healing, [55], and cancer, [56]. Although this theory is relatively new compared with Turing's idea, there is no doubt that these types of models have provided significant gain and a novel way of studying biological phenomena and, in particular, pattern formation.

Discrete Models

The previous mathematical theories for pattern formation, given above, have focused on the reactions occuring on a continuous scale. A more intricate modelling approach occurs via a discrete framework where consideration can be given to individual cells and the intricate details that are involved in biological processes. Within this, a number of approaches have been proposed.

A broad class of discrete models is the Cellular Automata approach where cells are defined on a regular grid and behave according to specific conditions. For example, a particular type of Cellular Automata is known as the Cellular Potts Model, [57], [58], which governs the potential behaviour of individual cells through probabilistic rules, typically based on mechanical forces and differences in energy, that effectively control cell interactions and migration. Based on these, cells are able to 'sort' themselves and simulations have been successful in emulating a variety of patterns in nature [see [59] and references therein]. Another example includes lattice gas models which consider cell changes in states, determined by boolean properties, at each point on a lattice. Once again, these models have been successful in replicating pattern formation, [see [59] and references therein].

Alternatively, discrete models that are lattice-free have also been considered. Clearly these provide reduced restriction on cell position but they also give greater flexibility in cell shape and control over cell interactions, see [60] and references therein. As a result, greater applicability to complex structures and behaviour in biology can be modelled.

In the context of this thesis, however, Turing proposed a discrete framework of the reaction diffusion equation where concentration levels on individual cells were considered, [9]. Moreover, Othmer & Scriven followed a similar approach to Turing's model with additional interactions from a surrounding bath of chemical, [61].

Moreover, one particularly prominent discrete approach considers cell signalling via receptor-ligand binding as a mechanism for pattern formation. This direct con-

nection and physical contact results in the exchange of information leading to the initiation and development of morphological changes within the receiving cell, [62]. A number of different signalling mechanisms are thought to be present within biological systems with these incorporating different degrees of interaction, [62]. In particular, a well studied mechanism is known as juxtacrine signalling which involves communication between adjacent cells, [63]. Within this, surface bound receptors bind to ligands situated on the surface of neighbouring cells.

A variety of growth factors have been identified as candidates for this type of process, [64]. However, one of the first to consider a mathematical approach with a candidate receptor-ligand binding process involved in juxtacrine signalling was Collier *et al*, [65]. By using Notch-Delta interactions as the basis of the model, the results showed the attainability of small wavelength patterns, describing activity on individual cells, which the authors suggested may capture fine grained patterns arising in nature. In this framework, a lateral inhibition mechanism was considered implementing a negative feedback loop which resulted in high activity cells suppressing the activity of neighbouring cells, [66]. These cells subsequently acquire opposing fates which are assumed to be interpreted through the description of individual cell activity.

A drawback of the model considered by Collier *et al* is that it is unable to robustly produce longer wavelength patterns. However, a number of models based on a mechanism known as lateral induction have been proposed by Owen, Sherratt and co-workers with the results of these showing the attainability of longer wavelength patterns, [67–71]. Within these, the application of wound healing is considered with the model formulated based on the juxtacrine signalling interactions between receptors and ligands. The lateral induction mechanism implements a positive feedback loop which acts to upregulate neighbouring cells and, in this way, provides a mechanism for systems exhibiting this type of interaction. In particular, the candidate receptor and ligand for the lateral induction studies above are given by the ligand TGFα binding to its receptor EGF-R.

1.3 Outline of Thesis

Turing's theory is amongst the leading theories for biological pattern formation and models based on his work provide a simple yet elegant way of studying these types of problems. However, the most simple mathematical models using Turing's famework ignore the impact of cellular influences and typically assume differentiation of cells in response to chemical concentration levels that are above an arbitrary threshold value. Although this has led to many insightful conclusions into pattern formation, it is an over-simplication of the role cell dynamics have in this process. As a result, this thesis will propose mathematical models that will attempt to describe two such

cellular processes that are fundamental in biological processes: cell differentiation and cell communication.

In Chapter 2, using a classical two species Turing system as a framework, we consider the incorporation of cell differentiation via precursor specification and asymmetric precursor differentiation. The former considers the possibility of cells moving between two different states depending on activator levels with the latter involving the transformation of an undetermined cell into two cells with different classifications: uncommitted and committed. Each of these models consider cell feedback in a number of ways to upregulate/downregulate activator and/or inhibitor levels. By considering feedback into activator levels, we show that we can relax some of the restrictions that have led to scepticism of Turing's theory. Specifically, the results suggest the possibility of equal chemical diffusion coefficients resulting in a relaxation of the long range inhibition, short range activation requirement of two species systems.

In Chapter 3, we propose a mathematical model with greater detail considering the transformation from a continuous activator-inhibitor model to a discrete model where individual cells have the possibility of communicating in a number of ways. In doing so, we replace the activator with a receptor-ligand binding process in the presence of an inhibitor and investigate possible short range cell communication effects and their impact on pattern formation. Reducing the three species model using a Quasi-Steady State Assumption (QSSA) results in a two species system that provides a direct comparison to the simplest classical activator-inhibitor model. Moreover, we propose kinetics similar to the classical Gierer-Meinhardt and Schnakenberg kinetics for comparative purposes and to illustrate the capabilities of a pure and cross type system.

Analysing these case studies in Chapter 4, we show that pattern formation can exist for a two species system considering one diffusible species together with an autocrine and/or juxtacrine signalling mechanism. Moreover, we can attain a variety of wavelength patterns, including both fine grained and longer wavelength patterns, that have applicability to a number of biological systems. Finally, the full three species system is analysed generally, and with focus on the validity of the two species reduction assumptions.

Chapter 2

Modelling Cell Differentiation in Turing Systems

Previous researchers have often only considered the chemicals when utilising reaction-diffusion based models; usually assuming that cells differentiate above a certain chemical concentration level. Here we formally introduce two possible types of cellular commitment and consider a three species reaction diffusion model capable of producing Diffusion Driven Instability (DDI). We incorporate cellular dynamics into a two species activator-inhibitor system to investigate the impact that cellular processes have on patterning. The first model considers precursor specification with the possibility of cells transferring back into an uncommitted state and the other asymmetric precursor differentiation. Possible feedback mechanisms on activator concentration are investigated with similar results observed between the two models. In particular, with the incorporation of cellular commitment processes with specific feedback mechanisms, the results suggest a relaxation of the two species Turing Instability requirement of long range inhibition, short range activation.

2.1 Introduction

Cell differentiation is one of the most fundamental processes occuring within all living organisms and involves the specialisation of a cell to perform a particular function. This complex process arises in many biological situations including tissue repair and regulation, cancer and fundamental embryogenesis. Of particular interest to scientists is the development of multicellular organisms where a single cell, the zygote, is transformed into a fully formed organism. Within this framework cell commitment plays a key role giving rise to the diverse cell types observed in organisms with differentiation recognisable through differences in cellular properties such as shape, size and molecular expression among others. However, exactly how these cells are defined and become restricted to a particular fate is still poorly understood and much research is

focussed on the mechanisms involved in the determination of cell fate.

A cell acquires a particular fate by responding to their environmental cues and differentiating accordingly. This causes a change in the intrinsic properties of the cell and results in a generic cell beholding the information required to perform some particular function, [72]. This information is brought about by changes in the gene expression of individual cells. However, the exact regulatory modules that determine the change in phenotype remain unclear. It is thought that one of the main factors is the cellular response to signalling molecules in their environment that change the morphology and phenotypic behaviour of a cell.

The morphological changes observed in cells occurs at the latter stage of the commitment process. This process begins with cell specification where cells, in response to external signals, become influenced to follow a particular differentiation pathway. Specification results in cells that still have the ability to revert back to a previous state. However, cells that continue on this developmental pathway undergo cell determination which involves further restriction to a more defined fate, [72]. Cells become irreversibly committed during the determination process but do not have the ability to perform a particular function. This exact function will be provided by differentiation where specific traits can be observed (see Fig. 2.1). Taking blood as an example, cell determination will put hematopoietic stem cells on a path to become blood cells. However, cell differentiation will specify whether these will be red blood cells, white blood cells or platelets, say.

Cells that have the capability to create the various cell types are referred to as stem cells. Typically these can be grouped into two distinct types: adult stem cells and embryonic stem cells. The latter have the ability to differentiate into all cell types and also have the capacity to self renew limitlessly. Conversely, adult stem cells are restricted in their renewal and differentiation properties having been already specialised in some way, [72]. Occurring after embryogenesis, they are focussed on their general area of applicable function differentiating to repair and regenerate particular areas within the organism. Most often they are used in processes such as wound healing and tissue homeostasis. For example, they have been found to be present within a number of systems such as the follicular bulge replenishing cells within the hair follicle and interfollicle epidermis, [73], and intestinal crypt, [74], among others.

2.1.1 Modelling Background

As we have already discussed, symmetry breaking phenomena involves the transformation of small disordered fluctuations within a system into an ordered state. It has been suggested that this mechanism is capable of describing pattern formation and one of the most recognisable and well studied examples of this in mathematics was proposed by A.M. Turing in 1952. In his seminal paper, [9], Turing introduced a

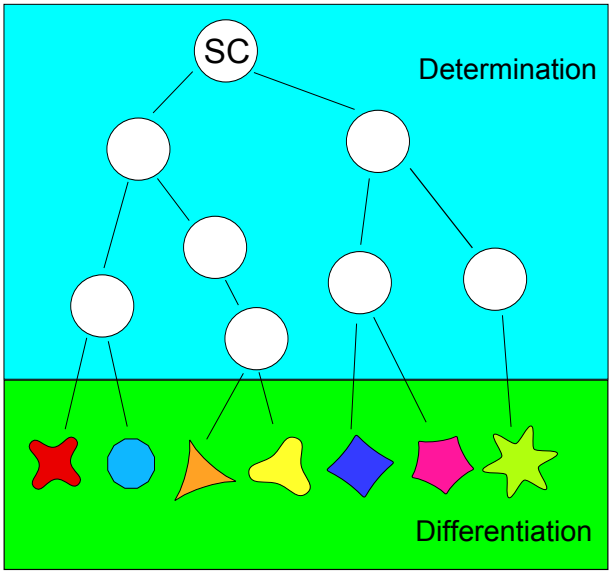

Figure 2.1: Schematic illustrating the process of commitment. Here during determination cells follow a developmental pathway until differentiation specifies particular functions for cells to perform. The morphological changes such as size, shape and gene expression occur within the differentiation process. SC stands for stem cell and the differences in shape and colour signify the assignment of a particular fate.

model that suggested diffusion may be the destabilising factor from which patterns can form. He used a system of reacting and diffusing chemicals, coining the now widely used term morphogens, and demonstrated that, under certain conditions the steady state can be stable to homogeneous perturbations but unstable to spatially inhomogeneous perturbations. In other words, the simple addition of diffusion could act as a destabilising mechanism generating spatial patterns from near homogeneity.

Together with the required conditions for DDI to exist (see Chapter 1) the analysis shows that the application of Turing theory requires the inhibitor to diffuse faster than the activator ($D_B > D_A$). This concept of long range inhibition, short range activation, [22], allows the activator to grow locally while the inhibitor suppresses it's activity at distant sites. While $D_A \neq D_B$, it can be arbitrarily close, [34]. However, generally we require $D_B >> D_A$ for pattern formation to exist, [75]. This inevitably gives a significant restriction on the diffusive capabilities of the two chemicals in question.

Moreover, in the simplest systems an oversimplication arises in the absence of any consideration of cellular dynamics. The significance of cell activity in the patterning process has been highlighted by a number of experimentalists. The self organisation of dissociated cells within feather bud formation [76] and interactions observed between pigmentation cells in zebrafish stripe formation [77], [78], [26] are just two such studies suggesting the importance of cell dynamics in pattern formation. As a result, the typical assumption of cell differentiation above a certain activator level may suggest

a naive approach to considering fundamental cell dynamics in Turing type systems. While less frequent, some mathematical studies have considered certain aspects of cell dynamics within Turing systems. For example, Rauch and Millionas, [79], proposed a Turing type model assuming that signal transduction leads to the production of messenger molecules diffusing at the same rate. Despite these and other recent advancements the explicit inclusion of cell behaviour in Turing models remains scarce.

2.1.2 Outline

This chapter considers the explicit introduction of precursor cell commitment in pattern formation to determine the significance of cell dynamics in biological phenomena. In §2.2 we explicitly introduce cellular dynamics into a Turing type model that is capable of spontaneously generating patterns. In doing so, we consider a general framework for the introduction of cell kinetics and restrict our study to two plausible representations: precursor specification and asymmetric precursor differentiation. We analyse the impact that the cell processes have on the patterning mechanism by incorporating distinct forms of feedback mechanisms, §2.2.3, and investigate their theoretical implications. Within this, we focus on the conceptually different activator-inhibitor schemes of pure and cross kinetics and use the Gierer-Meinhardt and Schnakenberg models as illustrative examples of these. Analysis on the models is undertaken in §2.3.2 and numerical simulations on one and two dimensional domains are investigated in §2.3.3.

2.2 Incorporation of Cellular Dynamics

The nature of Turing systems gives a simple and attractive way of using mathematics to simulate biological patterning. However, the question remains as to whether the simplest of these models under certain assumptions provides significant detail to describe biological complexity. Here we consider the generic reaction diffusion equation with the explicit incorporation of a cell population:

$$\frac{\partial \mathbf{m}}{\partial t} = D_m \nabla^2 \mathbf{m} + \mathbf{F}(\mathbf{m}, \mathbf{n}), \tag{2.1}$$

$$\frac{\partial \mathbf{n}}{\partial t} = -\nabla \cdot \mathbf{J} + \mathbf{H}(\mathbf{m}, \mathbf{n}), \tag{2.2}$$

where $\mathbf{m}(\mathbf{r}, t)$ and $\mathbf{n}(\mathbf{r}, t)$ are vectors of chemical concentrations and cell populations respectively at position $\mathbf{r}$ and time t, D_m is a matrix containing the chemical diffusion coefficients, $\mathbf{J}$ is the flux density describing the flow of cells and $\mathbf{F}(\mathbf{m}, \mathbf{n})$, $\mathbf{H}(\mathbf{m}, \mathbf{n})$ are vector functions representing the interactions between the chemicals and cells. This

general framework permits an investigation into the impact cell kinetics may have on the patterning process by explicitly incorporating the cell population, $\mathbf{n}$, into the chemical reaction kinetics, $\mathbf{F}(\mathbf{m}, \mathbf{n})$.

For the chemical dynamics we consider the simplest activator-inhibitor system consisting of two species, as discussed in Chapter 1. By incorporating this, the model then becomes

$$\frac{\partial A}{\partial t} = D_A \nabla^2 A + \begin{cases} F_p(A, B, \mathbf{n}) \\ F_c(A, B, \mathbf{n}) \end{cases}, \tag{2.3}$$

$$\frac{\partial B}{\partial t} = D_B \nabla^2 B + \begin{cases} G_p(A, B, \mathbf{n}) \\ G_c(A, B, \mathbf{n}) \end{cases}, \tag{2.4}$$

$$\frac{\partial \mathbf{n}}{\partial t} = -\nabla \cdot \mathbf{J} + \mathbf{H}(A, B, \mathbf{n}), \tag{2.5}$$

where A, B is the activator and inhibitor respectively and D_A, D_B are the diffusion coefficients. The reaction kinetics are incorporated through the functions F_p, G_p, F_c, G_c where p and c denote the two types of kinetic schemes in the activator-inhibitor framework. An explanation of these is given in Chapter 1 but the underlying interactions can be seen in Fig. 2.2.

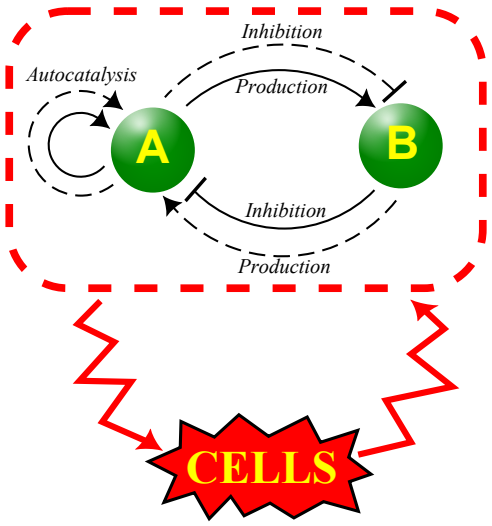

Figure 2.2: Schematic illustrating the modelling framework for the incorporation of cellular dynamics into a two species activator-inhibitor system. Here, A, B represent the activator and inhibitor respectively. The conceptually different interactions of pure (solid lines) and cross kinetics (dashed lines) can be seen and the explicit introduction of cells incorporates interactions with the patterning system. Specifically, we focus our study on cell commitment and the possible feedback effects from this process.

In the absence of cell interactions, the chemicals react and diffuse with one another and, under certain conditions, can produce pattern formation of Turing type. Within this, it is typically assumed that a homogeneous cell population interprets this information and differentiates according to some threshold level of chemical. However, here we investigate the impact cellular dynamics have on this process by considering interactions between a cell population and the patterning system, Fig. 2.2. In particular, we assume that cells becoming committed to a particular fate interact with the chemical system via feedback, effectively changing activator/inhibitor levels as the commitment process develops, and this study will focus on this fundamental process to determine its significance in pattern formation. The model given by (2.3)-(2.5) permits an investigation into this and here we concentrate on two conceptual models of cell commitment.

2.2.1 Precursor Specification

Consider a population of uncommitted cells that become specified directly. These cells, due to some external signal, become specified to begin a particular differentiation pathway at some rate, but we assume also that they have the ability to transfer back to the uncommitted cell population. In this way cells can 'pass' between two different states based upon their gene expression levels. Uncommitted cells can move to the committed class, becoming specified, by responding to environmental cues, however, specified cells also have the ability to become unspecified and as a result move back to the uncommitted class. This transfer from a specified state back to an uncommitted state can be thought of as the cell exhibiting a lack of sufficient gene expression creating cells that may be below the level required for determination to occur.

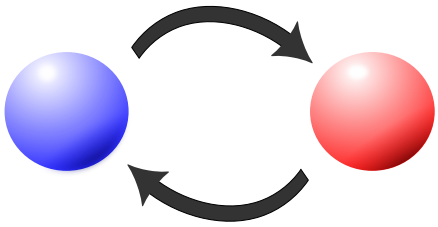

Figure 2.3: Illustration showing the modelling approach considered for the incorporation of a precursor specification process. Here cells transfer from an uncommitted to a specified state and have the possibility of undergoing a reversible process. The blue and red cell represent the uncommitted and committed (specified) class respectively.

Let U represent the uncommitted cell population and C be the specified leading to

the committed cell population. In doing so, we propose a rate diagram for a precursor specification process, illustrated in Fig. 2.3, as follows:

$$U \underset{k_6(\cdot)}{\overset{k_5(\cdot)}{\rightleftharpoons}} C,$$

where cells become specified at a rate dependent on some function, $k_5(\cdot)$, and are reversibly removed from the committed class at a rate $k_6(\cdot)$. Note that we assume that there is no cell proliferation and the cell population simply passes between an uncommitted and committed class. Now by adopting a Law of Mass Action (LMA) type argument applied to cell processes we can derive equations describing the evolution of the uncommitted and committed cell populations:

$$\frac{dU}{dt} = -k_5(\cdot)U + k_6(\cdot)C, \tag{2.6}$$

$$\frac{dC}{dt} = k_5(\cdot)U - k_6(\cdot)C. \tag{2.7}$$

From this we notice that there is a conservation equation: $\frac{dU}{dt} + \frac{dC}{dt} = 0$. On integrating we obtain $U + C = U_0$ where we assume U_0 is a constant representing the initial total population of uncommitted cells. Rearranging this gives $U = U_0 - C$ and substitution into the system, (2.6)-(2.7), reduces the number of equations to a single differential equation:

$$\frac{dC}{dt} = k_5(\cdot)(U_0 - C) - k_6(\cdot)C. \tag{2.8}$$

This equation describes the evolution of precursor specification and on combining this with the chemical concentration equation the system becomes

$$\frac{\partial A}{\partial t} = D_A \nabla^2 A + \begin{cases} F_p(A, B, C) \\ F_c(A, B, C) \end{cases}, \tag{2.9}$$

$$\frac{\partial B}{\partial t} = D_B \nabla^2 B + \begin{cases} G_p(A, B, C) \\ G_c(A, B, C) \end{cases}, \tag{2.10}$$

$$\frac{\partial C}{\partial t} = k_5(\cdot)(U_0 - C) - k_6(\cdot)C. \tag{2.11}$$

where now we have a model where the effect of committed cells on patterning is included through the chemical reaction terms dependence on the committed cell population, C. The functional forms remain generic to allow investigation into the possible

effects the chemical concentrations have on the committed cell population. We assume that the cells do not move ($\mathbf{J} = 0$ in (2.5)) so that only the effects of the commitment process are investigated. We next demonstrate a similar model for a different cell differentiation pathway.

2.2.2 Asymmetric Precursor Differentiation

Asymmetric division begins with an originally uncommitted parent cell dividing into two daughter cells with different cell fates. The schematic in Fig. 2.4 illustrates this process.

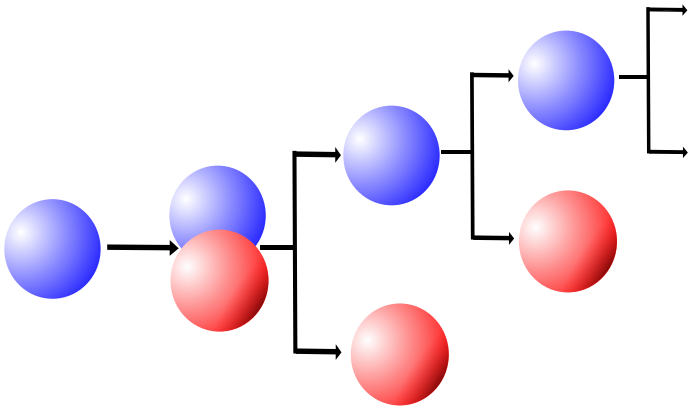

Figure 2.4: The division of a previously uncommitted cell into two cells; one being of identical type and the other differentiating due to the acquisition of a particular fate. The resulting identical type is known as an uncommited cell (blue) and the other a committed cell (red).

The commitment pattern of asymmetric division has been extensively studied in many model systems and development provides a number of situations where cell fate is controlled by this mechanism. For example, in the model organism Drosophila Melanogaster the formation of neurons occurs through the asymmetric division of precursor neuroblasts, [80], [81]. It has also been suggested that the asymmetric division of neuroblasts lacking tumor suppressor genes have the ability to become cancer stem cells ([82] and references therein).

Further to this, asymmetric division is believed to regulate tissue homeostasis. A prime example of this is in the regeneration and replenishment of cells in the skin. Studies have suggested that a stem cell population residing in the follicular bulge region of the hair follicle asymmetrically gives rise to cells required for the

maintenance of both the follicular and interfollicular regions, [73], [83]. Within our study we consider the effect of asymmetric precursor differentiation within pattern formation systems and propose a model to describe this process.

Consider a population of uncommitted cells that exhibit characteristics which are similar to a stem cell population. The uncommitted cells undergo an irreversible process of asymmetric division producing one unchanged uncommitted cell, thus replenishing the population for further division to occur, and one cell that has now undergone differentiation. In our modelling approach we consider the asymmetric division illustrated in Fig. 2.4 and assume that these committed cells differentiate at a rate proportional to some functional form, $k_5(\cdot)$, that depends on the chemical levels. We also include the possibility of cell apoptosis of the committed cell population. In this way, we incorporate the possibilty of cells undergoing programmed cell death which may arise due to morphological abnormalities, for example. This process is assumed to occur at rate $k_6(\cdot)$. By choosing general functional forms for these rates we can tailor the model to suit different biological systems. Formulating this as a rate diagram this would then become

$$U \overset{k_5(\cdot)}{\rightarrow} U + C \underset{k_6(\cdot)}{\hookrightarrow} \text{apoptosis}$$

which, using arguments as before, allows us to derive an equation for the evolution of the committed cell population:

$$\frac{dC}{dt} = k_5(\cdot)U_0 - k_6(\cdot)C, \tag{2.12}$$

where C denotes the committed cell population, U_0 is the initial uncommitted cell population and $k_5(\cdot)$, $k_6(\cdot)$ are functions regulating the rate of commitment and apoptosis respectively. We note the similarity between (2.8) and (2.12). The latter now does not include the possibility of transfer back to an uncommitted cell population and instead maintains an uncommitted cell population by replenishment due to division. Here, the rate coefficient $k_6(\cdot)$ now regulates apoptosis. Although we have only considered proliferation and apoptosis in the committed cell population equation above, (2.12), it should be noted that further cell dynamics can be incorporated as desired. Further to this, the rate of commitment, $k_5(\cdot)$, will be chosen using standard forms since there is little or no current experimental data on which to prescribe a particular form.

Now by combining the resultant committed cell population equation, describing asymmetric precursor differentiation, with the generic two species chemical system we

obtain

$$\frac{\partial A}{\partial t} = D_A \nabla^2 A + \begin{cases} F_p(A,B,C) \\ F_c(A,B,C) \end{cases}, \tag{2.13}$$

$$\frac{\partial B}{\partial t} = D_B \nabla^2 B + \begin{cases} G_p(A,B,C) \\ G_c(A,B,C) \end{cases}, \tag{2.14}$$

$$\frac{\partial C}{\partial t} = k_5(\cdot)U_0 - k_6(\cdot)C, \tag{2.15}$$

allowing us to investigate the impact cell commitment has on the patterning process through the dependence on the committed cell population in the chemical kinetics.

2.2.3 Chemical Kinetics and Feedback Mechanisms

Feedback mechanisms are common in biological systems where the response to external and internal signals is vitally important in the regulation and functioning of a system. Feedback mechanisms can take two different forms: positive feedback acts to upregulate a system or entity whereas negative feedback has the opposite effect, [62]. In the human body, for example, a number of feedback mechanisms exist to allow the body to maintain a fully functioning level and are often evident within homeostatic processes. Some examples of positive feedback include immune response to viruses, platelet accumulation in blood vessel maintenance and cellular response to wound healing. Negative feedback examples include the body's response to hyperglycemic blood-glucose levels, high blood pressure and metabolism. The chemical reaction networks given above provide a further example of feedback loops whereby the chemicals regulate each other such that they can lead to an inhomogeneous equilibrium state.

The two proposed models, (2.9)-(2.11) and (2.13)-(2.15), provide a framework for an investigation into the possible feedback effects a committed cell population can have on pattern formation. For the chemical kinetics we choose two classical schemes in the form of Gierer-Meinhardt, [22], and Schnakenberg, [43]. The committed cell populations interaction with the chemical system is considered through the functional forms Q_i, $i = 1, .., 4$. The full set of kinetics is given by

$$\begin{aligned} F_p &= k_1 \frac{A^2}{B} Q_1(\cdot) - k_2 A + Q_2(\cdot) & & F_c = k_1 + k_2 A^2 B Q_1(\cdot) - k_3 A + Q_2(\cdot) \\ & & \textit{and} & \\ G_p &= k_3 A^2 Q_3(\cdot) - k_4 B + Q_4(\cdot) & & G_c = k_4 - k_2 A^2 B Q_3(\cdot) + Q_4(\cdot) \end{aligned} \tag{2.16}$$

$$\text{Precursor Specification:} \quad H(A,C) = k_5(\cdot)(U_0 - C) - k_6(\cdot)C \tag{2.17}$$

$$\text{Asymmetric Precursor Differentiation:} \quad H(A,C) = k_5(\cdot)U_0 - k_6(\cdot)C \tag{2.18}$$

where A represents the activator and B the inhibitor, D_A, D_B are the diffusion coefficients and k_i, $i = 1, .., 4$ are positive rate constants which have different meanings within each model. A description of the underlying interactions of these chemical kinetics can be seen in Chapter 1. While these schemes are both simplistic and naive in nature, they serve to illustrate the principal findings.

The feedback functions, given by Q_i, $i = 1, .., 4$, affect the chemical concentrations within the system and, by incorporating them in this way, we can investigate different scenarios with the possibility of feedback from the cell population to upregulate/downregulate activator and/or inhibitor levels. In the absence of feedback, the uncommitted cell population produces a base rate of activator/inhibitor that allows for the beginning of pattern formation. After this initial point, the chemicals react and diffuse to amplify their levels such that pattern formation can arise from near homogeneity.

Typically, it is assumed that cells respond to chemical levels and differentiate accordingly. However, the explicit representation of cell commitment and implementation of feedback increases/decreases these levels and may lead to possible effects on patterning within the system. Using this, we assume that the committed cell population begins to increase or suppress chemical levels depending on the nature and type of feedback. The different types of feedback we consider can be seen in Fig. 2.5. Here, we explicitly incorporate positive/negative feedback into activator and/or inhibitor levels directly or through the regulatory processes.

Direct Feedback

For direct feedback (see Fig. 2.5(a)) we consider the case where the committed cell population impacts directly on activator/inhibitor concentrations through positive and negative feedback mechanisms. In this way, the committed cells are able to upregulate and downregulate the chemical concentrations and these can be considered either on their own as solitary effects or together as joint effects.

- *Activator Upregulation/Downregulation*

  The activator is upregulated/downregulated by the committed cell population creating a positive/negative feedback loop between these two entities. To incorporate this mathematically we choose the functions in the two models to be of

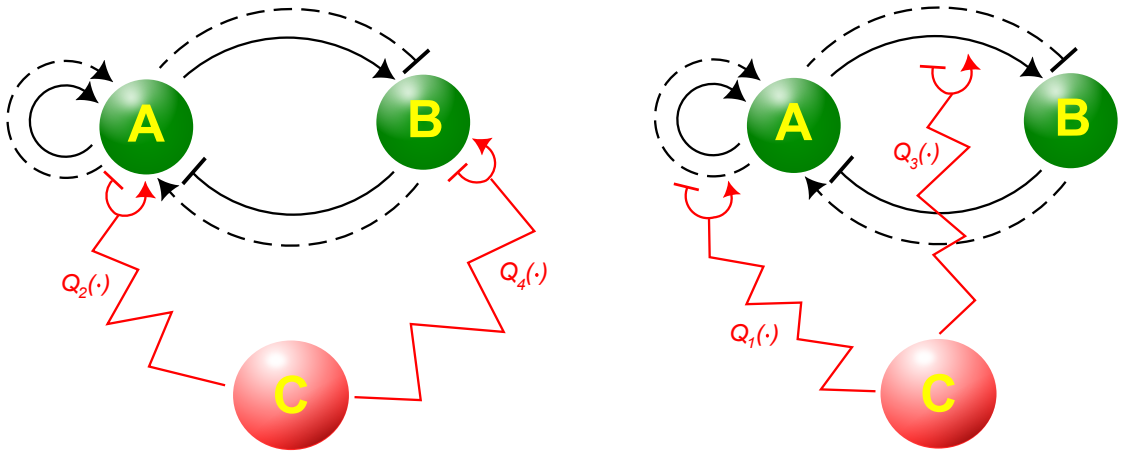

(a) Direct Feedback (b) Regulatory Feedback

Figure 2.5: Schematic illustrating the possible effects the committed cell population, C, can have on the two chemicals A (activator) and B (inhibitor). We see the underlying interactions proposed to implement (a) direct feedback and (b) regulatory feedback into the patterning mechanisms of pure (solid) and cross chemical kinetics (dashed). The feedback functions Q_i, $i = 1, .., 4$ are reference to the mathematical models (2.16)-(2.18).

the form

$$Q_1(\cdot) = Q_3(\cdot) = 1, Q_4(\cdot) = 0, \quad Q_2(\cdot) = \begin{cases} k_8 C, & \text{positive feedback} \\ -k_8 AC, & \text{negative feedback.} \end{cases} \tag{2.19}$$

where k_8 regulates the rate of positive/negative feedback. In this way, we assume that positive feedback derives from increased product by committed cells. The term incorporating negative feedback can be thought of as taking place when the activator comes into contact with a committed cell resulting in some form of activator-receptor binding & ubiquitination. The downstream effect being the supression of activator within the system.

- *Inhibitor Upregulation/Downregulation*

  Similarly to the previous case we assume that the cell population feeds back to upregulate or downregulate the chemical concentration. However this time the inhibitor concentration is affected. In this case, we propose the functions in the two models to be of the form

$$Q_1(\cdot) = Q_3(\cdot) = 1, Q_2(\cdot) = 0, \quad Q_4(\cdot) = \begin{cases} k_8 C, & \text{positive feedback} \\ -k_8 BC, & \text{negative feedback.} \end{cases} \tag{2.20}$$

where k_8 regulates the positive/negative feedback. Similar arguments can be put forth to those given above.

The above functional forms have been chosen primarily for their simplicity. Of course, many other functions can be implemented to describe this process. Note that for direct feedback we set $Q_1(\cdot) = Q_3(\cdot) = 1$ in our models.

Regulatory Feedback

By regulatory feedback we mean that the committed cell population affects the autocatalytic mechanism through which the activator is produced and also into the mechanism regulating the inhibitor (Fig. 2.5). Autocatalysis is the reaction process by which the chemical is self sustaining, continually replenishing itself if some chemical is present. In the Gierer-Meinhardt and Schnakenberg kinetics the activator produces itself via autocatalysis, regulating the process and allowing continued production of the activator in the system. The inhibitor is produced by the activator in the pure type kinetics but facilitates the reaction in the cross type kinetics with the inhibitor being depleted within this process. As a result, we consider the regulatory processes of the activator and inhibitor to be the autocatalytic reaction and inhibitor depletion respectively (see Fig. 2.5(b)).

- *Activator Upregulation/Downregulation*

  As in direct feedback, the activator is upregulated/downregulated by the committed cell population creating a positive/negative feedback loop. This time, however, the activator levels are affected via the regulatory processes. By choosing the functions below we can incorporate this into our model.

$$Q_2(\cdot) = Q_4(\cdot) = 0, Q_3(\cdot) = 1, \quad Q_1(\cdot) = \begin{cases} 1 + \frac{k_8}{k_1}C, & \text{positive feedback} \\ \frac{1}{1+k_8 C}, & \text{negative feedback.} \end{cases} \tag{2.21}$$

  where k_8 regulates the positive/negative feedback. Here, the positive feedback term assumes that the normal rate of autocatalysis from the uncommitted cell population continues but there is a further contribution from the committed cell population. The negative feedback term, however, involves suppression of the original autocatalysis mechanism, inhibiting the production.

- *Inhibitor Upregulation/Downregulation*

  The committed cell population imposes a positive/negative feedback loop changing inhibitor concentration levels through the regulatory term. Within the Gierer-Meinhardt kinetics for pattern formation systems we assumed that the inhibitor is stimulated by the activator, producing inhibitor at a rate proportional

to k_3A^2. In the Schnakenberg kinetics the inhibitor is depleted by the activator and is consumed through the facilitation of the reaction, $-k_2A^2B$. Therefore, it is through these regulatory mechanism that we assume feedback occurs. We propose similar functions to the activator upregulation/downregulation case and again assume that the cell population feeds back to upregulate or downregulate the chemical concentrations. However this time the inhibitor concentration is affected. In the case of the Gierer-Meinhardt kinetics, we can set the functions in the model to be of the form

$$Q_2(\cdot) = Q_4(\cdot) = 0, Q_1(\cdot) = 1, \quad Q_3(\cdot) = \begin{cases} 1 + \frac{k_8}{k_3}C, & \text{positive feedback} \\ \frac{1}{1+k_8C}, & \text{negative feedback.} \end{cases} \tag{2.22}$$

where again k_8 is the rate of positive/negative feedback into the inhibitor. The terms are assumed to similarly follow the activator upregulation/downregulation description above.

However, with the Schnakenberg kinetics we assume that inhibitor levels are altered via the activators suppressive effect on the inhibitor. In this case we need to minimise the suppression and, as a result, consider

$$Q_2(\cdot) = Q_4(\cdot) = 0, Q_1(\cdot) = 1, \quad Q_3(\cdot) = \begin{cases} \frac{1}{1+k_8C}, & \text{positive feedback} \\ 1 + \frac{k_8}{k_2}C, & \text{negative feedback.} \end{cases} \tag{2.23}$$

where k_8 is the rate of positive/negative feedback into the inhibitor.

For reference between the different models, it should be noted that $k_8 = 0$ will provide no feedback interaction and lead back to the two chemical species case.

2.3 Mathematical Models

The general three species system that incorporates both types of chemical kinetics and cell commitment processes is given by

$$\frac{\partial A}{\partial t} = D_A\nabla^2 A + \begin{cases} F_p(A,B,C) \\ F_c(A,B,C) \end{cases} \tag{2.24}$$

$$\frac{\partial B}{\partial t} = D_B\nabla^2 B + \begin{cases} G_p(A,B,C) \\ G_c(A,B,C) \end{cases} \tag{2.25}$$

$$\frac{\partial C}{\partial t} = H(\cdot) \tag{2.26}$$

where the subscripts p and c denote the pure and cross type reaction kinetics, respectively given by $F_p(A,B)$, $G_p(A,B)$ and $F_c(A,B)$, $G_c(A,B)$. We consider the cell dynamics in the absence of any taxis and incorporate the interactions through the function $H(\cdot)$. In line with the standard assumption that activator (or inhibitor levels) trigger commitment, we assume transfer to the committed cell population depends on the activator concentration. In particular, we consider a saturating form according to $k_5(\cdot) = \frac{k_5 A}{k_7+A}$. The coefficient regulating the transfer back and apoptosis of the precursor specification and asymmetric precursor differentiation kinetics respectively is simply assumed to be constant, $k_6(\cdot) = k_6$. Therefore, the kinetics are given by

$$\begin{aligned} F_p &= k_1\frac{A^2}{B}Q_1(\cdot) - k_2A + Q_2(\cdot) \qquad & F_c &= k_1 + k_2A^2BQ_1(\cdot) - k_3A + Q_2(\cdot) \\ & \qquad\qquad \textit{and} & & \\ G_p &= k_3A^2Q_3(\cdot) - k_4B + Q_4(\cdot) & G_c &= k_4 - k_2A^2BQ_3(\cdot) + Q_4(\cdot) \end{aligned} \tag{2.27}$$

$$\text{Precursor Specification:} \quad H(A,C) = \frac{k_5A(U_0-C)}{k_7+A} - k_6C, \tag{2.28}$$

$$\begin{matrix}\text{Asymmetric Precursor} \\ \text{Differentiation}\end{matrix}: \quad H(A,C) = \frac{k_5AU_0}{k_7+A} - k_6C, \tag{2.29}$$

where A, B denote the activator and inhibitor respectively, k_i, $i = 1,..,7$ are positive rate constants that may take different meanings depending on context, and D_A, D_B are the diffusion coefficients. Under a suitable nondimensionalisation (see Appendix A.1 and A.2), the model becomes,

$$\frac{\partial u}{\partial t} = \nabla^2 u + \begin{cases} f_p(u,v,w) \\ f_c(u,v,w) \end{cases} \tag{2.30}$$

$$\frac{\partial v}{\partial t} = d\nabla^2 v + \begin{cases} g_p(u,v,w) \\ g_c(u,v,w) \end{cases} \tag{2.31}$$

$$\frac{\partial w}{\partial t} = h(u,w) \tag{2.32}$$

with

$$\begin{aligned} f_p &= \frac{u^2}{v}q_1(\cdot) - \alpha u + q_2(\cdot) \qquad & \textit{and} \qquad & f_c = \delta + u^2 v q_1(\cdot) - u + q_2(\cdot) \\ g_p &= u^2 q_3(\cdot) - v + q_4(\cdot) & & g_c = \rho - u^2 v q_3(\cdot) + q_4(\cdot) \end{aligned} \tag{2.33}$$

$$\text{Precursor Specification:} \quad h(u,w) = \frac{u}{\kappa + u} - \beta w, \tag{2.34}$$

$$\begin{matrix}\text{Asymmetric Precursor} \\ \text{Differentiation}\end{matrix} : \quad h(u,w) = \frac{u(1-\nu w)}{\kappa + u} - \beta w. \tag{2.35}$$

Here u, v and w represent the activator, inhibitor and committed cell population respectively and α, δ, ρ and d are all positive parameters. Here, q_i, $i = 1, .., 4$ represent the nondimensionalised feedback functions which, by considering only activator feedback for illustration, now take the form

- Direct Feedback:

$$q_1(\cdot) = q_3(\cdot) = 1, q_4(\cdot) = 0 \quad q_2(\cdot) = \begin{cases} \gamma w, & \text{positive feedback} \\ -\gamma u w, & \text{negative feedback.} \end{cases} \tag{2.36}$$

- Regulatory Feedback:

$$q_2(\cdot) = q_4(\cdot) = 0, q_3(\cdot) = 0 \quad q_1(\cdot) = \begin{cases} 1 + \gamma w, & \text{positive feedback} \\ \frac{1}{1+\gamma w}, & \text{negative feedback.} \end{cases} \tag{2.37}$$

where γ is a positive parameter controlling the rate of feedback.

On comparison of the two models, although the underlying assumptions and derivation are different, we see that the only variation between them is the term $-\frac{\nu u}{\kappa + u}$ in the cell dynamics function $h(\cdot)$. As a result of the nondimensionalisation, if $\nu = 0$ we obtain the asymmetric precursor differentiation model and for $\nu \neq 0$ the precursor specification model is considered.

Using the model framework of (2.30)-(2.32) we first undertake a general linear stability analysis, encompassing both chemical and cell commitment mechanisms, in order to predict the theoretical implications of incorporating cell commitment in a pattern formation mechanism. Beyond this, we investigate the behaviour of the system with different feedback mechanisms and rates by undertaking analysis in §2.3.2, comparing the results with the system in the absence of feedback. Finally, we show numerical simulations on both one and two dimensional domains in §2.3.3 to reinforce the re-

sults of the analysis and to determine the impact cell commitment has on the resultant patterns.

2.3.1 General Stability Analysis and Behaviour

Considering the general nondimensionalised model, (2.30)-(2.32), we let general functions f and g represent both pure and cross specific functions, f_p, f_c, g_p, g_c. With this, we analyse the linear stability of this system and determine the conditions that will lead to Diffusion-Driven Instability (DDI). In doing so, we seek to determine when the homogeneous steady state is stable to a homogeneous perturbation while unstable to an inhomogeneous perturbation.

The homogeneous steady state (u_s, v_s, w_s) is given by $f(u_s, v_s, w_s) = g(u_s, v_s, w_s) = h(u_s, v_s, w_s) = 0$. Linearising about this steady state by setting

$$\mathbf{u} = \begin{pmatrix} u - u_s \\ v - v_s \\ w - w_s \end{pmatrix} \tag{2.38}$$

gives

$$\mathbf{u}_t = M\mathbf{u} + D\nabla^2\mathbf{u}, \quad D = \begin{pmatrix} 1 & 0 & 0 \\ 0 & d & 0 \\ 0 & 0 & 0 \end{pmatrix}, \tag{2.39}$$

where M is the Jacobian matrix at the steady state and D is the matrix of diffusion coefficients. Seeking solutions of the form $\mathbf{u} = \tilde{\mathbf{u}}exp(\lambda t + ik\mathbf{r})$ we substitute in and rearrange to give

$$(M - \lambda I - Dk^2)\tilde{\mathbf{u}} = 0, \tag{2.40}$$

where $\nabla^2 \sim -k^2$ from the spatial eigenvalue problem (see Murray [2]) with k the wavenumber and λ the temporal growth rate. Further to this, M is the matrix of partial derivatives at the steady state, I is the identity matrix and D is the matrix of diffusion coefficients. For nontrivial solutions we require

$$\left|M - \lambda I - Dk^2\right| = 0, \tag{2.41}$$

with the expansion of this leading to a characteristic polyniomial of the form

$$p(\lambda) = \lambda^3 + a_2(k)\lambda^2 + a_1(k)\lambda + a_0(k) = 0. \tag{2.42}$$

In the above

$$a_2(k) = -f_u - g_v - h_w + (1+d)k^2, \tag{2.43}$$

$$a_1(k) = dk^4 + (-f_u d - g_v - h_w - dh_w)k^2 + f_u g_v - g_u f_v + f_u h_w$$
$$- f_w h_u + g_v h_w - g_w h_v, \tag{2.44}$$

$$a_0(k) = -k^4 dh_w + (f_u dh_w + g_v h_w - g_w h_v - h_u f_w d)k^2$$
$$+ g_u f_v h_w + f_u g_w h_v - f_u g_v h_w - h_u f_v g_w + h_u f_w g_v - g_u f_w h_v, \tag{2.45}$$

where $f_u = \frac{\partial f}{\partial u}|_{(u_s,v_s,w_s)}$, $g_u = \frac{\partial g}{\partial u}|_{(u_s,v_s,w_s)}$, etc. and d is the diffusion parameter. We are now in a position to analyse the stability of the homogeneous steady state. Using the Routh Hurwitz conditions, [4], this leads to the requirements

- Stable to a homogeneous perturbation: in the absence of any spatial terms we set $k = 0$ and, to satisfy the stability criteria, we require, $a_2(k=0) > 0$, $a_0(k=0) > 0$ and $(a_1 a_2 - a_0)(k=0) > 0$. Explicitly, this leads to the following requirements

$$a_2(k=0) = -f_u - g_v - h_w > 0 \tag{2.46}$$

$$a_0(k=0) = g_u f_v h_w + f_u g_w h_v - f_u g_v h_w - h_u f_v g_w$$
$$+ h_u f_w g_v - g_u f_w h_v > 0, \tag{2.47}$$

$$(a_1 a_2 - a_0)(k=0) = (f_u g_v - g_u f_v + f_u h_w - f_w h_u$$
$$+ g_v h_w - g_w h_v)(-f_u - g_v - h_w),$$
$$- (g_u f_v h_w + f_u g_w h_v - f_u g_v h_w - h_u f_v g_w$$
$$+ h_u f_w g_v - g_u f_w h_v) > 0. \tag{2.48}$$

  The final of these conditions is only true if $a_1(k=0) > 0$:

$$f_u g_v - g_u f_v + f_u h_w - f_w h_u + g_v h_w - g_w h_v > 0. \tag{2.49}$$

  where f_u, g_u, etc. denote the partial derivative of the functions with respect to the subscripts evaluated at the steady state.

- Unstable to an inhomogeneous perturbation: in the presence of spatial terms we set $k \neq 0$ and look for instability from the diffusive terms. In this case, at

least one of $a_2(k)$, $a_0(k)$ or $(a_1a_2 - a_0)(k)$ must be negative for instability of the homogeneous steady state. A number of scenarios arise and we look at these separately below. Firstly, however, by using (2.46), we can see that for all cases,

$$a_2(k) = \overbrace{-F_A - G_B - H_C}^{>0} + \overbrace{(1 + D_B)k^2}^{>0} > 0. \tag{2.50}$$

As a result, instability can only be attained if $a_0(k) < 0$ and/or $(a_1a_2 - a_0)(k) < 0$. Note that if the coefficient $a_0(k) < 0$, we are guaranteed instability.

(i) $a_0(k) < 0$ with $a_1(k) > 0$ implies $(a_1a_2 - a_0)(k) > 0$, and so the conditions for instability become

$$-f_u d - g_v - h_w - dh_w > 0 \Rightarrow a_1(k) > 0, \tag{2.51}$$

$$a_0(k) = < 0. \tag{2.52}$$

This set of instability conditions leads to different forms for the characteristic polynomial $p(\lambda)$ and these are illustrated in Fig. 2.6(a). These suggest that there is the possibility of obtaining two negative and one positive real root or complex conjugate roots with negative real part and one positive real root. In this way, we are guranteed instability since $a_0(k) < 0$ which gives $Re(\lambda(k^2 \neq 0)) > 0$.

(ii) $a_0(k) < 0$ with $a_1(k) < 0$ implies $(a_1a_2 - a_0)(k) \lesseqgtr 0$ and the conditions for instability become

$$-f_u d - g_v - h_w - dh_w < 0, \tag{2.53}$$

$$a_1(k) < 0, \tag{2.54}$$

$$a_0(k) < 0 \quad \text{AND/OR} \quad (a_1a_2 - a_0)(k) < 0. \tag{2.55}$$

In this case, the typical forms of the characteristic polynomial can be seen in Fig. 2.6(b). Similarly to case (i), these suggest there is the possibility of obtaining two negative and one positive real root or complex conjugate roots with negative real part and one positive real root. Once again, we are guaranteed instability if either $a_0(k) < 0$, $a_1a_2 - a_0(k) < 0$ or both are satisfied since at least one $Re(\lambda) > 0$.

(iii) $a_0(k) > 0$ with $a_1(k) < 0$ implies $(a_1a_2 - a_0(k)) < 0$, and so the conditions

for instability become

$$-f_u d - g_v - h_w - d h_w < 0, \tag{2.56}$$

$$a_1(k) < 0, \tag{2.57}$$

$$a_0(k) > 0, \tag{2.58}$$

$$(a_1 a_2 - a_0)(k) < 0. \tag{2.59}$$

Here, the typical characteristic polynomial forms, Fig. 2.6(c), suggest the possibility of obtaining either two negative and one positive real root or one negative real root and complex conjugate roots with positive real part.

(iv) $a_0(k) > 0$ with $a_1(k) > 0$ implies $(a_1 a_2 - a_0)(k) \lesseqgtr 0$. Instability can only be achieved if $(a_1 a_2 - a_0)(k) < 0$, and so the conditions for instability become

$$-f_u d - g_v - h_w - d h_w > 0 \Rightarrow a_1(k) > 0, \tag{2.60}$$

$$a_0(k) > 0, \tag{2.61}$$

$$(a_1 a_2 - a_0)(k) < 0. \tag{2.62}$$

Finally, the illustrations in Fig. 2.6(d) suggest the characteristic polynomial can have either one negative real root and complex conjugate roots with positive real part or one negative real root and complex conjugate roots with negative real part. Therefore, the only way to instability is through the former case. In particular, via the complex eigenvalue with positive real part.

In the final two of these cases, (iii) and (iv), the theoretical suggestion is that one way to instability is through the appearance of the complex eigenvalue with positive real part. In fact, the latter of these can only be driven unstable if this scenario occurs. If an imaginary component appears, there is the possibility of oscillatory dynamics in time. Furthermore, if the imaginary eigenvalue also has positive real part the system can be driven unstable and we may expect to observe oscillatory behaviour in both space and time. An investigation of the dispersion relations and numerical simulations should determine whether this behaviour appears and therefore in our analysis, §2.3.2 and 2.3.3, we focus on this as a possibility.

Given plausible reaction kinetics we are able to use this information to determine the constraints on the parameters that, if satisfied, will produce patterned solutions in

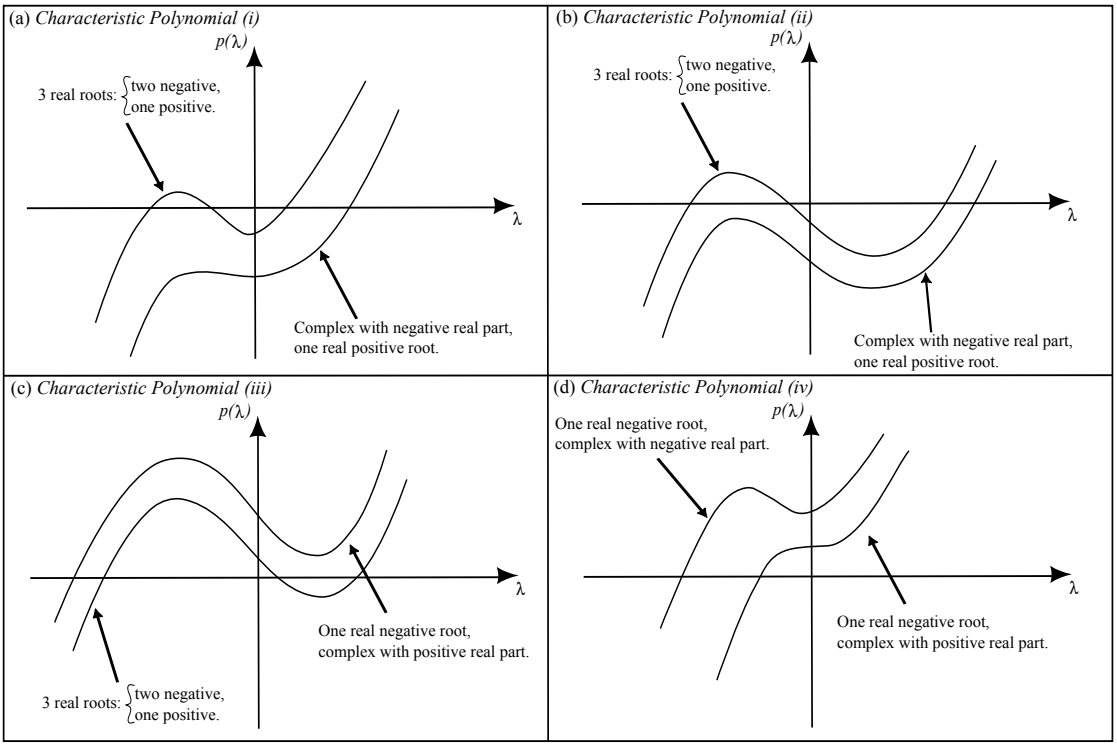

Figure 2.6: Typical solutions of the characteristic polynomial, $p(\lambda)$, for the instability conditions given above with (a)-(d) corresponding to instability conditions (i)-(iv) respectively. Instability conditions (i) and (ii) are unstable through the appearance of a positive real root. Conditions (iii) and (vi) indicate the possibility of complex roots with positive real part, suggesting the potential for oscillatory dynamics in both space and time.

simulations. By considering (2.33)- (2.35) with feedback into activator as a case study, (2.36)-(2.37), we are now in a position to investigate the impact cell differentiation has on pattern formation.

2.3.2 Analysis of Cell Feedback

Firstly, no feedback from the committed cell population ($\gamma = 0$) results in a system that is uncoupled from the chemical system in that it does not affect activator/inhibitor levels. In doing so, the pattern is driven by a two species activator-inhibitor system and the parameter space and one dimensional simulations for these models follow the standard two species system results shown in Fig. 1.5 of Chapter 1. These show the possible parameter values for which DDI will occur and typical corresponding simulations for a specific parameter set.

To demonstrate the impact of cell commitment we analyse the specific case of feedback affecting activator levels within the systems and incorporate the Asymmetric Precursor Differentiation (APD) and Precursor Specification (PS) commitment mechanisms. In particular, we look at both types of feedback, namely direct and regulatory feedback, separately and will consider the following in the analysis:

- Feedback effects on the parameter spaces;
- Lifting of restrictions in classical two species systems;
- Dispersion relations with potentially oscillatory dynamics;
- Numerical analysis of pattern development and above with one and two dimensional results.

Due to the complexity of the system, it becomes difficult to gain precise analytical relationships for pattern formation. Therefore, we investigate the model numerically in order to gain insight into the models capabilities. Details of the numerical methods can be seen in Appendix C.1. In the following investigation we analyse the cases when $\nu = 0$ (APD) and $\nu = 1$ (PS) to determine the results of each of the models.

Parameter Space Analysis

The parameter space provides an illustration of the region and parameters that will lead to pattern formation of Turing type. The different mechanism effects for increasing feedback ($\gamma \in [0\ \ 1]$) on the parameter spaces can be seen in Fig. 2.7. The changes in the parameter space for the different types of feedback are also summarised in the table and graphs of Fig. 2.8, illustrating the overall effects and percentage change of increasing feedback ($\gamma = 0, 0.25, 0.5, 0.75, 1$) in the parameter spaces.

From this, we can see that opposing effects are observed for the comparable feedback mechanisms in the pure and cross type chemical kinetics. Furthermore, the largest differences when feedback is increased is seen in direct feedback for pure kinetics and for all feedback mechanisms in the APD cross model but, in particular, the regulatory mechanisms. In the pure case, the positive feedback results in an increase

in the parameter space for increasing feedback parameter γ. Furthermore, the negative feedback into the pure type kinetics results in a decrease in the parameter space region. In contrast, feedback into the cross kinetic system has opposing actions with positive and negative feedback resulting in a decrease and increase in the parameter space region respectively.

For the pure type system these results would suggest that greater robustness in terms of parameter selection is gained from the inclusion of positive feedback. This parameter space expansion allows a wider range of parameters to be chosen. Although negative feedback results in a decrease, different scales of reductions are observed between the type of feedback imposed. For example, with direct negative feedback much larger decreases are evident compared to the regulatory negative mechanism. In fact, the results illustrate a loss of the parameter space for feedback values greater than 0.75 and 1 when considering the APD and PS model respectively. The decrease in the regulatory negative feedback mechanism shows only slight decreases in the parameter space. Therefore, the plots suggest that biological systems exhibiting high feedback from a committed cell population may not be amenable to the implementation of a direct negative feedback mechanism.

Opposing but similar results are observed for the cross type system with the largest increases and decreases in the parameter space regions observed for direct negative and positive feedback respectively. However, in this case, the plots show that feedback is limited to $\gamma < 0.75$ when considering direct positive feedback from an APD mechanism. Similarly to the pure type kinetics, this is rectified when considering the PS model with $\nu = 1$. However, this again is only up to a certain critical feedback value where after this point there is no DDI.

These results suggest that with the inclusion of positive feedback into pure type kinetics or negative feedback into cross kinetics the choice of parameter values can be less restricted giving a greater variability in the possible values that can be chosen. Where the classical two species system may fail to allow for any kind of perturbation to the parameters, the incorporation of cell differentiation with feedback mechanisms may permit fluctuations in parameters depending on the mechanism present and level of feedback. Therefore, for these cases, the explicit implementation of a committed cell population may create a more robust system with respect to parameter selection by making the model less sensitive to variability and often natural perturbations within biological systems. However, the distinct behaviours observed for the different kinetic forms suggests a subtle relationship.

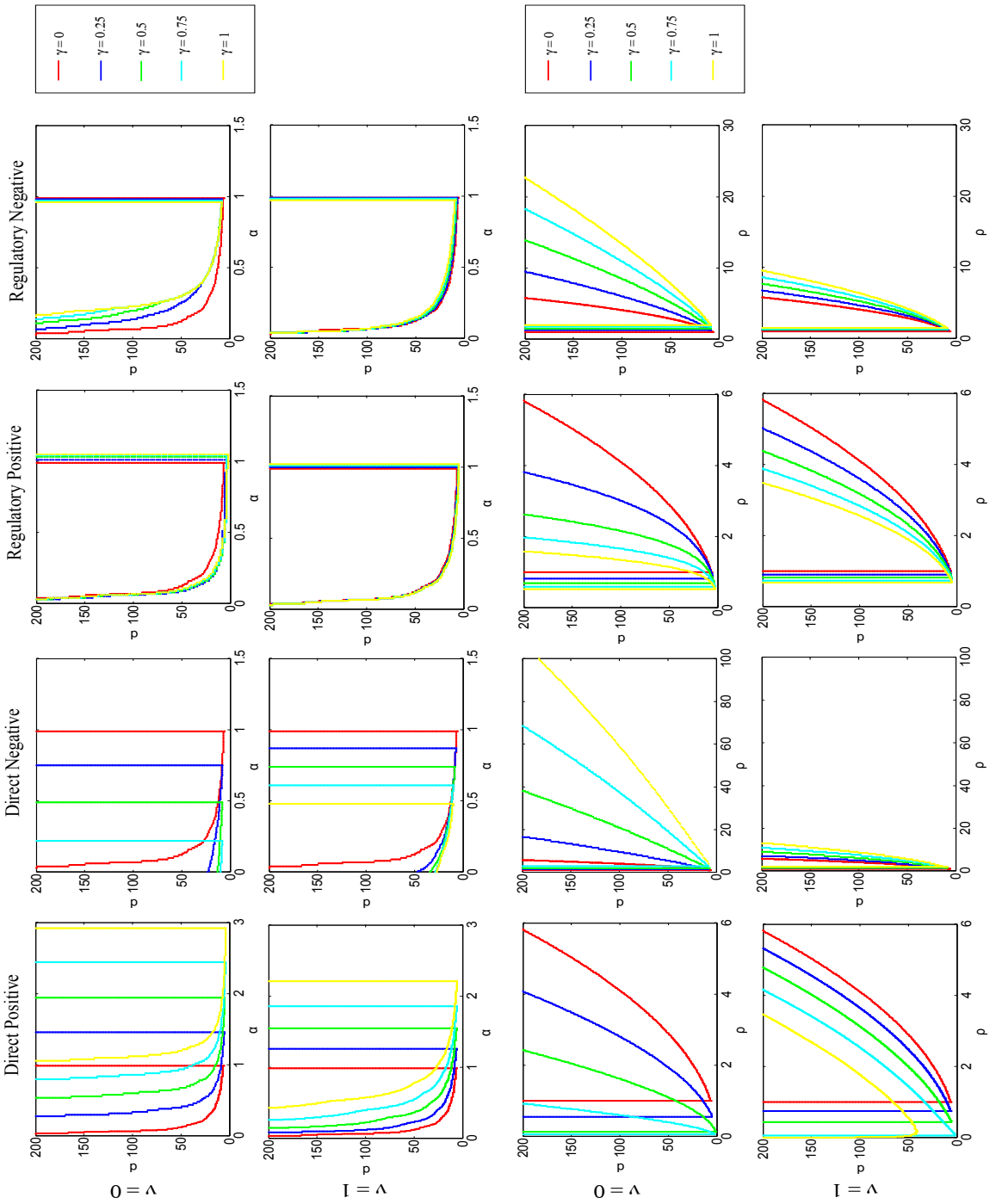

(a) Pure Kinetics

(b) Cross Kinetics

Figure 2.7: Plots of the $\alpha - d$ and $\rho - d$ parameter space for the two models: APD ($\nu = 0$) and PS ($\nu = 1$). Furthermore the impact of feedback is investigated for $\gamma \in [0\ 1]$ and the results are shown for both (a) pure (Gierer-Meinhardt) and (b) cross (Schnakenberg) kinetics. The other parameters are chosen as $\kappa = 10$, $\beta = 0.1$ and $\delta = 0$.

	Direct Pos.	*Direct Neg.*	*Regulatory Pos.*	*Regulatory Neg.*
(a) Pure	Increase	Decrease	Increase	Decrease
(b) Cross	Decrease	Increase	Decrease	Increase

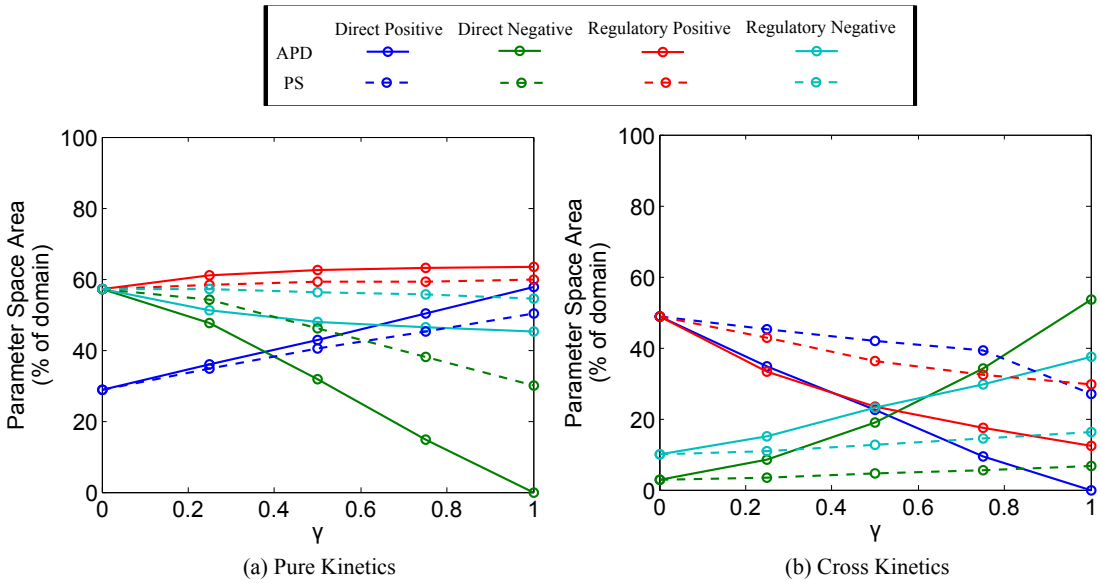

Figure 2.8: Plots of the percentage area covered by the parameter space over the domain shown in Fig. 2.7 and, above, a table indicating the changes in the parameter space when the feedback parameter, γ, is increased. The results are shown for (a) Pure Gierer-Meinhardt kinetics and (b) Cross Schnakenberg kinetics.

Equal Chemical Diffusion Coefficients

Further investigation reveals the possibility of identical chemical diffusion coefficients. This contradictary result (compared to a two species Turing model) is illustrated in Fig. 2.9. A plot of γ against α shows that the diffusion parameter $d = \frac{D_B}{D_A}$ can be chosen to be equal to one, Fig. 2.9, predicting that $D_A = D_B$. Here we set $d = 1$ and plot the parameter space for varying values of γ and α, with $\nu = 0$ (APD), $\nu = 0.5$ and $\nu = 1$.

The region enclosed by the lines indicate the possible parameter values that will produce spatially heterogeneous patterns when both chemicals diffuse at the same rate. In fact, with this model there is also the possibility of having $d < 1$ (not shown). The incorporation of this would then allow a choice of diffusion parameter, d, such that the activator diffusion is faster than its inhibitor. As a result of the similar

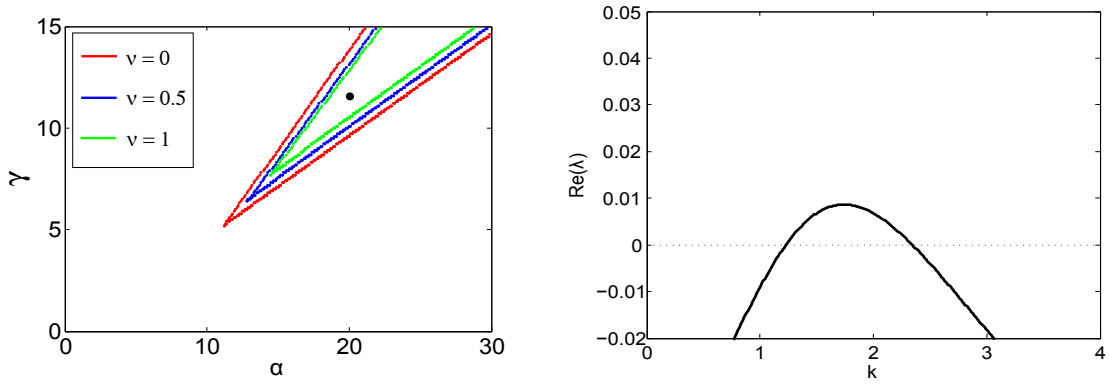

(a) Parameter Space (b) Dispersion Relation

Figure 2.9: Figure showing the possibility of DDI for $d = 1$ with (a) parameter space plot for $\nu = 0, 0.5, 1$ and (b) dispersion relation showing the possible unstable wavenumbers. The parameter values shown by the black dot are $\alpha = 20$, $\gamma = 12$, $\nu = 0$, $\kappa = 10$, $\beta = 0.1$, $d = 1$.

nondimensionalisation and DDI analysis of the two species models (see Chapter 1), in the absence of any cell dynamics, we require the diffusion parameter $d = \frac{D_B}{D_A} > 1$. Biologically speaking this incorporates the notion of short range activation, long range inhibition of the chemical species. As discussed, this has led to much scepticism in the use of Turing's theory due to the restriction on the dynamics of the chemical species.

Previous research by Rauch *et al*, however, has shown that spatial patterning can exist in Turing systems with equal diffusion coefficients by including the effects of subcellular dynamics, [79]. Moreover, a theoretical study based on the molecular signalling between the Eda, CTGF and BMP pathway has also shown the possibility of pattern formation with equal diffusion coefficients, [84]. Further to this, however, the figures above suggest that with a pure type system that explicitly couples cell differentiation with direct positive feedback we can not only have equal diffusion coefficients ($d = 1$) but can also have the activator diffusing faster than its inhibitor ($d < 1$).

The upregulation of activator through feedback clearly allows for increasing activator levels within the system. The spatially restricted committed cells amplify activator levels across the domain and, due to the form of pure kinetics, this results in an increase to inhibitor levels. This increase in inhibitor potency across the system may mean that the requirement for diffusion is reduced. In this way, this reduction can lead to the attainability of equal diffusion coefficients. Moreover, the form of the kinetics may also explain the selective appearance of this property in pure type kinetics since activator upregulation would lead to supression of inhibitor in cross kinetics.

Imaginary Part in Dispersion Relations

Our earlier consideration of the general system suggested eigenvalues with positive real and imaginary components are possible for the three species system. Investigating this phenomena, we consider plots of the dispersion relation that show the range of unstable wavenumbers that can grow exponentially to produce patterning of particular wavelengths. Typically, however, the wavenumber with largest $Re(\lambda) > 0$ dominates. Figure 2.10 and 2.11 show the dispersion relations for varying γ with $\nu = 0$ (APD) and $\nu = 1$ (PS) respectively. Moreover, we observe the results for the different chemical kinetics and feedback mechanisms.

Most notably, the negative feedback dispersion relations can introduce an imaginary component. This imaginary wavenumber suggests dynamics that are oscillatory in both space and time. With larger feedback we see the imaginary part becomes increasingly dominant as a result of a larger set of imaginary unstable wavenumbers within the spatial wavenumber range. Therefore, for higher feedback parameter, we would expect the temporal oscillations to be much more apparent in model simulations.

2.3.3 Numerical Analysis

The different sizes of the parameter spaces exhibited in the feedback mechanisms precludes a detailed study. Instead, we concentrate on some interesting phenomena that appear in the one and two dimensional simulations. Moreover, we will consider numerical simulations of the interesting behaviour highlighted in the previous section. We assume that the inhibitor decay is approximately one hour $k_4 = 0.7$ and diffusion of the activator and inhibitor is in the region of $\sim 10^{-7} - 10^{-9}$ cm^2/s. Note that these are not taken from specific sources. For an approximate reference point to biological timescales we will focus on the patterns formed after 48 hours.

Patterning in One Dimension

As we have seen from the analysis of the previous section, both models have the capability to produce spatial patterning of Turing type. The one dimensional simulations give a degree of insight and allow us to investigate some of the properties the systems exhibit. For reference, the one dimensional simulations with no feedback are given for both the APD model ($\nu = 0$) and PS model ($\nu = 1$), Fig. 2.12. These correspond to the simulations of the classical two species system and although the activator and inhibitor simulations remain the same, the evolution of the committed cell population show the differences in the cell simulations.

However, the main feature of the modelling is to determine the impact of cell commitment on pattern formation. In doing so, we analyse the simulations for an

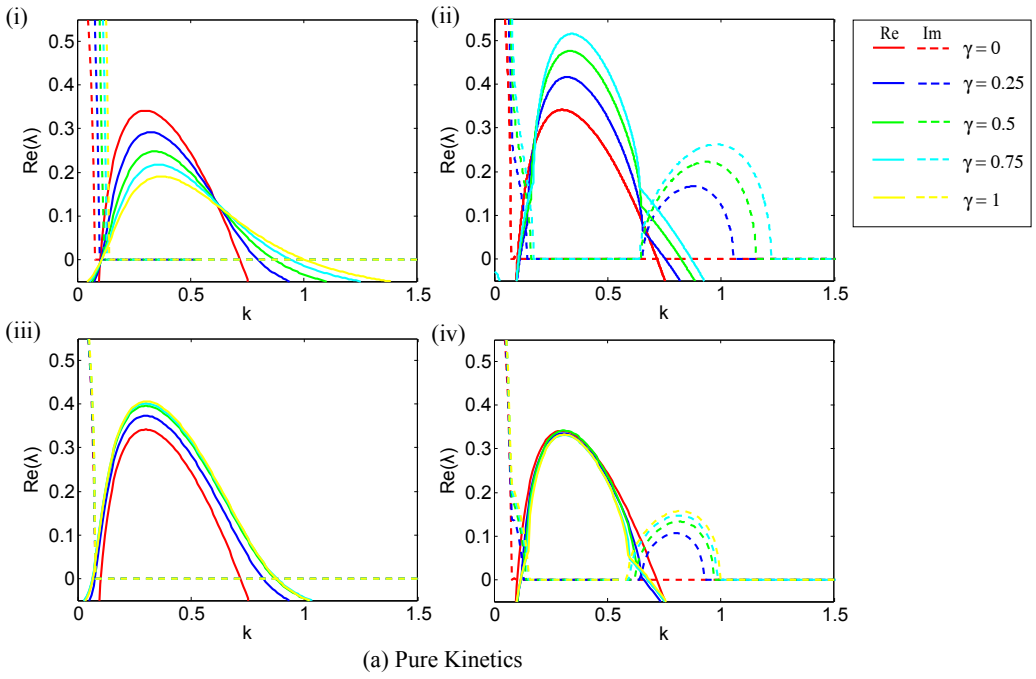

(a) Pure Kinetics

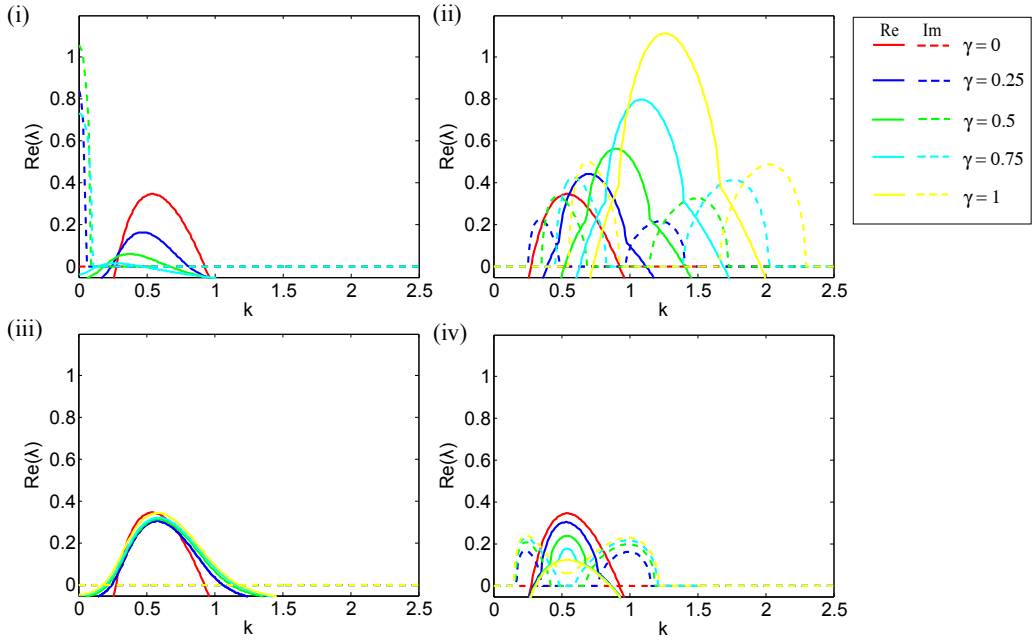

(b) Cross Kinetics

Figure 2.10: Dispersion relations for the APD ($\nu = 0$) model with different feedback mechanisms and increasing γ in (a) pure chemical kinetic model and (b) cross chemical kinetic model. The dispersion relations for different feedback mechanisms are shown as (i) direct positive, (ii) direct negative, (iii) regulatory positive and (iv) regulatory negative. The other parameters were chosen to be $\kappa = 10$, $\beta = 0.1$, $\delta = 0$ and setting α, ρ to be the midvalue of the parameter space at $d = 100$.

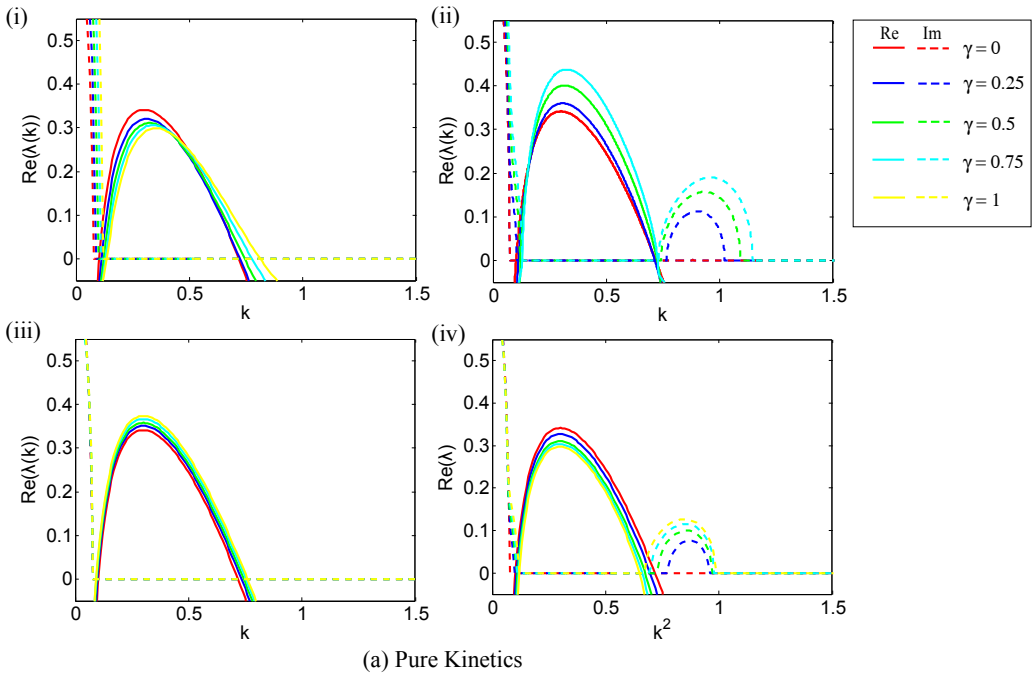

(a) Pure Kinetics

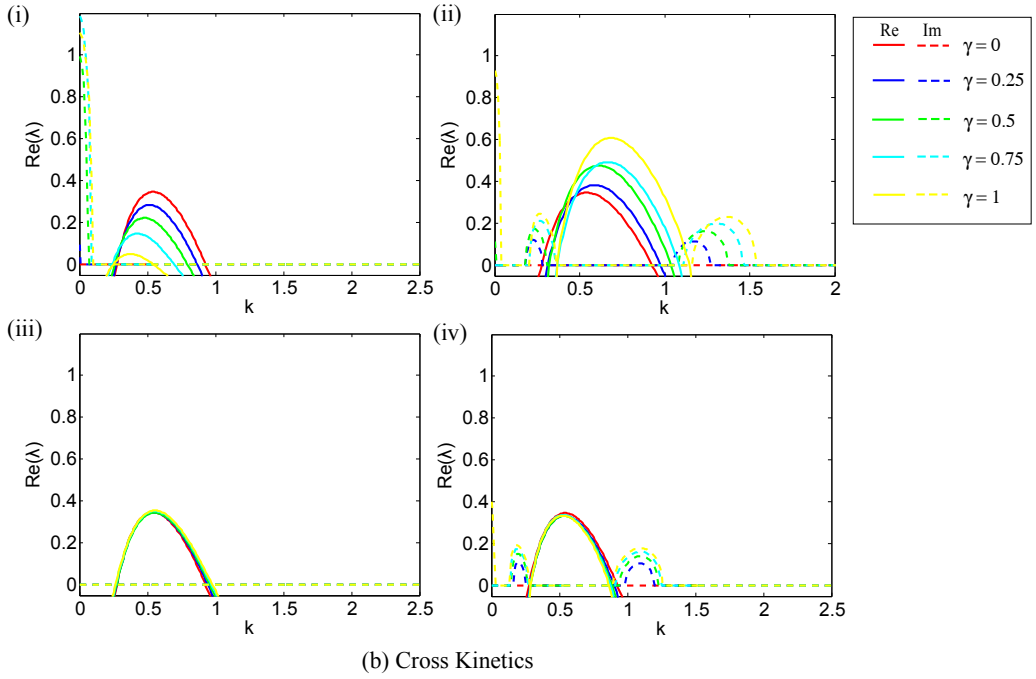

(b) Cross Kinetics

Figure 2.11: Dispersion relations for the PS ($\nu = 1$) model with different feedback mechanisms and increasing γ in (a) pure chemical kinetic model and (b) cross chemical kinetic model. The dispersion relations for different feedback mechanisms are shown as (i) direct positive, (ii) direct negative, (iii) regulatory positive and (iv) regulatory negative. The other parameters were chosen to be $\kappa = 10$, $\beta = 0.1$, $\delta = 0$ and setting α, ρ to be the midvalue of the parameter space at $d = 100$.

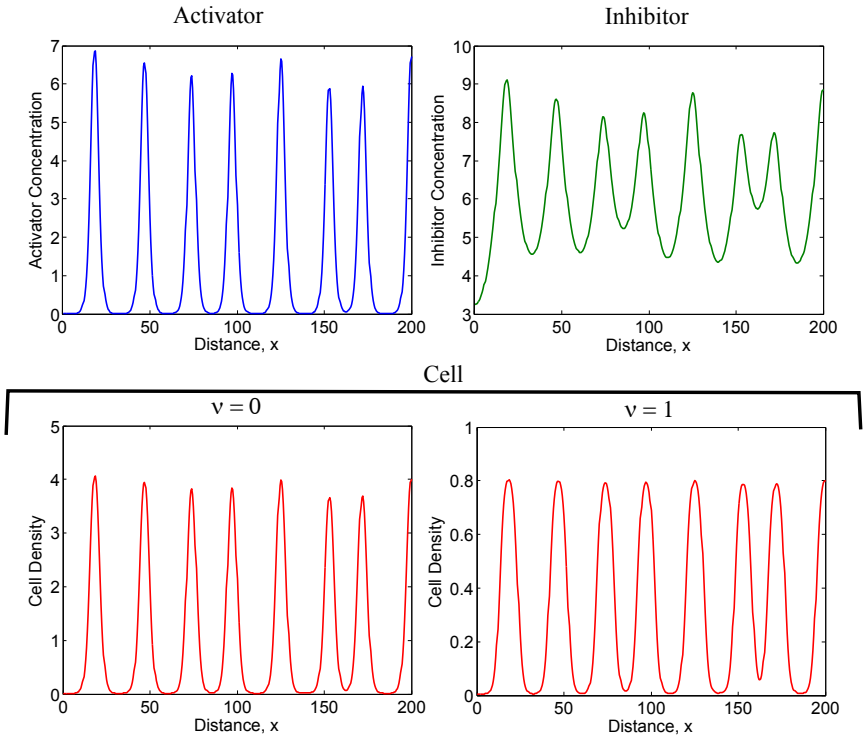

(a) Pure Kinetics

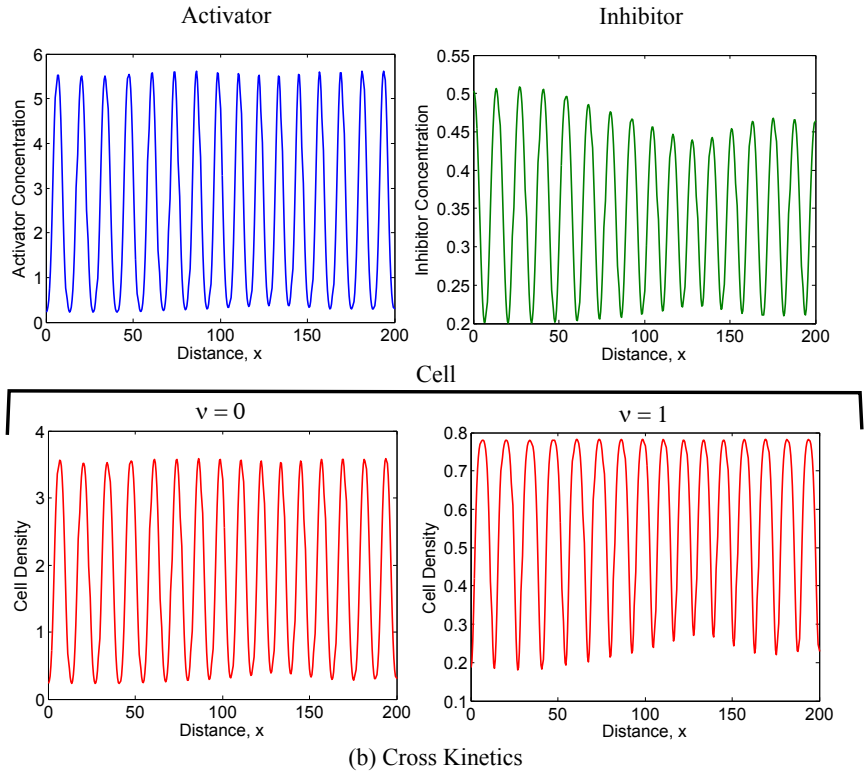

(b) Cross Kinetics

Figure 2.12: One dimensional simulations for no feedback ($\gamma = 0$) in the (a) pure kinetic and (b) cross kinetic models. Here the APD and PS models are shown when $\nu = 0$ and $\nu = 1$ respectively. The other parameters are chosen as $\kappa = 10$, $\beta = 0.1$, $\delta = 0$ and by setting α, ρ to be the midvalue of the parameter space at $d = 100$.

increased feedback function ($\gamma = 1$) in the APD model, Fig. 2.13, and PS model, Fig. 2.14.

The simulations show a difference in the pattern characteristics exhibited for the different feedback mechanisms and the different chemical kinetic schemes. Comparing the pure kinetics with feedback (Fig. 2.13(a)) against the no feedback case (Fig. 2.12(a)), the APD model shows a spiked peak solution and much more rounded peaks when considering direct positive feedback and regulatory positive feedback respectively. The negative feedback simulations are affected by the temporal oscillations predicted in the linear stability analysis. This temporal behaviour results in the solution changing over time and the simulations provide only a snapshot of a changing pattern. As a result, we observe an irregular solution compared to the no feedback case and other feedback mechanisms.

This temporal behaviour does not arise when considering the PS simulations, Fig. 2.14. These simulations show similar peak form characteristics to the APD simulations but the overall solutions result in greater regularity.

Patterning in Two Dimensions

Although the one dimensional results are useful as an indication for model results, it fails to determine the possible types of pattern that are comparable with nature. In this context, by analysing the two dimensional plots we can qualitatively compare the results to biological applications such as the patterning observed in epithelial layers for example. Firstly, as a reference, the results in the absence of any feedback ($\gamma = 0$) are given in Fig. 2.15.

Here, spot patterns arise in both of the models and the observations from the one dimensional simulations are evident. In particular, the rounded peaks result in larger spot sizes and, in the cross kinetic system, this enlargement results in reduced interpeak space. More importantly, however, the different activator, inhibitor and committed cell patterns illustrate the importance of explicitly considering cellular dynamics in pattern formation mechanisms since there is a marked difference between the activator (which is typically assumed to refer to cell commitment in a two species chemical system) and the cell commitment patterns.

The impact of feedback on the patterns can be seen in the two dimensional simulations of the APD model, Fig. 2.16, and PS model, Fig. 2.17. Considering the first of these, which investigates the APD model, the two dimensional simulations show that a variety of wavelength and spot size patterns can be obtained with different feedback mechanisms. For example, by incorporating regulatory feedback the patterns in cell commitment show larger spots appearing compared to much smaller spots with direct positive feedback. This may suggest that the regulatory mechanism may result in committed cells intracellularly retaining activator during cell mediated autocatalysis.

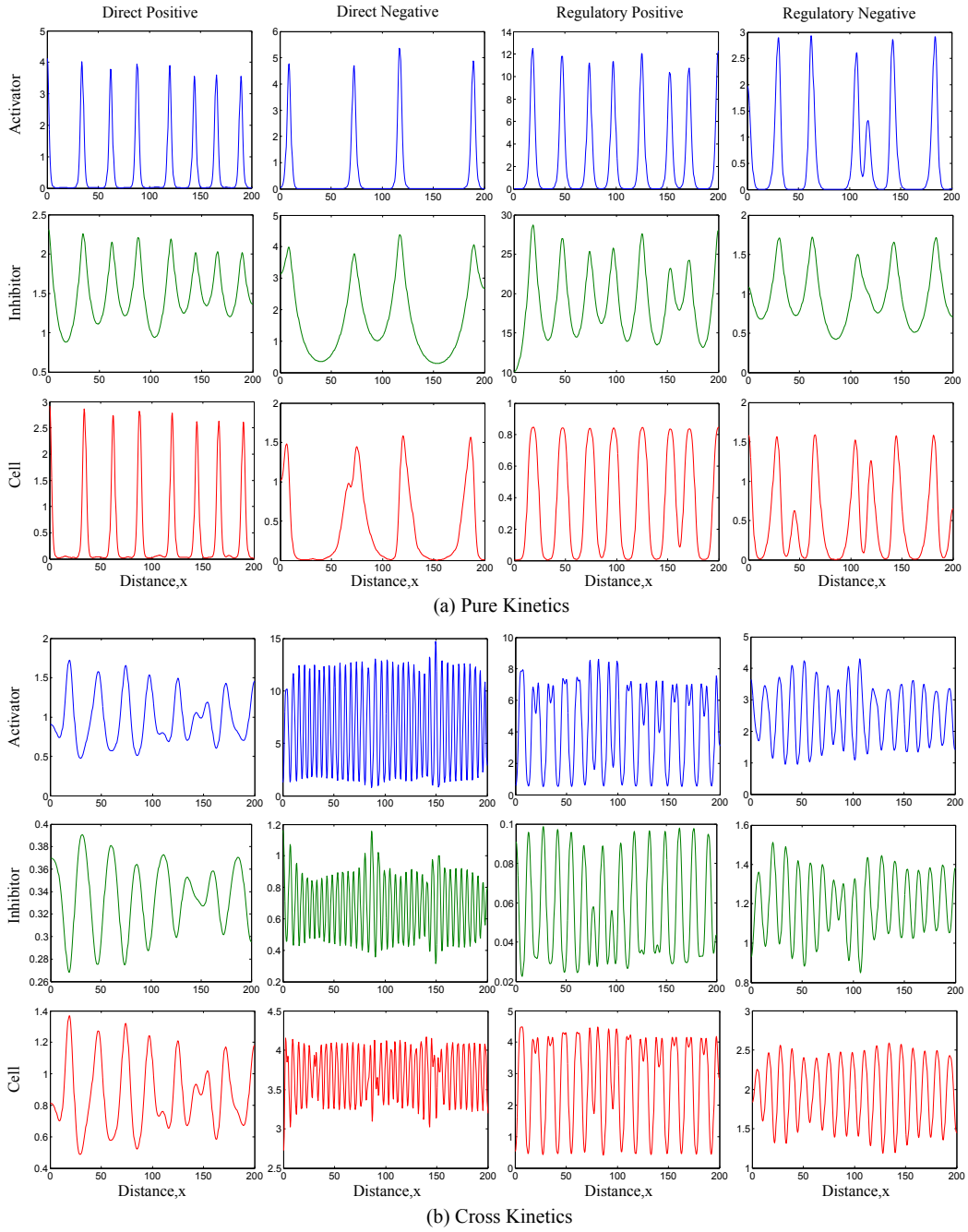

Figure 2.13: One dimensional simulations for the APD model with different feedback mechanisms. Here the two chemical dynamics are shown in (a) pure kinetics and (b) cross kinetics. The parameters are chosen as $\kappa = 10$, $\beta = 0.1$, $\delta = 0$, $\nu = 0$ and by setting α, ρ to be the midvalue of the $\gamma = 1$ ($\gamma = 0.75$ for pure direct negative and cross direct positive) parameter space at $d = 100$.

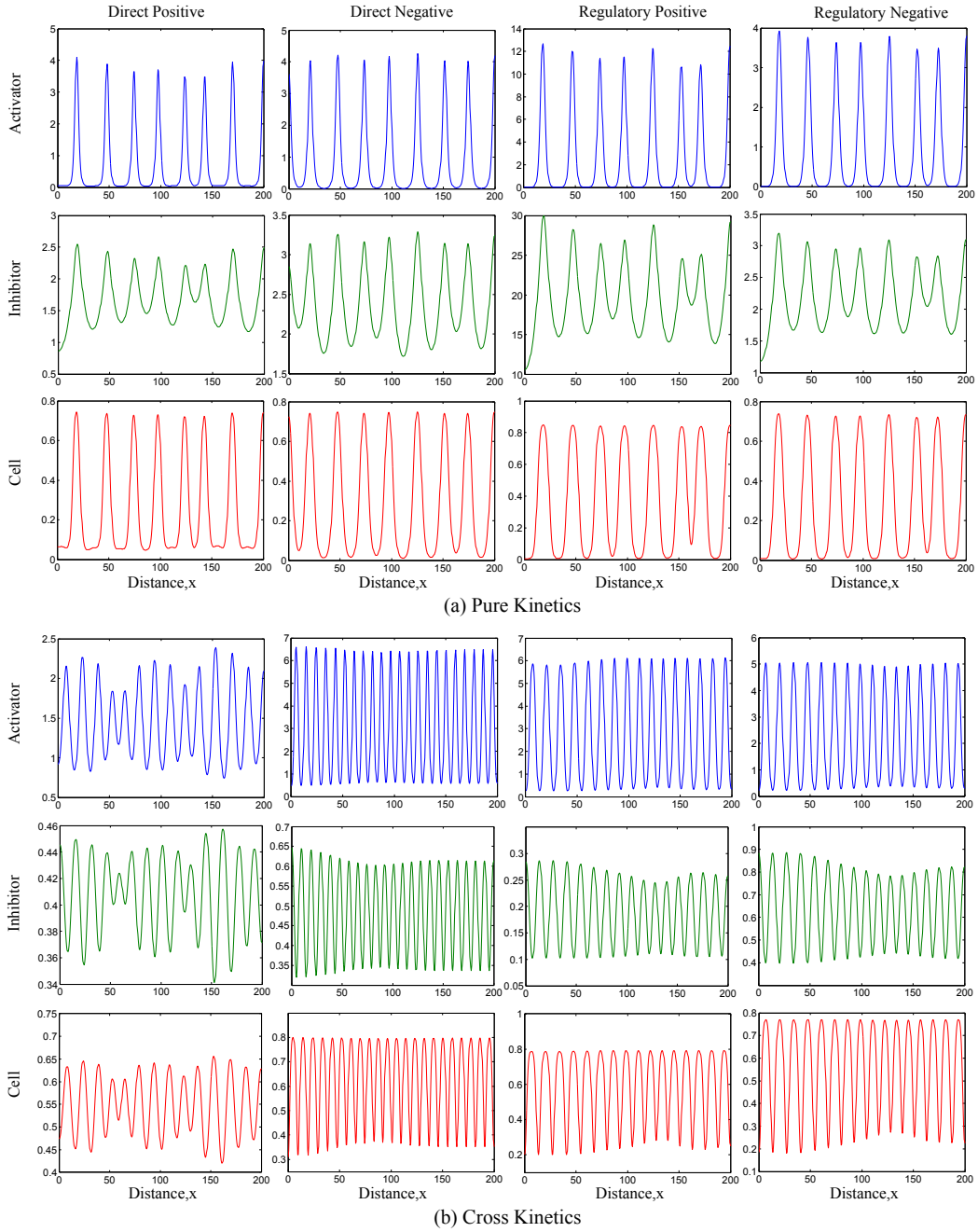

Figure 2.14: One dimensional simulations for the PS model with different feedback mechanisms. Here the two chemical dynamics are shown in (a) pure kinetics and (b) cross kinetics. The parameters are chosen as $\kappa = 10$, $\beta = 0.1$, $\delta = 0$, $\nu = 1$ and by setting α, ρ to be the midvalue of the $\gamma = 1$ parameter space at $d = 100$.

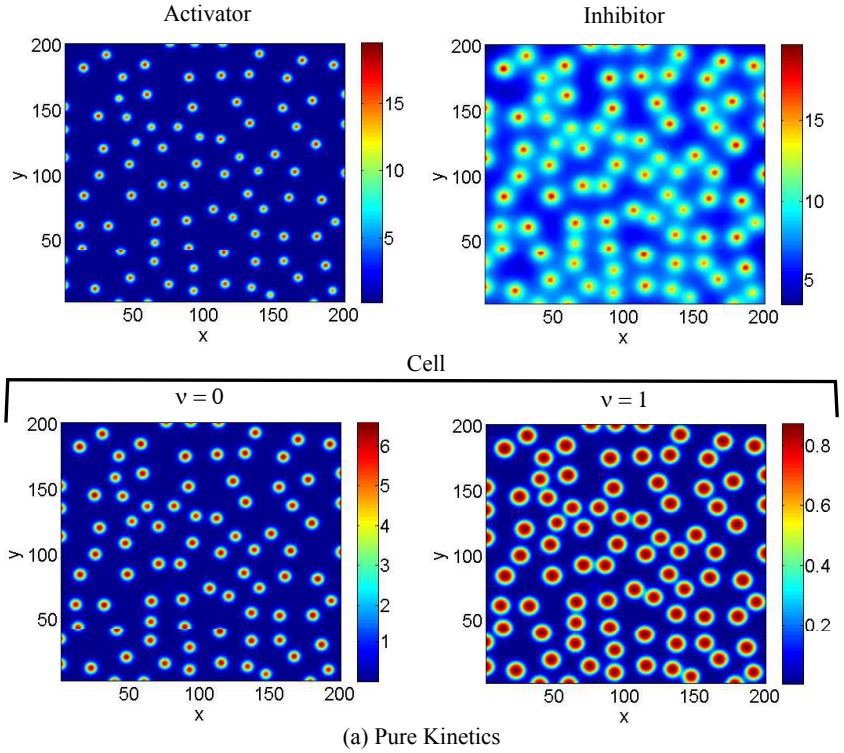

(a) Pure Kinetics

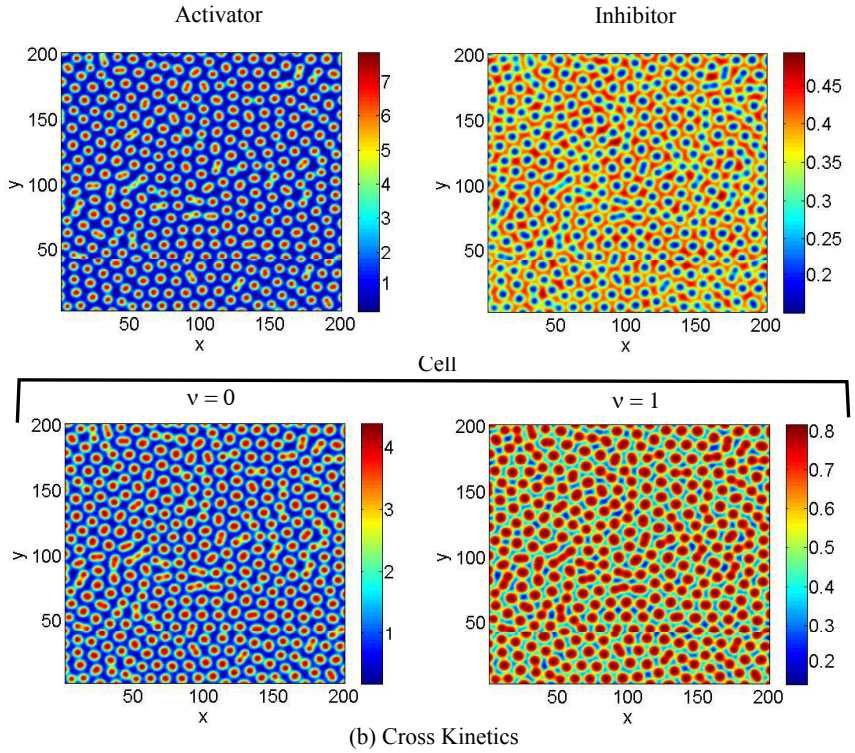

(b) Cross Kinetics

Figure 2.15: Two dimensional simulations for no feedback ($\gamma = 0$) in the (a) pure kinetic and (b) cross kinetic models. Here the APD and PS models are shown when $\nu = 0$ and $\nu = 1$ respectively. The other parameters are chosen as $\kappa = 10$, $\beta = 0.1$, $\delta = 0$ and by setting α, ρ to be the midvalue of the parameter space at $d = 100$.

In the case of regulatory positive feedback into pure kinetics, this could also account for the large differences in activator and inhibitor potency.

The Schnakenberg kinetics with different feedback mechanisms show the different types of patterns that can be obtained, Fig. 2.16(b). Similarly to the Gierer-Meinhardt kinetics, spot patterns arise in simulations but these are closely packed with little interpeak space. Labyrinth patterns are also observed with direct negative feedback, once again, suggesting applicability to a variety of applications such as the patterns observed on some fish, [85].

As we have discussed, spatio-temporal patterns are observed in the APD model with negative feedback. The effect that these have on the two dimensional patterns can be seen in Fig. 2.16. Within this, the pure kinetic patterns exhibit spots with a trailing edge that are continually moving across the domain with time. This moving spot pattern has been observed in mollusc shell patterns and it has also been suggested that this phenomena could explain long branching filamentous structures, [86]. The spatio-temporal patterns of cross kinetics, however, exhibit different characteristics with spot and labyrinth patterns arising when considering direct and regulatory negative feedback mechanisms respectively.

The simulations of the PS model with $\nu = 1$ illustrate spot patterns regardless of feedback mechanisms or chemical kinetics, Fig. 2.17. As we have seen, even without feedback, the cell population in the PS model produces larger spots than that of the APD model. However, similarly to the APD model, smaller/larger spots are observed in cell commitment patterns when regulatory feedback is implemented suggesting a consistent result when considering different positive feedback mechanisms. The negative feedback results differ, however, since the labyrinth patterns do not appear with the implementation of cross kinetics and, instead, the same feedback mechanism (direct negative) shows increased density of spots with each remaining distinct. Moreover, these negative feedback patterns do not exhibit temporal changes when $\nu = 1$. Broadly speaking, the cross kinetic cell patterns in the PS simulations illustrate closely packed spots with little interpeak space.

Numerical Simulations Reinforcing Model Behaviour:

Pattern Formation with Equal Diffusion Coefficients

As we have seen from the parameter space and dispersion relation plots of Fig. 2.9, the model with pure type kinetics is capable of producing pattern formation with equal diffusion coefficients. Here, we investigate the one and two dimensional patterns that can be obtained when $d = \frac{D_B}{D_A} = 1$, Fig. 2.18.

Similarly to the pure kinetics with different feedback mechanisms, these show that spot patterns arise in the two dimensional simulations. In comparison to the no

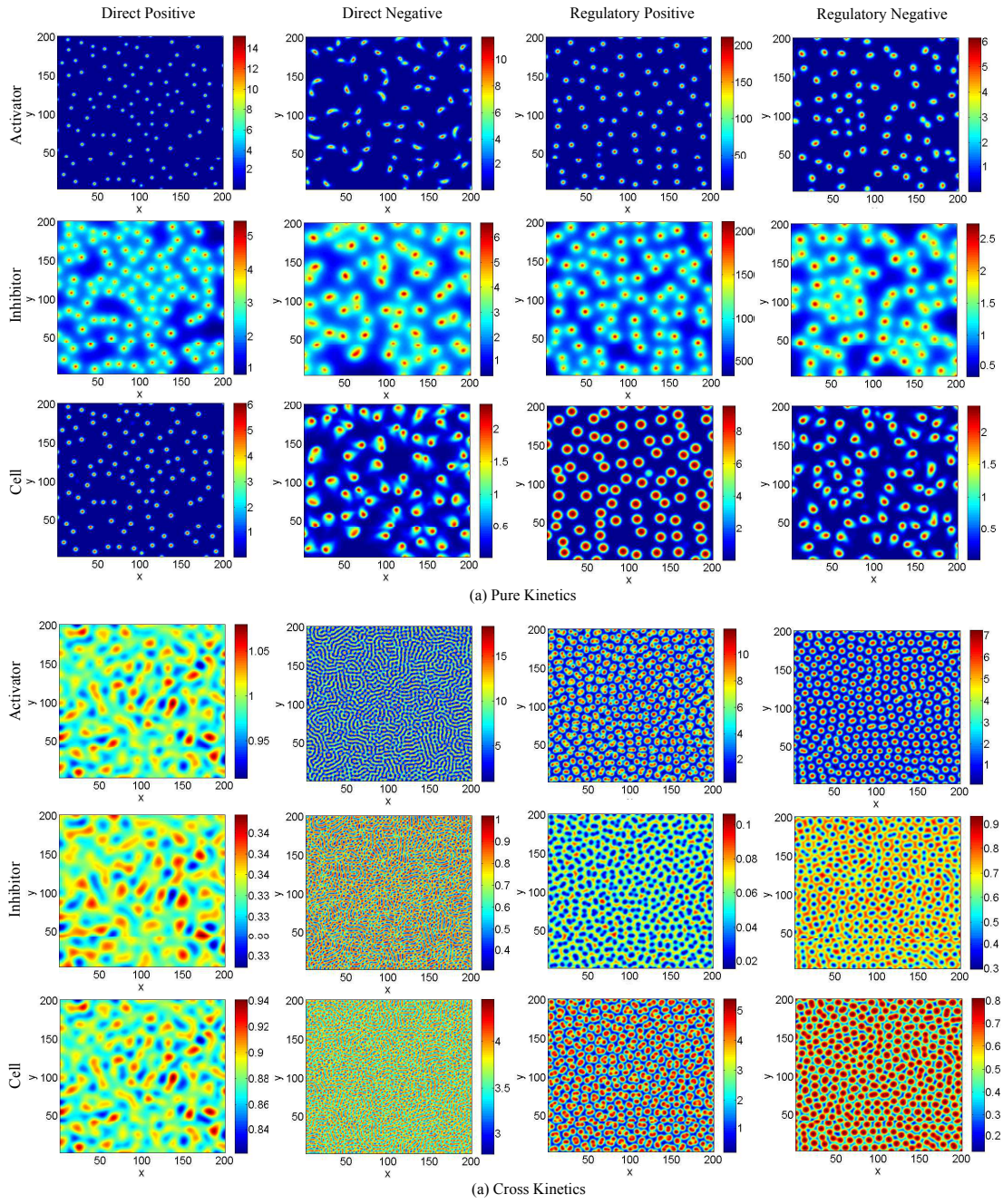

Figure 2.16: Two dimensional simulations for the APD model with different feedback mechanisms. Here the two chemical dynamics are shown in (a) pure kinetics and (b) cross kinetics. The parameters are chosen as $\kappa = 10$, $\beta = 0.1$, $\delta = 0$, $\nu = 0$ and by setting α, ρ to be the midvalue of the $\gamma = 1$ ($\gamma = 0.75$ for pure direct negative and cross direct positive)parameter space at $d = 100$.

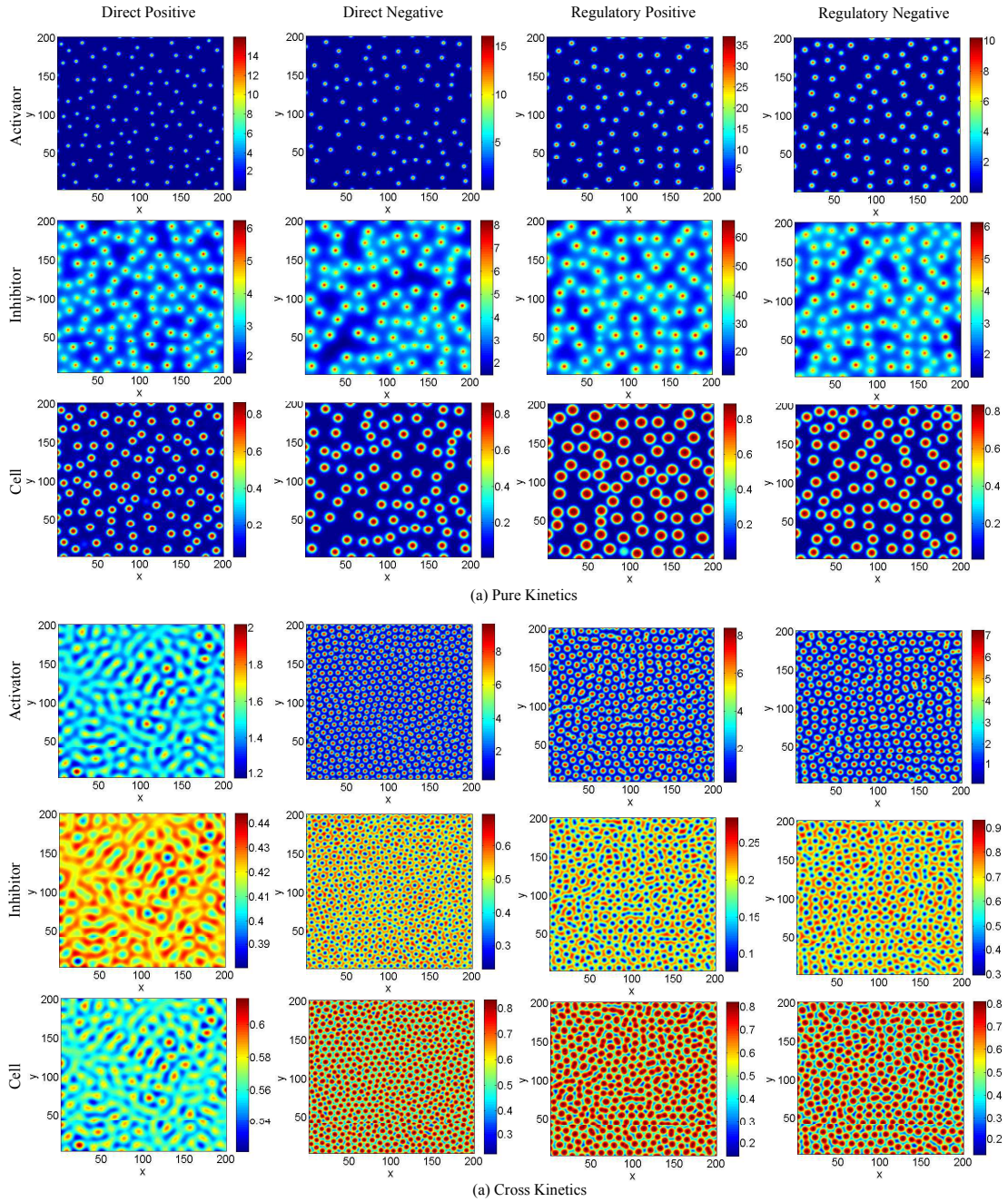

Figure 2.17: Two dimensional simulations for the PS model with different feedback mechanisms. Here the two chemical dynamics are shown in (a) pure kinetics and (b) cross kinetics. The parameters are chosen as $\kappa = 10$, $\beta = 0.1$, $\delta = 0$, $\nu = 1$ and by setting α, ρ to be the midvalue of the $\gamma = 1$ parameter space at $d = 100$.

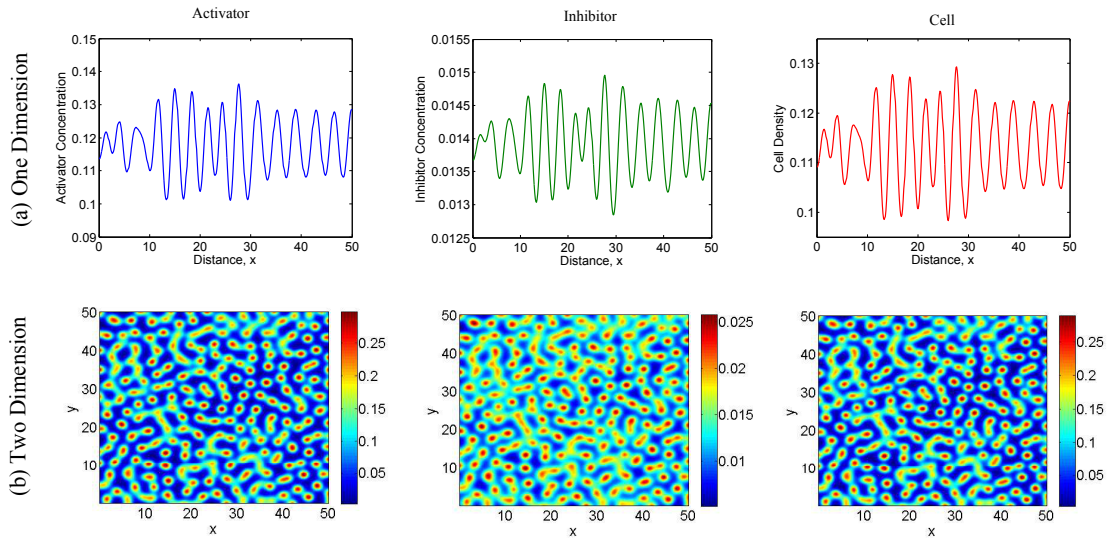

Figure 2.18: Plots of (a) the one dimensional simulations of the activator (blue), inhibitor (green) and committed cell evolution (red) and (b) the two dimensional simulations of the activator, inhibitor and committed cell patterns when $d = 1$. The simulations provide further evidence that pattern formation can occur with equal chemical diffusion coefficients. Similarly to the plots of the parameter space and dispersion relation considering equal diffusion coefficients, the parameter values were chosen as $\alpha = 20$, $\gamma = 12$, $\nu = 0$, $\kappa = 10$, $\beta = 0.1$, $d = 1$. To be consistent with the simulations in the chapter, these simulations are a snapshot in time at 48 hours. However, we consider a 50x50 domain due to increased high foci across the domain.

feedback case (which requires $D_B > D_A$), the pattern results in an increased density of spots. As a result, we consider a 50x50 domain so that the intricate details of the pattern are visible. Drawing on the explanation in the parameter space and dispersion relation analysis, the upregulation of activator from stationary committed cells together with identical diffusion rates will permit this observed increase in high activator spots. We note that the cell commitment pattern is identical to the activator evolution. More importantly, however, we can see that pattern formation is possible in a model with equal diffusion coefficients. In this case, the notion of long range inhibition, short range activation is not required leading to a distinct advantage when applying this model to biological applications.

The Appearance of Spatio-Temporal Patterns

As we have seen from the dispersion relations in Fig. 2.10 and 2.11, the imaginary component of the eigenvalue becomes more apparent as the feedback parameter is increased. The effect this component can have on the numerical solution has already been seen in the two dimensional plots of Fig. 2.16 but here we illustrate this through the space-time plots of Fig. 2.19.

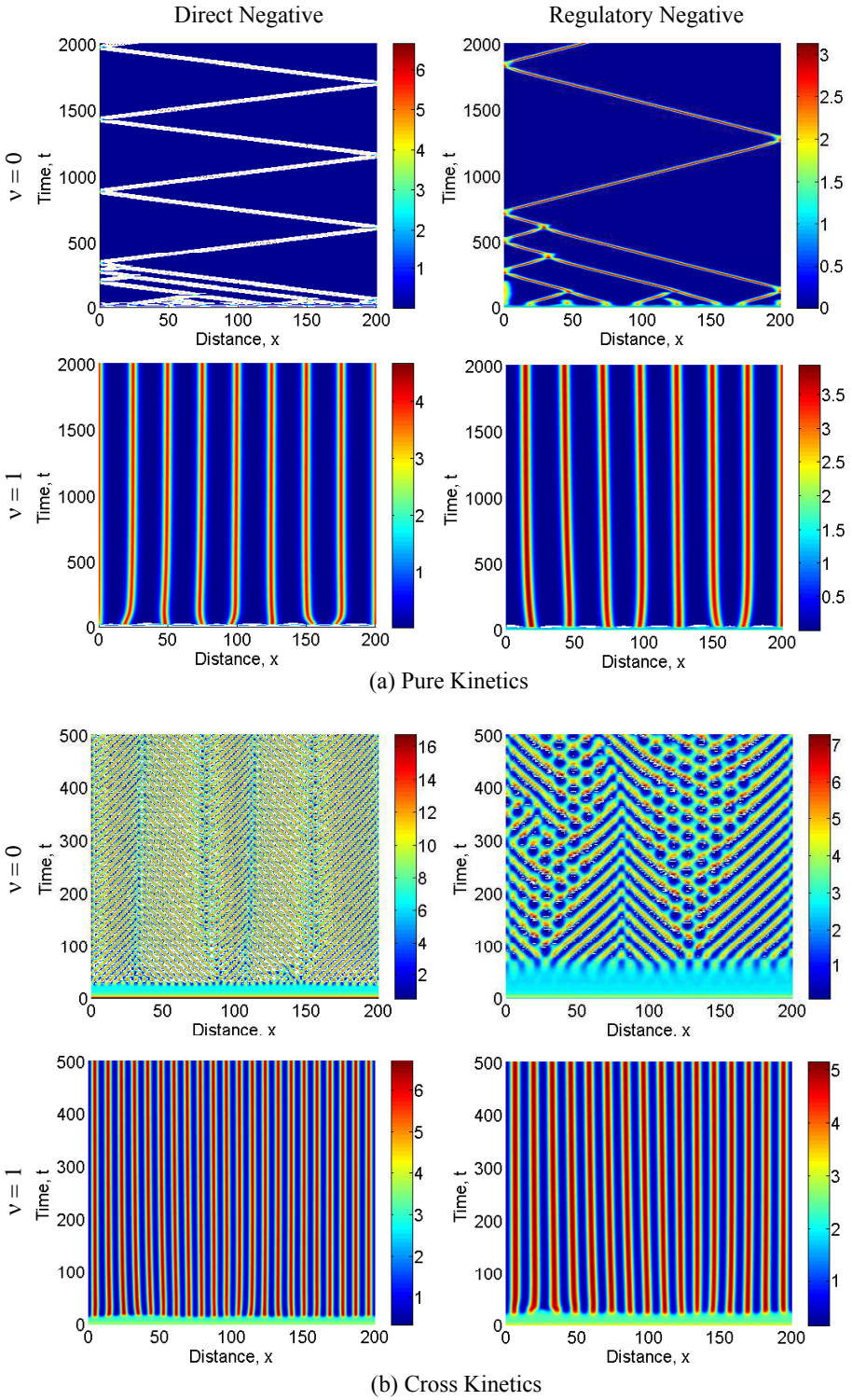

Figure 2.19: Activator Space-Time plots of the negative feedback mechanisms in a model with (a) pure kinetics and (b) cross kinetics. Here, we see the appearance of travelling wave type solutions with the APD model ($\nu = 0$) and an ordered spatial pattern of Turing type for the PS model ($\nu = 0$). The other parameters were chosen as $\kappa = 10$, $\beta = 0.1$, $\delta = 0$, and α, ρ to be the midvalue of the $\gamma = 1$ parameter space at $d = 100$.

From these, we observe changing spatial patterns with time but can see that this only arises when considering the asymmetric precursor differentiation model ($\nu = 0$). In this case, the imaginary part is within the unstable wavenumber range and we can obtain spatio-temporal patterns in simulations. In particular, direct or regulatory negative feedback results in travelling wave type solutions. The pure kinetics exhibit a more ordered temporal evolution where, after a specific time, there exists a single travelling wave in the one dimensional simulations at each time point.

Further interesting temporal changes occur when considering the regulatory positive feedback mechanism with cross kinetics, Fig. 2.20. In this case, the space-time plot indicates that a single phase of peak splitting occurs during the early development stage, Fig. 2.20(a). Furthermore, this is reinforced through the corresponding two dimensional simulations throughout time, Fig. 2.20(b). The two dimensional simulations illustrate the progression of the pattern and splitting from a single peak at $\sim 12 - 18$ hours into two or three peaks from ~ 18 hours onwards.

Feedback Produces Mechanism Dependent Results

In our study, an investigation of increased feedback levels via direct and regulatory mechanisms shows differences in pattern effects. This is illustrated by focussing on the upregulation of activator levels through the direct and regulatory positive feedback mechanisms. The two dimensional simulations for $\gamma = 0, 10, 25$ can be seen in Fig. 2.21.

From these, the different effects can be seen for the two different positive feedback mechanisms. In comparison to the patterns with no feedback, increasing levels of direct positive feedback leads to a decrease in the spot size and density. In contrast, increasing levels of regulatory positive feedback shows an increase in size and density. Furthermore, high levels of regulatory feedback ($\gamma = 25$) result in the loss of a coherant pattern, with spots increasing in size but becoming less defined. This suggests that, rather than generic explanations, intrinsic feedback properties should be used to explain the observations from exogenous activator. Feedback appears to produce mechanism dependent results and these results suggest that the type of mechanism has a significant and specific impact on the patterns.

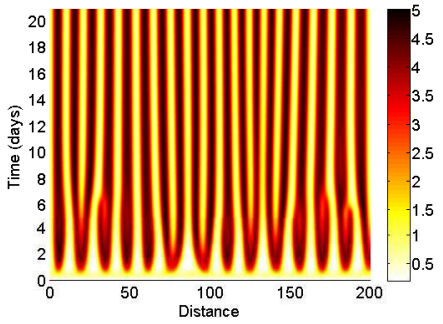

(a) Space-Time (One Dimension)

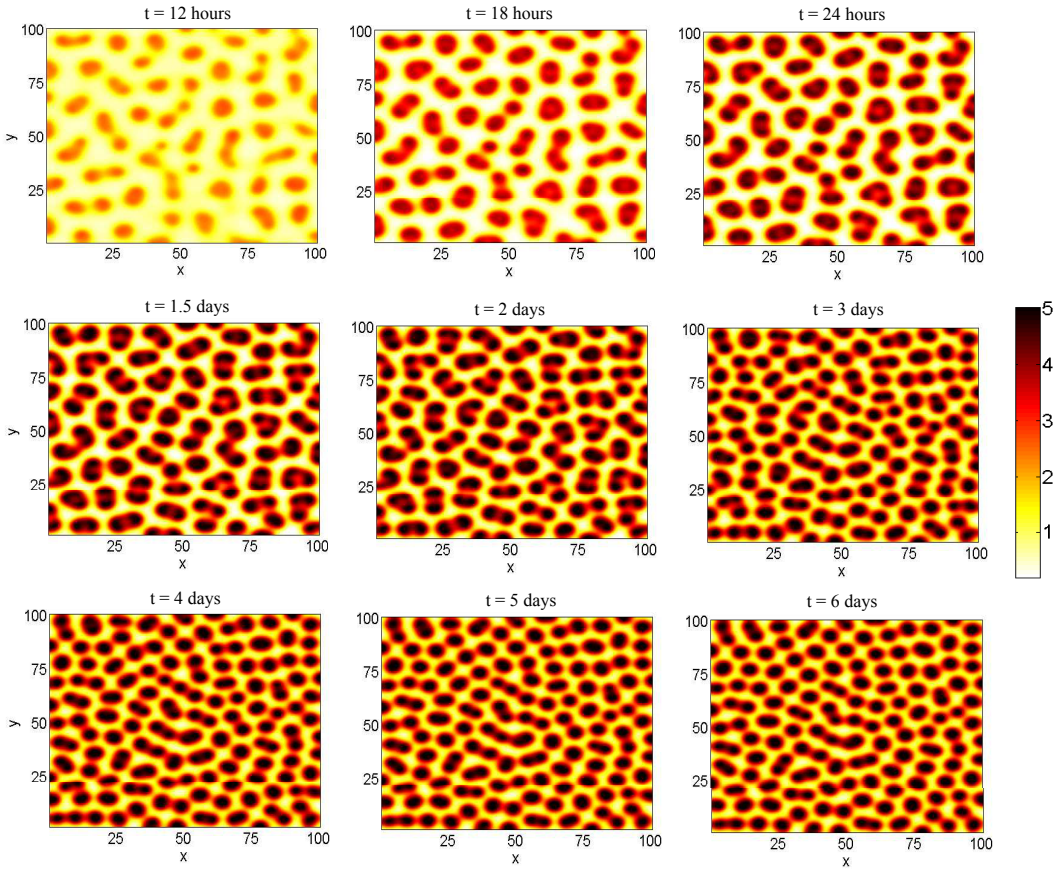

(b) Simulations Over Time (Two Dimensions)

Figure 2.20: Cell Space-Time plots of the regulatory positive feedback mechanisms in a model with cross kinetics. Here, we see the appearance of peak splitting with the APD model ($\nu = 0$). The other parameters were chosen as $\kappa = 10$, $\beta = 0.1$, $\delta = 0$, and $\rho = 0.92$, $\gamma = 1$ and $d = 100$.

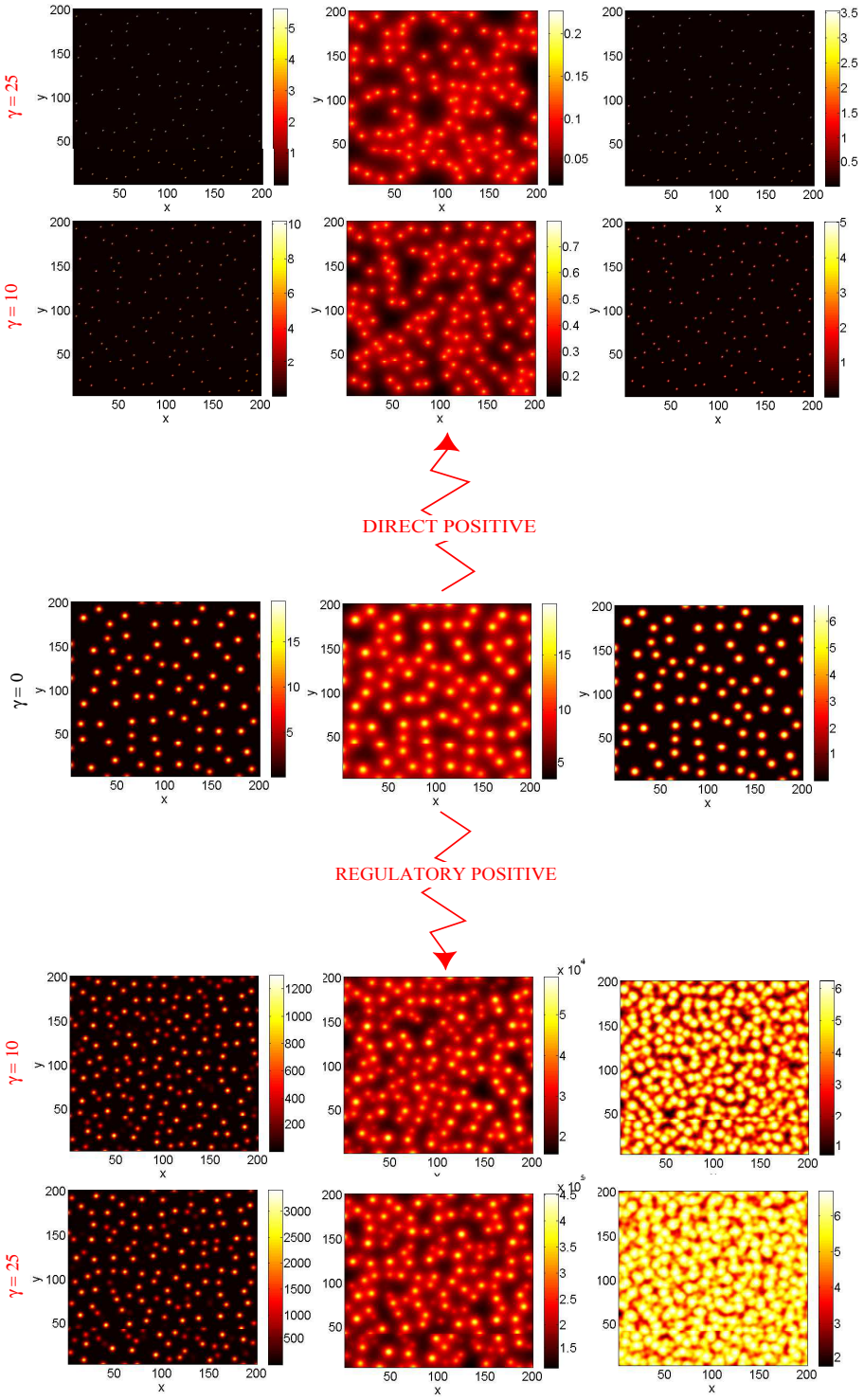

Figure 2.21: Two dimensional simulations for the APD model with pure kinetics and different positive feedback mechanisms for $\gamma = 0, 10, 25$. Here we consider the high feedback effects via direct positive and regulatory positive feedback mechanisms. The parameters are chosen as $\kappa = 10$, $\beta = 0.1$, $\nu = 0$ and α to be the midvalue of the parameter space at $d = 100$.

2.4 Summary and Discussion

Here we have proposed a three species model that considers a Turing type mechanism coupled, through the consideration of feedback, with the explicit modelling of cell differentiation processes. By firstly considering a general model we have shown that a variety of chemical and cell kinetics can be considered. Moreover, a range of feedback mechanisms can also be implemented to upregulate/downregulate activator and/or inhibitor levels. However, in this study we focussed on two conceptually different chemical kinetic schemes, namely the Gierer-Meinhardt and Schnakenberg kinetics, and considered two representations of cell differentiation: Asymmetric Precursor Differentiation (APD) and Precursor Specification (PS). Feedback effects from a committed cell population introduced upregulation/downregulation of activator levels and these were incorporated into the system directly and via regulatory mechanisms that affected different parts of the chemical network.

A numerical investigation into the three species models was undertaken to observe the significance and impact cell differentiation has on biological pattern formation. The main results, with reference to some applications, are summarised below.

- *Parameter Space Increase/Decrease*

  When considering increasing feedback parameter, γ, opposing effects on the parameter space are observed for the two different chemical kinetic schemes. In the pure case, positive feedback results in an increase in the parameter space whereas negative feedback produces a decrease. In contrast, cross kinetics show an increase with negative feedback and decrease with positive feedback. In particular, the largest changes are observed when considering the APD model with direct feedback. The results of the PS model appear to slow this increase/decrease.

- *Equal Chemical Diffusion Coefficients*

  Two species systems of Turing type require the notion of short range activation, long range inhibition and this is incorporated into the system through the choice of D_A and D_B which denote the activator and inhibitor diffusion coefficients respectively. Due to the lack of biological systems exhibiting this concept, this requirement has led to scepticism in the use of the theory to model biological systems. However, here we have shown that a model considering direct positive feedback from a committed cell population is capable of pattern formation when the activator and inhibitor diffuse at the same rate ($d = \frac{D_B}{D_A} = 1$). In fact, it is possible to produce pattern formation when the activator diffuses faster than the inhibitor ($d < 1$).

- *Imaginary Part of Eigenvalue and Spatio-Temporal Patterns*

  The theoretical predictions from the linear stability analysis suggested that oscillatory temporal behaviour may be possible within these models. An investigation of the dispersion relations confirmed this with the appearance of an imaginary component with $Re(\lambda) > 0$ when considering APD negative feedback. Together with this, the numerical simulations showed that spatio-temporal patterns appear which, at a specific timeframe, illustrate spots of high activator with a trailing edge in pure kinetics and labyrinth/spot patterns with cross kinetics. Moreover, the space-time plots illustrate that with direct or regulatory negative feedback travelling wave type solutions are observed. The relevance of the travelling wave phenomena seen in this model may suggest the applicability of the system to embryogenesis. In fact, one such example is the developing pigmentation pattern exhibited on the skin of a mutant mouse, [87]. Within this, travelling waves of stripes form across the body and models exhibiting travelling wave behaviour may be able to explain these results.

  Further to this, observations of the pattern progressions show that a peak splitting phenomena occurs when considering regulatory positive feedback into cross kinetics. This phenomena has been extensively studied in Turing systems on growing domains, [88], [89], and can continually occur with growth. However, these studies have consisted of continuous peak splitting throughout time. In contrast, our model exhibits a single phase of peak splitting which occurs early in pattern formation.

  As an example, this pattern progression may explain the early patterning observed in the developing coat of the jaguar or the animal coat pattern of the leopard. Within these biological systems, there is a transformation from spots that split to produce rosette type patterns once maturity is reached. A Turing model to account for the development of these patterns has already been considered by Liu *et al*, [90] and simulations have successfully replicated the desired patterns by implementing the model over two stages. The first of these produced spot patterns, corresponding to early development, which subsequently became broken rings as parameters were changed in the second stage.

  Our results illustrate that throughout time there is a transition from spots which split to produce a greater density of spots across the domain. However, intermediate stages appear to exhibit rosette type patterns together with spots and, in this way, may suggest that it can replicate the specified patterns in na-

ture, Fig. 2.22.

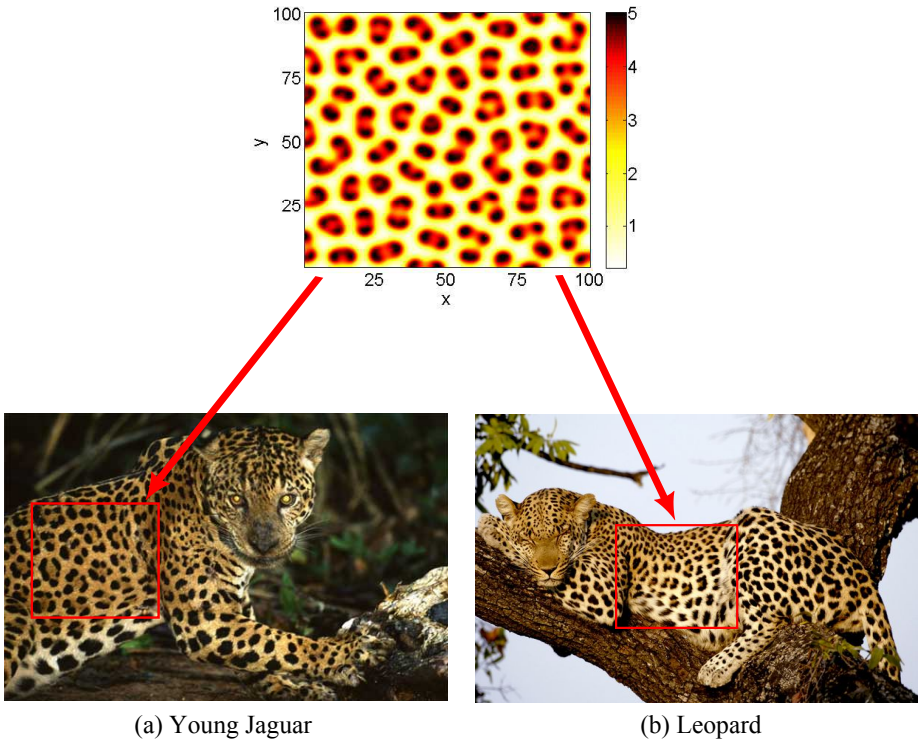

(a) Young Jaguar (b) Leopard

Figure 2.22: Comparison of the animal coat patterns in nature with a two dimensional simulation of the cross APD model with regulatory positive feedback. The results suggest that the single phase of peak splitting observed during early pattern formation shows similarities to (a) young jaguar pigmentation and (b) leopard pigmentation patterns in nature. The simulation is a snapshot at 36 hours and the parameters are chosen as $\kappa = 10$, $\beta = 0.1$, $\delta = 0$, and $\rho = 0.92$, $\gamma = 1$ and $d = 100$. Pictures taken from (a) `http://animals.nationalgeographic.com/animals/mammals/jaguar/`, (b) `http://animals.nationalgeographic.com/animals/mammals/leopard/`

- *Feedback Mechanism Dependent Patterns*

  By considering the upregulation of activator levels with two different feedback mechanisms the simulations illustrated opposing effects. In particular, the results showed that with the promotion of activator directly from a committed cell population spot size and density decreased. In contrast, positive feedback via a regulatory mechanism produced increased spot density with high levels of

feedback resulting in a loss of a coherent cell commitment pattern. However, the activator pattern remained largely unchanged. As a result, this suggests that results observed from experimental perturbation analysis may need to be explained in a more concise and mechanism dependent manner.

For example, one of the first attempts to link the mathematical results with molecular research was undertaken by Sick *et al*, [18]. Within this, an activator-inhibitor model with pure kinetics was proposed to account for the patterning observed in mouse hair follicle development. Perturbation analysis is undertaken with results suggesting that a moderate overexpression of activator resulted in increased follicle density. Further to this, strong overexpression resulted in a disruption to patterning.

The simulations match experimentally predicted results but our simulations would suggest the generic explanation given, that exogenous activator produces the phenomena, may not capture the underlying interactions and complexity of the system. More appropriately, these could be explained through a more concise approach and by considering specific feedback mechanisms that are fundamentally regulating the system. In particular, the results of our model suggests that the regulatory positive feedback mechanism is more applicable to the results observed in Sick *et al* and would give greater insight into the underlying mechanisms involved in pattern formation. Together with this, our model gives an explicit representation for cell commitment that may actually be the preferred mechanism within the system.

These results illustrate the effects that feedback from a cell population may have on patterning. Compared to a two species system, that implicitly assumes cell differentiation via arbitrary activator levels, the results from this model indicate the importance of explicitly including cell dynamics in models. In particular, the consideration of feedback from the differentiating cell population has a significant impact on model results and behaviour. The simplest two species system may provide a framework but its limitations and naivity may prevent important and intrinsic behaviour from being captured.

Chapter 3

Modelling Discrete Cell Signalling via Turing Systems

Cell communication is one of the fundamental mechanisms involved in the development of biological phenomena and can occur in a variety of contexts. Studies considering continuous mathematical models of Turing type can often ignore these precise cellular level details that are essential in many biological processes. Turing's theory has given us some concept of understanding and a fundamental mechanism for patterning to occur but it has been suggested that it lacks the detailed description of the complicated processes and specific cellular/environmental mechanisms involved in biology. In this chapter we propose a discrete mathematical model, based on Turing's classical continuous framework, that considers the activity of receptor, ligand and inhibitor. In doing so, we replace the autocatalytic process of the activator with a receptor-ligand binding process in the presence of an inhibitor and consider the significance of fundamental cell signalling mechanisms in pattern formation systems. Under certain assumptions we can reduce the model to a form similar to the simplest two species activator-inhibitor system and the results suggest patterning can arise in a system considering one diffusible species together with localised signalling. Further to this, both the two and full three species systems are capable of pattern formation for a variety of wavelengths from fine grained to longer wavelength patterns.

3.1 Introduction

The understanding of cell dynamics is of particular importance in the study of all biological processes. Throughout nature, the varied and spectacular patterning is a consequence of intricate interactions between the cells and their environment. In particular, one of the key processes involved is cell communication where cells undergo signalling to transfer information that develops and regulates the system. A number of studies have suggested that this process is key in pattern formation systems such as

sensory bristle formation, [66], feather and hair arrangement in birds and mammals, [76], [17], and zebrafish stripe formation, [91], among others. These types of patterns (see Fig. 3.1) illustrate the diversity of nature but also suggest that detail at the level of cells is fundamentally important to describe the intrinsic processes that exist in development. Research attempts to explain biological phenomena and unearth the elusive drivers of morphogenesis.

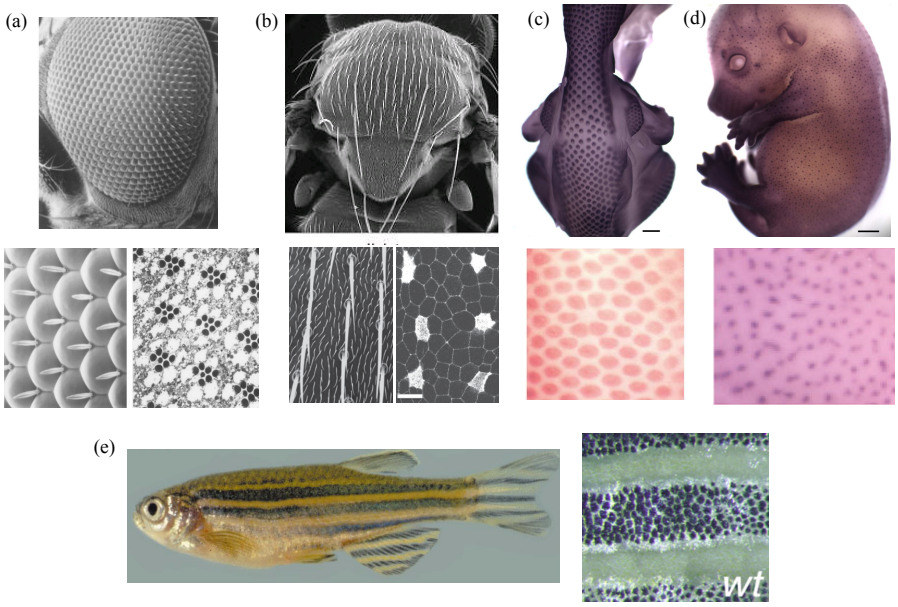

Figure 3.1: Pattern formation of (a) drosophila photoreceptors, [92], (b) drosophila sensory bristle formation, [93], (c) chick feather placode formation, [32], (d) mouse hair follicle development, [32], and (e) zebrafish stripe formation, [94]. Each of the systems show an overview and more detailed snapshot of the pattern, indicating the intricate details. Furthermore, they show the diversity of patterning and the capability of fine grained to longer range wavelength patterns in biology.

This study focusses on fundamental cell signalling and analyses its significance in mathematical models and developmental biology. In particular we suggest that a classical activator-inhibitor approach may fail to capture the important details and processes involved in complex biological phenomena and propose a more detailed discrete approach that is based on the underlying framework of this well studied classical system. Moreover, we attempt to propose a system that will determine the fine grained and longer range wavelength patterns that can be seen in Fig. 3.1, focussing on the detailed cellular level to describe systems such as these.

3.1.1 Signalling Mechanisms

A variety of signalling processes have been proposed as mechanisms for cell communication and these are often categorised into three distinct types: autocrine, paracrine and endocrine, [62]. Paracrine signalling describes communication often between nearby cells due to an extracellular diffusible ligand and endocrine signalling assumes possible interaction with all cells within a tissue via the transfer of molecules in the bloodstream. Autocrine signalling is the process by which an individual cell regulates its own activity. For example, a cell produces a molecule that subsequently binds to and activates receptors on its own surface, Fig. 3.2(a). In this way cells can self regulate themselves. Signalling between adjacent cells does not occur and individual cells are responsible for their own activity.

A more recent cell communication mechanism, termed juxtacrine signalling, has been suggested as a possible mechanism for cell communication. This type of signalling allows adjacent cells to transfer information via receptor-ligand binding. Figure 3.2(b) below illustrates the receptor-ligand binding occuring between cells j and $j+1$. Membrane receptors bind to the ligand on adjacent cells resulting in signal transduction within the receiving cell. The downstream effect being changes in the activity of the receiving cell.

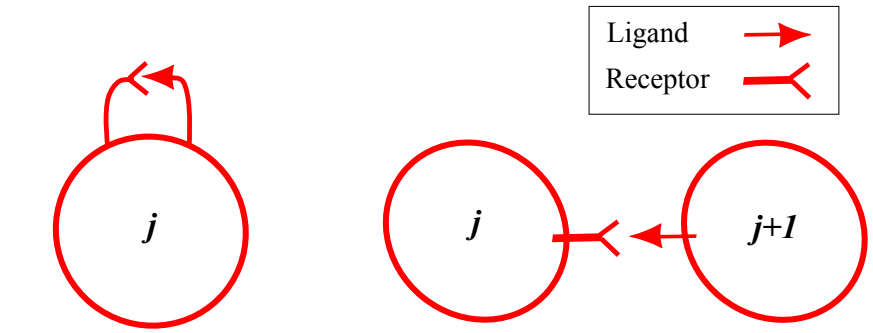

Figure 3.2: Diagram illustrating receptor-ligand binding in (a) autocrine signalling and (b) juxtacrine signalling. The receiving cell j has a membrane receptor which becomes bound to the ligand on the surface of the same cell and neighbouring cell $(j + 1)$ for autocrine and juxtacrine signalling respectively. This process results in signal transduction changing the morphology of the receiving cell, j.

The term juxtacrine was coined in 1990, [63], and has been found to be present within a number of biological processes, an example being the activity of Delta and Notch. The Notch gene was first discovered in 1917 by Thomas Hunt Morgan whilst

studying the fruit fly Drosophila Melanogaster, [95], but it was not until the 1980s that more detailed molecular analysis was undertaken, [96], [97]. This Notch-Delta receptor-ligand complex has been widely studied, most commonly in the study of drosophila development, [98]. Within this, it has been suggested that a lateral inhibition mechanism is regulating, for example, patterning phenomena such as sensory bristle formation, Fig. 3.1(b).

However, the precise interactions still remain unclear and therefore the determination of specific signalling mechanisms as stand alone regulators and mediators of biological phenomena may not occur in some cases. Together with the distinct activity of autocrine and juxtacrine signalling, studies have also suggested that a number of signalling mechanisms may be simultaneously at work. For example, the healing of the intestinal muscosa after inflammation is thought to consist of both autocrine and juxtacrine signalling mechanisms, [99].

Moreover, other factors are believed to affect the signalling process, with various researchers suggesting the presence of inhibitors in these cell based systems that suppress the activity of receptor/ligand. Such inhibitors have been observed in a variety of biological systems. For example, in cancer, it has been suggested that agents inhibiting the production of VEGF via autocrine signalling may reduce angiogenic factors in mesothelioma cancer, [100], allowing research to focus on possible anti-angiogenic factors that may be used to target the receptor-ligand binding process of VEGF [101]. Precisely how these are implemented remains an open question since a number of theories have been suggested. For example, the Wnt family have a number of inhibitors and antagonistic agents which supress the production of growth factors in different ways. It has been suggested that the sFRP (secreted Frizzled-related protein) family, WIF (Wnt inhibitory factor)-1 and Cerberus bind to WNT proteins whereas specific members of the Dickkopf (Dkk) family bind to the receptor of Wnt, [102]. Furthermore, in a study considering the antagonistic effect of EGF-R on Notch activity in the development of sensory organ precursors in Drosophila sensory bristle formation, [103], the authors suggest that after the activation of EGF-R there is an intracellular inhibitory mechanism supressing the activity of Notch production.

As a result, it is clear that many factors may affect the biological system and, therefore, it may become difficult to determine these experimentally. However, mathematics can be used in these situations to hypothesise and test theories that may be currently beyond the constraints of experimentation. In particular, it can be used to elucidate the signalling mechanisms that may arise within particular systems. In fact, previous research into pattern formation and cell signalling mechanisms in biological processes have already been undertaken and these are discussed below.

3.1.2 Modelling Background

Discrete Models of Signalling

Discrete mathememattical models have been used to describe the cellular level details and processes that are fundamental within biological phenomena, [9], [61]. Although most commomly used as a continuous model, A.M. Turing's seminal paper included a discretised version of the reaction-diffusion system where individual cells exhibited chemical concentration levels, [9]. A similar approach was considered by Othmer & Scriven, [61].

However, discrete models have been utilised to describe the cell signalling interactions that are regulating biological processes and one of the most well studied signalling mechanisms is juxtacrine where information is transferred between neighbouring cells. A mathematical model of juxtacrine signalling in pattern formation was proposed by Collier *et al* in 1996, [65]. Within this, a model is used to account for juxtacrine signalling via a receptor Notch binding to its ligand Delta, situated on the surface of adjacent cells, which after mutually inhibiting one another, amplify small differences in activity levels, [62]. This process, known as lateral inhibition, produces a pattern of small isolated clusters of cells with high receptor activity surrounded by cells with low ligand activity. In modelling this concept, they showed that a lateral inhibition model was capable of simulating patterns with a variety of wavelengths, but most notably of just two cells, capturing fine grained patterns observed in vertebrates and worms.

This work resulted in further mathematical studies of juxtacrine signalling within the development of epithelial patterning, [69], [70], wound healing, [67], [68], among others. However, these models are based on a lateral induction mechanism which considers different behaviour to the previous lateral inhibition mechanism. Lateral induction considers a positive feedback loop in activity arising from the interactions via cell communication. The results of the mathematical modelling of this type of mechanism suggests the possibility of longer wavelength patterns.

Continuous Models

Together with these fairly recent discrete mathematical models describing lateral inhibition/induction mechanisms, a number of continuous mathematical models and theories already exist to study pattern formation in biological systems. As discussed in Chapter 1, one of the most notable models is the work of A.M. Turing which considers a symmetry-breaking phenomena where the chemical interactions and destabilising effect of diffusion gives rise to pattern formation from near homogeneity, [9]. In the simplest case, this focusses on the interplay of two chemicals, termed the activator and inhibitor, that react and diffuse to produce spatially heterogeneous patterns. The

underlying interactions follow two concepts which are evident through the form of the kinetics and these are categorised as pure and cross, [21]. A detailed description of these can be seen in Chapter 1. However, a schematic of the interactions can be seen in Fig. 3.4. Within these simple systems, the significance and explicit representation of the cellular dynamics are often ignored and, as a result, the purely chemical system may fail to capture the precise cellular influences and molecular interactions between both the cells and their environment that are fundamentally important in initiating and maintaining biological phenomena.

The complex signalling pathways that arise in biological processes involve a multitude of interactions between various signalling factors. As an example, consider the molecular interactions that are thought to be present in the initiation of mouse hair follicles (see Fig. 3.3). Specifically, the Eda ligand binds to its receptor Edar, resulting in self-activation, whilst also promoting the production of an inhibitor (BMP). This inhibitor acts at a distance from its site of synthesis to suppress the activity of Edar. Within these main interactions, CTGF is upregulated by Edar and suppresses the inhibitory action of BMP. Moreover, BMP also suppresses the activity of β-catenin. The interplay between the receptors, ligands and inhibitors illustrates the complexity and intricate nature of the process and the corresponding pattern showing the positions of hair follicle initiation can be seen in Fig. 3.1(d).

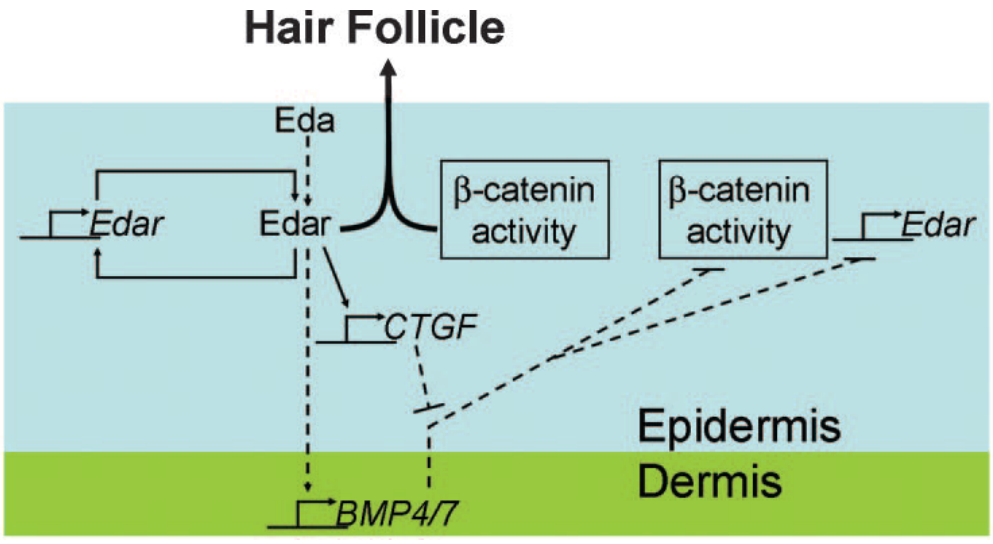

Figure 3.3: Schematic of the signalling pathway and molecular interactions involved in the inititiation of mouse hair follicles (pattern can be seen in Fig. 3.1(d)). Here, the interactions between a variety of signalling factors leads to the formation of the hair follicles where the solid lines indicate local signalling and dashed lines signifying action at a distance. Picture taken from [17].

Therefore, while Turing's theory has remained amongst the leading models of biological pattern formation, its most often studied form, consisting of a system of continuous reacting and diffusing chemical species, suggests a naive view of the intricacies of cell signalling. In this study we propose a discrete model incorporating a more detailed description at a cellular level, that is based on the simplest classical activator-inhibitor system. Specifically, we replace the activator autocatalysis, which acts to promote its own synthesis, with a receptor-ligand binding process in the presence of an inhibitor, Fig. 3.4. In this way, we hope to capture at least a subset of the

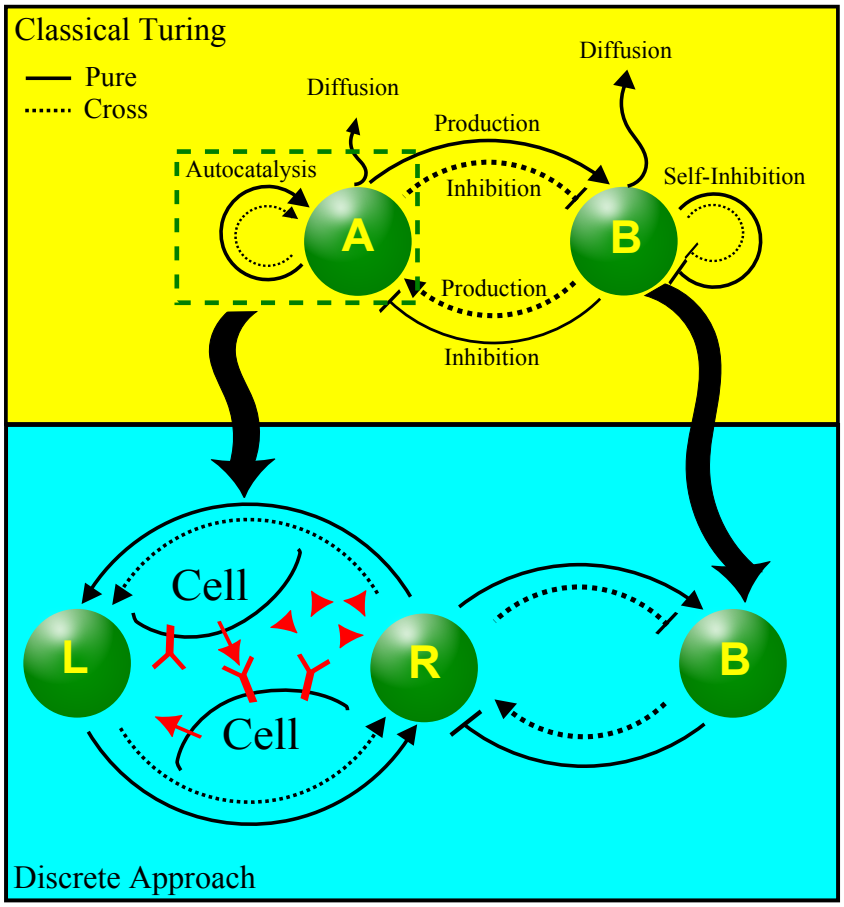

Figure 3.4: Schematic illustrating the underlying framework of a classical two species activator-inhibitor system and its comparison with a more detailed discrete approach. The discrete approach incorporates greater detail by expanding the autocatalytic process of an activator-inhibitor system into a process of receptor-ligand binding. The classical approach considers A and B representing the activator and inhibitor respectively with R, L and B respectively representing the receptor, ligand and inhibitor of the discrete approach.

intrinsic processes the activator incorporates and produce a more detailed framework, originating from a well studied pattern formation mechanism, which now considers cellular dynamics. In particular, using the receptor-ligand binding process we investigate cell signalling mechanisms and determine the impact and significance of cell signalling in both the modelling approach and biological phenomena.

3.1.3 Outline

In §3.2 we propose a general discrete model that extends the classical two species activator-inhibitor system of Turing type. We propose a general three species model consisting of receptor, ligand and inhibitor activity and discuss possible reaction kinetics in §3.3 that incorporate distinct modes of cellular communication as discussed above. For tractability, the model is reduced to a two species system in §3.4 using a Quasi Steady State Assumption (QSSA), aiding comparison with the continuous activator-inhibitor models of Turing type.

Analysing this discrete two species model in Chapter 4, through a linear stability analysis similar to Turing's approach, leads to a picture of how patterns vary according to different signalling mechanisms. In particular, we observe pattern formation in a two species model considering only one diffusible species and a form of autocatalysis via autocrine or juxtacrine cell signalling mechanism. In Chapter 5 we undergo a numerical investigation into the case studies and reinforce the results of the previous chapter through one and two dimensional simulations, illustrating the typical patterns that can be produced. In studying the chosen reaction kinetics we hope to capture a variety of patterns with different wavelengths suggesting the applicability of the model to a variety of systems that involve longer wavelength and fine grained patterns. Further to this, by modelling a more detailed version of the continuous system we are keen to see if this offers greater robustness with regards to the various drawbacks of Turing's theory previously discussed.

3.2 Mathematical Model: General Framework

The processes involved in development involve understanding on different scales from micro, at the level of cells, to macro, involving the whole organism. However, at any level of description the fundamental cellular dynamics are vitally important since the cells become the mediators for complex biological processes. Therefore, to gain greater insight into the signalling mechanisms occurring within biological phenomena we split the activator process in a classical activator-inhibitor system into a receptor-ligand binding process, Fig. 3.4. In this way, we consider the interactions of receptors (R) and ligands (L), replacing the autocatalytic process that occurs in a continuous activator-

inhibitor system with a receptor-ligand binding process that considers details on the level of cells. The ligand binds to membrane receptors situated on the cell surface and, once bound, triggers signal transduction within the receiving cell. This process results in a cascade of intracellular interactions leading to morphological changes within receiving cells. In doing so, these cells may now exhibit certain characteristics and perform particular functions. However, similarly to the supression of an activator, the activity of receptors/ligands can be supressed by the presence of an inhibitor.

We consider a discrete model that describes the evolution of signalling molecules at cell position p:

$$\frac{d\mathbf{W}_p}{dt} = \mathbf{F}(\cdot) + D_W \Delta \mathbf{W}_p \tag{3.1}$$

where $\mathbf{W}_p$ represents a vector of variables at cell p, $\mathbf{F}$ incorporates their interactions and D_W is a matrix of diffusion rates. The notation for diffusion is given by $\Delta \mathbf{W}_p$ and this may take different forms according to the lattice that describes the arrangement of cells, Fig. 3.5. For example, for a one dimensional line or two dimensional square

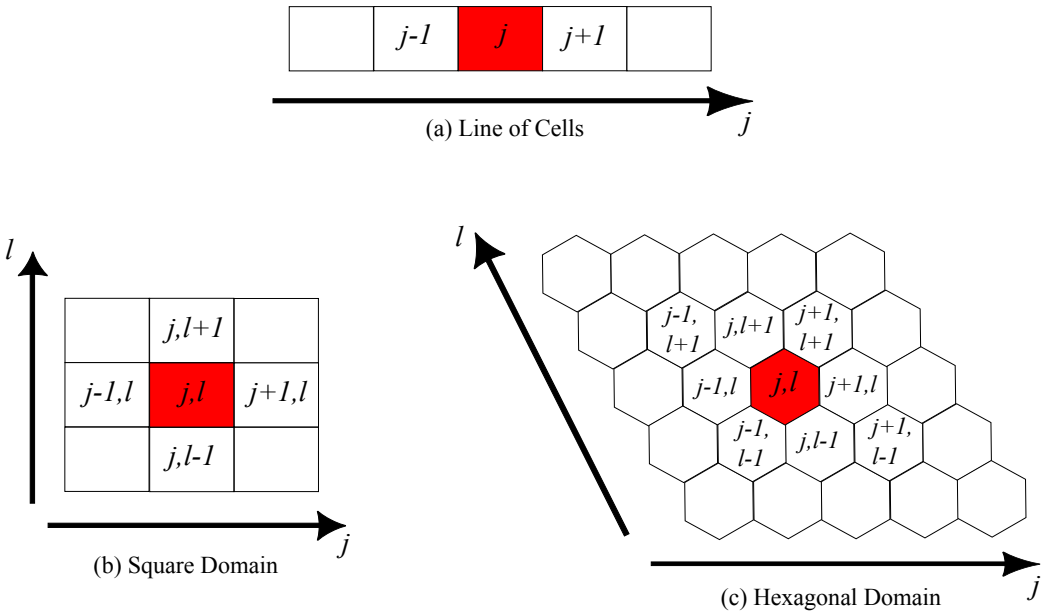

Figure 3.5: Schematic illustrating the types of domains considered in one and two dimensions. Here, we consider (a) a line of cells in one dimension and (b) square cell array, (c) hexagonal cell array for two dimensions. Within this j and l are indices corresponding to the horizontal and vertical directions respectively.

or hexagon we consider

$$\text{1D:} \quad \mathbf{W}_{j+1} + \mathbf{W}_{j-1} - 2\mathbf{W}_j, \tag{3.2}$$

$$\text{2D SQUARE:} \quad \mathbf{W}_{j,l+1} + \mathbf{W}_{j+1,l} + \mathbf{W}_{j,l-1} + \mathbf{W}_{j-1,l} - 4\mathbf{W}_{j,l} \tag{3.3}$$

$$\text{2D HEXAGON:} \quad \mathbf{W}_{j,l+1} + \mathbf{W}_{j+1,l+1} + \mathbf{W}_{j+1,l} + \mathbf{W}_{j,l-1} + \mathbf{W}_{j-1,l-1} + \mathbf{W}_{j-1,l} - 6\mathbf{W}_{j,l} \tag{3.4}$$

where j and l denote the horizontal and vertical directions respectively.

Taking as our starting point a classic activator-inhibitor type system, we consider the interactions between receptor, ligand and inhibitor as illustrated in Fig. 3.6. Within this, we incorporate the possibility of both receptor-ligand and receptor-inhibitor binding whilst retaining the main network interactions of a classical activator-inhibitor system. For the remainder of the formulation we restrict our attention to one dimension and consider the interactions occuring between receptor, ligand and inhibitor in a line of cells where j denotes cell position. A model considering these reactions can be given as

$$\frac{dR_j}{dt} = F(R_j, L_j, B_j, \bar{L}_j, \bar{B}_j), \tag{3.5}$$

$$\frac{dL_j}{dt} = G(R_j, L_j, B_j, \bar{L}_j, \bar{B}_j) + D_L(L_{j+1} - 2L_j + L_{j-1}), \tag{3.6}$$

$$\frac{dB_j}{dt} = H(R_j, L_j, B_j, \bar{L}_j, \bar{B}_j) + D_B(B_{j+1} - 2B_j + B_{j-1}), \tag{3.7}$$

where the variables R_j, L_j, B_j represent activity of the receptor, ligand and inhibitor at cell j. The functional forms F, G and H incorporate the interactions between the receptors, ligand and inhibitor, and D_L, D_B are the diffusion rates of ligand and inhibitor. In the above model we do not consider diffusion of the receptor, assuming it to be bound to the cell membrane and restricted in motion.

In order to investigate possible cell signalling mechanisms within the system we consider terms to describe the interactions involved in both the receptor-ligand binding, $\bar{L}_p$, and receptor-inhibitor binding, $\bar{B}_p$. Each consider the types of interactions that occur in cell signalling and can be broadly described as terms involving the activity on individual cells and the effect of surrounding cells. Consequently, we can have a wide variety of interactions within the system that may range from individual to multiple cells, for example interactions involving cellular self-regulation through filopodia extensions, [104]. In general, therefore, $\bar{L}_j$, $\bar{B}_j$ could involve possible interactions with the ligand/inhibitor activity levels on cells $j, j \pm 1, j \pm 2, j \pm 3$. Here,

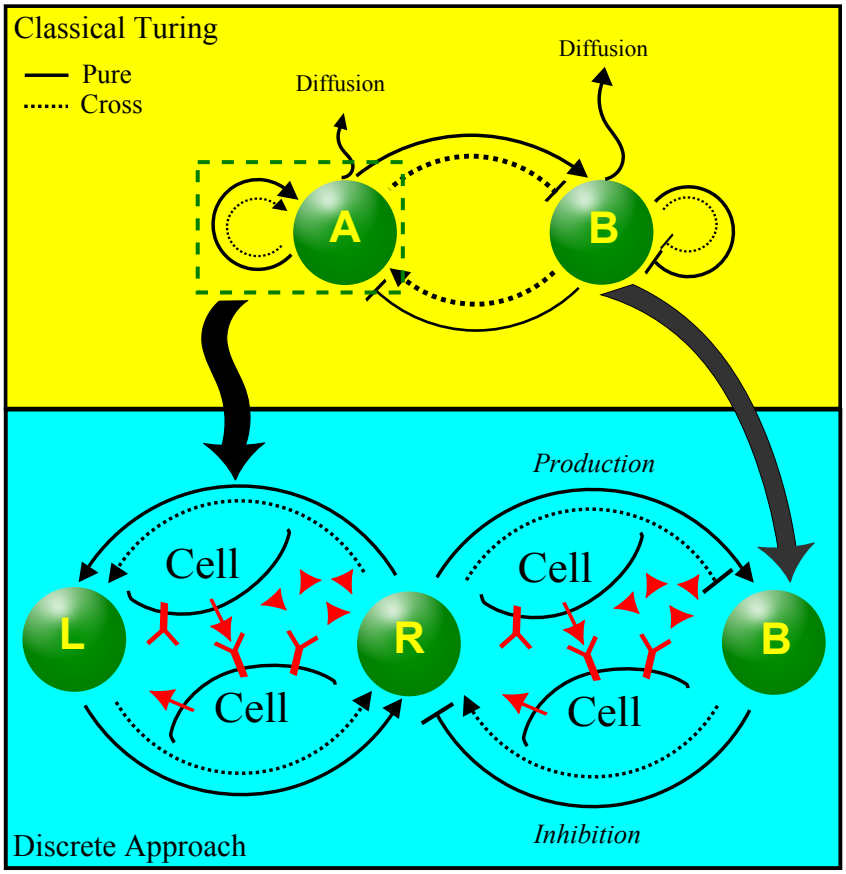

Figure 3.6: Schematic illustrating the underlying framework of a classical two species activator-inhibitor system and its comparison with a more detailed discrete approach. The discrete approach considers the incorporation of greater detail by expanding the autocatalytic process in an activator-inhibitor system by introducing the intrinsic process of receptor-ligand binding and receptor-inhibitor binding. The classical approach considers A and B representing the activator and inhibitor respectively with R, L and B respectively representing the receptor, ligand and inhibitor of the discrete approach.

we restrict the interactions to either autocrine or direct neighbour (juxtacrine) signalling, setting $\bar{L}_j = \bar{L}_j(L_j, L_{j\pm1})$ and similarly $\bar{B}_j = \bar{B}_j(B_j, B_{j\pm1})$. As discussed in the introduction, autocrine signalling involves self regulation: we assume ligands bind to receptors at the surface of the same cell resulting in a cascade of intracellular signals. In contrast, juxtacrine signalling involves communication between cells in direct contact with ligands on neighbouring cells $j \pm 1$ binding to receptors on the receiving

cell j. Here we present one way that these mechanisms can be modelled:

$$\bar{L}_j = \underbrace{\frac{\alpha_L}{2}(L_{j+1} + L_{j-1})}_{Juxtacrine} + \underbrace{(1-\alpha_L)L_j}_{Autocrine}, \tag{3.8}$$

$$\bar{B}_j = \underbrace{\frac{\alpha_B}{2}(B_{j+1} + B_{j-1})}_{Juxtacrine} + \underbrace{(1-\alpha_B)B_j}_{Autocrine}, \tag{3.9}$$

where we incorporate an averaging term to describe juxtacrine signalling and a linear term for autocrine signalling. We note that the juxtacrine signalling term is the same as that proposed by [65]. The parameters $\alpha_L, \alpha_B \in [0\ ,\ 1]$ in the above control the degree of each signalling mechanism within the system:

$$\alpha_L, \alpha_B \begin{cases} = 0 & \text{Autocrine Signalling} \\ \in (0\ \ 1) & \text{Autocrine + Juxtacrine} \\ = 1 & \text{Juxtacrine Signalling} \end{cases} \tag{3.10}$$

For example, choosing $\alpha_L = 0$ and $\alpha_B = 1$ will produce a system that considers an autocrine signalling process between receptor-ligand and juxtacrine signalling for receptor-inhibitor binding. These effects will be combined with the existing diffusive effects.

Similarly to the inhibitor attributes in the classical Turing model, we assume the inhibitor exists in a diffusible form that permeates throughout the extracellular space. Inhibitor may suppress the activity of receptor/ligand both directly by occupying receptors on the cell surface or indirectly by binding to ligands to reduce their physical attributes and effects. Further to this, we also assume ligand diffusion since previous research has suggested the presence of ligand molecules in both a cleaved, allowing a ligand molecule to diffuse through the extracellular space, and uncleaved form, resulting in membrane bound ligand on the cell surface, [105].

3.3 A Basic Model and Its Motivation

In this section we consider various reductions of the equations (3.5)-(3.7) into an analytically convenient two species model, facilitating a comparison with classical activator-inhibitor models. The general form of this is given by

$$\frac{dU_j}{dt} = F(U_j, B_j, \bar{U}_j, \bar{B}_j) + D_U(U_{j+1} - 2U_j + U_{j-1}), \tag{3.11}$$

$$\frac{dB_j}{dt} = H(U_j, B_j, \bar{U}_j, \bar{B}_j) + D_B(B_{j+1} - 2B_j + B_{j-1}), \tag{3.12}$$

$$\bar{U}_j = \underbrace{\frac{\alpha_U}{2}(U_{j+1} + U_{j-1})}_{Juxtacrine} + \underbrace{(1-\alpha_U)L_j}_{Autocrine}, \tag{3.13}$$

$$\bar{B}_j = \underbrace{\frac{\alpha_B}{2}(B_{j+1} + B_{j-1})}_{Juxtacrine} + \underbrace{(1-\alpha_B)B_j}_{Autocrine}, \tag{3.14}$$

where U_j is now a 'lumped' activity of receptor/ligand, while B_j represents the inhibitor as before. F is reinterpreted to incorporate the kinetics of both receptor and ligand, while, D_U, D_B denote diffusion rates. Note that for $D_U, D_B > 0$ and $\alpha_U = \alpha_B = 0$ we derive a general discretised two species Turing system, [9]. We consider the two classical conceptual models of Gierer-Meinhardt, [22], and Schnakenberg, [43], to motivate the kinetic choices.

3.3.1 Derivation via a Gierer-Meinhardt Type Scheme

The Gierer-Meinhardt kinetics, [22], are one of the most well known kinetic schemes, especially in the study of developmental patterning. The simplest system consists of a two species model:

$$\frac{dA_j}{dt} = k_1\frac{A_j^2}{B_j} - k_2 A_j + D_A(A_{j+1} - 2A_j + A_{j-1}), \tag{3.15}$$

$$\frac{dB_j}{dt} = k_3 A_j^2 - k_4 B_j + D_B(B_{j+1} - 2B_j + B_{j-1}), \tag{3.16}$$

where A_j, B_j represent the activator and inhibitor respectively at cell j, D_A, D_B are the diffusion coefficients of the activator and inhibitor and k_i, $i = 1, ..4$ are the rate constants. Under a suitable nondimensionalisation, the model becomes

$$\frac{du_j}{dt} = \frac{u_j^2}{w_j} - \delta_u u_j + d_u(u_{j+1} - 2u_j + u_{j-1}), \tag{3.17}$$

$$\frac{dw_j}{dt} = u_j^2 - w_j + d_w(w_{j+1} - 2w_j + w_{j-1}), \tag{3.18}$$

where u_j, w_j are the activator and inhibitor respectively and δ_u, d_w are positive parameters. The exact properties of pure kinetic systems can be seen in Chapter 1.

Here we discuss a possible pure-based kinetic scheme in discrete form using the expanded cell based approach given by (3.5)-(3.7), with its resultant reaction kinetics showing similarities to the pure type Gierer-Meinhardt kinetics given above. The

model is given by,

$$\frac{dR_j}{dt} = k_1(\cdot) - k_2 R_j, \tag{3.19}$$

$$\frac{dL_j}{dt} = k_3(\cdot) - k_4 L_j + D_L(L_{j+1} - 2L_j + L_{j-1}), \tag{3.20}$$

$$\frac{dB_j}{dt} = k_5(\cdot) - k_6 B_j + D_B(B_{j+1} - 2B_j + B_{j-1}), \tag{3.21}$$

where R_j, L_j, B_j represent the activity of the receptor, ligand and inhibitor at cell j respectively. Here, we only consider receptor-ligand binding and assume that cell signalling is regulated by a positive parameter $\alpha \in [0\,,\,1]$, where $\alpha = 0$ and $\alpha = 1$ incorporates autocrine signalling and juxtacrine signalling respectively, within a function of the form $\bar{L}_j = \frac{\alpha}{2}(L_{j+1} + L_{j-1}) + (1-\alpha)L_j$, as previously discussed. The consideration of the reaction kinetics in this case is phenomenological, motivated from (3.15)-(3.16), but adapted as follows

- The term given by $k_1(\cdot)$ in (3.19) considers the upregulation of receptor activity due to receptor-ligand binding. A receptor R_j situated on the surface of cell j binds to a ligand via juxtacrine signalling and/or autocrine signalling, $\bar{L}_j$, (depending on the value of α) with the downstream effect being upregulation of receptor activity. However, since there is no explicit representation of bound and unbound receptors we note that the form of the production function assumes an autocatalytic reaction: the rate of receptor activity is proportional to the amount of receptor. Using this we can recover a form that is similar to the classical Gierer-Meinhardt kinetics. To incorporate the possible suppressive action of the inhibitor we consider a rate constant dependent on the inhibitor activity: again motivated by the Gierer-Meinhardt kinetics we take $k_1(\cdot) = k_1\frac{R_j\bar{L}_j}{B_j}$. More generally, this function could take a number of further forms according to the inhibition. For example, the inhibitor could bind to receptors on the cell surface, occupying a receptor site and suppressing receptor-ligand binding.

- The functional form given by $k_3(\cdot)$ in (3.20) describes upregulation of ligand activity. While, generally this could be functionally dependent on all the variables, here we simply assume that the ligand activity is directly upregulated by receptor activity in the cell. For simplicity we assume that the ligand production depends linearly on receptor activity, $k_3(\cdot) = k_3 R_j$.

- The inhibitor production term is proposed to be $k_5(\cdot) = k_5 R_j^2$, consistent with the assumption in the classical Gierer-Meinhardt model, (3.15)-(3.16).

- In each equation we also assume a simple sink term describing the degradation/decay. With this, the ligand and inhibitor sink terms can represent the degradation or signalling decay of these molecules. The receptor sink term is likely to account for the internalisation of receptors by the cell. For simplicity and comparison to the continuous model, each of the above equations consider linear degradation/decay.

With the above kinetics and nondimensionalisation, $u_j = \frac{k_4 k_5}{k_1 k_3} R_j$, $v_j = \frac{k_4^2 k_5}{k_1 k_3^2} L_j$, $w_j = \frac{k_4^2 k_5 k_6}{k_1^2 k_3^2} B_j$, $t^* = k_6 t$, $\delta_u = \frac{k_2}{k_6}$, $\mu = \frac{k_4}{k_6}$, $d_v = \frac{D_L}{k_6}$, $\frac{D_B}{k_6}$, the model becomes

$$\frac{du_j}{dt} = \frac{u_j \bar{v}_j}{w_j} - \delta_u u_j, \tag{3.22}$$

$$\frac{dv_j}{dt} = \mu(u_j - v_j) + d_v(v_{j+1} - 2v_j + v_{j-1}), \tag{3.23}$$

$$\frac{dw_j}{dt} = u_j^2 - w_j + d_w(w_{j+1} - 2w_j + w_{j-1}), \tag{3.24}$$

where the nondimensionalised variables u_j, v_j, w_j represent the activity of the receptor, ligand and inhibitor at cell j respectively and δ_u, μ, d_v, d_w are all positive parameters.

Reduction to Two Species

Although the three species model above is not overly complicated, it becomes valuable to reduce higher order models to gain analytical tractability. If we assume that ligand activities are fast in comparison with those of receptor, then the ligand is assumed to be at quasi-equilibrium. To impose this we assume the parameter μ is large such that the rate of change of ligand is approximately zero ($\frac{dL_j}{dt} \approx 0$) and negligible ligand diffusion. This equation can then be rearranged to give an approximated solution in terms of the other dependent variables and in this case becomes $u_j \sim v_j$. With these, the reduced two species model becomes

$$\frac{du_j}{dt} = \frac{u_j \bar{u}_j}{v_j} - \delta_u u_j, \tag{3.25}$$

$$\frac{dw_j}{dt} = u_j^2 - w_j + d_w(w_{j+1} - 2w_j + w_{j-1}), \tag{3.26}$$

where we reinterpret the variables to consider the activity of the receptor/ligand u_j and inhibitor activity w_j. Note that d_w and δ_u are positive parameters while the communication term becomes $\bar{u}_j = \frac{\alpha}{2}(u_{j+1} + u_{j-1}) + (1 - \alpha)u_j$.

Clearly (3.25)-(3.26) is similar to the classical activator-inhibitor model, (3.17)-(3.18), however with diffusion of u replaced with a localised signalling form. An

amalgamated version of (3.17)-(3.18) can be given by

$$\frac{du_j}{dt} = \frac{u_j \bar{u}_j}{v_j} - \delta_u u_j + d_u(u_{j+1} - 2u_j + u_{j-1}) \tag{3.27}$$

$$\frac{dw_j}{dt} = u_j^2 - w_j + d_w(w_{j+1} - 2w_j + w_{j-1}) \tag{3.28}$$

where the variables are as defined before together with $d_u \geq 0$. We investigate this model in order to determine whether pattern formation can occur and, in doing so, present the results in a manner that compares and contrasts the two models: the model (3.25)-(3.26) in the absence of receptor/ligand diffusion ($d_u = 0$), as in the reduction assumptions, and the model (3.27)-(3.28) that is similar to a classical activator-inhibitor motivated model, incorporating receptor/ligand diffusion ($d_u \neq 0$).

3.3.2 Derivation via a Schnakenberg Type Scheme

The Schnakenberg kinetics proposed in 1979, [43], form an example of 'cross kinetic' reactions and can be formulated according to rate reactions as follows:

$$X \underset{k_3}{\overset{k_1}{\rightleftharpoons}} A_j, \quad Y \overset{k_4}{\to} B_j, \quad 2A_j + B_j \overset{k_2}{\to} 3A_j.$$

Using the Law of Mass Action, we have

$$\frac{dA_j}{dt} = k_1 + k_2 A_j^2 B_j - k_3 A_j, \tag{3.29}$$

$$\frac{dB_j}{dt} = k_4 - k_2 A_j^2 B_j. \tag{3.30}$$

Here, A_j and B_j is the activator and inhibitor respectively at cell j and k_i, $i = 1, .., 4$ are rate reaction constants. The addition of discrete diffusion will allow the study of this as a discrete Turing model.

In our extended model we consider an adaptation to include the receptor-ligand binding. Specifically, we let

$$X \underset{k_3}{\overset{k_1}{\rightleftharpoons}} R_j, \quad Y \underset{k_5}{\overset{k_4}{\rightleftharpoons}} L_j, \quad Z \overset{k_6}{\to} B_j, \tag{3.31}$$

$$\begin{cases} R_j + L_{j+1} + B_j & \overset{k_{2a}}{\to} 2R_j + L_{j+1}, \\ R_j + L_{j-1} + B_j & \overset{k_{2a}}{\to} 2R_j + L_{j-1}, \\ R_j + L_j + B_j & \overset{k_{2b}}{\to} 2R_j + L_j. \end{cases} \tag{3.32}$$

This set of reactions describes proposed interaction of receptor R_j, ligand L_j and

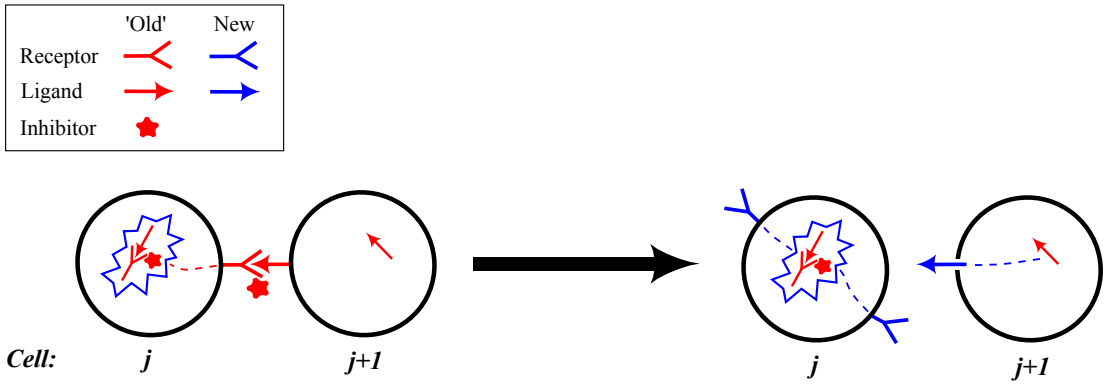

Figure 3.7: Schematic illustrating the interactions involved in the first of the proposed autocatalytic reactions, (3.32). Firstly, a receptor situated on the surface of cell j binds to a ligand on cell $j+1$ in the presence of an inhibitor which freely diffuses. This complex involving a receptor-ligand binding with inhibitor is then internalised and intracellularly processed resulting, via numerous complex interactions, in two new receptors on j and one replaced ligand on cell $j+1$. The inhibitor facilitates the reaction and gets used up in the process. The 'old' and new receptors/ligands are denoted by red and blue colours respectively.

inhibitor B_j where the index j denotes the position of cell j. We assume a set of autocatalytic binding processes considered in (3.32) which results in an upregulation of receptor. In this way, we can recover a similar form to the classical Schnakenberg kinetics. Here we note that the different reactions assume receptors interact with ligands on different cells and the rate constants regulating these reactions are different depending on the form of signalling. In particular, k_{2a}, k_{2b} denote the rates of reaction/signalling between neighbouring (juxtacrine) and individual cells (autocrine) respectively. From this, it is implicitly assumed that the binding process results in a cascade of intracellular signalling due to the internalisation of bound receptors with the downstream effects leading to receptor upregulation and production/replacement of a ligand on cells j and $j \pm 1$ (see Fig. 3.7). Note that the 'inhibitor', B_j, contributes towards the upregulation whilst being consumed in the reaction. Thus, it may be better to think of the inhibitor as a mediator of the reaction. For example, the 'inhibitor' may change the receptors morphology to admit the binding of a ligand to possible receptors. By using a similar argument to the LMA we obtain the model,

$$\frac{dR_j}{dt} = k_1 + R_j \bar{L}_j B_j - k_3 R_j, \tag{3.33}$$

$$\frac{dL_j}{dt} = k_4 - k_5 L_j + D_L(L_{j+1} - 2L_j + L_{j-1}), \tag{3.34}$$

$$\frac{dB_j}{dt} = k_6 - k_2 R_j \bar{L}_j B_j + D_B(B_{j+1} - 2B_j + B_{j-1}), \tag{3.35}$$

where R_j, L_j, B_j represent the receptor, ligand and inhibitor respectively, k_i, $i = 1,..6$ are rate constants, D_L, D_B are the diffusion rates of the ligand and inhibitor respectively. The signalling term $\bar{L}_j = \frac{\alpha}{2}(L_{j+1}+L_{j-1})+(1-\alpha)L_j$ and incorporates the different rate reactions regulating the signalling mechanisms via $\alpha = 2k_{2a} = 1 - k_{2b}$, with $\alpha \in [0\ ,\ 1]$. In considering the ligand production there are a number of possible interactions that can be considered. However, we simply assume linear reactions which are in reality likely to result from numerous internal signalling cascades. Although the above assumptions are highly restrictive, and a wide variety of other forms may be appropriate in a given system, the aim is for comparitive purposes.

Under the nondimensionalisation $u_j = \sqrt{\frac{k_4}{k_3k_5}}R_j$, $v_j = \sqrt{\frac{k_5}{k_3k_4}}L_j$, $w_j = \sqrt{\frac{k_4}{k_3k_5}}B_j$, $\beta = \frac{k_1}{k_3}\sqrt{\frac{k_4}{k_3k_5}}$, $\mu = \frac{k_5}{k_3}$, $\rho = \frac{k_6}{k_3}\sqrt{\frac{k_4}{k_3k_5}}$, $d_v = \frac{D_L}{k_3}$, $d_w = \frac{D_B}{k_3}$,

$$\frac{du_j}{dt} = \beta + u_j\bar{v}_jw_j - u_j, \tag{3.36}$$

$$\frac{dv_j}{dt} = \mu(u_j - v_j) + d_v(v_{j+1} - 2v_j + v_{j-1}), \tag{3.37}$$

$$\frac{dw_j}{dt} = \rho - u_j\bar{v}_jw_j + d_w(w_{j+1} - 2w_j + w_{j-1}), \tag{3.38}$$

where u_j, v_j, w_j represent the receptor, ligand and inhibitor activities respectively and β, μ, ρ, d_v, d_w are all positive parameters.

Reduction

As before, we now reduce the three species model to a simpler two species system to facilitate a comparison to the classical Turing system. Assuming the same QSSA we can reduce the model to a two species framework that considers the receptor/ligand activity u_j and inhibitor activity w_j. After substitution of the expression for v_j the model becomes

$$\frac{du_j}{dt} = \beta + u_j\bar{u}_jw_j - u_j \tag{3.39}$$

$$\frac{dw_j}{dt} = \rho - u_j\bar{u}_jw_j + d_w(w_{j+1} - 2w_j + w_{j-1}) \tag{3.40}$$

where now $\bar{u}_j = \frac{\alpha}{2}(u_{j+1} + u_{j-1}) + (1 - \alpha)u_j$. To also permit comparisons with the classical Schnakenberg model we state the generalised model:

$$\frac{du_j}{dt} = \beta + u_j\bar{u}_jw_j - u_j + d_u(u_{j+1} - 2u_j + u_{j-1}), \tag{3.41}$$

$$\frac{dw_j}{dt} = \rho - u_j\bar{u}_jw_j + d_w(w_{j+1} - 2w_j + w_{j-1}), \tag{3.42}$$

where the variables are as defined before but now with $d_u \geq 0$.

3.4 Summary

A model such as (3.5)-(3.7) allows pattern formation to be studied at a cell based level, with cell-interaction detail that may be lacking in continuous models. This three species model offers great scope, and to perform a useful comparison we motivated this study by formulating it with a direct comparison to a classical activator-inhibitor type mechanism. Using a QSSA, a reduced two species system has been derived that is of the general form

$$\frac{dU_j}{dt} = F(U_j, B_j, \bar{U}_j, \bar{B}_j) + D_U(U_{j+1} - 2U_j + U_{j-1}), \tag{3.43}$$

$$\frac{dB_j}{dt} = G(U_j, B_j, \bar{U}_j, \bar{B}_j) + D_B(B_{j+1} - 2B_j + B_{j-1}), \tag{3.44}$$

where U_j, B_j represent the activity of receptor/ligand and inhibitor on cell j respectively, with the communication terms

$$\bar{U}_j = \frac{\alpha_U}{2}(U_{j+1} + U_{j-1}) + (1 - \alpha_U)U_j, \tag{3.45}$$

$$\bar{B}_j = \frac{\alpha_B}{2}(B_{j+1} + B_{j-1}) + (1 - \alpha_B)B_j, \tag{3.46}$$

to model autocrine and juxtacrine signalling.

In the next chapter we undertake a linear stability analysis to analyse the general model and find the conditions that will lead to pattern formation. In doing so, the analysis follows a similar framework to the Turing type stability analysis of the classical activator-inhibitor system. Using the two case studies formulated in §3.3.1 and §3.3.2 as possible kinetic schemes, we investigate the importance of cell signalling mechanisms in biological applications by investigating the analytical and numerical results. We discuss the pattern forming potentials of the two different models and discuss the impact different cell signalling mechanisms have on pattern formation.

Chapter 4

Impact of Cell Signalling on Pattern Formation

In this chapter we investigate the impact cell signalling mechanisms have on pattern formation by undertaking analysis of the reduced two species model and full three species system. We consider the Gierer-Meinhardt and Schnakenberg motivated schemes of the previous chapter to permit a direct comparison to Turing's classical approach. The analysis demonstrates that both the two and three species models similarly exhibit a variety of characteristics. In particular, both fine grained to longer range wavelength patterns are attainable, with numerical simulations also illustrating particular traits according to the signalling mechanism. The results indicate the potential application of the models to a range of biological systems.

4.1 Introduction

Motivated by well studied Turing type models, in the previous section we proposed two case studies for Turing systems at the level of cell detail, specifically interacting cells via autocrine and juxtacrine signalling. Furthermore, using the QSSA, a reduced form of the model kinetics were formulated to generate a direct comparison to a discrete Turing model. Throughout our analysis we will relate the results with classical activator-inhibitor systems to see how autocrine and juxtacrine signalling mechanisms impact on pattern formation.

In the next section we consider the generic form of the model from which all cases analysed can be explicitly stated. Undertaking a linear stability analysis on this model in §4.2.1 allows for a universal stability analysis for all subsequent cases. These follow the form of analysing the impact of autocrine, juxtacrine and a combination of the two signalling mechanisms in a model with Gierer-Meinhardt, §4.3, and Schnakenberg type kinetics, §4.4, proposed in Chapter 3. Moreover, we undertake a detailed numerical investigation on these kinetics schemes in §4.5 that considers

both one and two dimensional domains. In this way, we hope to determine the effects that these signalling mechanisms have in pattern formation and observe whether the results support the predictions from the linear stability analysis. In particular, we are keen to determine the effect of signalling mechanisms on wavelength and patterning. Further to this, we explore whether formulating the model in this way generates any advantages/disadvantages over 'typical' Turing systems. Finally, we consider the full three species model in §4.7 to investigate the general results and determine whether the reduced model is a reasonable approximation of this system.

4.2 Mathematical Models

As well as providing a more detailed approach to modelling pattern formation, the formulation of the general model in the previous chapter and given below, results in a diverse framework that can be used to investigate a number of different scenarios. As a result, we consider all the mathematical models separately below and make reference to them in the analysis.

(I) Principal Model: A general two species model with both localised and diffusion based signalling:

$$\frac{dU_j}{dt} = F(U_j, B_j, \bar{U}_j, \bar{B}_j) + D_U(U_{j+1} - 2U_j + U_{j-1}), \tag{4.1}$$

$$\frac{dB_j}{dt} = G(U_j, B_j, \bar{U}_j, \bar{B}_j) + D_B(B_{j+1} - 2B_j + B_{j-1}). \tag{4.2}$$

Within this U_j, B_j represent the receptor/ligand and inhibitor activity respectively, F and G incorporate the reaction kinetics of the receptor/ligand and inhibitor, both species diffuse with diffusion coefficients D_U, D_B and t is the time. Autocrine and/or juxtacrine cell signalling are included through the terms $\bar{U}_j$ and $\bar{B}_j$, respectively, and are assumed to take the form

$$\begin{aligned} \bar{U}_j &= \frac{\alpha_U}{2}(U_{j+1} + U_{j-1}) + (1 - \alpha_U)U_j \\ \bar{B}_j &= \frac{\alpha_B}{2}(B_{j+1} + B_{j-1}) + (1 - \alpha_B)B_j \end{aligned} \tag{4.3}$$

where

$$\alpha_U, \alpha_B \begin{cases} = 0 & \text{Autocrine Signalling} \\ \in (0\ \ 1) & \text{Autocrine + Juxtacrine} \\ = 1 & \text{Juxtacrine Signalling} \end{cases} \tag{4.4}$$

The following models, that are subsets of (4.1)-(4.2), are provided to highlight

the case studies that we will consider.

(I)*(a)* General Discrete Turing: Here we consider the principal model in the absence of localised signalling:

$$\frac{dU_j}{dt} = F(U_j, B_j) + D_U(U_{j+1} - 2U_j + U_{j-1}), \tag{4.5}$$

$$\frac{dB_j}{dt} = G(U_j, B_j) + D_B(B_{j+1} - 2B_j + B_{j-1}). \tag{4.6}$$

(I)*(b)* Autocrine: Here we consider only inhibitor diffusing, with receptor/ligand diffusion replaced by a purely autocrine signalling mechanism ($\alpha = 0$) via receptor-ligand binding:

$$\frac{dU_j}{dt} = F(U_j, B_j, \bar{U}_j), \tag{4.7}$$

$$\frac{dB_j}{dt} = G(U_j, B_j, \bar{U}_j) + D_B(B_{j+1} - 2B_j + B_{j-1}), \tag{4.8}$$

with

$$\bar{U}_j = U_j. \tag{4.9}$$

(I)*(c)* Juxtacrine: Here we consider only diffusion of the inhibitor, with receptor/ligand diffusion being replaced by purely juxtacrine signalling ($\alpha = 1$) via receptor-ligand binding:

$$\frac{dU_j}{dt} = F(U_j, B_j, \bar{U}_j), \tag{4.10}$$

$$\frac{dB_j}{dt} = G(U_j, B_j, \bar{U}_j) + D_B(B_{j+1} - 2B_j + B_{j-1}), \tag{4.11}$$

with

$$\bar{U}_j = \frac{1}{2}(U_{j+1} + U_{j-1}). \tag{4.12}$$

(I)*(d)* Mixed: Here we consider a model that involves both autocrine and juxtacrine signalling ($\alpha \in (0\ 1)$) via receptor-ligand binding, together with longer range diffusion based signalling:

$$\frac{dU_j}{dt} = F(U_j, B_j, \bar{U}_j) + D_U(U_{j+1} - 2U_j + U_{j-1}), \tag{4.13}$$

$$\frac{dB_j}{dt} = G(U_j, B_j, \bar{U}_j) + D_B(B_{j+1} - 2B_j + B_{j-1}), \tag{4.14}$$

with

$$\bar{U}_j = \frac{\alpha}{2}(U_{j+1} + U_{j-1}) + \alpha U_j. \tag{4.15}$$

We investigate the pattern forming potential of each scenario in the proceeding sections, beginning with a linear stability analysis of the principal model, (I).

4.2.1 Linear Stability Analysis

Consider the general mathematical model given by

$$\frac{dU_j}{dt} = F(U_j, B_j, \bar{U}_j, \bar{B}_j) + D_U(U_{j+1} - 2U_j + U_{j-1}), \tag{4.16}$$

$$\frac{dB_j}{dt} = G(U_j, B_j, \bar{U}_j, \bar{B}_j) + D_B(B_{j+1} - 2B_j + B_{j-1}). \tag{4.17}$$

We analyse this reduced general model such that, depending on the biological application, we can investigate possible interactions and binding processes between receptor/ligand, U_j, and inhibitor, B_j. The impact of autocrine/juxtacrine receptor-ligand binding and inhibitor binding processes can be implemented through functional forms of $\bar{U}_j$ and $\bar{B}_j$ respectively. For the purposes of the analysis and to be consistent with the main text, we assume that these terms take similar forms: $\bar{U}_j = \frac{\alpha_U}{2}(U_{j+1} + U_{j-1}) + (1 - \alpha_U)U_j$ and $\bar{B}_j = \frac{\alpha_B}{2}(B_{j+1} + B_{j-1}) + (1 - \alpha_B)B_j$. However, one noticeable difference are the signalling parameters α_U and α_B. In this way, the different parameters will allow for differences in the mechanisms occurring in the receptor-ligand and receptor-inhibitor binding processes.

The positive homogeneous steady state (U_s, B_s) of the system satisfies $F(U_s, B_s, U_s, B_s) = G(U_s, B_s, U_s, B_s) = 0$ and we analyse the stability of the system by considering small perturbations to this steady state. Therefore we set

$$U_j = U_s + \hat{U}_j,$$

$$B_j = B_s + \hat{B}_j,$$

where $\hat{U}_j$, $\hat{B}_j$ are small perturbations. Substituting in, expanding by the Taylor series and ignoring higher order terms,

$$\frac{d\hat{U}_j}{dt} = F_U\hat{U}_j + F_B\hat{B}_j + F_{\bar{U}}\hat{\bar{U}}_j + F_{\bar{B}}\hat{\bar{B}}_j + D_U(\hat{U}_{j+1} - 2\hat{U}_j + \hat{U}_{j-1}). \tag{4.18}$$

Here, $F_U = \frac{\partial F}{\partial U_j}|_{(U_s,B_s)}$, $F_B = \frac{\partial F}{\partial B_j}|_{(U_s,B_s)}$, $F_{\bar{U}} = \frac{\partial F}{\partial \bar{U}_j}|_{(U_s,B_s)}$, $F_{\bar{B}} = \frac{\partial F}{\partial \bar{B}_j}|_{(U_s,B_s)}$. Similarly

for B_j,

$$\frac{d\hat{B}_j}{dt} = G_U\hat{U}_j + G_B\hat{B}_j + G_{\bar{U}}\hat{\bar{U}}_j + G_{\bar{B}}\hat{\bar{B}}_j + D_B(\hat{B}_{j+1} - 2\hat{B}_j + \hat{B}_{j-1}) \tag{4.19}$$

where $G_U = \frac{\partial G}{\partial U_j}|_{(U_s,B_s)}$, $G_{\bar{B}} = \frac{\partial G}{\partial B_j}|_{(U_s,B_s)}$, etc. From now on, this notation will be used to denote the partial derivatives evaluated at the steady state. Now seek solutions of the form,

$$\begin{pmatrix} \hat{U}_j \\ \hat{B}_j \end{pmatrix} \sim \begin{pmatrix} \check{U}(t) \\ \check{B}(t) \end{pmatrix} e^{ijk} \tag{4.20}$$

where $k \in \mathbb{Z}^+$ is the wavenumber. Since we are considering a discrete system involving measurements on the scale of individual cells the wavelength of any relevant pattern must be greater than or equal to two cells. Substituting in and dividing throughout by e^{ijk} reduces the system, in matrix vector form, to,

$$\frac{d}{dt}\begin{pmatrix} \check{U}(t) \\ \check{B}(t) \end{pmatrix} = \underbrace{\begin{pmatrix} F_U + F_{\bar{U}}K_{c_U} + D_U K_{diff} & F_B + F_{\bar{B}}K_{c_B} \\ G_U + G_{\bar{U}}K_{c_U} & G_B + G_{\bar{B}}K_{c_B} + D_B K_{diff} \end{pmatrix}}_{A} \begin{pmatrix} \check{U}(t) \\ \check{B}(t) \end{pmatrix} \tag{4.21}$$

where, based on the assumed communication term:

$$\begin{aligned} K_{c_U}(k) &= \frac{\alpha_U}{2}(e^{ik} + e^{-ik}) + (1 - \alpha_U) \\ &= \alpha_U \cos(k) + (1 - \alpha_U); \end{aligned} \tag{4.22}$$

$$K_{c_B}(k) = \alpha_B \cos(k) + (1 - \alpha_B); \tag{4.23}$$

$$\begin{aligned} K_{diff}(k) &= e^{ik} - 2 + e^{-ik} \\ &= 2(\cos(k) - 1), \end{aligned} \tag{4.24}$$

by using Euler's formula. Considering the temporal part, we now seek solutions of the form

$$\begin{pmatrix} \check{U}(t) \\ \check{B}(t) \end{pmatrix} \sim \begin{pmatrix} \check{U} \\ \check{B} \end{pmatrix} e^{\lambda t} \tag{4.25}$$

where λ is the temporal growth rate. Substituting into the system and dividing throughout by $e^{\lambda t}$ yields a system of the form

$$\begin{pmatrix} F_U + F_{\bar{U}}K_{c_U} - \lambda + D_U K_{diff} & F_B + F_{\bar{B}}K_{c_B} \\ G_U + G_{\bar{U}}K_{c_U} & G_B + G_{\bar{B}}K_{c_B} - \lambda + D_B K_{diff} \end{pmatrix} \begin{pmatrix} \check{U} \\ \check{B} \end{pmatrix} = 0. \tag{4.26}$$

For nontrivial solutions we require

$$\begin{vmatrix} F_U + F_{\bar{U}}K_{c_U} - \lambda + D_U K_{diff} & F_B + F_{\bar{B}}K_{c_B} \\ G_U + G_{\bar{U}}K_{c_U} & G_B + G_{\bar{B}}K_{c_B} - \lambda + D_B K_{diff} \end{vmatrix} = 0. \tag{4.27}$$

On expanding this leads to a characteristic polynomial of the form

$$\lambda^2 + a_1(k)\lambda + a_0(k) = 0, \tag{4.28}$$

where

$$\begin{aligned} a_1(k) &= -tr(A) \\ &= -(F_U + G_B + F_{\bar{U}}K_{c_U} + G_{\bar{B}}K_{c_B}) - (D_U + D_B)K_{diff}, \end{aligned} \tag{4.29}$$

$$\begin{aligned} a_0(k) &= -det(A), \\ &= D_U D_B K_{diff}^2 + (F_{\bar{U}}K_{c_U}D_B + D_U G_B + F_U D_B + D_U G_{\bar{B}}K_{c_B})K_{diff} \\ &\quad - F_{\bar{B}}K_{c_B}G_U + F_U G_B + F_U G_{\bar{B}}K_{c_B} - F_B G_U + F_{\bar{U}}K_{c_U}G_B \\ &\quad + F_{\bar{U}}K_{c_U}G_{\bar{B}}K_{c_B} - F_{\bar{B}}K_{c_B}G_{\bar{U}}K_{c_U} - F_B G_{\bar{U}}K_{c_U}. \end{aligned} \tag{4.30}$$

We are now in a position to analyse the stability of the homogeneous steady state. We perform a DDI-type analysis by examining scenarios under which the homogeneous steady state is (i) stable to a homogeneous perturbation and (ii) unstable to an inhomogeneous perturbation. In doing so, we obtain the general conditions

$$(F_U + G_B + F_{\bar{U}} + G_{\bar{B}}) < 0, \tag{4.31}$$

$$F_U G_B - F_B G_U + F_U G_{\bar{B}} - F_B G_{\bar{U}} - F_{\bar{B}} G_U + F_{\bar{U}} G_B + F_{\bar{U}} G_{\bar{B}} - F_{\bar{B}} G_{\bar{U}} > 0, \tag{4.32}$$

$$D_U G_B + F_U D_B + F_{\bar{U}}K_{c_U}D_B + D_U G_{\bar{B}}K_{c_B} > 0, \tag{4.33}$$

$$b_1^2 - 4b_2 b_0 > 0. \tag{4.34}$$

In the above

$$b_2 = (4D_U D_B + 2F_{\bar{U}}\alpha_U D_B + 2D_U G_{\bar{B}}\alpha_B - F_{\bar{B}}\alpha_B G_{\bar{U}}\alpha_U + F_{\bar{U}}\alpha_U G_{\bar{B}}\alpha_B), \tag{4.35}$$

$$\begin{aligned} b_1 = {} & F_{\bar{U}}(1-\alpha_U)G_{\bar{B}}\alpha_B + F_{\bar{U}}\alpha_U G_{\bar{B}}(1-\alpha_B) - F_{\bar{B}}(1-\alpha_B)G_{\bar{U}}\alpha_U \\ & - F_{\bar{B}}\alpha_B G_{\bar{U}}(1-\alpha_U) + F_U G_{\bar{B}}\alpha_B + F_{\bar{U}}\alpha_U G_B - 8D_U D_B - F_{\bar{B}}\alpha_B G_U \\ & + 2F_{\bar{U}}(1-\alpha_U)D_B + 2D_U G_B + 2F_U D_B + 2D_U G_{\bar{B}}(1-\alpha_B) \\ & - 2F_{\bar{U}}\alpha_U D_B - 2D_U G_{\bar{B}}\alpha_B - F_B G_{\bar{U}}\alpha_U, \end{aligned} \tag{4.36}$$

$$\begin{aligned} b_0 = {} & 4D_U D_B + F_{\bar{U}}(1-\alpha_U)G_{\bar{B}}(1-\alpha_B) - F_{\bar{B}}(1-\alpha_B)G_U - 2F_{\bar{U}}(1-\alpha_U)D_B \\ & - 2D_U G_B - 2F_U D_B - 2D_U G_{\bar{B}}(1-\alpha_B) - F_{\bar{B}}(1-\alpha_B)G_{\bar{U}}(1-\alpha_U) + F_U G_{\bar{B}}(1-\alpha_B) \\ & - F_B G_{\bar{U}}(1-\alpha_U) + F_U G_B - F_B G_U + F_{\bar{U}}(1-\alpha_U)G_B. \end{aligned} \tag{4.37}$$

Provided plausible reaction kinetics that adhere to a relative discrete formulation, the linear stability analysis will provide conditions on parameters within the model that, if satisfied, will lead to pattern formation. The case studies of the previous chapter, motivated by Gierer-Meinhardt and Schnakenberg type systems, provide a framework to study the possible interactions within a specific application.

4.3 Analysis of Case Study I: Gierer-Meinhardt

We follow the general stability analysis derived in §4.2.1 and reproduce it for the nondimensionalised Gierer-Meinhardt type model from Chapter 1. In the augmented form

$$\frac{du_j}{dt} = \frac{u_j \bar{u}_j}{w_j} - \delta_u u_j + d_u(u_{j+1} - 2u_j + u_{j-1}), \tag{4.38}$$

$$\frac{dw_j}{dt} = u_j^2 - w_j + d_w(w_{j+1} - 2w_j + w_{j-1}), \tag{4.39}$$

where u_j, w_j are the receptor/ligand and inhibitor activity respectively at cell j and δ_u, d_w are positive parameters with $d_u \geq 0$. As before, the communication term $\bar{u}_j = \frac{\alpha}{2}(u_{j+1} + u_{j-1}) + (1-\alpha)u_j$ where $\alpha \in [0\ 1]$ regulates the signalling. Therefore, by setting $d_u > 0$ we have a comparitive model to the discrete Turing but with localised signalling. The full linear stability analysis can be seen in Appendix B.1 but

the set of conditions for pattern formation are given by,

$$0 < \delta_u < 1, \tag{4.40}$$

$$\delta_u d_w K_c - d_u > 0, \tag{4.41}$$

$$d_w > \frac{(3+2\sqrt{2})(2d_u + \delta_u \alpha)}{2\delta_u}. \tag{4.42}$$

The above conditions, (4.40)-(4.42), correspond to the 'standard' case when either $d_u > 0$ or $d_u = 0$ & $\alpha \geq 0.5$. However, together with (4.40)-(4.41), when $d_u = 0$ & $0 \leq \alpha < 0.5$ we require

$$d_w > \frac{(1+2\alpha)}{4(1-2\alpha)}, \tag{4.43}$$

where $K_c(k) = \alpha\cos(k) + (1-\alpha)$ (see Appendix B.1 for details). The condition (4.41) above provides a bound on the wavenumber such that admissible wavenumbers must lie between the range $[0\ ,\ k_c]$ where k_c is the critical upper wavenumber. More specifically, by solving (4.41) for k we obtain $k_c = \cos^{-1}\left(\frac{\delta_u d_w(\alpha-1)+d_u}{\delta_u d_w \alpha}\right)$. Therefore, depending on the parameter values the wavenumber range will vary and only the wavenumbers within the relevant range will lead to pattern formation. In the subsequent analysis the conditions (4.40), (4.42) ($d_u > 0$ or $d_u = 0$ & $\alpha \geq 0.5$ case) and (4.40), (4.43) ($d_u = 0$ & $0 \leq \alpha < 0.5$ case) are the conditions that delimit the parameter regions for pattern formation.

In numerical simulations used to validate the analysis, the models are numerically solved for an initial activity level given by a 2% random perturbation to the homogeneous steady state. The boundary conditions are considered to be periodic and, in this way, implement a closed system. Details of the numerical methods can be seen in Appendix C.2.

4.3.1 Autocrine Signalling ($\alpha = 0$)

We refer to the model given by (4.38)-(4.39) and set $\alpha = 0$ to incorporate an autocrine signalling mechanism within the system. Here, the model is the same as the discrete Turing system. However, for $\alpha = 0$ and $d_u = 0$, the short range activation mediated by diffusion is replaced with a purely local self-activation process.

In both cases, we can obtain a region of parameter space where parameters chosen within this will lead to pattern formation in simulations, 4.1(a)(i) and (b)(i). The $\delta_u - d_w$ parameter space for the discrete Turing model can be seen in Fig. 4.1(a)(i). From this we obtain the results of the classical activator-inhibitor system with Gierer-Meinhardt kinetics and therefore we can see a comparison between the two diffusible model with autocrine signalling and the continuous system (c.f. Fig. 1.5 in Chapter

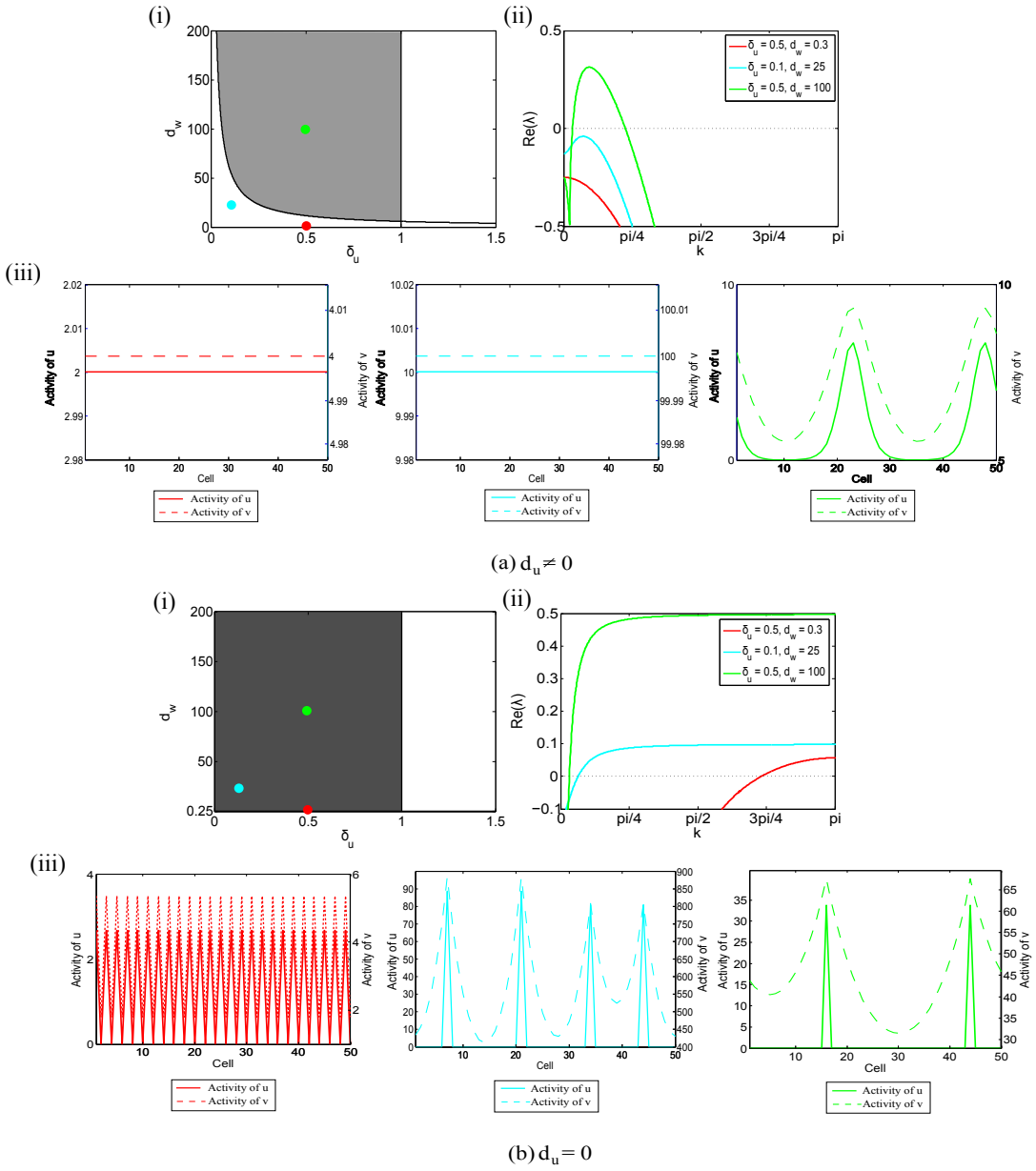

Figure 4.1: Investigation of the Gierer-Meinhardt model with an autocrine signalling mechanism ($\alpha = 0$) for (a) discrete Turing (with $d_u = 1$) and (b) diffusion replaced by purely local self activation ($d_u = 0$). Within these, we show (i) parameter space, (ii) dispersion relations, and (iii) simulations, for the parameter sets denoted by the coloured dots (see legends in (ii)). Parameters chosen within the grey parameter regions will lead to pattern formation. In particular, the light and dark grey regions consider the different instability conditions when $d_u \neq 0$ and $d_u = 0 \& 0 \leq \alpha < 0.5$.

1).

However, we also observe a region of parameter space in a model replacing short range diffusion with self-activating autocrine signalling ($d_u = 0$), Fig. 4.1(b)(i). In comparison to the two diffusible species region, the parameter space changes shape and becomes larger, incorporating a greater range of parameters. This enlargement of the parameter space suggests greater robustness of the model, since we can now include parameters that were originally outwith the region for pattern formation when both species diffuse ($d_u \neq 0$). In fact, by choosing the same parameter set in both parameter space regions we observe a transition from no pattern formation to patterning in simulations, Fig. 4.1(iii). Firstly, when $d_u \neq 0$, Fig. 4.1(a), the parameter sets given by the cyan and red coloured dots lead to the decay of the random initial conditions to the steady state values. In this case the linear stability analysis predicts no patterning. However, with $d_u = 0$, Fig. 4.1(b), the solution evolves to produce pattern formation with peaks and troughs in activity levels.

This is reinforced through plots of the dispersion relations showing the possible unstable wavenumbers, Fig. 4.1(ii). The different parameter sets illustrate dispersion relations that have $Re(\lambda) < 0$ and $Re(\lambda) > 0$ corresponding to parameter sets chosen outwith and within the parameter space respectively. These would indicate that patterns are possible through the appearance of unstable wavenumbers with positive real part of λ.

Further to this, the dispersion relations of the discrete Turing model ($d_u \neq 0$) have an upper and lower bound on the unstable wavenumbers, Fig. 4.1(a)(ii). In contrast, the one diffusible species model, Fig. 4.1(b)(ii), shows what appears to be an unbounded set of wavenumbers and, in this case, we consider the dispersion relations for the relevant wavenumber range for individual cell-based patterns. In particular, the choice of wavenumber is only relevant to a maximum of $k = \pi$, since this will lead to a wavelength greater than or equal to two cells. This minimum wavelength pattern is observed for the parameter set given in red in the one diffusible species model, Fig. 4.1(b)(iii). Here, the simulations show that we can obtain fine grained patterns and, although this has been found in both lateral induction and lateral inhibition models, the result would suggest that when diffusion is replaced by a self-activating autocrine mechanism the system may be similarly able to capture patterns that have periodicity on a much smaller scale such as patterning exhibited on the fruit fly Drosophila Melanogaster. The cyan and green simulations in Fig. 4.1(b)(iii) further illustrate the capabilities of the model and, in particular, the possibility of longer wavelength patterns.

In the continuous system each of the dispersion relation forms also arise but when there is an unbounded wavenumber range the system may exhibit infinitesimal patterning. As a result, these may not be justifiable in biological applications, [84]. This

in itself leads to an advantage of using the discrete model since the maximum relevant wavenumber can permit biologically plausible pattern formation in a model with one diffusible species. Moreover, the generated patterns produce specified activity levels for individual cells and, from these quantifiable results, cell differentiation can be easily determined.

Stability Analysis Predictions Versus Actual Wavelengths

Over the entire parameter space the linear stability analysis predicts wavelengths, which we typically expect to observe, that corresponds to the wavenumber with largest $Re(\lambda) > 0$. We refer to this throughout our analysis as the 'expected wavelength'. For the discrete Turing (two diffusible species) model and the model with diffusion replaced by short range activation via autocrine signalling (one diffusible species), these can be seen in Fig. 4.2(a) and Fig. 4.3(a) respectively. The predictions given by the linear stability analysis are reinforced with numerical simulations for possible parameter set choices. Moreover, the parameters are chosen to show the range of wavelengths that are possible in simulations and give an indication of the resultant patterns.

The simulations produced in Fig. 4.2(a)(i)-(iii) appear to produce the characteristic wavelengths synonymous with Turing patterns. From these, expected wavelengths of $\omega = 50$ can be obtained for high values of d_w and the corresponding simulations for chosen parameter sets predict close agreement with the linear stability analysis, Fig. 4.2(i)-(iii). In contrast, the stability analysis of the one diffusible species model predicts that expected wavelengths of only two cells can be obtained over the entire parameter space, Fig. 4.3(a). Furthermore, the simulations do not appear to be in close agreement with the predicted wavelength, Fig. 4.3(i)-(iii).

The typical dispersion relations suggest an explanation for this (compare Fig. 4.2(b) and 4.3(b)). The first of these (discrete Turing) illustrates a dispersion relation with a small bounded range of unstable wavelengths. This form is typical across the parameter space and the selection of the unstable wavelength with largest $Re(\lambda) > 0$ (expected wavelength) can be easily identified. However, the one diffusible species model with autocrine signalling exhibits a dispersion relation that has a number of possible unstable wavelengths, Fig. 4.3(b). This wide range results in a difficulty selecting the expected wavelength, leading to unreasonable predictions. In this case, the linear stability analysis is not a good predictor of the resultant pattern.

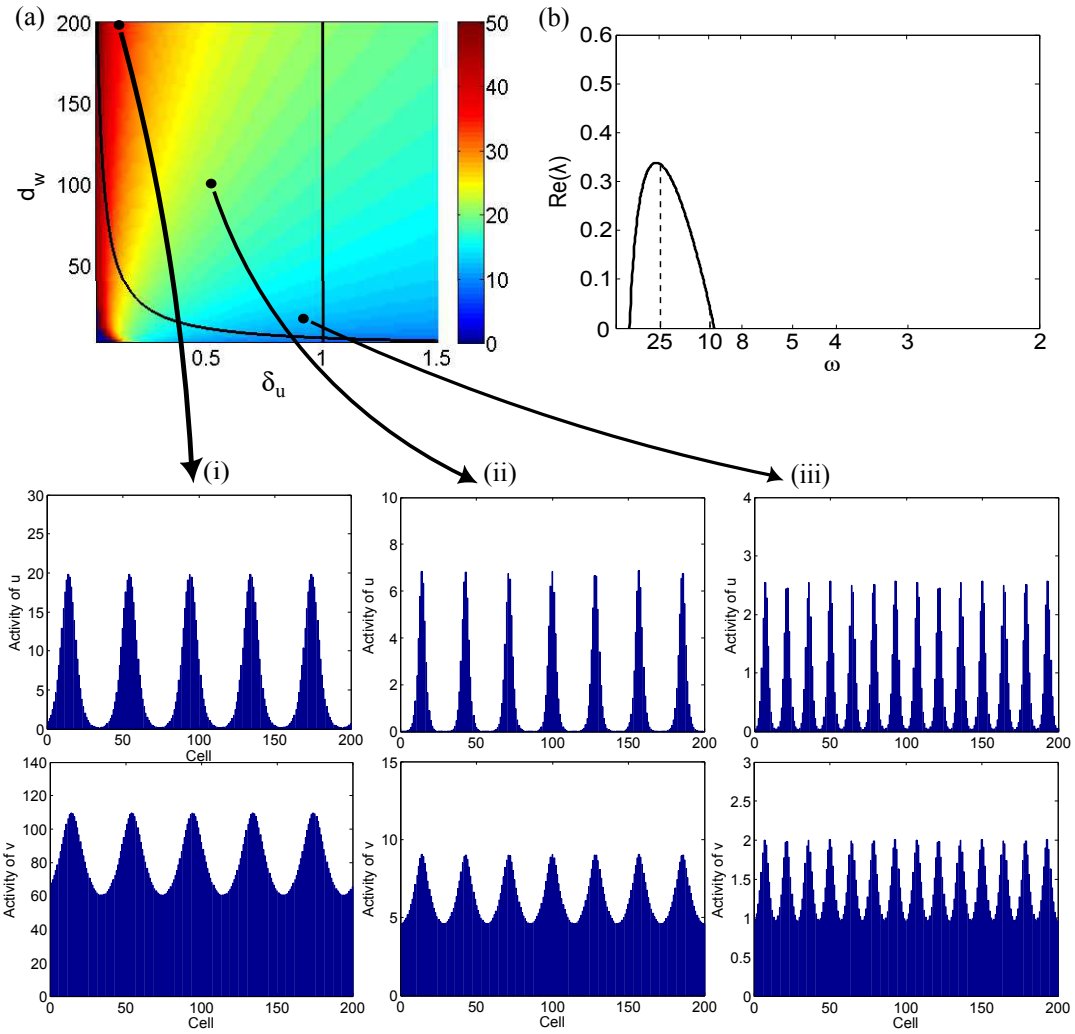

Figure 4.2: Plots showing (a) expected wavelengths over the parameter space for the discrete Turing model ($d_u = 1$), (b) dispersion relation for parameter set within the parameter space range and (i)-(iii) simulations across the parameter space. Parameters for the simulations are given by (i) $d_w = 200$, $\delta_u = 0.13$ (10% in from parameter space edge), (ii) $d_w = 100$, $\delta_u = 0.53$ (50% in), (iii) $d_w = 20$, $\delta_u = 0.93$ (90% in). Moreover, the dispersion relation, given in (b), illutrates the possible unstable wavelengths and corresponds to parameter set (ii). The range of expected wavelengths over the parameter space are referenced through the colorbar and the model is numerically solved for 200 cells.

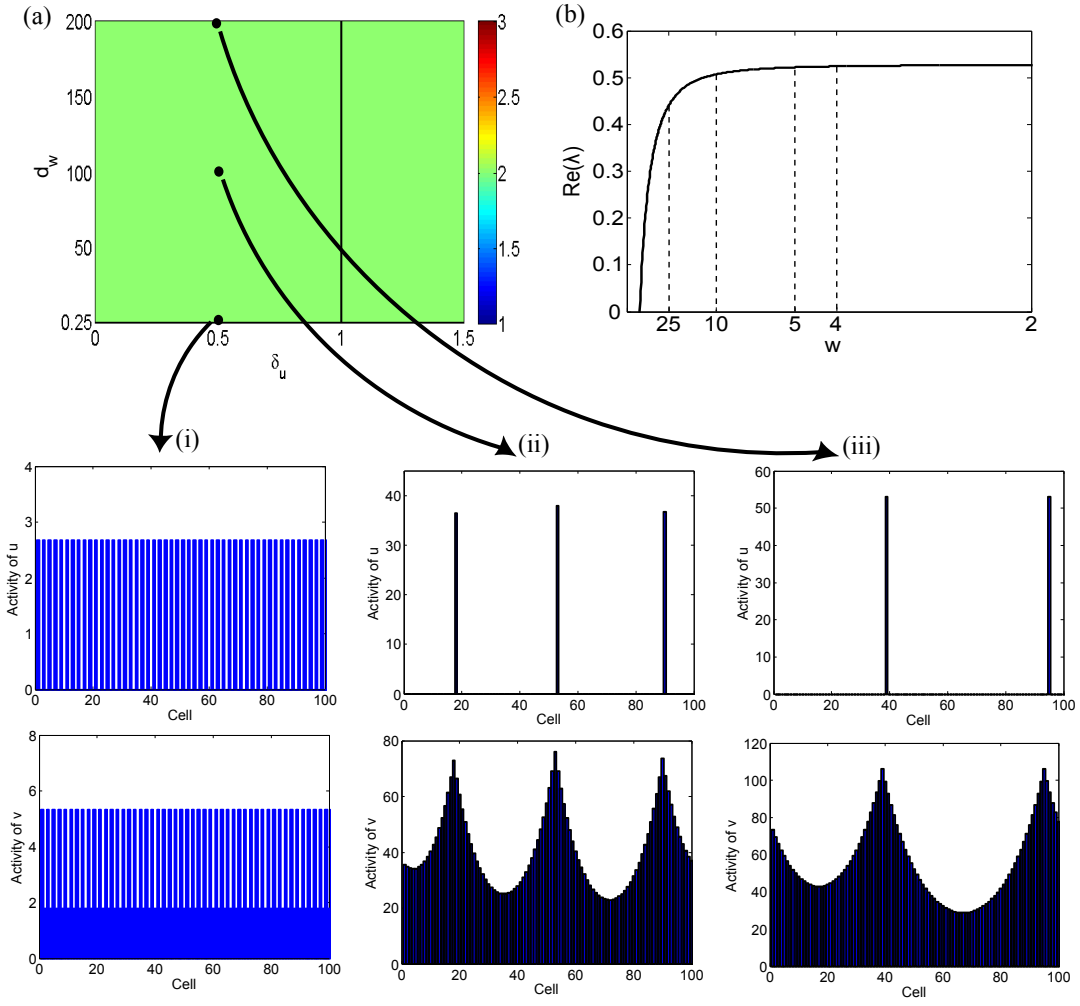

Figure 4.3: Plots showing (a) expected wavelengths over the parameter space for the one diffusible species model with autocrine signalling ($d_u = 0$), (b) dispersion relation for parameter set within the parameter space range and (i)-(iii) simulations across the parameter space. Parameters for the simulations are given by $\delta_u = 0.5$ and (i) $d_w = 0.2525$, (ii) $d_w = 100$, (iii) $d_w = 200$. Moreover, the dispersion relation, given in (b), illutrates the possible unstable wavelengths and corresponds to parameter set (ii). The range of expected wavelengths over the parameter space are referenced through the colorbar and the model is numerically solved for 100 cells.

Determining Excited Modes Through Fourier Series Analysis

The Fourier series decomposes some periodic solution into a function involving the linear combination of sines and cosines using the approximation,

$$f(x) = \sum_{n=1}^{\infty} a_n \cos\left(\frac{n\pi x}{L}\right) + b_n \sin\left(\frac{n\pi x}{L}\right), \tag{4.44}$$

with coefficients

$$a_0 = \frac{1}{L}\int_0^L f(x)dx; \tag{4.45}$$

$$a_n = \frac{2}{L}\int_0^L f(x)\cos\left(\frac{n\pi x}{L}\right)dx, \quad n \geq 1; \tag{4.46}$$

$$b_n = \frac{2}{L}\int_0^L f(x)\sin\left(\frac{n\pi x}{L}\right)dx \quad n \geq 0. \tag{4.47}$$

In this way, we can determine the dominant coefficients and periodicity of the solution by calculating the Fourier series coefficients. We observe the dominant coefficients and their corresponding simulations for the one diffusible species model in Fig. 4.4. The plots show the Fourier series coefficients, a_n, b_n, for increasing inhibitor diffusion parameter, d_w. The dominant coefficients give rise to the wavelengths, ω, in simulations. The predictions from the Fourier series analysis correspond to the aligned simulations.

Transitioning through values of d_w, it becomes difficult to determine the periodicity and wavelength of the solution even at small values of d_w, Fig 4.4(iii), since we have coefficient contributions over a large range. These contributions become increasingly spread incorporating more terms to determine a Fourier series approximation. This reinforces the previous suggestion that, as we consider increasing d_w values, the wavelength becomes difficult to predict and results in irregular wavelength patterns.

Observations of Patterns in Simulations

The simulations in the previous figures illustrate the diversity of the patterns that can be produced for either of the diffusivity scenarios studied. The two diffusible species model produces patterns with multiple cell contributions to peaks which depend on the wavelength of the pattern. As we have seen, these patterns are much more regular and ordered following the characteristic wavelengths that are synonymous with Turing systems. In contrast, for the one diffusible species model the patterns formed are generally less regular and result in peaks in receptor/ligand activity levels of single cell contributions, Fig. 4.4. Further to this, the inter-peak activity levels are approximately zero and therefore we observe distinct single cell peaks arising.

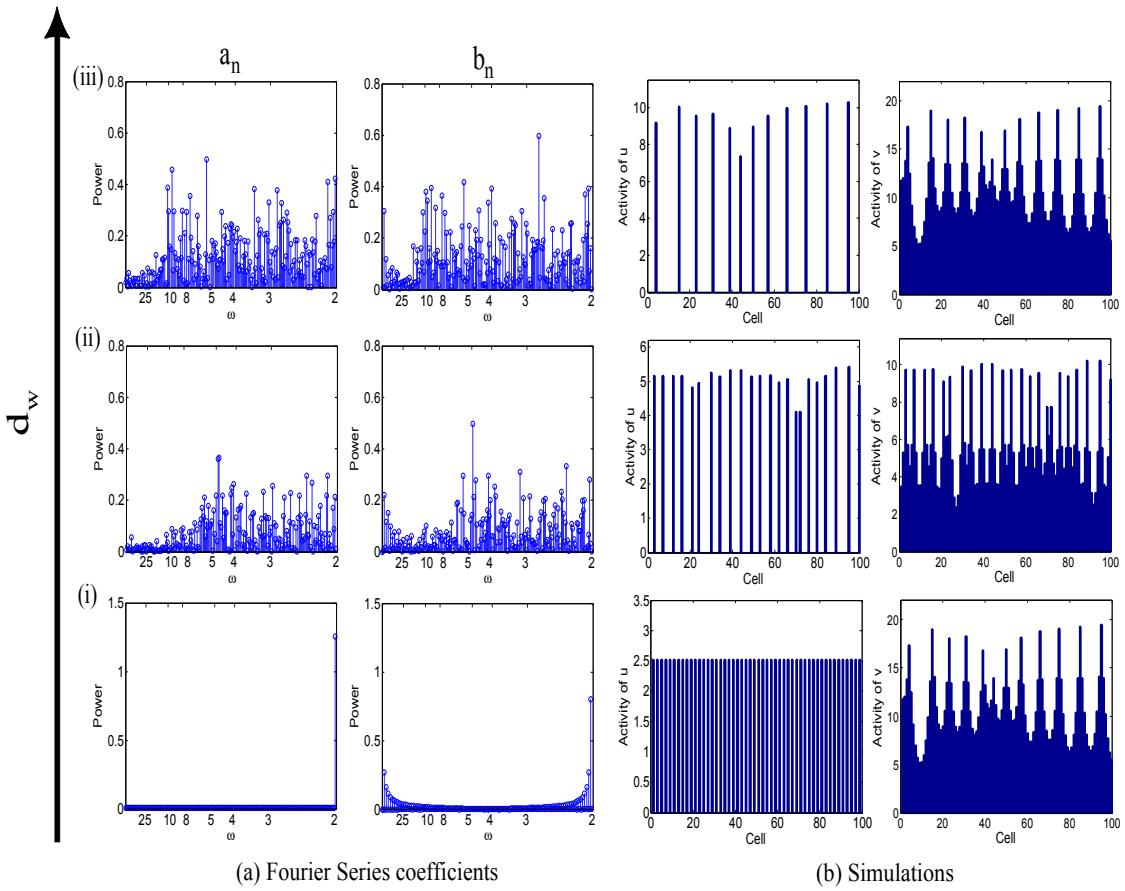

Figure 4.4: Plots of (a) Fourier series coefficients and (b) corresponding simulations. Here we show coefficients up to 200 terms for $\alpha = 0$, $d_u = 0$, $\delta_u = 0.5$ and for increasing d_w with (i) $d_w = 0.3$, (ii) $d_w = 2$, (iii) $d_w = 8$. The plots indicate greater contributions over a larger range of coefficients as d_w is increased.

A reason for this is that the self regulatory effect of autocrine signalling is amplifying differences in activity levels and producing the single cell amplification that we see in simulations. The arguments supporting this are (i) comparing different model simulations the discrete Turing system (considering receptor/ligand diffusion) results in a wider contribution of cells to both peaks and troughs, and (ii) inhibitor patterns, in both diffusivity cases, exhibit multiple cell contributions. Each of these suggests that the presence of diffusion is creating larger cell aggregations and, therefore, the single cell peak phenomena is as a result of short range autocrine signalling replacing diffusion. Furthermore, this may also suggest that autocrine signalling is being made largely redundant when diffusion is present.

4.3.2 Juxtacrine ($\alpha = 1$)

We refer to the Gierer-Meinhardt based model, (4.38)-(4.39), and set $\alpha = 1$ in the communication term. In this way, the signalling mechanism involves a receptor situated on the cell surface binding to a ligand on a neighbouring cell with the downstream effect being morphological changes to the receiving cell. Once again, we investigate how juxtacrine signalling mediates pattern formation by considering a model with either one ($d_u = 0$) or two ($d_u \neq 0$) diffusible species, analysing the wavelengths and pattern form in simulations.

Parameter Space Analysis

The distinct parameter regimes for the cases (a) $d_u \neq 0$ and (b) $d_u = 0$ are shown in Fig. 4.5.

These regions, although relatively unchanged from the autocrine case, are reduced in size. However, this does not really affect the overall choice of parameters that will lead to pattern formation unless there is a specific requirement to select parameter values near the d_w bifurcation points. Therefore, the model considering one diffusible species may offer greater robustness with regards to parameter selection.

Moreover, the consideration of a discrete model suggests that we can now obtain pattern formation by introducing a juxtacrine signalling mechanism together with at least one diffusible species.

Predicted Versus Actual Wavelength

Previous modelling of juxtacrine signalling predicts a variety of patterns in simulations - from fine grained patterns with lateral inhibition, [65], to longer wavelength patterns using lateral induction, [70]. As we have seen in the autocrine case, we can obtain a range of different wavelength patterns over the parameter space range. Similarly, we can produce a range of wavelength patterns in a model now considering juxtacrine

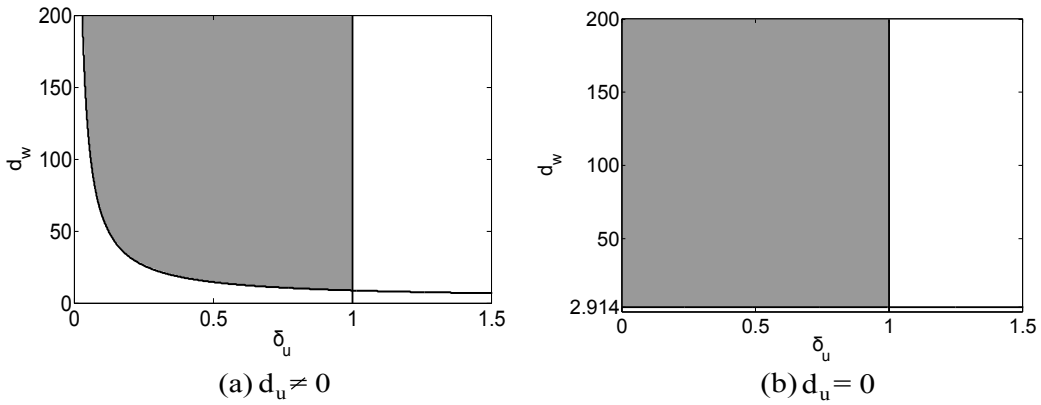

Figure 4.5: Comparison of the parameter space with (a) juxtacrine signalling and two diffusible species ($d_u = 1$) and (b) juxtacrine signalling and one diffusible species ($d_u = 0$). The grey regions indicate the choices of δ_u and d_w that will lead to pattern formation in simulations with the light grey corresponding to the constraints on the parameters, (4.40)-(4.42), with $\alpha = 1$.

signalling and one diffusible species, Fig. 4.6. We omit the details of patterns for the two diffusible species case since it remains unchanged from the autocrine case (see Fig. 4.2(a)).

We simulate the one diffusible species model over the parameter space range to observe the relationship between the predicted wavelength and simulated wavelengths. In doing so, transitioning through the δ_u range, Fig. 4.6(a)-(c), we notice that the simulated wavelengths are relatively unchanged and differ slightly from the predicted wavelength.

Numerical simulations for three seperate δ_u values with $d_w = 100$ and $n = 200$ cells show that the patterns formed are of a similar nature. This indicates a form of robustness since, regardless of the nondimensional δ_u values, the patterns are of similar wavelength. This suggests that we need only specify the nondimensional d_w value to generate a pattern of a particular wavelength. The range of wavelengths can be observed by choosing different diffusion coefficients and simulating the model for parameter sets over this d_w range, Fig. 4.6 (d), (e). The numerical simulations reinforce the predictions of longer wavelength patterns with increasing d_w. These ranging patterns illustrate the capabilities of the juxtacrine based model and how diverse patterns can be by scaling a single parameter.

Over the parameter space we can see that the model with one diffusible species is in closer agreement with the predicted wavelengths when juxtacrine signalling is present. However, there are small discrepencies in this predicted versus simulated wavelength and the irregularity in activity peak levels and wavelengths. Once again, the typical dispersion relation can infer this, Fig. 4.6(b). In this case, the one diffusible species model with juxtacrine signalling has a bounded region of unstable wavelengths that

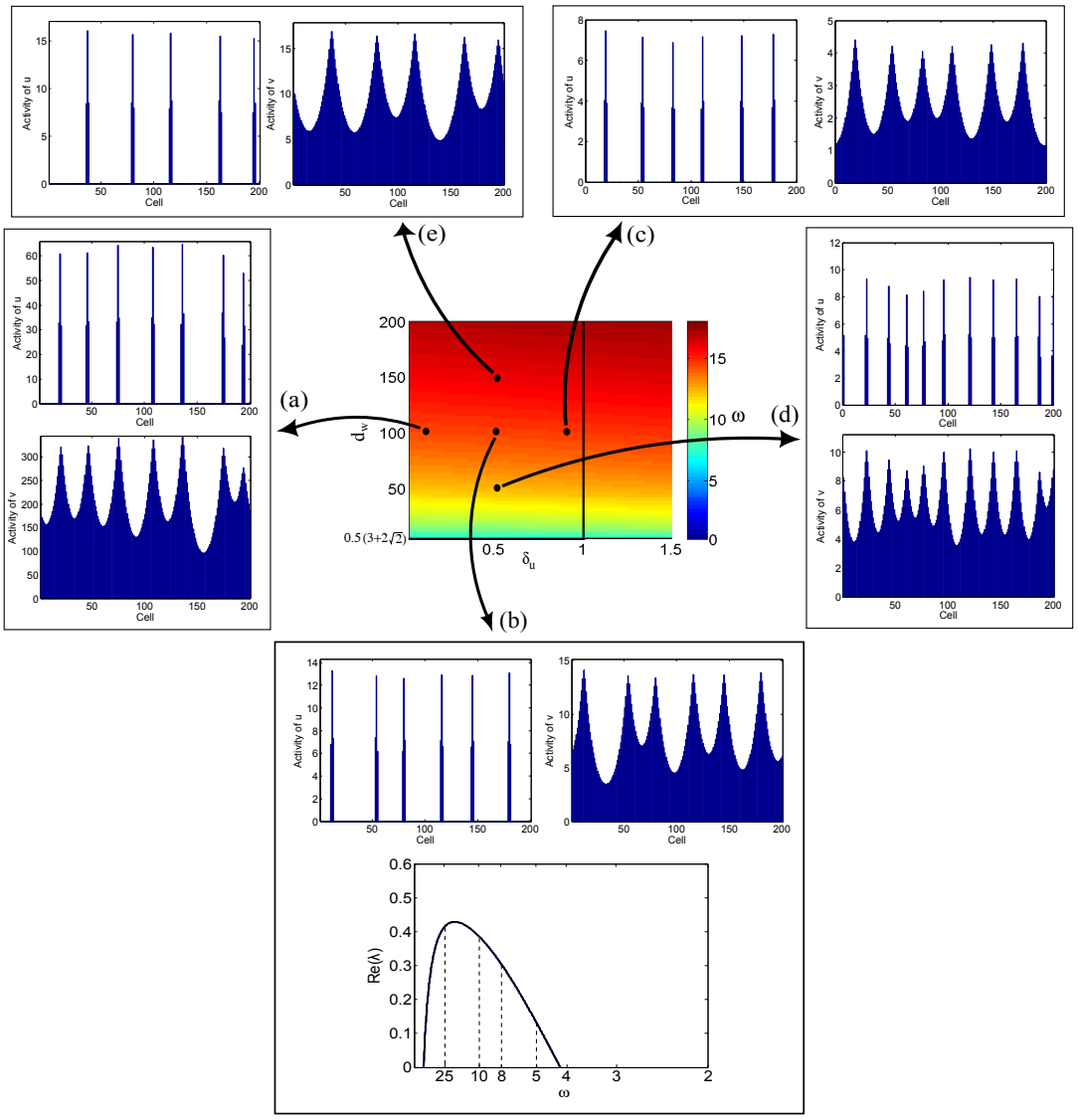

Figure 4.6: Plot of the parameter space for $d_u = 0$ with the superimposed colour scale indicating wavelengths corresponding to the maximum wavenumber. These wavelength predictions are reinforced with simulations over the parameter space range in both the vertical and horizontal directions: (a) $\delta_u = 0.1$, $d_w = 100$; (b) $\delta_u = 0.5$, $d_w = 100$; (c) $\delta_u = 0.9$, $d_w = 100$; (d) $\delta_u = 0.5$, $d_w = 50$; (e) $\delta_u = 0.5$ $d_w = 150$. In (b) the dispersion relation is also shown indicating the unstable wavelengths ($Re(\lambda) > 0$). This bounded form is typical across the parameter space and illustrates a dispersion relation with a smaller range of unstable wavelengths compared to the one diffusible species model with autocrine signalling.

is similar to the discrete Turing model. However, there are a larger set of unstable wavelengths from which to select and this suggests that competition between these leads to the small discrepencies between predicted and simulated wavelengths.

The Fourier series analysis supports this slight irregularity in activity since we see the inclusion of a number of terms in the Fourier series approximation when $d_u = 0$, Fig. 4.7. However, in comparison to the autocrine Fourier series analysis (Fig. 4.4) there are less contributing terms suggesting a more ordered solution with juxtacrine over autocrine. This overall suggests that local communication between the cells may act to 'regularise' patterning. The self regulation in autocrine signalling only permits self-amplification of activity in selected cells. Thus, the only mediation results from the longer range inhibitory effect in the population. In contrast, juxtacrine signalling accomodates some communication and transfer of information. The more ordered pattern suggests juxtacrine signalling may provide a more regular pattern, yet there is an overall reduced region of parameter selection.

Observations of Patterns in Simulations

As in the autocrine case, simulations reveal the diversity of patterns that can be produced. The two diffusible species model produces patterns that have characteristic wavelengths and multiple cell contributions to peaks. Here, the model is effectively of Turing type and the minor differences in results indicate this. This time, however, patterns formed for the one diffusible species model (diffusion replaced by short range activation via juxtacrine signalling) produces activated peaks featuring contributions from multiple cells, Fig. 4.6, 4.7. In particular, these appear to consist of $4 - 5$ cell contributions near bifurcation to three cell contributions as we move away from this. Inter-peak activity levels are approximately zero and therefore we observe distinct peaks arising in receptor/ligand simulations. In contrast to autocrine signalling, juxtacrine involves communication between neighbouring cells and, as a result, a suggested reason for the multiple cell contributions in peaks could be that the local signalling mechanism mediates the activity levels in the neighbouring cells, producing high single peaks with lower activity level peaks either side. Similarly to autocrine signalling, inhibitor activity peaks consist of contributions from a number of cells with decreasing activity levels as we move away from either side of a dominant cell exhibiting highest activity.

4.3.3 Autocrine + Juxtacrine ($\alpha \in (0\ 1)$)

The exact communication mechanism present within pattern formation systems remains unknown. However, a number of mechanisms have been suggested. The analysis so far suggests that the short range activation of an activator-inhibitor system

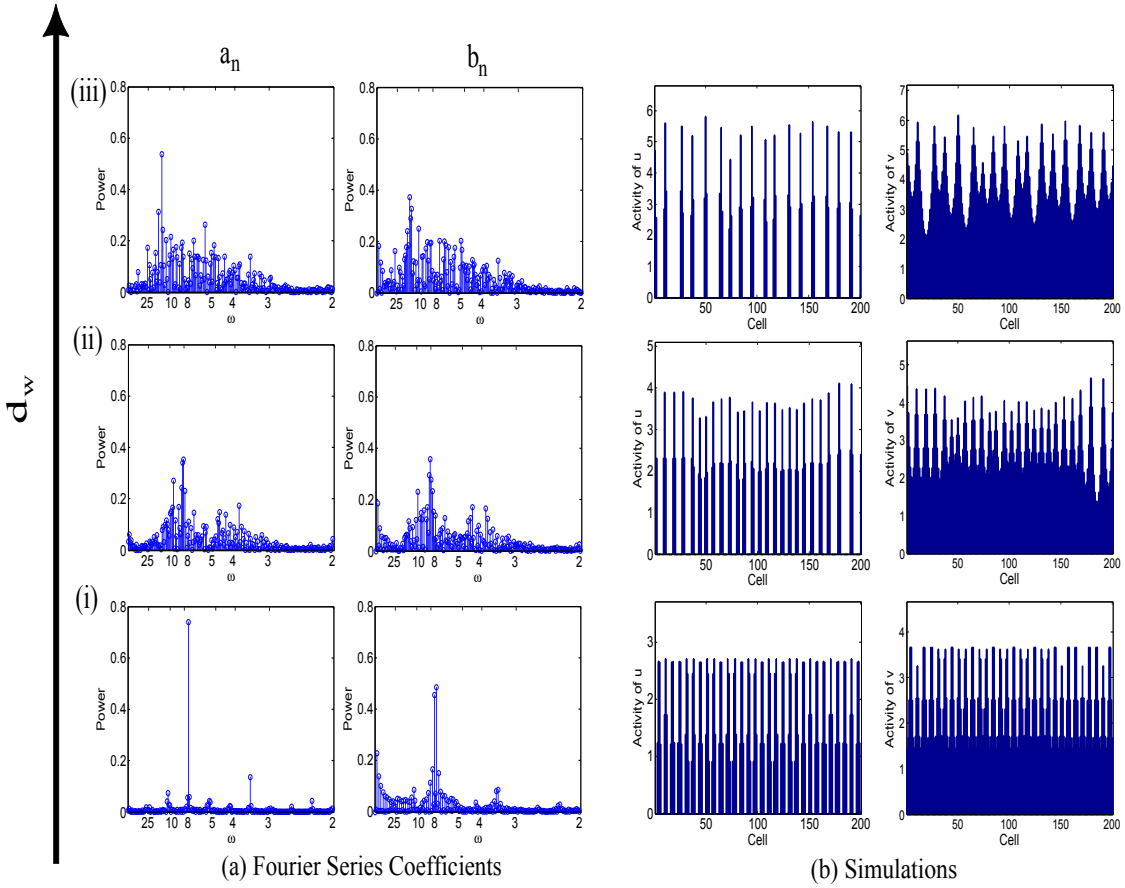

Figure 4.7: Plots of the coefficients in the fourier series with 200 terms. In this case, we consider $\alpha = 1$ and increasing d_w with $\delta_u = 0.5$, (a) fourier coefficients and (b) corresponding simulations with $d_u = 0$ and (i) $d_w = 3$, (ii) $d_w = 8$ (iii) $d_w = 20$.

can be replaced with either autocrine or juxtacrine mediated autocatalysis, with the resultant patterns at the scale of individual cells. Here we assume that two cell communication mechanisms, namely autocrine and juxtacrine signalling, are present within a system and seek to investigate the impact this joint effect has on pattern formation.

In this case, we consider the model given by (4.38)-(4.39) that incorporates both a local averaging term describing juxtacrine signalling and linear term describing autocrine signalling and investigate a combination of both signalling mechanisms by scaling the parameter $\alpha \in (0\ 1)$. This parameter will define the relative strength of each signalling mechanism. As can be seen from the equation, a value of $\alpha > 0.5$ corresponds to greater impact from juxtacrine signalling, with the reverse true for $\alpha < 0.5$. Clearly, $\alpha = 0.5$ corresponds to equal activity of autocrine and juxtacrine signalling. As before, both one ($d_u = 0$) and two ($d_u \neq 0$) diffusible species will be considered.

Parameter Space Analysis

Similar to the autocrine and juxtacrine specific cases we investigate the region where spatial pattern formation exists over both $\delta_u - d_w$ and $\alpha - d_w$ parameter space, Fig. 4.8. The latter allows an investigation into the possible parameter values that will lead to pattern formation for varying signalling strength α, whereas the former facilitates comparison to the earlier studies. As we transition from autocrine signalling ($\alpha = 0$) to juxtacrine signalling ($\alpha = 1$) we observe a decrease in the parameter regime (Fig. 4.8(a),(b)(i)) meaning a restriction in the size of d_w for patterning as the signalling strength parameter α is increased. However, this change is slight and only of concern under fine-tuning of parameters at low diffusion rates.

The parameter spaces in Fig. 4.8(a),(b)(ii) show the possible $\alpha - d_w$ parameter choices that will produce pattern formation in simulations. The different grey colours represent the appropriate conditions for pattern formation: light grey regions follow the 'standard' analysis ($d_u > 0$ or $d_u = 0$ & $\alpha \geq 0.5$) and darker grey regions ($d_u = 0$ & $0 \leq \alpha < 0.5$) require different conditions (see Appendix B.1 for details).

Investigation of Dispersion Relations

For two diffusible species, or one diffusible species with $\alpha > 0.5$, dispersion relations showing the unstable wavelengths feature a bounded region, similar to the standard continuous case. Moreover, with a bias towards juxtacrine signalling ($\alpha > 0.5$), in the absence of short range diffusion, the model is also capable of producing a bounded set of wavelengths. However, for $\alpha < 0.5$ a single root of $a_0(k)$ lies in the range $k \in [0\ \pi]$ and, as a result, we obtain only one root in the dispersion relation, Fig. 4.9.

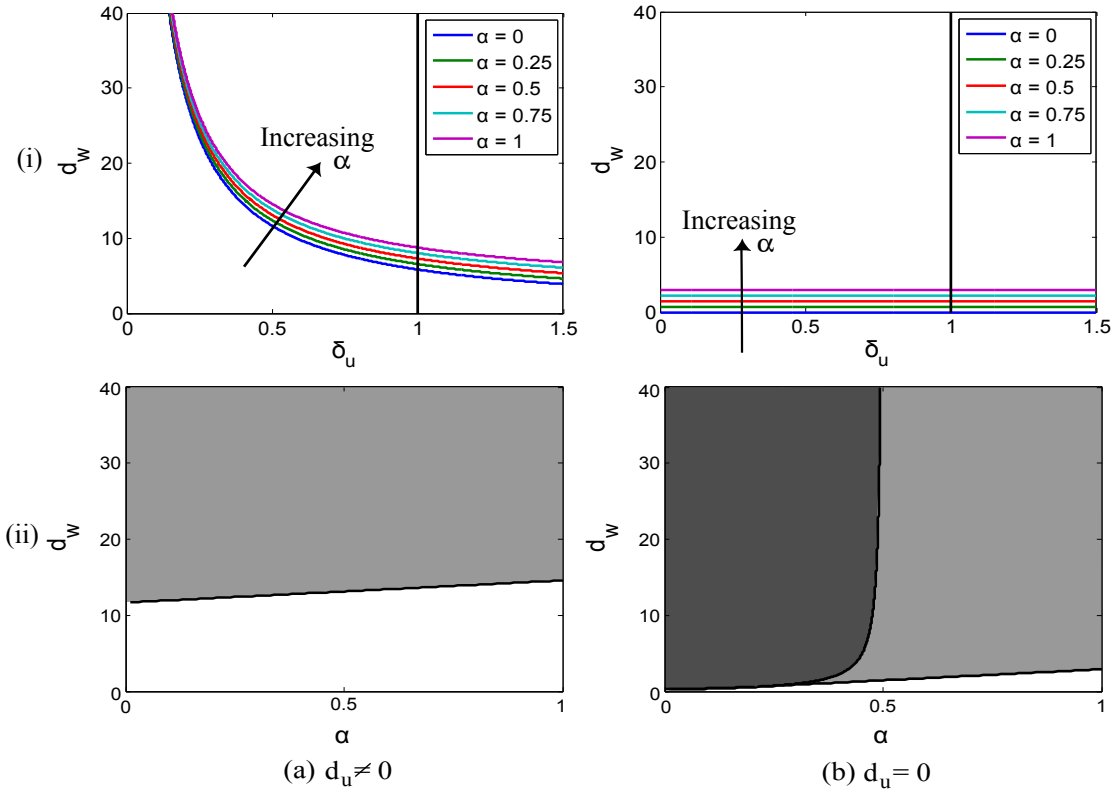

Figure 4.8: Plots of (i) $\delta_u - d_w$ and (ii) $\alpha - d_w$ parameter space in a model with (a) $d_u = 1$ and (b) $d_u = 0$. The plots in (a),(b)(i) indicate the parameter space for increasing α showing the parameter space for the previously distinct signalling mechanisms of autocrine ($\alpha = 0$) and juxtacrine ($\alpha = 1$). The $\alpha - d_w$ parameter spaces in Fig. (a)(b)(ii) illustrate the possible choice of α, d_w parameters that will lead to pattern formation when $\delta_u = 0.5$. These regions are indicated by light grey with the second of these figures (Fig. (b)(ii)) segmented into the two conditions that are required for pattern formation when $\alpha < 0.5$ and $\alpha > 0.5$ (see Appendix B.1)

.

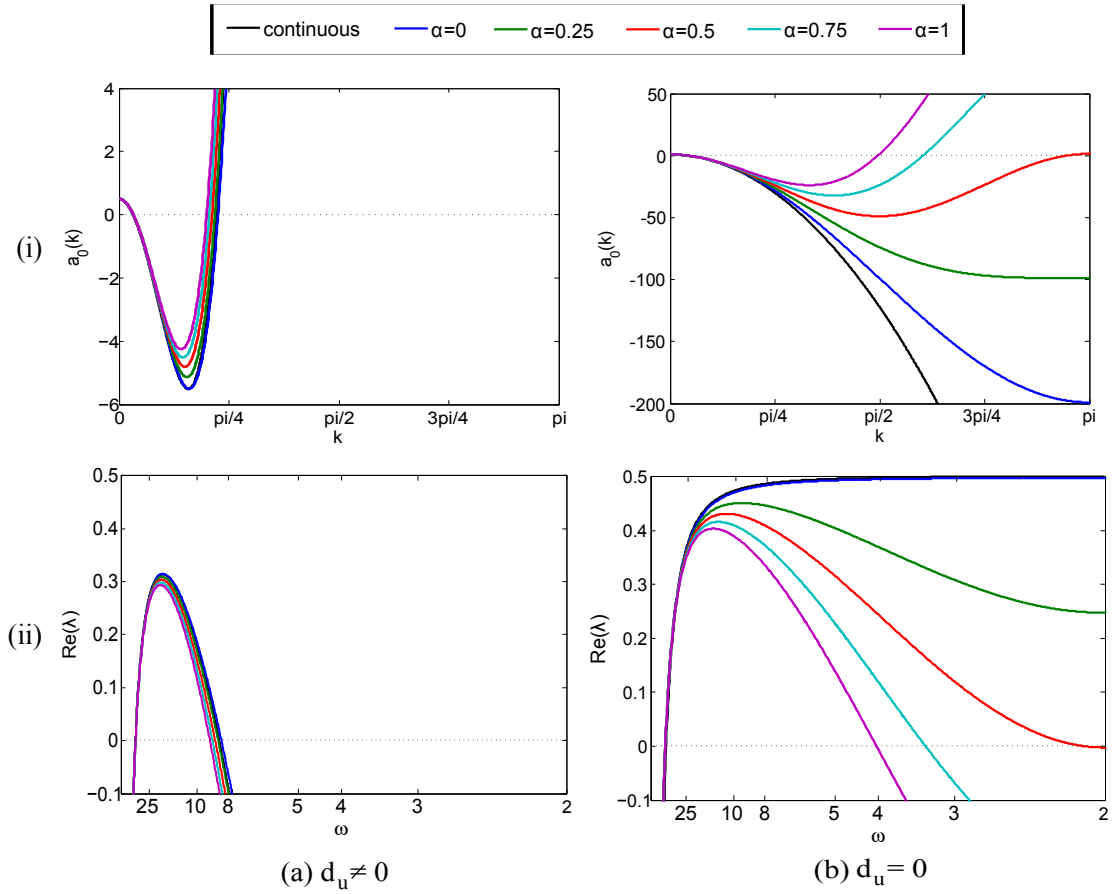

Figure 4.9: Plots of the (i) condition required for instability ($a_0(k) < 0$) and (ii) corresponding dispersion relations, in models with (a) two diffusible species ($d_u = 1$) and (b) one diffusible species ($d_u = 0$). The other parameters were chosen as $\delta_u = 0.5$, $d_w = 100$ with the same parameters chosen for the continuous case. Note that these are not directly comparable but are for illustration purposes.

From this we observe the relationship between the form of $a_0(k)$ and the dispersion relations for increasing α. For reference, the corresponding continuous models $a_0(k)$ and dispersion relation form is shown in black. The plots of the two diffusible species model, for various α, illustrate similar forms to the continuous case and result in two distinct roots with a bounded set of unstable wavenumbers, Fig. 4.9(a). Note that with autocrine signalling ($\alpha = 0$ resulting in discrete Turing form) the dispersion relations show near identical results to the continuous case.

However, with one diffusible species the continuous form of $a_0(k)$ shows a monotonic decrease. Moreover, the dispersion relation results in a single distinct root. Similarly, in the discrete system, $\alpha < 0.5$ results in a single distinct root but, in this case, the set of unstable wavenumbers are limited through the maximum relevant wavenumber for patterning, $k = \pi$, corresponding to a minimum wavelength of $\omega = 2$. Since this is not applicable in a continuous system, using the discrete framework provides a distinct advantage. In particular, the unbounded set of wavenumbers in the continuous case may lead to infinitesimal wavenumbers exhibiting 'salt and pepper' type patterning, [84].

As already discussed, the dispersion relation plots may suggest that closer agreement to wavelength predictions from the linear stability analysis are possible when there are two distinct roots. In this way, a bounded set of wavenumbers provides a restricted range of possible unstable wavelengths, Fig. 4.9(a)(ii). Typically, the mode with largest $Re(\lambda) > 0$ dominates. With few unstable modes this will be selected without much competition from other unstable modes. However, the selection of unstable modes in $d_u = 0$ scenarios admits greater competition from other wavenumbers. This would suggest a reason for the large range of coefficient contributions observed in the one diffusible autocrine/juxtacrine Fourier series analysis (see Fig. 4.4, 4.7) and also the pattern irregularity observed in these models.

Wavelength and Pattern Observations

The plots in Fig. 4.10, 4.11 show that a combination of both juxtacrine and autocrine signalling is also capable of producing a variety of wavelength patterns from fine grained patterns near bifurcation to longer range patterns further from this. Longer wavelength patterns can be obtained for high d_w values with the two diffusible species model and high d_w, δ_u values in the one diffusible species model. Fine grained patterns are observed with low d_w, δ_u. This suggests the models based on Gierer-Meinhardt kinetics are capable of producing patterns from the scale of insects to large animals, according to the mechanism of short range activation.

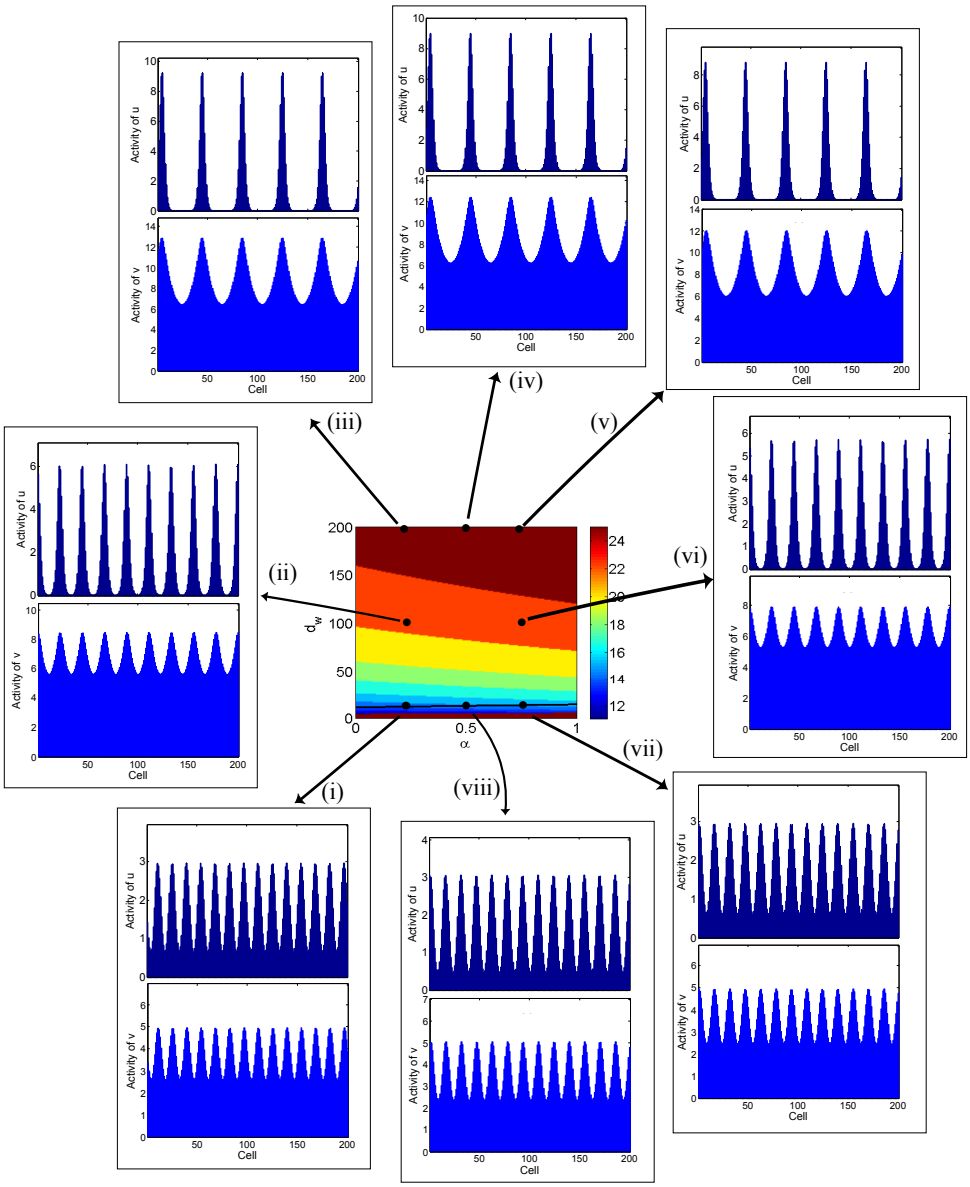

Figure 4.10: Plot of the expected wavelength over the parameter space for $d_u = 1$. The one dimensional simulations are shown to support the wavelength predictions from the linear stability analysis. The parameters are given as $\delta_u = 0.5$ and (i)-(iii) $\alpha = 0.25$ with $d_w = 13, 100, 200$, (iv) $\alpha = 0.5$, $d_w = 200$, (v)-(vii) $\alpha = 0.75$, $d_w = 200, 100, 15$, (viii) $\alpha = 0.5$, $d_w = 14$.

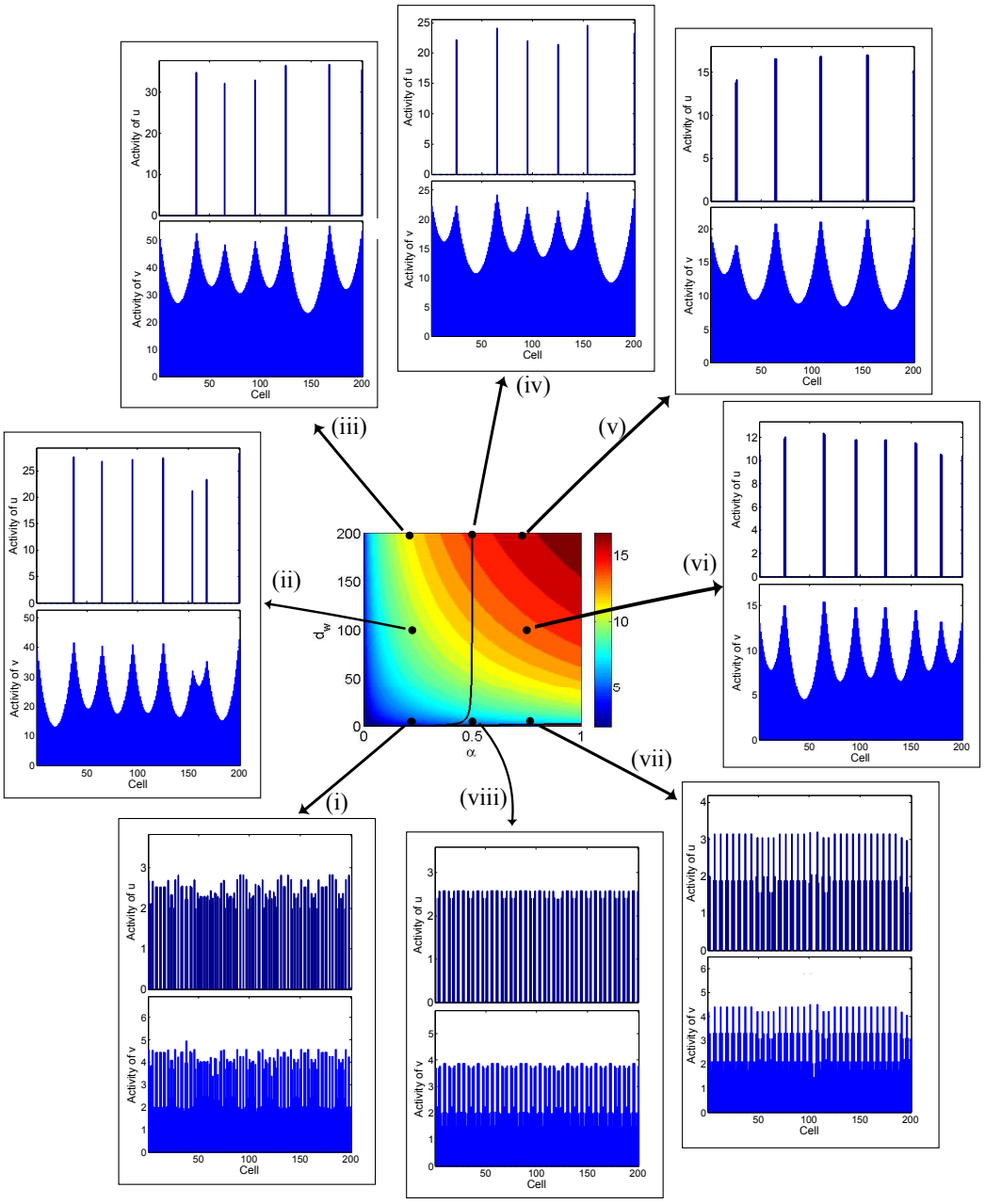

Figure 4.11: Plot of the expected wavelength over the parameter space for $d_u = 0$. The one dimensional simulations are shown to support the wavelength predictions from the linear stability analysis. The parameters are given as $\delta_u = 0.5$ and (i)-(iii) $\alpha = 0.25$ with $d_w = 1.5, 100, 200$, (iv) $\alpha = 0.5$, $d_w = 200$, (v)-(vii) $\alpha = 0.75$, $d_w = 200, 100, 2.5$, (viii) $\alpha = 0.5$, $d_w = 2$.

4.4 Analysis of Case Study II: Schnakenberg

We continue our investigation of the model by considering the conceptually different Schnakenberg kinetics. In this way, we will be able to investigate the model with comparisons to the classical activator-inhibitor approach but also observe whether the general results are consistent regardless of the precise kinetics. The model with Schnakenberg type kinetics is given by

$$\frac{du_j}{dt} = \beta + u_j\bar{u}_j w_j - u_j + d_u(u_{j+1} - 2u_j + u_{j-1}), \tag{4.48}$$

$$\frac{dw_j}{dt} = \rho - u_j\bar{u}_j w_j + d_w(w_{j+1} - 2w_j + w_{j-1}). \tag{4.49}$$

As before, we investigate mechanisms in which activator signalling is via autocrine, juxtacrine or diffusion. Similarly to the Gierer-Meinhardt based kinetics of the previous section, we investigate the pattern forming potential of the model. Specifically, we first undertake a linear stability analysis (details of this can be seen in Appendix B.2). From this, the conditions for pattern formation are given by:

$$(\beta+\rho)^2 - \frac{2\rho}{(\beta+\rho)} + 1 > 0; \tag{4.50}$$

$$-\left(\frac{\rho}{(\beta+\rho)} - 1\right)(\beta+\rho)^2 + (\beta+\rho)\rho > 0; \tag{4.51}$$

$$\left(\frac{\rho}{(\beta+\rho)} - 1\right)d_w + \frac{\rho K_c d_w}{(\beta+\rho)} - d_u(\beta+\rho)^2 > 0; \tag{4.52}$$

$$d_w > \frac{\left(\rho\alpha + 3d_u\rho + d_u\beta + \sqrt{(\rho^2\alpha^2 + 6d_u\rho^2\alpha + 2d_u\beta\rho\alpha + 8d_u^2\rho^2 + 8d_u^2\beta\rho)}\right)(\beta+\rho)^3}{(\beta^2+\rho^2-2\beta\rho)}, \tag{4.53}$$

where $K_c(k) = \alpha\cos(k) + (1-\alpha)$. The above conditions, (4.50)-(4.53), correspond to the 'standard' case when either $d_u > 0$ or $d_u = 0$ & $\alpha \geq 0.5$. However, together with (4.50)-(4.52), when $d_u = 0$ & $0 \leq \alpha < 0.5$ we require

$$d_w > \frac{(\beta^3 + 3\beta^2\rho + 3\beta\rho^2 + \rho^3)}{(4(\rho - \beta - 2\rho\alpha))}. \tag{4.54}$$

A simplification is achieved via the special case $\beta = 0$. Equations (4.50)-(4.54) reduce to

$$\rho > 1; \tag{4.55}$$

$$K_c d_w - d_u \rho^2 > 0; \tag{4.56}$$

$$d_w > \left(3d_u\rho + \rho\alpha + \sqrt{(8d_u^2\rho^2 + 6d_u\rho^2\alpha + \rho^2\alpha^2)}\right)\rho, \tag{4.57}$$

and, together with (4.55)-(4.56), when $d_u = 0$ & $0 \leq \alpha < 0.5$ we require

$$d_w > \frac{\rho^2}{4(1-2\alpha)}. \tag{4.58}$$

Similarly to the Gierer-Meinhardt analysis of the previous section, by solving (4.56) for k we obtain a bound on the wavenumber range: $k \in [0\ ,\ k_c]$ where $k_c = \cos^{-1}\left(\frac{(\alpha-1)d_w + d_u\rho^2}{d_w\alpha}\right)$. Therefore, the wavenumber range will vary depending on the parameter values. Moreover, we note that the conditions (4.55), (4.57) ($d_u > 0$ or $d_u = 0$ & $\alpha \geq 0.5$ case) and (4.55), (4.58) ($d_u = 0$ & $0 \leq \alpha < 0.5$ case) delimit the $\rho - d_w$ and $\alpha - d_w$ parameter spaces given in the analysis. The $\rho - d_w$, for $\alpha = 0, 0.25, 0.5, 0.75, 1$, and the $\alpha - d_w$ parameter space showing the possible parameter values that will lead to pattern formation can be seen in Fig. 4.12.

In figure 4.12(i) we observe a decrease in the $\rho - d_w$ parameter space when α is increased from $\alpha = 0$ (autocrine signalling) to $\alpha = 1$ (juxtacrine signalling). The intermediate values represent a combination of both signalling mechanisms and the plots indicate that we have a reduction in the choice of parameter values that give pattern formation when α is increased. However, in comparison to the two diffusible species model, the parameter space with one diffusible species admits a greater range of parameter values (compare Fig. 4.12(a) with (b)). In particular, for low d_w values there are now parameters that predict pattern formation that would not have done for the model with two diffusible species. This can be clearly seen when comparing the parameter spaces but is made more obvious by plotting the critical d_w values over α, Fig. 4.13. The red region indicates the choice of parameter values that lead to pattern formation in the one diffusible case but no patterning in the two diffusible case and these analytical results are reinforced through numerical simulations. For the same parameter sets, numerical solutions of the model with two diffusible species shows the decay of the random initial conditions to the homogeneous steady state.

These results suggest an expanded range for pattern formation and potentially greater robustness. Thus, we observe broadly consistent results between the two different kinetics suggesting that the phenomena observed is not kinetics dependent and the effects on the parameter space and patterns may be a general feature of the

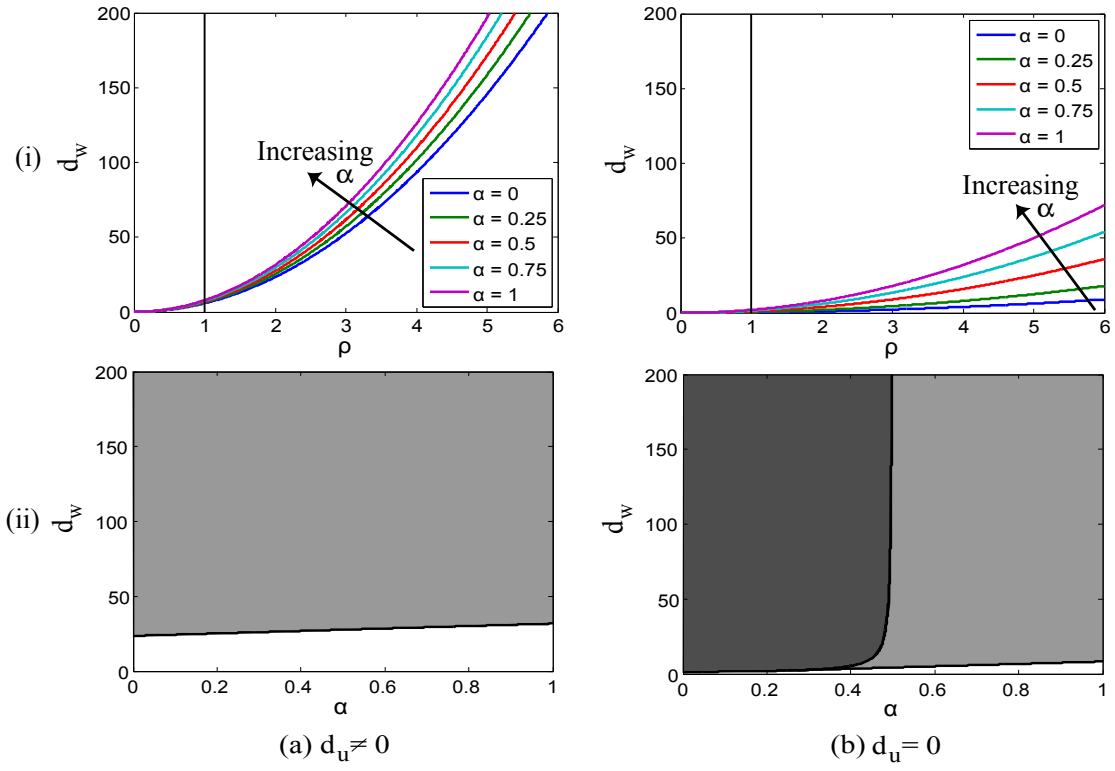

Figure 4.12: Plots of the parameter space and superimposed expected wavelength for increasing signalling parameter α with (a) $d_u = 1$, (b) $d_u = 0$. Here we show (i) $\rho - d_w$ parameter space, (ii) $\alpha - d_w$ parameter space and (iii) expected wavelength over the $d_w - \alpha$ parameter space range. Similarly to the Gierer-Meinhardt model, the parameter space in Fig. (b)(ii) is segemented into the appropriate cases required for pattern formation.

discrete signalling model.

Wavelength and Pattern Observations

Further to the consistency observed in the parameter space analysis, a model based on Schnakenberg type kinetics is also capable of producing a variety of wavelength patterns, Fig. 4.14. Similar wavelength patterns can be obtained in both systems and, as a result, this shows that the general system (independent of reaction kinetics) is capable of producing a wide range of patterns in simulations. Typical one dimensional simulations for the model considering two diffusible species ($d_u \neq 0$) and one diffusible species ($d_u = 0$) are given in Fig. 4.15 and 4.16 respectively. Apart from the one diffusible species model with autocrine signalling, the two models appear to approximately match the predicted wavelengths from the linear stability analysis (c.f. Fig. 4.14).

Once again, these results corroborate the earlier findings and indicate similarities in the general behaviour. In particular, the one diffusible species model exhibits single

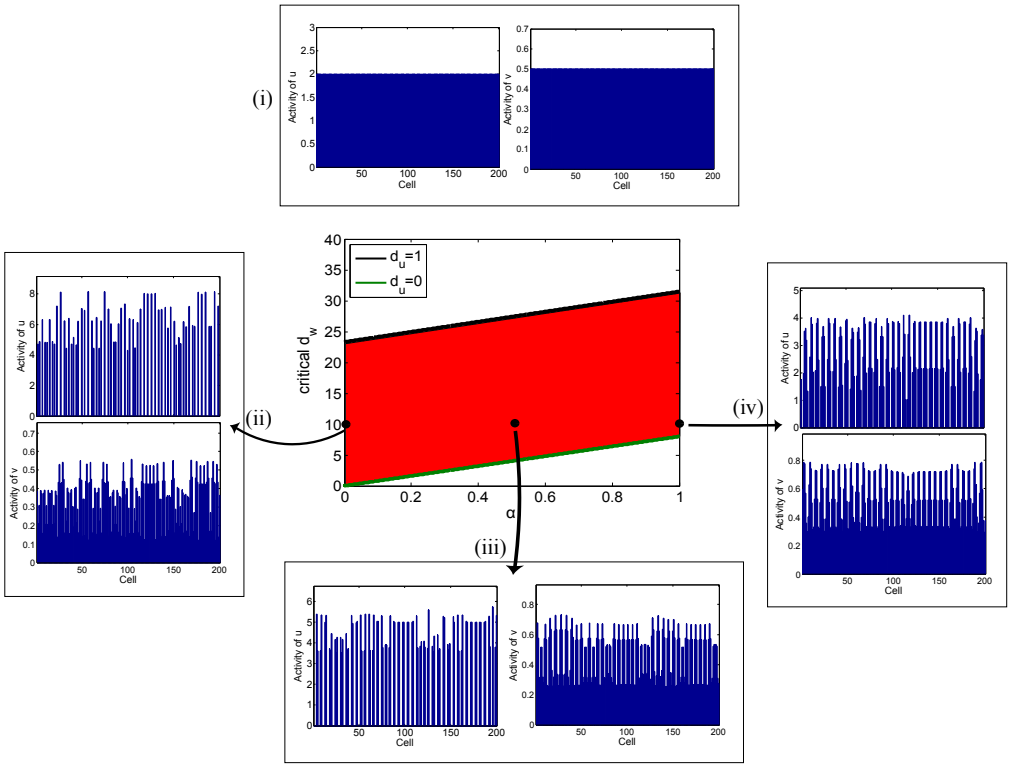

Figure 4.13: Plot of the comparitive critical $\alpha - d_w$ parameter space (centre) that give pattern formation for the two diffusible model (above black line) and one diffusible model (above green line). The red region indicates parameter values that suggest pattern formation in the one diffusible species model but not in the two diffusible species case. To illustrate this, numerical solutions of (i) the two diffusible case showing decay to the steady state and (ii)-(iv) the one diffusible model showing pattern formation with $\alpha = 0, 0.5, 1$ respectively are given. The other parameters are chosen as $\rho = 2$, $\beta = 0$, $d_u = 0$ and $d_w = 10$.

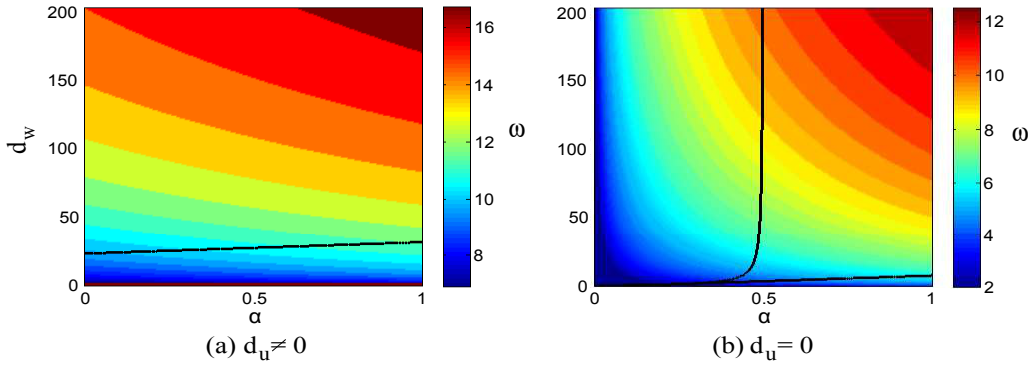

Figure 4.14: Plots of the expected wavelength over the $\alpha - d_w$ parameter space for increasing signalling parameter α with (a) $d_u = 1$, (b) $d_u = 0$. We see a range of predicted wavelengths for both the one and two diffusible species model. The other parameters are given as $\rho = 2$, $\beta = 0$.

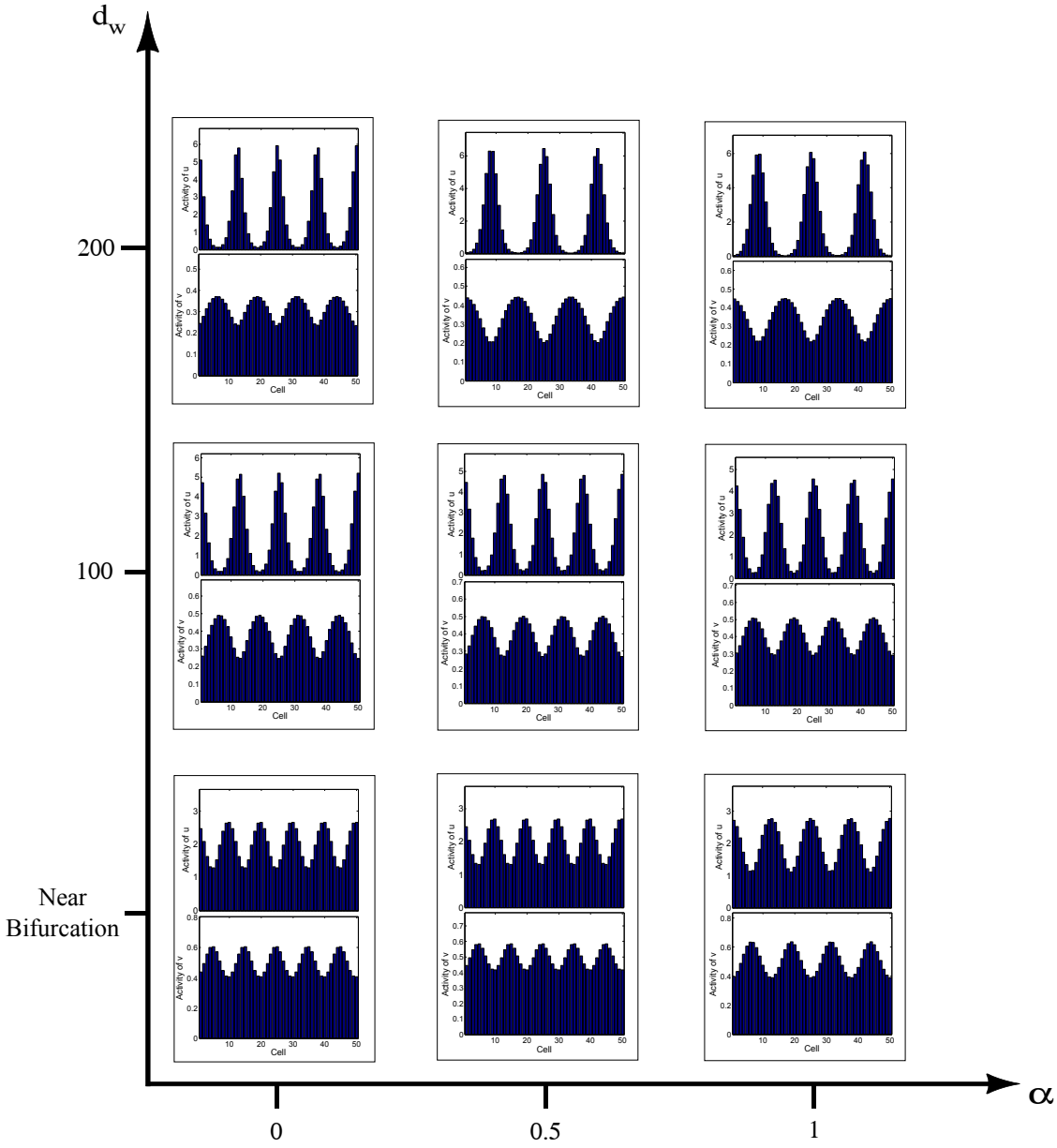

Figure 4.15: Numerical simulations of the discrete model with Schnakenberg type kinetics and two diffusible species for $\alpha = 0, 0.5, 1$ and d_w near bifurcation, $d_w = 100$ and $d_w = 200$. From this we can see the out-of-phase peaks and troughs in the activity levels of receptor/ligand (u) and inhibitor w. The other parameters are chosen as $\rho = 2$, $\beta = 0$ and $d_u = 1$.

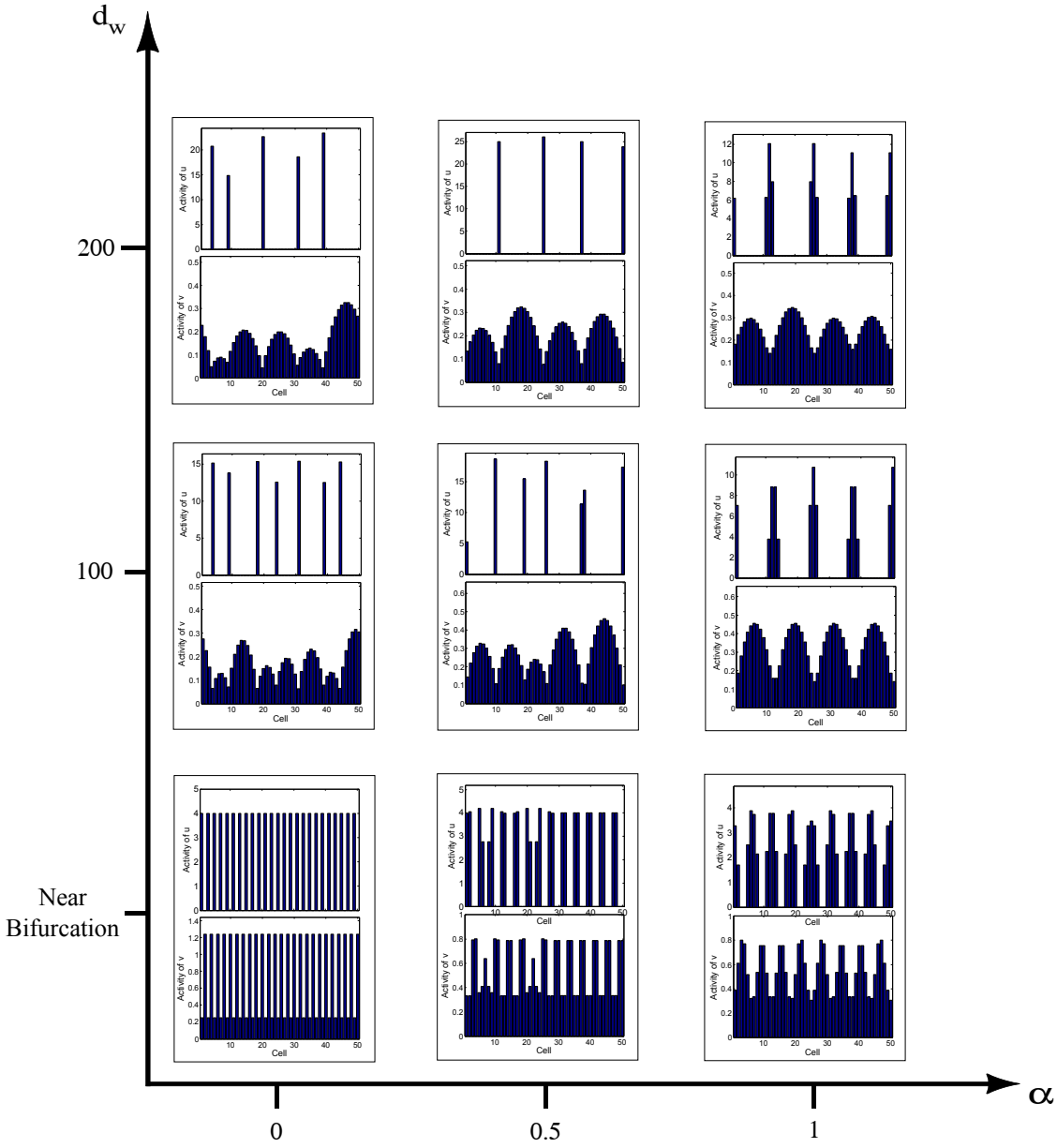

Figure 4.16: Numerical simulations of the discrete model with Schnakenberg type kinetics and one diffusible species for $\alpha = 0, 0.5, 1$ and d_w near bifurcation, $d_w = 100$ and $d_w = 200$. From this we can see the out-of-phase peaks and troughs in the activity levels of receptor/ligand (u) and inhibitor w. The other parameters are chosen as $\rho = 2$, $\beta = 0$ and $d_u = 0$.

cell to few cell peak patterns in receptor/ligand activity with increasing signalling parameter α, and larger numbers of cells contributing to inhibitor peaks.

Greater regularity is observed as we transition through α, with autocrine signalling ($\alpha = 0$) simulations showing irregular activity levels and wavelength compared with the ordered juxtacrine ($\alpha = 1$) simulations. Simulations of the two diffusible species model give regular solutions with peak contributions from multiple cells. The main differences arise through the in-phase/out-of-phase activity peaks.

4.5 A Detailed Numerical Investigation

In the previous sections we explored dynamics of the two species model predicted by a linear stability analysis. In doing so, we used one dimensional simulations to support the results in the context of a line of cells. A natural extension, particularly relevant to biological pattern formation, is to consider two dimensional dynamics.

In this section, we also consider domains composed of cells arranged on either a square or hexagonal lattice. Finally, the full three species system with Gierer-Meinhardt type kinetics, given in Chapter 3: (3.22)-(3.24), is analysed generally and also used to determine the validity of the reduction assumptions, §4.7.

4.5.1 Multi-Dimensional General Model

As discussed in Chapter 3 §3.2, the consideration of multi-dimensional domains involves the implementation of different terms describing diffusion. However, here we consider terms describing both diffusion and signalling. As a reminder, we refer to the model in its most general form:

$$\frac{d\mathbf{W}_p}{dt} = \mathbf{F}(\mathbf{W}_p, \bar{\mathbf{W}}_p) + D_W \Delta \mathbf{W}_p \tag{4.59}$$

where $\mathbf{W}_p$ is a vector of variables at cell p and D_W is the matrix of diffusion rates. Here, $\bar{\mathbf{W}}_p$ and $\Delta \mathbf{W}_p$ are the diffusion and communication terms and are implemented according to

Communication Term ($\bar{\mathbf{W}}_j$)

$$\text{1D:} \quad \frac{\alpha_W}{2}(\mathbf{W}_{j+1} + \mathbf{W}_{j-1}) + (1 - \alpha_W)\mathbf{W}_j, \tag{4.60}$$

$$\text{2D SQUARE:} \quad \frac{\alpha_W}{4}(\mathbf{W}_{j,l+1} + \mathbf{W}_{j+1,l} + \mathbf{W}_{j,l-1} + \mathbf{W}_{j-1,l}) + (1 - \alpha_W)\mathbf{W}_{j,l}, \tag{4.61}$$

$$\text{2D HEXAGON:} \quad \frac{\alpha_W}{6}(\mathbf{W}_{j,l+1} + \mathbf{W}_{j+1,l+1} + \mathbf{W}_{j+1,l} + \mathbf{W}_{j,l-1} + \mathbf{W}_{j-1,l-1} + \mathbf{W}_{j-1,l}) + (1 - \alpha_W)\mathbf{W}_{j,l}, \tag{4.62}$$

where α_W is a vector of signalling parameters that can take the value,

$$\alpha_W \begin{cases} = 0 & \text{Autocrine Signalling} \\ \in (0\ \ 1) & \text{Autocrine + Juxtacrine} \\ = 1 & \text{Juxtacrine Signalling.} \end{cases} \tag{4.63}$$

Diffusion Term ($\Delta\mathbf{W}_p$)

$$\text{1D:} \quad \mathbf{W}_{j+1} + \mathbf{W}_{j-1} - 2\mathbf{W}_j, \tag{4.64}$$

$$\text{2D SQUARE:} \quad \mathbf{W}_{j,l+1} + \mathbf{W}_{j+1,l} + \mathbf{W}_{j,l-1} + \mathbf{W}_{j-1,l} - 4\mathbf{W}_{j,l}, \tag{4.65}$$

$$\text{2D HEXAGON:} \quad \mathbf{W}_{j,l+1} + \mathbf{W}_{j+1,l+1} + \mathbf{W}_{j+1,l} + \mathbf{W}_{j,l-1} + \mathbf{W}_{j-1,l-1} + \mathbf{W}_{j-1,l} - 6\mathbf{W}_{j,l}. \tag{4.66}$$

In this way, we consider domains consisting of a line of cells with cell j and neighbouring cells $j \pm 1$, square cells with each cell j, l surrounded by four other cells, $j \pm 1, l$ and $j, l \pm 1$, and hexagonal cells with cell j, l surrounded by six cells, (see Fig. 3.5). Although still a simplification of cell geometries, the latter obviously offers greatest applicability to biology.

4.6 Numerical Analysis of Reduced Models (Two Species)

4.6.1 Case Study I: Gierer-Meinhardt

As a reminder, the nondimensionalised two species model with Gierer-Meinhardt kinetics is given by

$$\frac{du_p}{dt} = \frac{u_j \bar{u}_p}{v_p} - \delta_u u_p + d_u \Delta u_p \tag{4.67}$$

$$\frac{dw_p}{dt} = u_p^2 - w_p + d_w \Delta w_p \tag{4.68}$$

where u_p, w_p denote the receptor/ligand and inhibitor activities at cell p, the communication term, $\bar{u}_p$, and diffusion terms, Δu_p and Δw_p, similarly follow the general model framework given in (4.60)-(4.66), and d_u, d_w, δ_u are all positive parameters.

To focus our simulations we consider a parameterised set as follows. Firstly, we set the time, t, to be on the scale of hours and set the inhibitor decay to be $k_6 = 0.7$/hr, [see [67] and references therein]. This would imply an inhibitor half-life of approximately one hour. Moreover, we set the inhibitor diffusion to be $D_B \sim 40$/hr ($d_w = \frac{D_B}{k_6} = 60$) corresponding to diffusion coefficients in the continuous case of the order $D_B \sim 10^{-8}$ cm^2/s (see for example EGF diffusion in rats, [106]). These calculations are based on an average cell diameter of 10μm. Using these parameters, we are now in a position to track the pattern over time periods and view snapshots of the evolving pattern for certain timeframes. In the two dimensional simulations consisting of square cells we consider a 200x200 domain and simulate the model up to $t = 48$ hrs. The two dimensional simulations with hexagonal cells focus on a smaller 50x50 domain. Similarly to the simulations of the previous sections, the models are numerically solved for an initial activity level given by a 2 % random perturbation to the homogeneous steady state and the boundary conditions are periodic. Details of the numerical methods can be seen in Appendix C.2.

Temporal Evolution of Pattern

Here, we consider snapshots of the pattern for increasing time points $t = 12$, 18, 24, 36 and 48 hours. Firstly, in the simulations of the one diffusible species model, Fig. 4.17(ii), we notice amplifications in activity levels at 18 hours with the refinement of the pattern seen at subsequent time points. This amplification is more apparent when considering autocrine signalling. Here, cells self-activate without any interaction with surrounding cells and, as a result, time delays resulting from interactions may be reduced. For example, juxtacrine signalling will involve interactions with surrounding

cells and this signalling may increase the time of pattern development. Further to this, we note that the differences between 36 and 48 hour simulations appear slight in this model, suggesting that the pattern has almost evolved by 36 hours.

In contrast, the two diffusible species model shows no significant amplification until 36 hours, Fig. 4.17(i). Supposing cell differentiation corresponds to high activity levels, it may be possible to determine the differentiated cells earlier in the pattern formation of the one diffusible species model than in the two diffusible species case. Moreover, this suggests that short range activation driven by diffusion is slowing pattern formation.

Overall, each of the simulated patterns over a much longer time period, do not differ greatly from the patterns formed after 48 hrs. Therefore, with these parameters the pattern appears to be sufficiently formed in both models to determine patterning by this time.

Pattern Observations Over Time

As discussed in the previous chapter, in a model with two diffusible species and an autocrine/juxtacrine signalling mechanism, Fig. 4.17(i), we observe peaks and troughs in activity levels involving multiple cells contributing to peaks. Furthermore, these patterns show an ordered solution with a characteristic wavelength beginning to appear as time progresses. Simulations of the one diffusible species model shows a less regular pattern, Fig. 4.17(ii), with single to few cell peaks arising, according to the signalling parameter, α.

With autocrine signalling, single cell peaks arise early in pattern development with a refinement over time. Patterns with few cell peaks are evident with juxtacrine signalling. Therefore, the number of cell numbers contributing to peaks appear to depend on the signalling mechanism present. Autocrine signalling amplifies differences in activity levels individually with no communication with surrounding cells. In contrast, juxtacrine signalling involves near neighbour communication with adjacent cells. As a result, this would suggest that the independence of autocrine signalling leads to single cell peaks and the regulation occuring in juxtacrine permits activity levels to be spread between a cluster.

Two Dimensional Domains

The two dimensional simulations show the activity levels of receptor/ligand and inhibitor as indicated by the colorbar. Here, Fig. 4.18 illustrates the patterns formed after 48 hours from a model involving pure Gierer-Meinhardt type kinetics with autocrine, autocrine and juxtacrine, and juxtacrine signalling mechanisms. Once again, we consider both the two, Fig. 4.18(a), and one, Fig. 4.18(b), diffusible species cases.

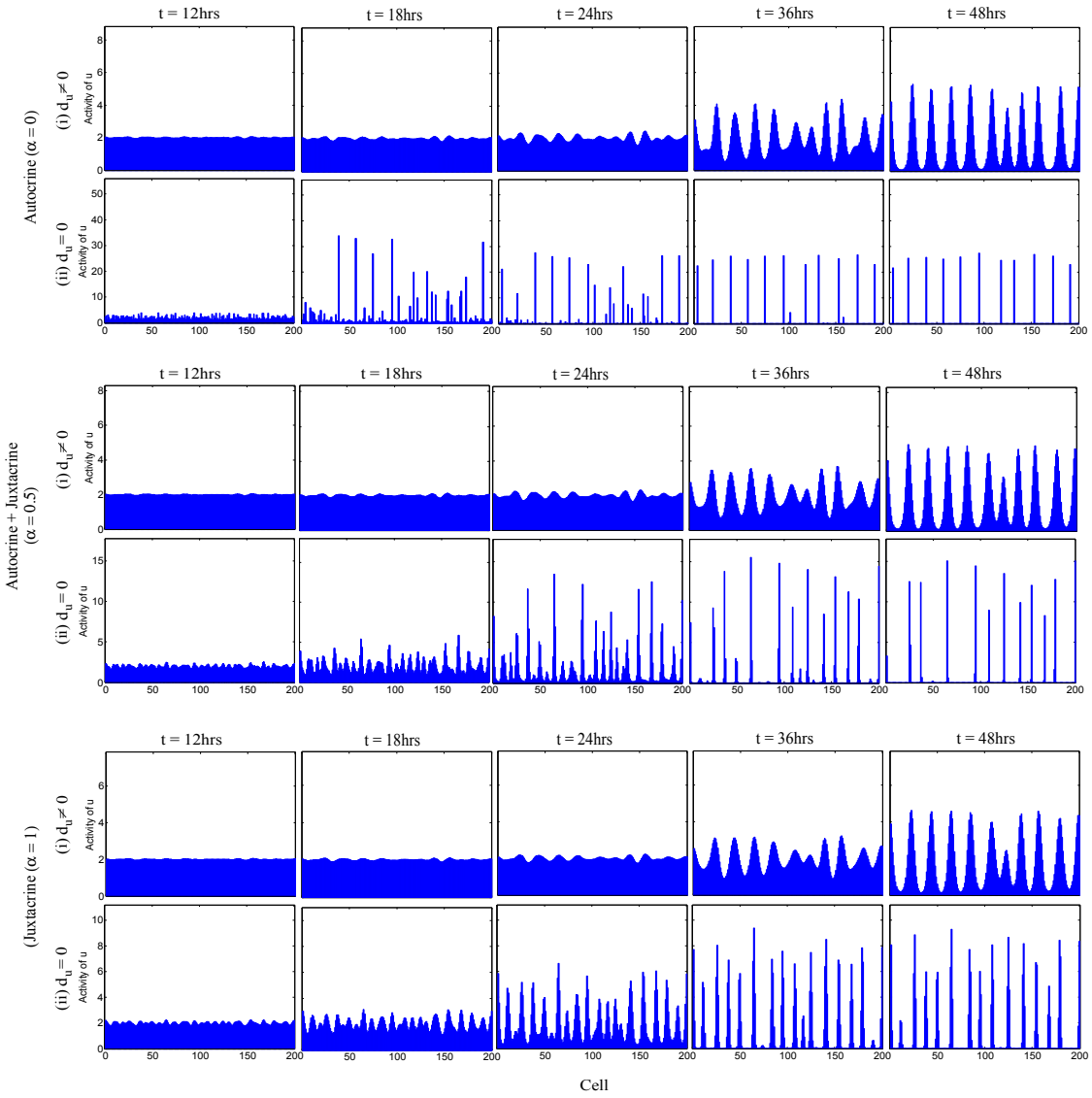

Figure 4.17: Snapshots in time ($t = 12, 18, 24, 36, 48$hrs) for simulations of the Gierer-Mienhardt model considering autocrine signalling ($\alpha = 0$), juxtacrine signalling ($\alpha = 1$) and a combination of both ($\alpha = 0.5$) with (a) $d_u = 1$ and (b) $d_u = 0$. The other parameters are $\delta_u = 0.5$, $d_w = 60$.

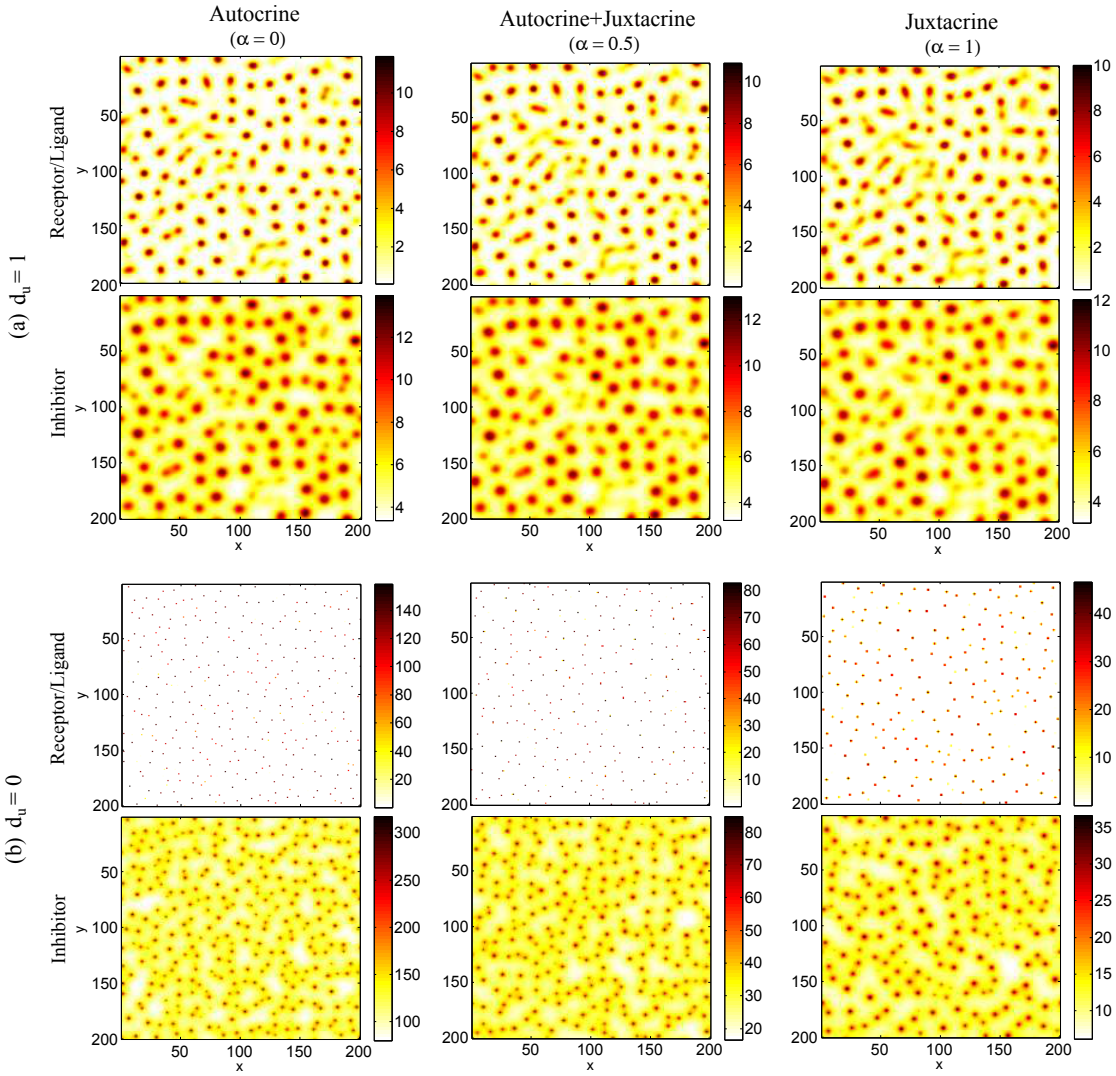

Figure 4.18: Two dimensional simulations with square cells for a model with Gierer-Meinhardt kinetics. The simulations are given on a 200x200 grid at $t = 48$ hrs and show both the (a) two ($d_u = 1$) diffusible and (b) one ($d_u = 0$) diffusible cases with autocrine ($\alpha = 0$), juxtacrine ($\alpha = 1$) and a combination of the two signalling mechanisms ($\alpha = 0.5$). Spot patterns are produced in each case with varying spot size depending on the number of diffusible species. The other parameters were chosen as $\delta_u = 0.5$, $d_w = 60$.

From these figures we observe spot patterns involving in-phase peaks and troughs of receptor/ligand and inhibitor levels. In comparison to the one and two diffusible species simulations, larger spots are visible when both species diffuse with the appearance of single to few cell peaks in receptor/ligand activity levels when only inhibitor diffuses. These results support the observations of the one dimensional simulations.

These signalling dependent characteristics are clearly seen in the 50x50 domain consisting of hexagonal cells, Fig. 4.19. However, in both receptor/ligand and inhibitor simulations of the two diffusible species system, central cells within peaks are surrounded by a ring of cells with lower activity levels. This phenomena has been observed in applications such as neuromast development in the mechanosensory system of fish and amphibians, [107]. Within this, a group of cells are surrounded by supporting cells and, assuming cell differentiation corresponds to activity levels, the medium levels surrounding high activity cells may account for the neuromast ring.

The simulations of the different models and, in particular, the specific mechanism of short range activation within the system illustrates the diversity and capabilities of the model. Together with neuromast development, the results of the different combinations show an applicability to a variety of biological systems such as drosophila patterning, mouse follicle development and chick placode formation. We discuss these applications in more detail in §4.8.

4.6.2 Case Study II: Schnakenberg

The analysis of §4.4 showed broadly consistent results when considering the two conceptually different reaction kinetics. Here, we briefly discuss the numerical results of the model with Schnakenberg kinetics to see if this continues. Similarly to the previous section we undertake a one dimensional analysis into the timeframes required for pattern formation and investigate the two dimensional results with focus on the pattern formation that arises.

Model and Parameterisation

As a reminder, the two species model with nondimensionalised Schnakenberg kinetics is given by

$$\frac{du_p}{dt} = \beta + u_p\bar{u}_p w_p - u_p + d_u \Delta u_p \tag{4.69}$$

$$\frac{dw_p}{dt} = \rho - u_p\bar{u}_p w_p + d_w \Delta w_p \tag{4.70}$$

where u_p, w_p denote the receptor/ligand and inhibitor activities at cell p, the communication term, $\bar{u}_p$, and diffusion terms, Δu_p and Δw_p, respectively follow the general

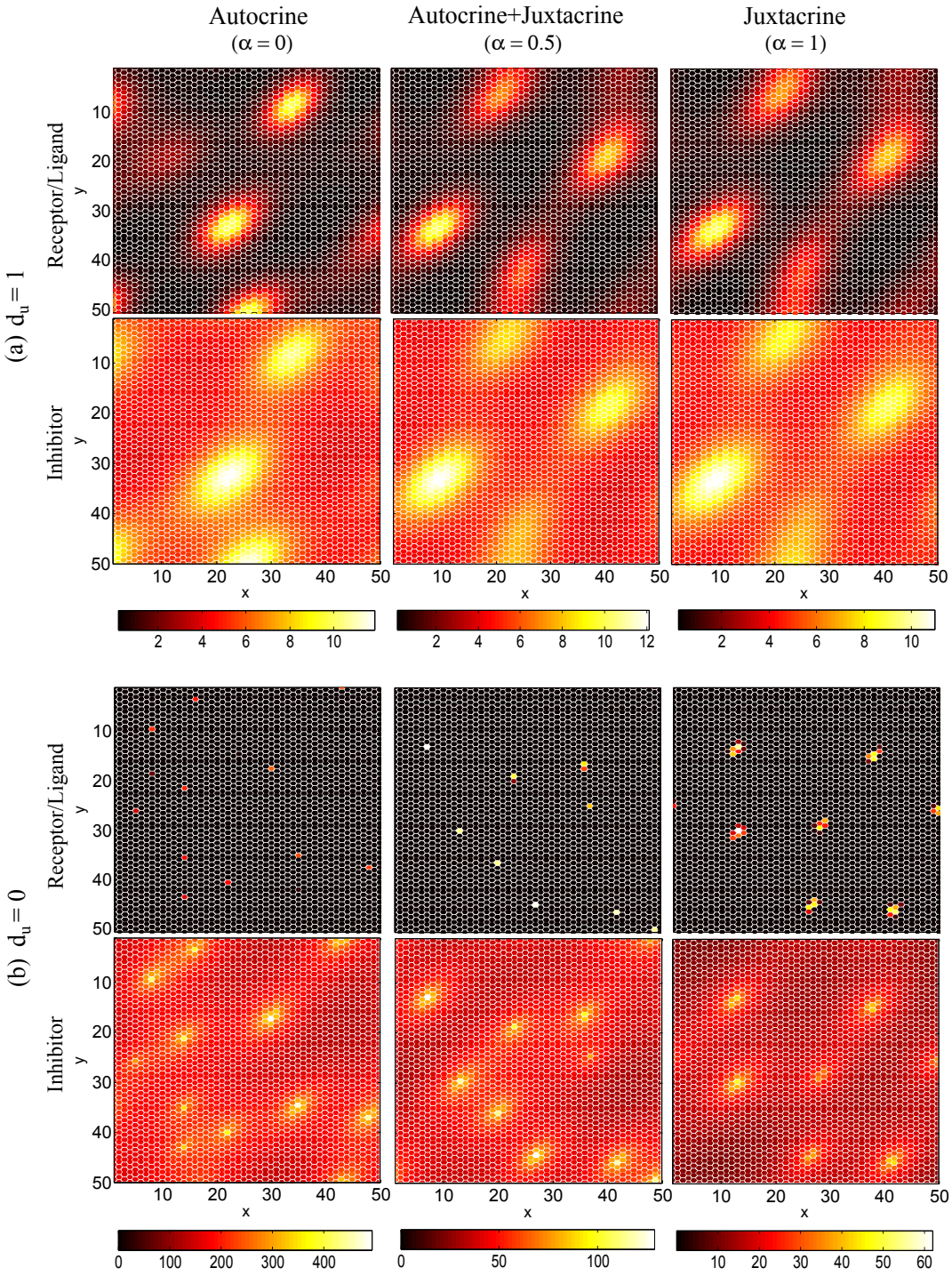

Figure 4.19: Two dimensional simulations with hexagonal cells for a model with Gierer-Meinhardt kinetics. The simulations are given on a 50x50 grid at $t = 48$ hrs and show both the (a) two ($d_u = 1$) diffusible and (b) one ($d_u = 0$) diffusible cases with autocrine ($\alpha = 0$), juxtacrine ($\alpha = 1$) and a combination of the two signalling mechanisms ($\alpha = 0.5$). Spot patterns are produced in each case with varying spot size depending on the number of diffusible species. The other parameters were chosen as $\delta_u = 0.5$, $d_w = 60$.

multi-dimensional model framework in §4.5.1, and d_u, d_w, ρ, β are all positive parameters.

The parameters used in the simulations are given by similar values to the Gierer-Meinhardt investigation (see §4.6.1). However, this time we set the receptor decay to be approximately one hour ($k_3 = 0.7$).

Temporal Evolution and Observations of Patterning

Once again, by considering both one ($d_u = 0$) and two ($d_u \neq 0$) diffusible species we can simulate the model over specific timeframes and investigate the temporal evolution of patterning for a model with cross type kinetics, Fig. 4.20.

Despite the phase differences, the patterns that arise from cross kinetics show largely consistent results with the Gierer-Meinhardt (pure) scheme. In particular, the patterns are generated within the 48 hour timeframe with significant amplitude changes observed earlier in the development of the one diffusible species model compared to the two diffusible species system. Moreover, we see similar cell numbers contributing to activity peaks: the two diffusible species model produces patterns with multiple cell peaks and a model with one diffusible species shows single to few cell peaks, according to the signalling mechanism.

The two dimensional simulations also show broadly consistent results, Fig. 4.21. The patterns generated are at 48 hours and from these cells with high receptor/ligand activity arise in spot patterns. The intricate detail of the spots can be clearly seen in Fig. 4.22, which considers a 50x50 domain with hexagonal cells. Once again, compared to the one diffusible species system, a larger number of cells with high receptor/ligand activity are apparent and a surrounding ring of cells with lower activity is also visible.

To summarise, the results of the Schnakenberg model show consistent general results to the Gierer-Meinhardt kinetics. Therefore, this suggests that the results of the model are independent of reaction kinetics and are a general feature of the modelling framework.

4.7 Investigation of the Full Three Species Model

The three species discrete model, based on the classical activator-inhibitor system, considers a more detailed approach to the continuous system. In doing so, it splits the autocatalytic reaction of the activator into a receptor-ligand binding process in the presence of an inhibitor. In this way, cell signalling interactions can be investigated to determine their significance in pattern formation. The details of the system and proposed kinetics can be seen in Chapter 3 but, as a reminder, the non-dimensionalised

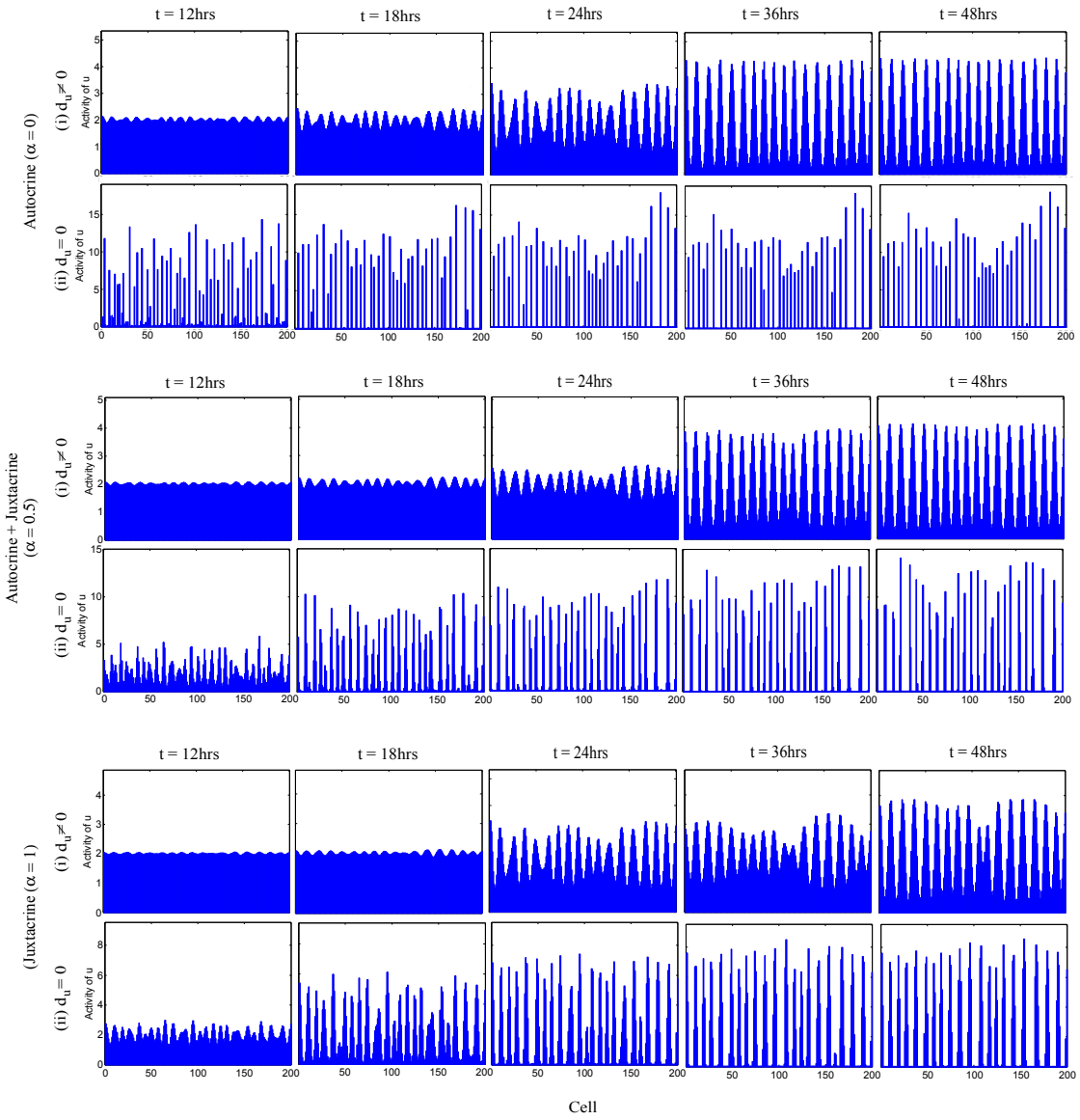

Figure 4.20: Snapshots in time ($t = 12, 18, 24, 36, 48$hrs) for simulations of the Schnakenberg model considering autocrine signalling ($\alpha = 0$), juxtacrine signalling ($\alpha = 1$) and a combination of both ($\alpha = 0.5$) with (a) $d_u = 1$ and (b) $d_u = 0$. The other parameters are $d_w = 60$, $\beta = 0$, $\rho = 2$.

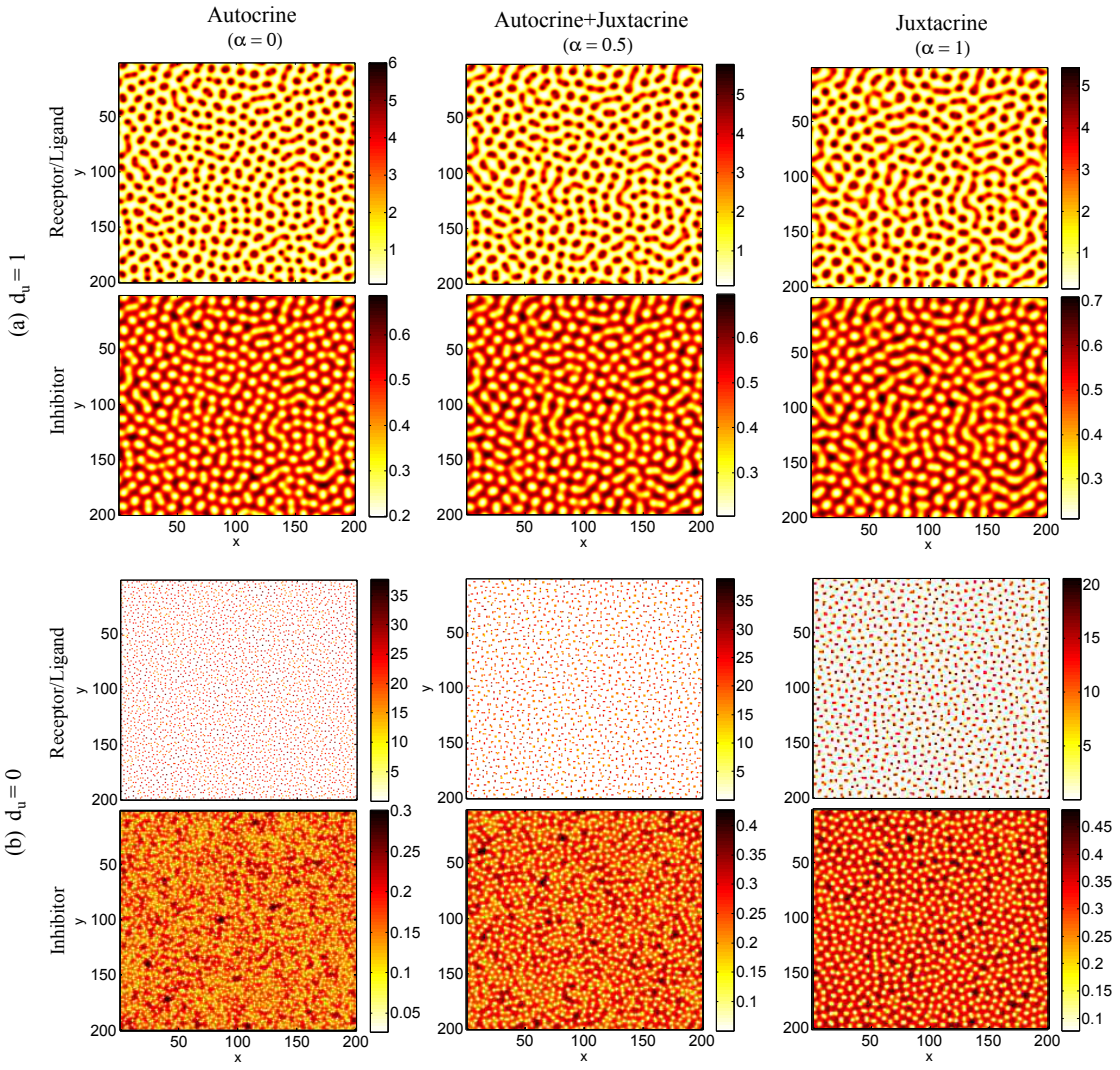

Figure 4.21: Two dimensional simulations with square cells for a model with Schnakenberg kinetics. The simulations are given on a 200x200 grid at $t = 48$ hrs and show both the (a) two ($d_u = 1$) diffusible and (b) one ($d_u = 0$) diffusible cases with autocrine ($\alpha = 0$), juxtacrine ($\alpha = 1$) and a combination of the two signalling mechanisms ($\alpha = 0.5$). Spot patterns are produced in each case with varying spot size depending on the number of diffusible species. The other parameters are given as $\beta = 0$, $\rho = 2$, $d_w = 60$.

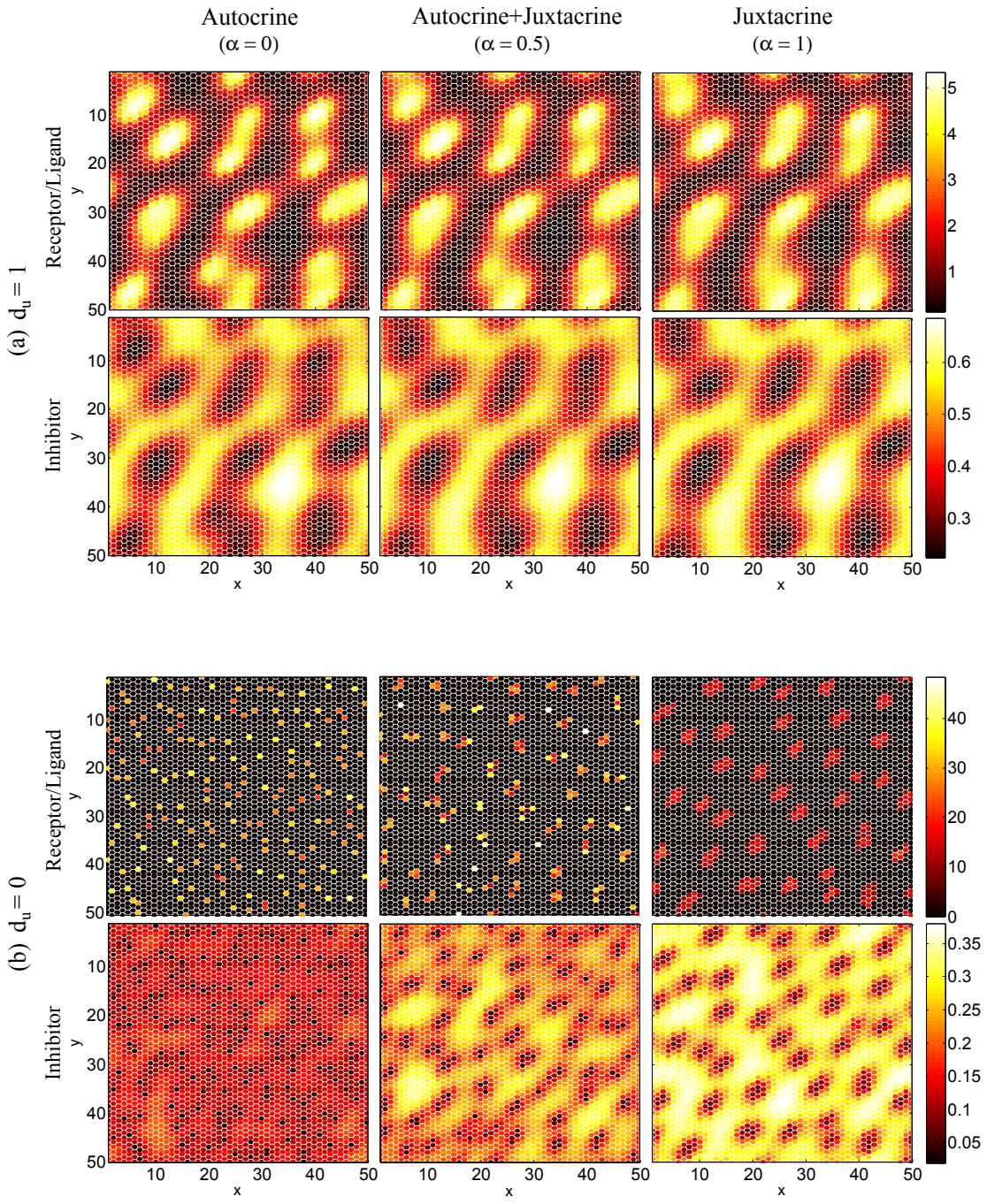

Figure 4.22: Two dimensional simulations with hexagonal cells for a model with Schnakeneberg kinetics. The simulations are given on a 50x50 grid at $t = 48$ hrs and show both the (a) two ($d_u = 1$) diffusible and (b) one ($d_u = 0$) diffusible cases with autocrine ($\alpha = 0$), juxtacrine ($\alpha = 1$) and a combination of the two signalling mechanisms ($\alpha = 0.5$). Spot patterns are produced in each case with varying spot size depending on the number of diffusible species. The other parameters are given as $\beta = 0$, $\rho = 2$, $d_w = 60$.

model with Gierer-Meinhardt kinetics as a case study is given below:

$$\frac{du_p}{dt} = \frac{u_p \bar{v}_p}{w_p} - \delta_u u_p; \tag{4.71}$$

$$\frac{dv_p}{dt} = \mu(u_p - v_p) + d_v \Delta v_p; \tag{4.72}$$

$$\frac{dw_p}{dt} = u_p^2 - w_p + d_w \Delta w_p. \tag{4.73}$$

u_p, v_p, w_p are the receptor, ligand and inhibitor activities at cell p respectively, while d_v, d_w, δ_u, μ are all positive parameters. The diffusion and cell signalling terms follow the different dimensional forms in §4.5.1.

The previous chapters have shown that, under certain assumptions and conditions on the parameters, the reduced two species model is capable of producing pattern formation in simulations. This two species model was obtained using a Quasi-Steady State Assumption (QSSA) and provided an analytically convenient form which permitted direct comparison with Turing's classical approach. However, a number of assumptions were made and here we consider the full three species system in order to determine its behaviour. We perform similar analysis to the reduced system to show that behaviour exhibited in this can be obtained. Furthermore, the assumptions that led to the reduced model were proposed without any real consideration to their validity. Therefore, we also analyse a relaxation of these assumptions to determine the extent to which the two species model approximates the full three species system and whether there is any additional behaviour. For illustrative purposes we consider only the model with Gierer-Meinhardt based kinetics.

4.7.1 Analytical Results from a Linear Stability Analysis

Firstly, we undertake a linear stability analysis of the three species model. The details can be seen in Appendix B.3 but the conditions which arise from this are given by

$$\mu > 0, \tag{4.74}$$

$$0 < \delta_u < \sqrt{2}, \tag{4.75}$$

$$-\frac{2d_v}{\delta_u} + \delta_u \mu d_w K_c(k) > 0, \tag{4.76}$$

$$d_w > \frac{\left(-\frac{1}{2}\delta_u^2 \mu\alpha + 2\mu\alpha + 2d_v + \sqrt{2\delta_u^2\mu^2\alpha^2 - 4\delta_u^2\mu\alpha d_v + 4\mu^2\alpha^2 + 8d_v\alpha\mu}\right)}{\delta_u^2 \mu}. \tag{4.77}$$

The above conditions, (4.74)-(4.77), are applicable when $\alpha \geq 0.5$. However, together with (4.74)-(4.76), when $0 \leq \alpha < 0.5$ we require,

$$d_w > \frac{(\delta_u^2\mu + 2\mu + 2\delta_u^2\mu\alpha + 8d_v)}{4\mu\delta_u^2(1-2\alpha)}. \tag{4.78}$$

where, as before, $K_c(k) = \alpha\cos(k)+(1-\alpha)$. Similar to the two species model analysis, solving condition (4.76) leads to the requirement that the wavenumber lies between $[0\ ,\ k_c]$, where $k_c = \cos^{-1}\left(\frac{\delta_u(\alpha-1)-\delta_u^2\mu d_w+2d_v}{\delta_u\alpha}\right)$. Therefore, across the parameter space region the relevant wavenumber range will vary. We note that in the following analysis the parameter space plots use the conditions (4.75), (4.77) when $\alpha \geq 0.5$ and (4.75), (4.78) for $0 \leq \alpha < 0.5$ to delimit the region for pattern formation.

General Analysis

Using the conditions, (4.74)-(4.78), the parameter spaces, indicating the region of pattern formation, can be seen in Fig. 4.23.

Comparing the results with the reduced system (Fig. 4.8(i)), we can see that the $\delta_u - d_w$ parameter space of the two diffusible species model is unchanged in the d_w parameter range. However, there is an enlargement in the possible δ_u choices with the stability conditions now permitting values up to $\sqrt{2}$. This greater choice of δ_u values is also apparent in the one diffusible species parameter space but we observe the opposite behaviour in the d_w range, Fig. 4.23(b)(i). In this case, the d_w range is reduced when comparing it with the two species model analysis.

A comparison of the parameter spaces in the full three species model shows similar regions for pattern formation. However, there is a slightly larger choice of d_w parameters that can be chosen for a model with only one diffusible species. This is also apparent in the $\alpha - d_w$ parameter regions, Fig. 4.23(ii). Furthermore, this parameter space is relatively unchanged from the reduced two species system.

However, the conditions from a linear stability analysis of the three species model show that it is purely the choice of α that determines the relevant conditions and therefore we now see the segregated parameter space arising in the two diffusible species model. Similarly to the reduced system, these different parameter regimes have a consequence on the form of the dispersion relations, Fig. 4.23(iii). The dispersion relations of Fig. 4.23(iii) also indicate that the two diffusible species model is more sensitive to the μ parameter selection than the one diffusible species system. For example, a model considering juxtacrine signalling with two diffusible species, Fig. 4.23(a)(iii) (dashed lines), shows an unstable wavenumber range when $\mu \geq 0.3$ whereas a one diffusible species model predicts unstable wavenumbers for $\mu > 0$, Fig. 4.23(b)(iii) (dashed lines).

Typically the wavenumber with the maximum $Re(\lambda) > 0$ dominates to form a

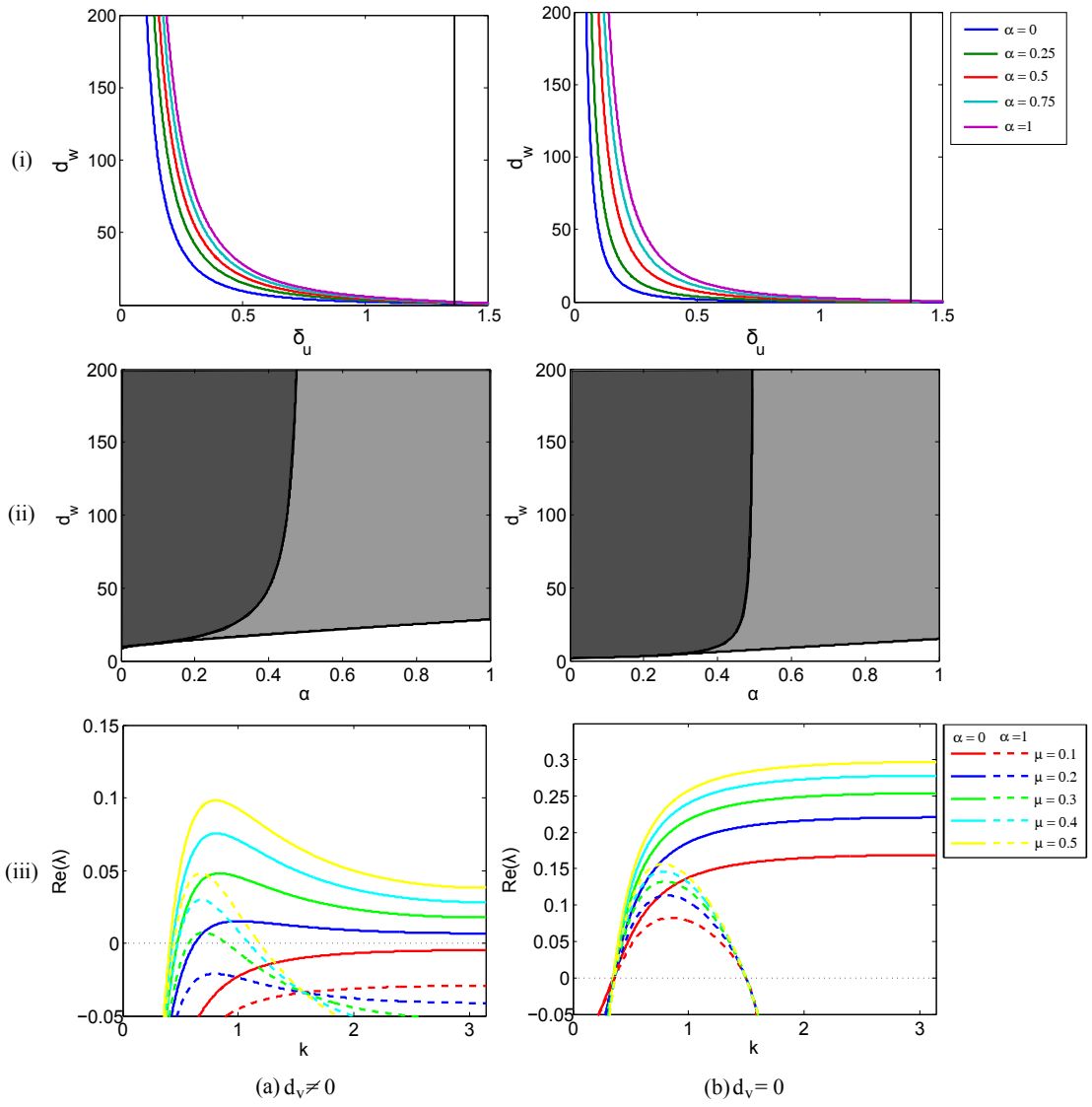

Figure 4.23: Plots of (i) $\delta_u - d_w$ parameter spaces for increasing μ, (b) $\alpha - d_w$ parameter spaces and (c) dispersion relations for increasing μ, in a model with (a) $d_v = 1$, (b) $d_v = 0$. The shades of grey in the parameter space indicate the conditions on instability and the dispersion relations are shown for $\alpha = 0$ (solid lines), $\alpha = 1$ (dashed lines) for increasing $\mu = 0.1, 0.2, 0.3, 0.4, 0.5$. The other parameters were chosen as $\delta_u = 0.5$, $\mu = 1$ for the parameter space and $\delta_u = 0.5$, $d_w = 60$ for the dispersion relations.

pattern with the corresponding wavelength. As discussed in the previous analysis, we refer to this as the 'expected wavelength' and over the parameter space these can be seen for both the one and two diffusible model in Fig. 4.24. This suggests that a variety of wavelength patterns are attainable with either diffusivity scenario. In particular, the linear stability analysis predicts that both fine grained and longer wavelength patterns are possible. These expected wavelength ranges show good agreement with the reduced two species system (c.f. Fig. 4.10 and 4.11).

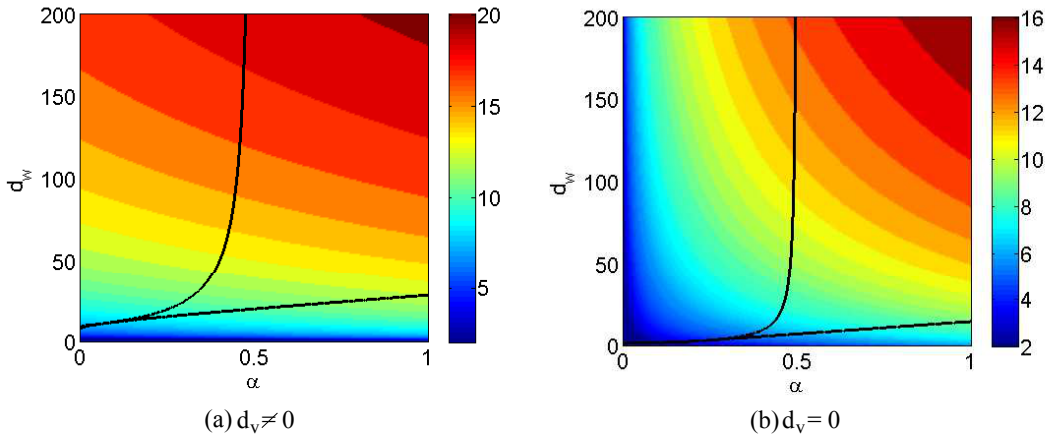

Figure 4.24: Plot of the expected wavelengths across the $\alpha - d_w$ parameter space for a model with (a) $d_v = 1$, (b) $d_v = 0$. The colorbar respresents the corresponding predicted expected wavelength that will is predicted to arise in simulations.

Validity of Reduction Assumptions

The general analysis of the previous section suggests a reasonable approximation can be gained when reducing the model to a two species form. However, the question arises as to whether the reduction assumptions hold when considering the full system and whether they have any effect on the model outcomes. Here we investigate the validity of these assumptions using the three species model.

The QSSAs that led to the reduced system were the following,

- The ligand production is initially fast in comparison with receptor activity so that it is assumed to be at equilibrium at all times ($\frac{dv_j}{dt} = 0$)
- Ligand diffusion is negligible ($d_v << \mu$)

Due to the nondimensionalisation, the first of these conditions can be satisfied by assuming μ is large and the second of these through $d_v \approx 0$. As a result, in the study of the validity of these QSSA assumptions we use these particular conditions as the basis of the investigation and focus on the effect these two parameters have on the model. Here, we consider the $\delta_u - d_w$ parameter spaces to observe the effect of ligand diffusion with increasing μ. Figure 4.25 shows the effect of varying the parameter μ.

As we discussed in the previous section, when μ is small ($\mu = 1$) the $\delta_u - d_w$ parameter space plots differ when $d_v \neq 0$ and $d_v = 0$. However, when μ is increased the two diffusivity scenarios begin to show similar parameter space plots suggesting that diffusion of the ligand may be considered negligible for large μ, Fig. 4.25(a) and (b).

The differences in the parameter spaces between $\mu = 1$ and $\mu = 100$ can be seen in the final plots in Fig. 4.25(a),(b). Here, we concentrate on the parameter spaces changes in the autocrine ($\alpha = 0$) and juxtacrine ($\alpha = 1$) specific mechanisms. In the two diffusible species model there is a shift in the possible d_w range such that there is a greater parameter choice as μ is increased, Fig. 4.25(a). In contrast, a model with one diffusible species produces an unchanged d_w range and, regardless of μ, the parameter space is defined by the solid line, Fig. 4.25(b). Moreover, this shift indicates that the parameter space of the two diffusible species model tends to the one diffusible species region for increasing μ.

This observation is reinforced by analysing the differences in the l_2-norm of the parameter space curves. Figure 4.25(c) shows that for increasing μ the $d_v \neq 0$ parameter space tends to the $d_v = 0$ region. In particular, when $\mu = 200$ there is close agreement between the two parameter space regions suggesting that when μ is large diffusion can be considered negligible.

Despite the differences in the δ_u range, the results suggest that for large μ the two species system provides a good approximation to the reduced system. Referring to the general analysis, Fig. 4.23(b) and 4.24(b) will show applicability to both the full three species model with large μ and reduced two species system. We now undertake a numerical investigation to determine whether this produces consistent results.

4.7.2 Numerical Investigation of Reduction Assumptions

Here, we follow a similar analysis to the previous section by considering the one diffusible species simulations to show that comparable results between the two models can be observed when μ is increased. For comparison to the reduced system analysis, we chose the same parameter values in this study: $\delta_u = 0.5$, $d_w = 60$.

The one dimensional simulations of the one ($d_v = 0$) and two ($d_v \neq 0$) diffusible species systems can be seen in Fig. 4.26. As we increase μ, the simulations begin to conform to the one diffusible species results and at $\mu = 300$ the simulations are

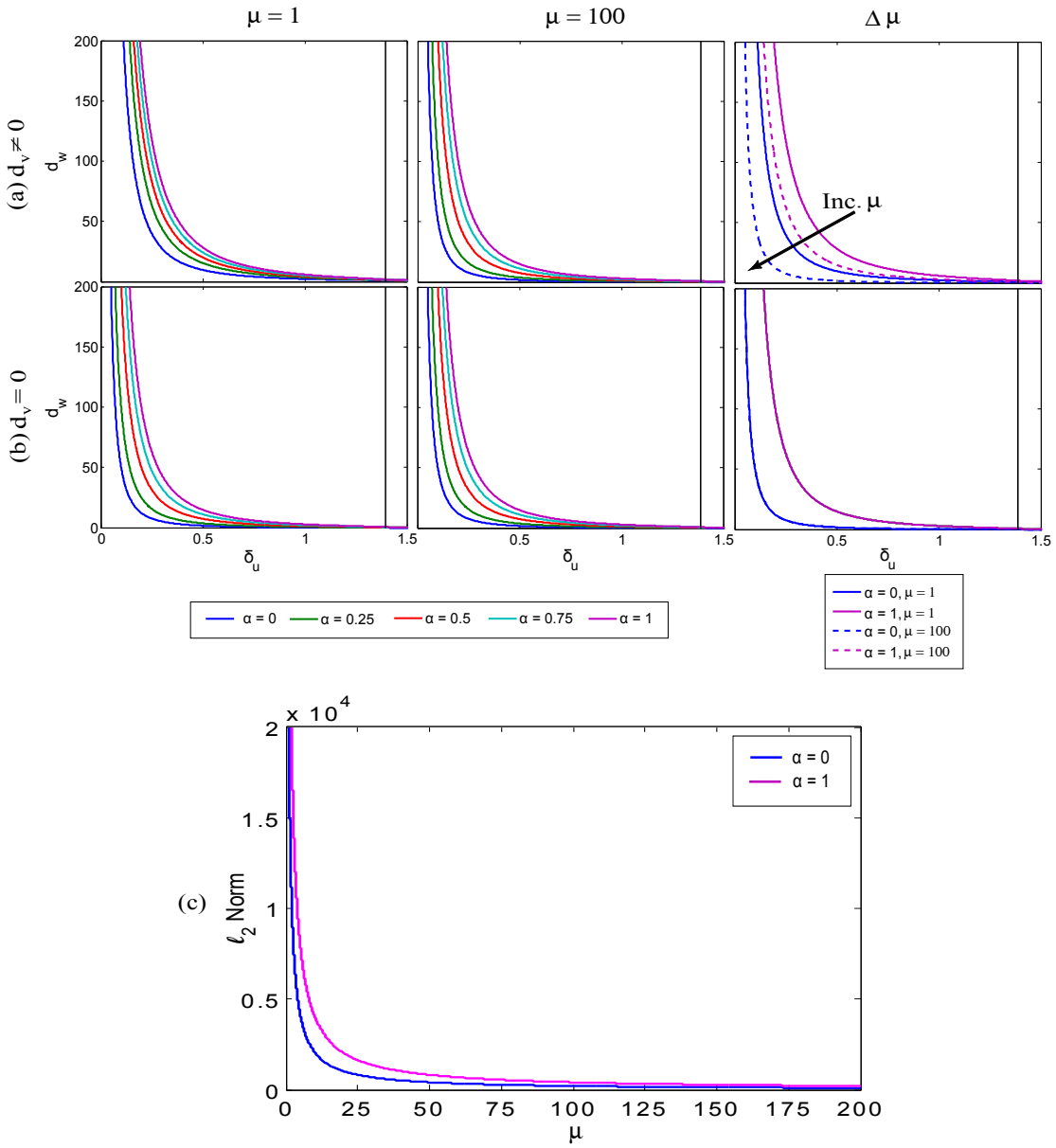

Figure 4.25: Plots of the $\delta_u - d_w$ parameter space for increasing μ with (a) $d_v = 1$, (b) $d_v = 0$. The figures reveal the changes in the parameter space for each $\alpha = 0, 0.25, 0.5, 0.75, 1$ with $\mu = 1$ and $\mu = 100$. The final plot in (a), (b) shows the change from $\mu = 1$ (solid line) to $\mu = 100$ (dashed line) for the two outer extremes parameter space curves of $\alpha = 0$ and $\alpha = 1$. This suggests that as μ increases the parameter space tends towards the $d_v = 0$ parameter space. This can be seen clearer seen in (c) a plot of the difference in the l_2-norm between the $d_v = 1$ curves for increasing values of μ, and $d_v = 0$ curve (unchanged by μ) to which it tends to. Details of the numerical method can be seen in Appendix C.2.

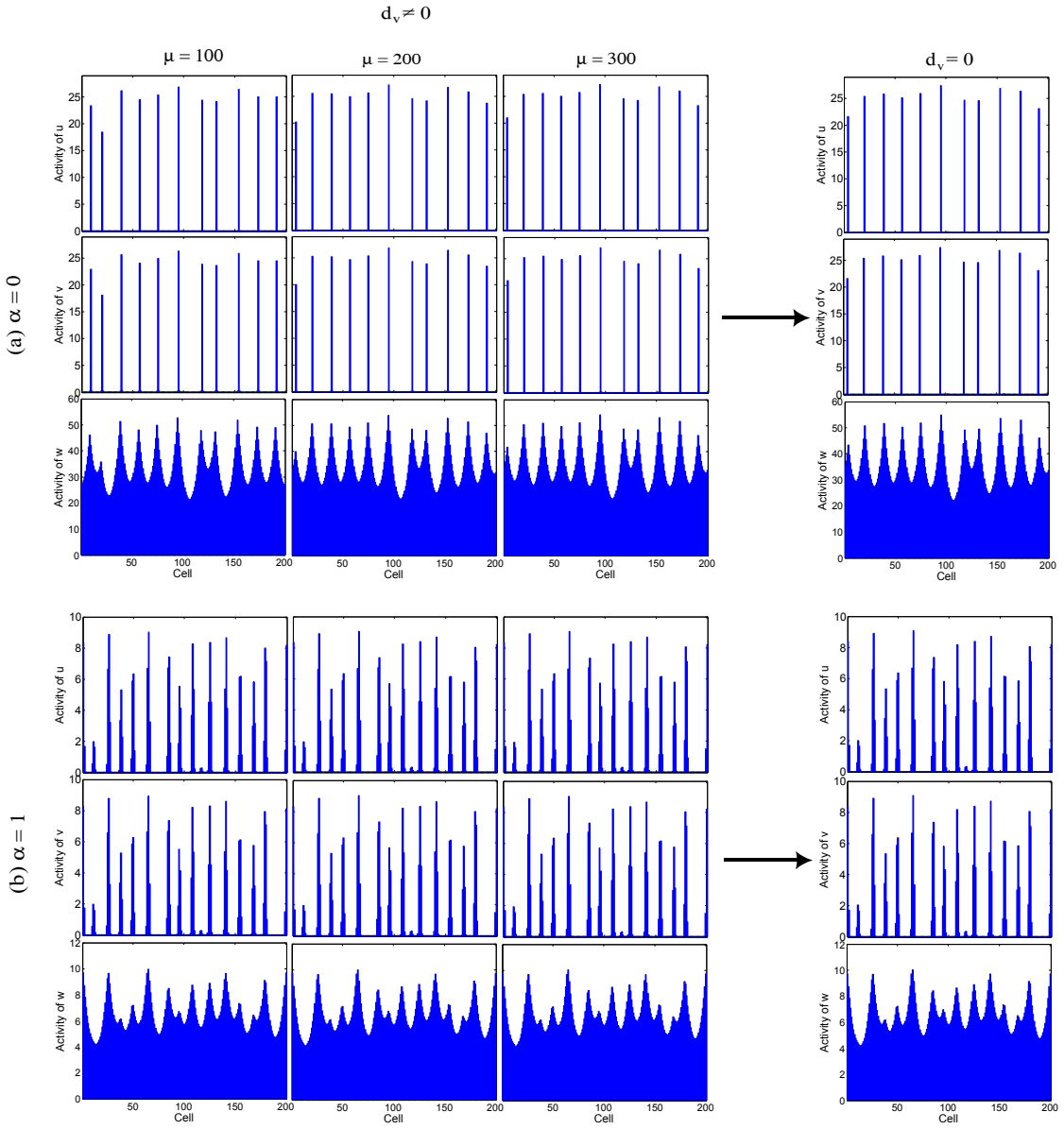

Figure 4.26: Plots of the one dimensional simulations for increasing μ and (a) $\alpha = 0$ and (b) $\alpha = 1$. Here we see the simulations tend towards the one diffusible models simulations. The other parameter was chosen as $\delta_u = 0.5$, $d_w = 60$.

in close agreement with one another. However, even at $\mu = 100$ the simulations are similar. As a result, this reinforces the observations of the parameter space analysis suggesting that, for increasing μ, the results of the two diffusible species model tend towards those of the one diffusible species case.

In comparison to the reduced two species system, the form and characteristics of the pattern are also in agreement (c.f. Fig. 4.17(ii)). At the same timepoints similar patterns appear and we see single cell peaks with autocrine signalling to few cell peaks with juxtacrine.

Finally, we consider two dimensional simulations on a hexagonal lattice, Fig. 4.27. Here, we only show simulations of the one diffusible species model since this gives a comparison to the reduced two species system. In this way, the patterns produced show that for large μ (negligible diffusion) the results are identical to the reduced model (c.f. Fig. 4.17). All of these results then suggest that for large enough μ ligand diffusion can be largely ignored. Moreover, the two species model gives a good approximation when the QSSAs are satisfied.

4.7.3 General Numerical Investigation of the Full Model

The linear stability analysis predicted that an increased range of parameters can be chosen when the full three species model is analysed. Moreover, depending on α, different forms for the dispersion relation can be obtained. In the reduced system, however, this had a direct consequence on the pattern and here we analyse the one and two dimensional simulations to see if similar or any new behaviour can be observed. As we have seen from the analysis of the reduction assumptions, the simulations of the full model in the absence of ligand diffusion (or large μ) is identical to the reduced system. Here, the model is numerically solved for a similar set of parameters to the reduced two species system with the addition of $\mu = 1$ (see §4.6.1 for details). Once again, the patterns are simulated up to 48 hours (see Appendix C.2 for details of the numerical method). Considering the one dimensional simulations we can see that similar behaviour is exhibited in a system with one diffusible species ($d_v = 0$). Notably, a model considering autocrine signalling with no ligand diffusion ($d_v = 0$) results in higher activity levels in simulations. This is due to the self-amplification of activity, thus preventing regulation from surrounding cells. For example, much lower activity is observed in systems involving juxtacrine signalling and those considering two diffusible species since these consider interactions with neigbouring cells.

Simulations of the two diffusible species system ($d_v \neq 0$) shows receptor and ligand activity peaks with multiple cell aggregations. Although these show fewer peak cell numbers than the reduced system, by considering faster ligand diffusion a greater number of cells with high activity can be obtained.

Comparing the simulations with Fig. 4.24, largely inconsistent predictions in

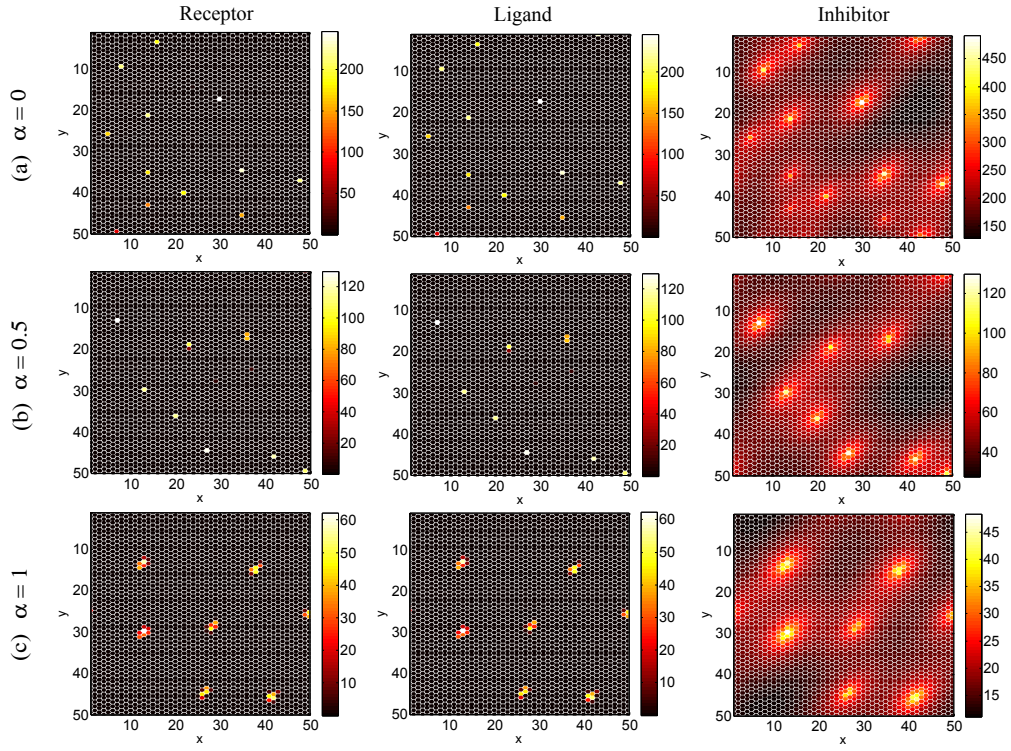

Figure 4.27: Two dimensional simulations with hexagonal cells for a three species model with Gierer-Meinhardt kinetics. The simulations are given on a 50x50 grid at $t = 48$ hrs and show the receptor, ligand and inhibitor activity of the one diffusible model with $\mu = 100$. This case also incorporates the two diffusible case when $d_v << \mu$ since diffusion can be considered negligible at these values. Furthermore, the signalling mechanisms of autocrine ($\alpha = 0$), juxtacrine ($\alpha = 1$) and a combination of the two signalling mechanisms ($\alpha = 0.5$) are considered. The results show close agreement with the reduced two species model with one diffusible species. The other parameters are given as $\delta_u = 0.5$, $d_w = 60$.

wavelength are again observed for a one diffusible species system considering autocrine signalling ($\alpha = 0$). Here, the linear stability analysis predicts wavelengths of two cell lengths but the simulations illustrate much larger wavelength patterns arise. However, the other cases are in reasonable agreement with the predicted wavelengths, once again, suggesting that the form of the dispersion relation has a direct effect on the predictions from the linear stability analysis. In particular, when $0 \leq \alpha < 0.5$ the wavelength with largest $Re(\lambda) > 0$ is not easily identified. Within this regime, we observe closer agreement when both ligand and inhibitor diffuse since the curve is more defined leading to easier selection (see Appendix B.3: Fig. B.2 for typical forms).

The two dimensional simulations show spot patterns arising with these supporting the observed characteristics of the one dimensional simulations. In each case, the patterns all show a similarity to the results observed in the reduced two species model that considers only one diffusible species with autocrine and/or juxtacrine signalling.

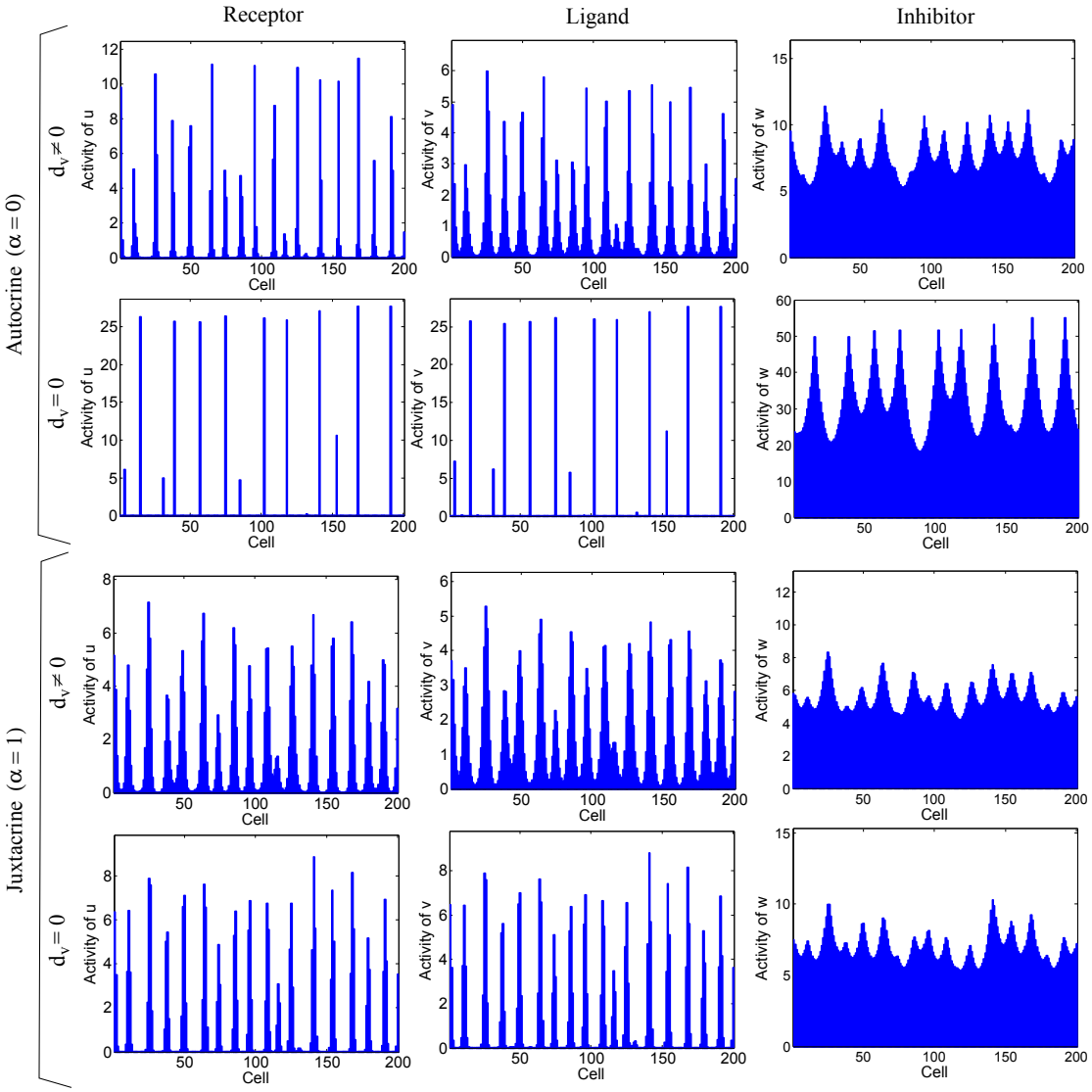

Figure 4.28: One dimensional simulations of the three species model for autocrine ($\alpha = 0$) and juxtacrine ($\alpha = 1$) signalling. We also consider both one ($d_v = 0$) and two diffusible species ($d_v = 1$). The other parameter were chosen as $\delta_u = 0.5$, $\mu = 1$, $d_w = 60$.

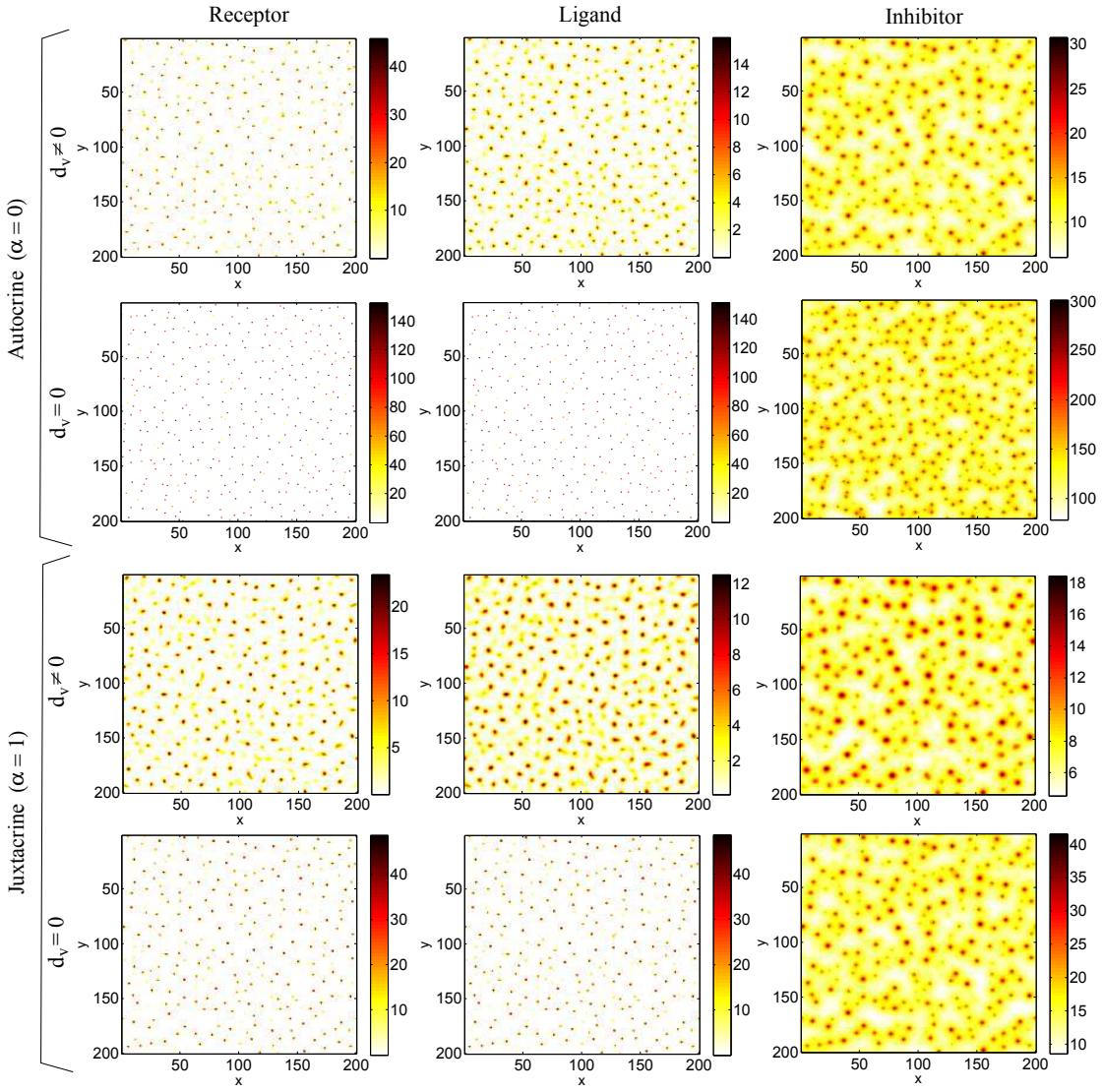

Figure 4.29: Two dimensional simulations of the three species model for autocrine ($\alpha = 0$) and juxtacrine ($\alpha = 1$) signalling together with one ($d_v = 0$) and two diffusible species ($d_v = 1$). The other parameter were chosen as $\delta_u = 0.5$, $\mu = 1$, $d_w = 60$.

4.8 Summary and Discussion

In this chapter we have undertaken analysis to determine the impact cell signalling has on pattern formation. In doing so, we have considered two conceptually different reaction kinetics based on the well studied Gierer-Meinhardt and Schnakenberg systems which, in the reduced two species form, have provided a direct comparison to Turing's classical approach. However, we have also considered the replacement of short-range activation via diffusion with an explicit cell based model in which signalling is mediated either by autocrine, juxtacrine or longer range (diffusive) signalling.

The analytical results and numerical simulations of the two case studies reveal general characteristics, suggesting that the effects of the model may be broadly consistent regardless of kinetic choice. Moreover, analysis of the full three species system with Gierer-Meinhardt type kinetics showed similar behaviour to the reduced system arising. We summarise the main results below.

- *Increased Parameter Choice When Considering Localised Signalling With One Diffusible Species*

  The results of the reduced model with two diffusible species is closely related to the classical Turing-type systems and there is a corresponding similarity in behaviour. However, when the short range activation is only via autocrine and/or juxtacrine signalling the parameter space analysis indicates a wider regime of pattern generating parameters. Consequently this confers greater robustness with regards to parameter selection.

  Similar behaviour arises in the full three species model but there is an increase in the δ_u parameter range. Furthermore, a model in the absence of ligand diffusion results in a decrease in the d_w range.

- *The Attainability of a Variety of Wavelengths*

  A variety of patterns are attainable ranging from fine grained (alternating high/low) to longer wavelengths according to the signalling and diffusing species present. For example, patterns consisting of only two cell lengths can be obtained in a system with one diffusible species and autocrine signalling, longer wavelengths at other parameter regimes. As a result, this shows the diversity of the model with the different possibilities allowing a wide variety of patterns. Although this all encompassing mechanism offers an advantage over the lateral inhibition and induction mechanisms, comparisons between the predicted-simulated wavelengths and Fourier series analysis shows that the linear stability analysis is not a good predictor of wavelength in a model considering one dif-

fusible species with autocrine signalling. Moreover, the forms of the dispersion relations reinforce this since a wider range of unstable wavelengths are possible.

These results are consistent with the three species model.

- *Pattern Observations*

  Simulations of the models show patterning with peaks and troughs in activity levels. However, the exact nature of the patterns depend on the signalling and number of diffusible species within the system. A model consisting of one diffusible model gives patterns that range from single cell peaks to multiple cell peaks, depending on the signalling mechanism. For example, a one diffusible species model with autocrine signalling gives single cell peak patterns whereas juxtacrine signalling produces patterns with peaks of $3-5$ cells. Simulations of a model with two diffusible species indicate patterns with peaks of multiple cells. The two dimensional simulations also exhibit these properties and result in spot patterns in both diffusive conditions.

  These results are consistent with the three species model.

- *Reduced System Provides A Good Approximation*

  We have shown that similar results to the reduced two species system can be observed for a three species system with large μ. Despite the increase in the δ_u range, the regions of parameter space indicate reasonable agreement. Moreover, as μ is increased the two diffusible species parameter space tends to the one diffusible species model. This suggests that diffusion can be considered negligible for large μ and therefore satisfies the reduction assumptions. Further to this, the one and two dimensional simulations appear identical to the reduced one diffusible species model when $\mu = 300$.

  Therefore, the reduced model provides a reasonable approximation to the full three species system.

In the beginning of this study (see Chapter 3: Introduction) we showed a variety of detailed patterning on a cellular level that illustrated the intricate detail required to emulate varied biological pattern formation. The results of this study have shown that the model is capable of producing a variety of patterns which may be applicable to these and other biological systems.

Depending on kinetic choice, we have shown that it is possible to produce out-of-phase peaks, similar to lateral inhibition, with cross type kinetics and in-phase peaks,

similar to lateral induction, by considering pure type kinetics. It has been widely suggested that a lateral inhibition mechanism is involved in drosophila sensory bristle formation, [66]. Furthermore, a single cell develops a dominant neural fate within a small group of approximately $7-9$ cells called a proneural cluster with this dominant cell selected by means of cellular interactions between the group, [66]. Our one and two dimensional simulations considering juxtacrine signalling within Schnakenberg kinetics show similar behaviour and also emulate the observed cellular interactions through near neighbour communication. The spots with high activity predict similar cell numbers and these cell clusters exhibit single cells with highest receptor/ligand activity suggesting that dominant neural fate may be easily identified by comparing activity levels. However, it should also be noted that a model considering Gierer-Meinhardt kinetics is capable of producing consistent characteristics suggesting a different mechanism can also explain this patterning phenomena.

Together with sensory bristle development, our model could be applicable to a variety of skin appendage pattern formation including feather placode and hair follicle patterns. These systems result in spot patterns which are often considered using a pure type continuous activator-inhibitor system, [29]- [31], [37], [18], [39], [32]. In particular, based on a molecular system exhibiting pure type reactions, [17], a continuous three species model describing the interactions between Edar, BMP and CTGF was proposed by Klika *et al*, [84]. The theoretical implications on patterning was considered with a specific application to hair follicle development in mouse, [17]. This molecular framework could also be used in an application of our study. For example, by considering the Edar, Eda and BMP interactions in [17] (see also Fig. 4.30) we could assume that the receptor, ligand and inhibitor represent these.

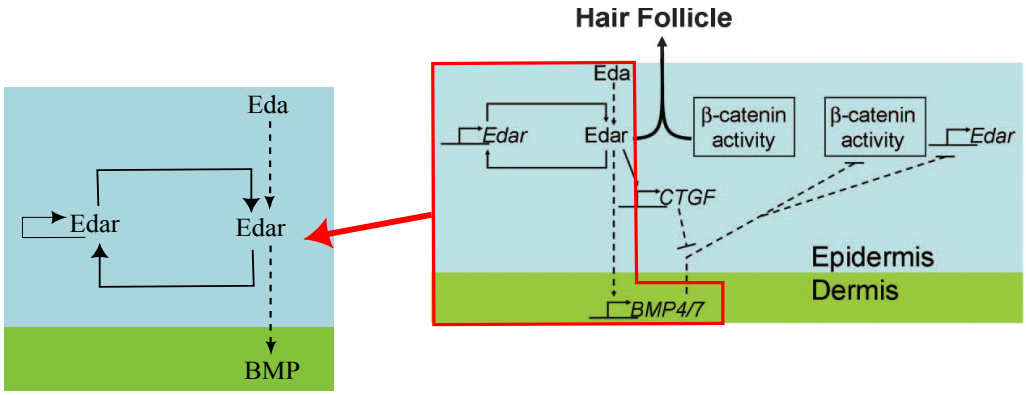

Figure 4.30: Schematic of the signalling pathway and molecular interactions involved in mouse hair follicle formation. A subset of this molecular system is considered for the purposes of our model but the full schematic is taken from [17].

In this way, we would now have a system modelling a subset of the molecular interactions involved in mouse hair follicle development. Using this, we can gain insight into the mechanisms regulating pattern formation. For example, studies have calculated mouse hair follicles to have mean follicle size (high Eda) of ~ 40 cells, [108], and the results from the reduced two diffusible species case or full three species model with high ligand and inhibitor diffusion would show good agreement with this.

These applications show that the model is capable of producing fine detailed and varied patterning observed in biological applications. Moreover, the different interactions that can be considered illustrates the diversity of the model and the all encompassing approach that it provides.

Chapter 5

Discussion

Turing's classical approach is undoubtedly a powerful framework to gain insight into the mechanisms initiating development. However, in its most simplest form it lacks the fundamental detail required to sufficiently describe biological complexity. In particular, the two species chemical system in the absence of any cell dynamics is an oversimplication and suggests a naive approach to modelling biological processes. This thesis investigates a more detailed consideration of Turing's simplest mechanism by using the two species activator-inhibitor model as a framework. In particular, we focussed on fundamental cell processes and their impact on biological phenomena, thus determining their significance in development.

In Chapter 2 we considered explicit representations of cell commitment and coupled this with a two species activator-inhibitor model of Turing type. In doing so, two conceptually different chemical kinetics and cell commitment processes were implemented. The chemical dynamics followed the pure and cross kinetic models of classical Turing systems and we considered the simplest Gierer-Meinhardt and Schnakenberg kinetics. The commitment processes consisted of a precursor specification mechanism and asymmetric precursor differentiation process. The first of these considered the transfer between an uncommitted and committed class depending on the expression levels and the latter involved a previously uncommitted cell becoming two cells: one committed and another uncommitted. In both cases, commitment resulted in changes to the chemical system through the implementation of a variety of feedback mechanisms. Essentially, these acted to upregulate/downregulate activator and/or inhibitor levels but the specific mechanisms targeted different parts of the chemical interaction network.

For illustration, the analysis focussed on positive/negative feedback from the committed cell population to affect activator levels and the significance of cell commitment processes in pattern formation was determined by observing the model behaviour compared to the classical two species system. The results suggest that with pure kinetics and the explicit representation of cell commitment, direct positive feedback can pro-

duce pattern formation when the activator and inhibitor diffuse at the same rate. This would lead to a relaxation in the long range inhibition, short range activation that is required in the simplest two species system of Turing type.

Further to this, a variety of patterns were possible with different chemical kinetics and types of feedback suggesting applicability to a number of systems. In particular, a single phase of peak splitting phenomena occurs in a model with Schnakenberg kinetics coupled with asymmetric precursor differentiation. Here, patterns involving the mechanism of regulatory positive feedback, upregulating activator via autocatalysis, could be applied to young jaguar and leopard patterning, [90]. Generally, early pattern development of these systems exhibit spots which subsequently break into multiple spots to develop rosette patterns as time progresses. Although Liu *et al* captured this temporal phenomena, their model involved a two stage Turing system which used two separate parameter sets for its evolution. In contrast, our model predicts this phenomena for one parameter set and therefore further investigation into the credible parameter values involved in this process will need to be determined to justify each models outcomes.

A detailed investigation of the peak splitting phenomena may indeed permit an application into developing jaguar/leopard pigmentation patterns. If this is favourable to these systems it could provide a hypothesis to test the possible commitment and feedback mechanisms that may be fundamentally active in these systems. Moreover, this will provide focus on particular areas of the interaction network in further research.

More significant oscillatory behaviour in space and time was shown to potentially occur theoretically from the linear stability analysis and this was then supported through numerical simulations in the study of a model involving asymmetric precursor differentiation with negative feedback. Within this, travelling wave type behaviour was observed. Biologically, this has been observed in a variety of systems such as mollusc shell patterns, [28], and hair patterns, [87], among others. Focussing on one particular example, Suzuki *et al* illustrated that a wave of pigment travels across the skin of mutant mice that are defective in splicing of the Foxn1 gene, [87], ultimately showing that this phenomena can indeed be present in embryogenesis. Early development $(30 - 60$ days after birth) results in pigmented skin across the whole body. However, as time progresses this pigment appears to oscillate across the skin where cells at the travelling front are stimulated to now produce the pigment while trailing cells are 'switched off', see Fig. 5.1. Within this study, the authors also measure the speed of the developing wave suggesting that with particular applications comparisons can be made between the application and theory in order to validate the model and perform more extensive analysis.

Further results regarding positive feedback showed no temporal behaviour. How-

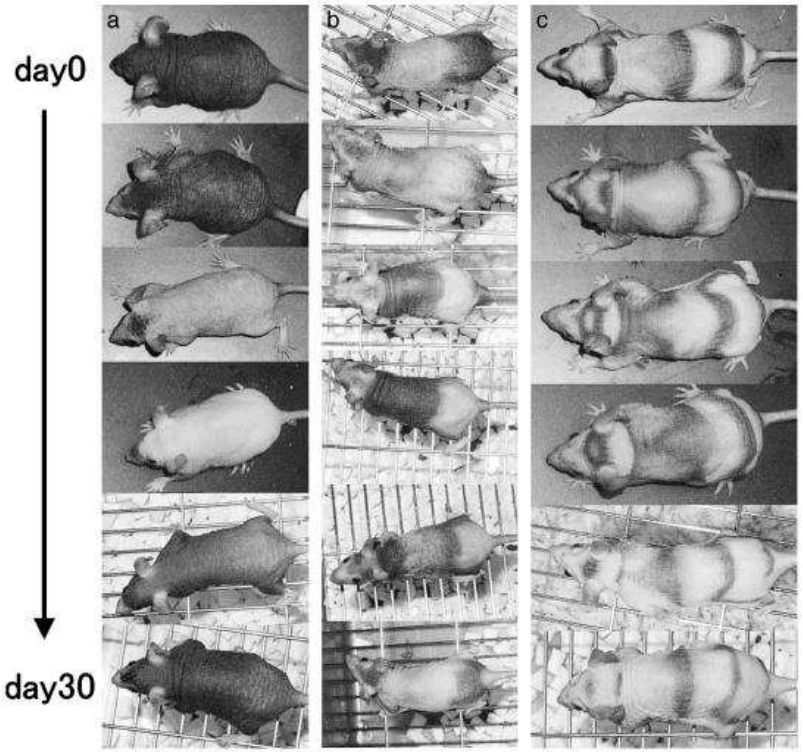

Figure 5.1: Time progressing photographs of pattern fomation in mutant mouse skin for (a) 30-60 days (b) 90-120 days and (c) 210-240 days after birth. Here, a travelling wave phenomena occurs as time progresses where pigmented skin appears to oscillate across the skin. Taken from [87].

ever, comparing the results of the two different positive feedback mechanisms suggested that the specific mechanism present in the system has significant ramifications on the patterns. Feedback implemented directly reduced spot size and density whereas regulatory feedback produced larger spots with the loss of a coherent pattern when feedback is increased further. Focussing on the work of Sick *et al*, which blended theory and application to mouse hair follicle patterning, perturbation analysis suggested that exogenous activator resulted in loss of patterning, [18]. However, our results suggest that a far more subtle relationship is present and that the observations from the perturbation analysis should be described more concisely using particular feedback mechanisms. In doing so, it could provide a much more detailed overview of the cellular mechanisms regulating biological processes.

Although the models formulated in this chapter capture greater biological complexity, the framework produced from this study also permits the inclusion of other cellular processes. For example, research focussed on fish pigmentation patterns have highlighted the importance of cell migration in pattern formation, [50], [78]. For exam-

ple, it has been suggested that melanocyte precursors migrate dorsolaterally, passing through the dermis and basal lamina to pigment the epidermis, [72]. As a result, cell migration and other fundamental cell processes such as proliferation should be considered to provide a more realistic cell population and to determine the significance of these in pattern formation. A specific application will provide a robust framework from which to test these processes and gain insight into the fundamental mechanisms.

In Chapter 3 we proposed a more detailed approach to the classical activator-inhibitor model of Turing type. Using a two species continuous system we explored the interactions that the activator/inhibitor intrinsically incorporate and formulated a discrete model that considered a receptor-ligand binding process in the presence of an inhibitor. Within this, we focussed on two mechanisms of cell signalling to determine their impact in pattern formation. Here, we considered autocrine signalling, juxtacrine signalling and the joint effects of these. Autocrine signalling involves receptor-ligand binding on the surface of individual cells resulting in self-regulation. Juxtacrine signalling involves communication between neighbouring cells. To permit a comparison to the classical activator-inhibitor system, we proposed reaction kinetics that followed similar forms to the Gierer-Meinhardt and Schnakenberg kinetics. Under certain assumptions, an analytically convenient 'reduced' form resulted in a direct comparison to Turing's simplest approach involving a two species model. In addition to this, a model with diffusion replaced by short range activation via cell signalling was also considered.

The analysis of these models was undertaken in Chapter 4 to determine the significance of cell signalling in pattern formation. Firstly, by undertaking a linear stability analysis on the reduced form we found that parameter regions indicating pattern formation were increased when considering one diffusible species with autocrine and/or juxtacrine signalling. Over the different parameter spaces, however, a variety of wavelength patterns were attainable - from fine grained to longer range wavelength patterns. Minimum wavelengths of $\omega = 2$ can be obtained for autocrine signalling with the smallest for juxtacrine being $\omega = 4$. Despite largely inconsistent results when diffusion is replaced by autocrine signalling, the numerical simulations show reasonable agreement with the predicted wavelengths.

Simulations exhibit mechanism dependent characteristics with single to few cell peaks arising depending on the signalling mechanism. However, when diffusion is present the local interactions involved in cell signalling are made largely redundant and we observe multiple cell contributions to peaks that are similar to the classical approach. The two dimensional simulations illustrate patterns with spots of high activity. More importantly, however, all the results are broadly consistent when considering the two conceptually different reaction kinetics suggesting that the behaviour is a general feature of the model.

Despite an increased range of parameters that can produce pattern formation, an investigation of the full three species model showed similar results to the reduced system. Moreover, the model incorporating the reduction assumptions showed good agreement with the results of the two species system. Therefore, the reduced two species model provides a reasonable approximation to the full system.

Furthermore, both the full three species and reduced model provide an ideal framework from which to investigate further biological factors. For example, in the development of mouse hair follicles research suggests that inhibitor could be mediated via receptor-inhibitor binding (see Fig. 5.2), [17], and therefore this model already provides a framework to investigate this. In fact, the system schematised in Fig. 5.2 would provide an ideal application of the model to determine whether the results can be explained in the context of specific biological systems. Moreover, due to its simplified form the reduced two species system could also be used to incorporate other important molecular factors arising within this particular system. For example, the role of Connective Tissue Growth Factor (CTGF), illustrated in Fig. 5.2, could be examined to determine its effect on mouse follicle patterning. This would then provide clearer insight into the primary factors involved in this system and give an indication of where further work should be focussed.

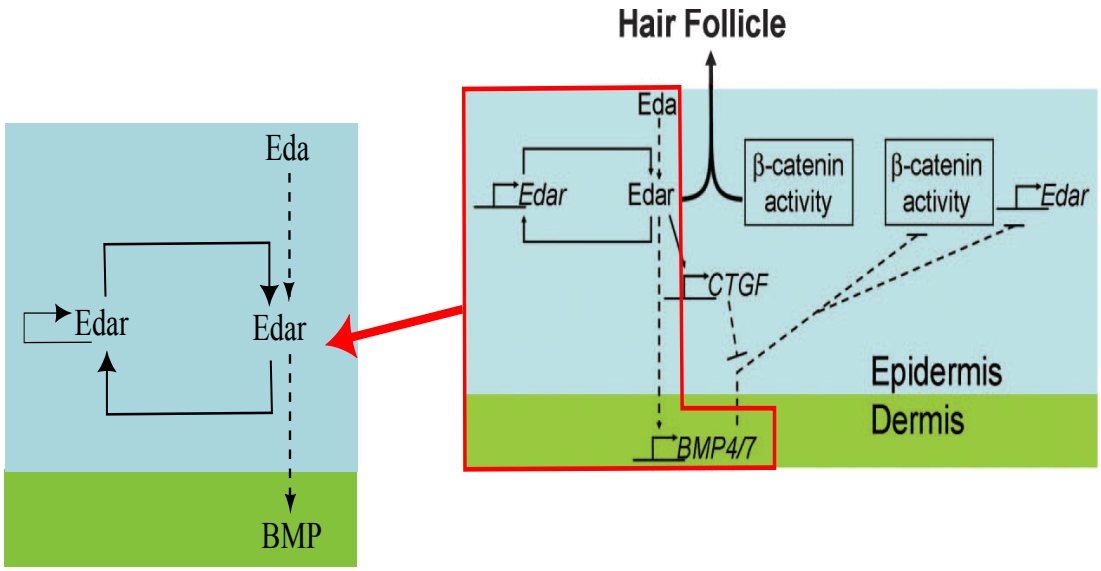

Figure 5.2: Schematic of the signalling pathway and molecular interactions involved in mouse hair follicle formation. A subset of this molecular system is considered for a possible application of the model but the full schematic is taken from [17]. The interactions between a variety of signalling factors leads to the formation of the hair follicles where the solid lines indicate local signalling and dashed lines signifying action at a distance.

As we have already discussed, another candidate system would be the sensory bristle development in Drosophila. Within this, wild type sensory bristles are arranged in an equidistant manner, initially arising from a sequence of proneural clusters consisting of approximately $7 - 9$ cells. A dominant neural fate cell within the cluster is determined via the amplification of small differences in activity levels, [109]. This neural fate cell is thought to inhibit the activity of adjacent cells and, therefore, the process is predominantly thought to consist of a lateral inhibition mechanism, [66]. However, our results suggest that a similar pattern can be obtained by implementing a model consisting of long range diffusion with short range activation via cell signalling. More significantly, we have shown that within this framework either a pure or cross type mechanism is capable of producing these types of patterns.

Notable experimental work that is thought to determine the mechanism of lateral inhibition in grasshopper embryos was undertaken by Doe and Goodman in 1985, [110, 111]. When the developing neural cell is ablated by a laser, one of the neighbouring cells replaces the ablated cell by taking the dominant neural fate. This suggests that the neighbouring cells, usually adopting a secondary fate, could escape inhibition and amplify activity. The indication from this is that lateral inhibition is the underlying mechanism driving pattern formation. The similar process of sensory bristle formation is also thought to follow this framework. Therefore, since our model indicates good agreement with the patterns arising in drosophila development we could, in some way, mimic the cell ablation experiment by decreasing cell activity in the dominant cell during pattern development of both the pure & cross type systems. Clearly, if one of the neighbouring cells then takes dominance this may cast doubt on the largely universal agreement that lateral inhibition is the specific mechanism involved in this process. Moreover, it would provide a framework for further investigation to determine the possible mechanisms initiating phenomena in these types of systems.

Together with sensory bristle formation the drosophila organism provides other examples of pattern formation in its development. For example, the drosophila eye is composed of 800 ommatidia arranged in regular sets of eight photoreceptors, known as ommatidium. In addition to lateral inhibition, however, recent research has suggested that this determination of pattern may also involve other mechanisms, see [112] and references therein. As a result, this could indicate that the mechanisms involved in our models, which show similar results to these types of systems, may be active in conjunction with lateral inhibition leading to further experimental work to determine the possible molecular factors that are involved in each mechanism.

Within this thesis, we have separately focussed on cell commitment and cell signalling as fundamental processes, with each showing a range of effects on pattern formation. Compared to the simplest system consisting of purely chemical dynamics these differences are considerable. Therefore, the significance of cell processes are

clearly highlighted and the results of both models stress the importance of incorporating cell behaviour in pattern formation mechanisms.

Appendix A

Nondimensionalisation of Cell Differentiation Models

A.1 Non-dimensionalisation of Gierer-Meinhardt Model

Consider the Precursor Specification model with pure type (Gierer-Meinhardt) kinetics given by,

$$\frac{\partial A}{\partial t} = k_1 \frac{A^2}{B} Q_1(\cdot) - k_2 A + Q_2(\cdot) + D_A \frac{\partial^2 A}{\partial x^2} \tag{A.1}$$

$$\frac{\partial B}{\partial t} = k_3 A^2 Q_3(\cdot) - k_4 B + Q_4(\cdot) + D_B \frac{\partial^2 B}{\partial x^2} \tag{A.2}$$

$$\frac{\partial C}{\partial t} = \frac{k_5 A(U_0 - C)}{k_7 + A} - k_6 C \tag{A.3}$$

By setting $A = u_0 u$, $B = v_0 v$, $C = w_0 w$, $x = x_0 x^*$, $t = t_0 t^*$ and substituting into the above equations we can reduce the number of parameters in the system. On dropping the asterisks, the nondimensionalisation reduces the system to one of the form,

$$\frac{\partial u}{\partial t} = \frac{u^2}{v} q_1(\cdot) - \alpha u + q_2(\cdot) + \frac{\partial^2 u}{\partial x^2} \tag{A.4}$$

$$\frac{\partial v}{\partial t} = u^2 q_3(\cdot) - v + q_4(\cdot) + d \frac{\partial^2 v}{\partial x^2} \tag{A.5}$$

$$\frac{\partial w}{\partial t} = \frac{u(1 - \nu w)}{\kappa + u} - \beta w \tag{A.6}$$

where α, β, κ and d are all positive parameters. The nondimensionalised variables and parameters are composed of the following:

Feedback Type	$q_1(\cdot)$	$q_2(\cdot)$	$q_3(\cdot)$	$q_4(\cdot)$	γ
Direct Positive (Activator)	0	γw	1	0	$\frac{k_3k_5k_8U_0}{k_1k_4^2}$
Direct Negative (Activator)	0	$-\gamma uw$	1	0	$\frac{k_5k_8U_0}{k_4^2}$
Regulatory Positive (Activator)	$(1+\gamma w)$	0	1	0	$\frac{k_5k_8U_0}{k_1k_4}$
Regulatory Negative (Activator)	$\frac{1}{(1+\gamma w)}$	0	1	0	$\frac{k_5k_8U_0}{k_4}$
Direct Positive (Inhibitor)	1	0	1	γw	$\frac{k_3k_5k_8U_0}{k_1^2k_4}$
Direct Negative (Inhibitor)	1	0	1	$-\gamma uw$	$\frac{k_5k_8U_0}{k_4^2}$
Regulatory Positive (Inhibitor)	1	0	$(1+\gamma w)$	0	$\frac{k_5k_8U_0}{k_3k_4}$
Regulatory Negative (Inhibitor)	1	0	$\frac{1}{(1+\gamma w)}$	0	$\frac{k_5k_8U_0}{k_4}$

with the nondimensionalised variables and other parameters composed of the following:

u_0	v_0	w_0	x_0	t_0	α	β	ν	κ	d	γ
$\frac{k_1}{k_3}$	$\frac{k_1^2}{k_3k_4}$	$\frac{k_5U_0}{k_4}$	$\sqrt{\frac{D_A}{k_4}}$	$\frac{1}{k_4}$	$\frac{k_2}{k_4}$	$\frac{k_6}{k_4}$	$\frac{k_5}{k_4}$	$\frac{k_3k_7}{k_1}$	$\frac{D_B}{D_A}$	$\frac{k_3k_5k_8U_0}{k_1k_4^2}$

A.2 Non-dimensionalisation of Schnakenberg Model

Consider the Precursor Specification model with cross type (Schnakenberg) kinetics given by,

$$\frac{\partial A}{\partial t} = k_1 + k_2A^2BQ_1(\cdot) - k_3A + Q_2(\cdot) + D_A\frac{\partial^2 A}{\partial x^2} \tag{A.7}$$

$$\frac{\partial B}{\partial t} = k_4 - k_2A^2BQ_3(\cdot) + Q_4(\cdot) + D_B\frac{\partial^2 B}{\partial x^2} \tag{A.8}$$

$$\frac{\partial C}{\partial t} = \frac{k_5A(U_0 - C)}{k_7 + A} - k_6C \tag{A.9}$$

By setting $A = u_0u$, $B = v_0v$, $C = w_0w$, $x = x_0x^*$, $t = t_0t^*$ and substituting into the above equations we can reduce the number of parameters in the system. On dropping the tildes, the nondimensionalisation reduces the system to one of the form,

$$\frac{\partial u}{\partial t} = \delta + u^2 v q_1(\cdot) - u + q_2(\cdot) + \frac{\partial^2 u}{\partial x^2} \tag{A.10}$$

$$\frac{\partial v}{\partial t} = \rho - u^2 v q_3(\cdot) + q_4(\cdot) + d\frac{\partial^2 v}{\partial x^2} \tag{A.11}$$

$$\frac{\partial w}{\partial t} = \frac{u(1-\nu w)}{\kappa + u} - \beta w \tag{A.12}$$

where δ, ρ, β, κ and d are all positive parameters. The feedback scenarios and parameter are given by

Feedback Type	$q_1(\cdot)$	$q_2(\cdot)$	$q_3(\cdot)$	$q_4(\cdot)$	γ
Direct Positive (Activator)	0	γw	1	0	$\frac{k_5 k_8 U_0}{k_3^2}\left(\frac{k_2}{k_3}\right)^{\frac{1}{2}}$
Direct Negative (Activator)	0	$-\gamma u w$	1	0	$\frac{k_5 k_8 U_0}{k_3^2}$
Regulatory Positive (Activator)	$(1+\gamma w)$	0	1	0	$\frac{k_5 k_8 U_0}{k_2 k_3}$
Regulatory Negative (Activator)	$\frac{1}{(1+\gamma w)}$	0	1	0	$\frac{k_5 k_8 U_0}{k_3}$
Direct Positive (Inhibitor)	1	0	1	γw	$\frac{k_5 k_8 U_0}{k_3^2}\left(\frac{k_2}{k_3}\right)^{\frac{1}{2}}$
Direct Negative (Inhibitor)	1	0	1	$-\gamma u w$	$\frac{k_5 k_8 U_0}{k_3^2}$
Regulatory Positive (Inhibitor)	1	0	$\frac{1}{(1+\gamma w)}$	0	$\frac{k_5 k_8 U_0}{k_3}$
Regulatory Negative (Inhibitor)	1	0	$(1+\gamma w)$	0	$\frac{k_5 k_8 U_0}{k_2 k_3}$

with the nondimensionalised variables and other parameters composed of the following:

u_0	v_0	w_0	x_0	t_0	δ	ρ	β	ν	κ	d
$\left(\frac{k_3}{k_2}\right)^{\frac{1}{2}}$	$\left(\frac{k_3}{k_2}\right)^{\frac{1}{2}}$	$\frac{k_5 U_0}{k_4}$	$\left(\frac{D_A}{k_3}\right)^{\frac{1}{2}}$	$\frac{1}{k_3}$	$\frac{k_1}{k_3}\left(\frac{k_2}{k_3}\right)^{\frac{1}{2}}$	$\frac{k_4}{k_3}\left(\frac{k_2}{k_3}\right)^{\frac{1}{2}}$	$\frac{k_6}{k_3}$	$\frac{k_5}{k_3}$	$\left(\frac{k_7^2 k_2}{k_3}\right)^{\frac{1}{2}}$	$\frac{D_B}{D_A}$

Appendix B

Linear Stability Analysis of Cell Signalling Case Studies

B.1 Linear Stability Analysis: Case Study I

We undertake a linear stability analysis for the nondimensionalised two species discrete model based on Gierer-Meinhardt reaction kinetics:

$$\frac{du_j}{dt} = \frac{u_j \bar{u}_j}{w_j} - \delta_u u_j + d_u(u_{j+1} - 2u_j + u_{j-1}), \tag{B.1}$$

$$\frac{dv_j}{dt} = u_j^2 - w_j + d_w(w_{j+1} - 2w_j + w_{j-1}), \tag{B.2}$$

The homogeneous steady state is given by $(u_s, w_s) = (\frac{1}{\delta_u}, \frac{1}{\delta_u^2})$. Using the framework set out in Chapter 4 §4.2.1, we evaluate the partial derivatives of the reaction terms such that for nontrivial solutions we require,

$$\begin{vmatrix} \delta_u K_c - \lambda + d_u K_{diff} & -\delta_u^2 \\ \frac{2}{\delta_u} & -1 - \lambda + d_w K_{diff} \end{vmatrix} = 0. \tag{B.3}$$

On expanding, this leads to a characteristic polynomial of the form,

$$\lambda^2 + a_1(k)\lambda + a_0(k) = 0, \tag{B.4}$$

where

$$a_1(k) = 1 - \delta_u K_c - (d_u + d_w)K_{diff}, \tag{B.5}$$

$$a_0(k) = d_u d_w K_{diff}^2 + (\delta_u K_c d_w - d_u)K_{diff} + 2\delta_u - \delta_u K_c. \tag{B.6}$$

Here, $K_c = \alpha\cos(k) + (1-\alpha)$ and $K_{diff} = 2(\cos(k)-1)$. We now look for the conditions under which the homogeneous steady state is *[i]* stable to a homogeneous perturbation and *[ii]* unstable to an inhomogeneous perturbation.

[*i*] Stable to a homogeneous perturbation. We look for solutions where, in the absence of spatially varying terms, $Re(\lambda(k=0)) < 0$. Using the characteristic polynomial, (B.4), we require the coefficients $a_1 > 0$ and $a_0 > 0$ for stability. Furthermore, in the absence of spatial terms, we set $k = 0 \Rightarrow K_c(0) = 1$ and $K_{diff}(0) = 0$. This gives

$$a_1(k=0) = 1 - \delta_u > 0 \Rightarrow \delta_u < 1 \tag{B.7}$$

$$a_0(k=0) = \delta_u > 0 \tag{B.8}$$

i.e. the homogeneous steady state is stable iff

$$0 < \delta_u < 1. \tag{B.9}$$

[*ii*] For the homogenoeous steady state to be unstable to an inhomogeneous perturbation we either require $a_1(k) < 0$ or $a_0(k) < 0$ for $k > 0$. However,

$$a_1(k) = \underbrace{1 - \delta_u K_c}_{>0} - (d_u + d_v)\underbrace{K_{diff}}_{<0} > 0 \tag{B.10}$$

So we can only have instability if $a_0(k) < 0$:

$$a_0(k) = \underbrace{d_u d_w K_{diff}^2}_{>0} + (\delta_u K_c d_w - d_u)\underbrace{K_{diff}}_{<0} + \underbrace{2\delta_u - \delta_u K_c}_{>0} \tag{B.11}$$

$$\begin{aligned} =&(2\delta_u\alpha d_w + 4d_u d_w)K^2 \\ &-(\delta_u\alpha + 4\delta_u\alpha d_w - 2\delta_u d_w + 8d_u d_w + 2d_u)K \\ &+4d_u d_w - 2\delta_u d_w + \delta_u\alpha + \delta_u + 2\delta_u\alpha d_w + 2d_u \end{aligned} \tag{B.12}$$

$$= a_0(K) \tag{B.13}$$

where $K = \cos(k)$. From (B.11) we see that since $K_{diff} < 0$, $\delta_u K_c d_w - d_u > 0$ is a necessary condition for $a_0(K) < 0$. For this to be satisfied we require $K_c > \frac{d_u}{\delta_u d_w}$ and, as a result, this imposes restrictions on the possible wavenumbers and corresponding wavelengths for varying parameter values. Specifically, $K = \cos(k) \in [\cos(k_c)\ \ 1]$

where $k_c = \Re(\cos^{-1}(\frac{\delta_u d_w(\alpha-1)+d_u}{\delta_u d_w \alpha}))$ is the critical wavenumber. Hence, we have minimum wavelengths ranging from $\omega = 2$ for $\alpha = 0$ to $\omega = 4$ for $\alpha = 1$. This means for autocrine signalling the model can generate patterns with alternating high/low activity levels whereas juctacrine signalling can produce minimum high activity levels every 4 cells.

These conditions are not sufficient, however, and for $a_0(K) < 0$ the minimum $a_0(K_{min})$ must also be negative. Therefore,

$$K_{min} = \frac{(\delta_u\alpha + 4\delta_u\alpha d_w - 2\delta_u d_w + 8d_u d_w + 2d_u)}{(4d_w(\delta_u\alpha + 2d_u))} \tag{B.14}$$

$$\begin{aligned} a_0(K_{min}) = &- \frac{(\delta_u\alpha + 4\delta_u\alpha d_w - 2\delta_u d_w + 8d_u d_w + 2d_u)^2}{8d_w(\delta_u\alpha + 2d_u)} \\ &+4d_u d_w - 2\delta_u d_w + \delta_u\alpha + \delta_u + 2\delta_u\alpha d_w + 2d_u \end{aligned} \tag{B.15}$$

Solving for d_w gives

$$d_w > \frac{(3+2\sqrt{2})(2d_u + \delta_u\alpha)}{2\delta_u}. \tag{B.16}$$

This situation leads to a typical form for $a_0(K)$ that follows that given by the parabola in Fig. B.1(a)(i). Moreover, the corresponding dispersion relation is shown in Fig. B.1(a)(ii). These correspond to the 'standard' analysis and are typical of forms observed in the continuous case (see [2]). In particular, there are two distinct roots, K_1, K_2, that bound the unstable wavenumbers. Specifically,

$$\begin{aligned} K_1 = &\frac{1}{4d_w(2d_u + \delta_u\alpha)}(4\delta_u d_w\alpha - 2\delta_u d_w + 2d_u + \delta_u\alpha + 8d_u d_w \\ &+\sqrt{4d_u^2 - 24\delta_u d_w d_u - 12\delta_u^2 d_w\alpha + 4d_u\delta_u\alpha + 4\delta_u^2 d_w^2 + \delta_u^2\alpha^2}), \end{aligned} \tag{B.17}$$

$$\begin{aligned} K_2 = &\frac{1}{4d_w(2d_u + \delta_u\alpha)}(4\delta_u d_w\alpha - 2\delta_u d_w + 2d_u + \delta_u\alpha + 8d_u d_w \\ &-\sqrt{4d_u^2 - 24\delta_u d_w d_u - 12\delta_u^2 d_w\alpha + 4d_u\delta_u\alpha + 4\delta_u^2 d_w^2 + \delta_u^2\alpha^2}). \end{aligned} \tag{B.18}$$

However, for certain parameter choices the form of $a_0(K)$ takes a different form in Fig. B.1(b)(i). In particular, for $d_u = 0$ & $0 \leq \alpha < 0.5$ only a single root of $a_0(K)$ is within the appropriate range ($K \in [-1\ 1]$) and some $a_0(K) < 0$ for $K_2 > -1$. The standard condition given by (B.16) is not satisfied and, in this case, we require

$$d_w > \frac{(1+2\alpha)}{4(1-2\alpha)}. \tag{B.19}$$

This time, the typical dispersion relation also has a single root but, since we are con-

sidering a discrete system, the maximum relevant wavenumber is given by $k = \pi$, Fig. B.1(b)(ii). If attainable, this wavenumber would generate patterns with a minimum wavelength of only 2 cell lengths. As a result of this, these types of dispersion relations (only one distinct root) can still correspond to pattern formation but there will be many competing unstable wavenumbers that may lead to erroneous predictions from the linear stability analysis (see for example §4.3.1: Fig. 4.3).

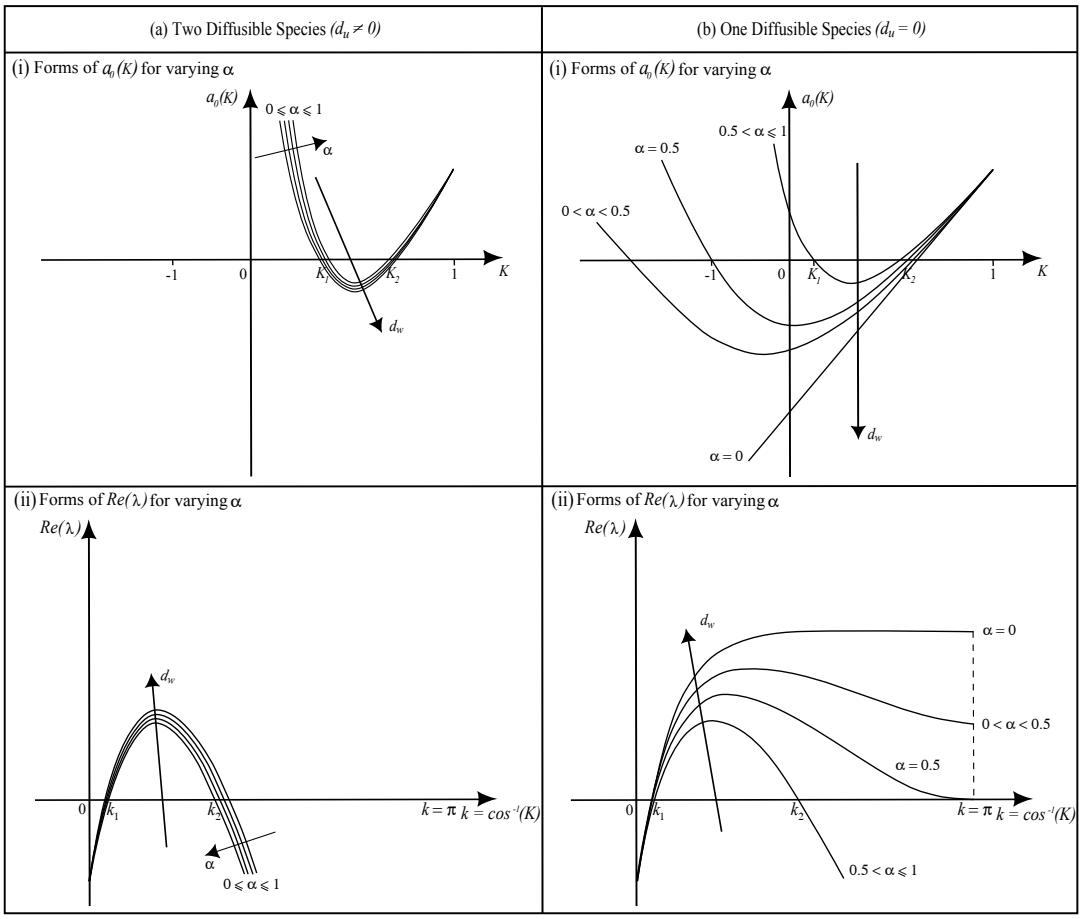

Figure B.1: Schematic illustrating the typical forms of (i) $a_0(K)$ and (ii) $Re(\lambda)$ for different parameter regimes. In particular, the models with (a) two ($d_u \neq 0$) (b) one ($d_u = 0$) diffusible species are shown, with the latter case exhibiting $a_0(k)$ and $Re(\lambda)$ forms with only a single root for $\alpha < 0.5$. In this case, the maximum attainable wavelength limits the relevant unstable wavenumbers, thus predicting pattern formation for wavenumbers within this range.

In summary, the conditions for pattern formation in the 'standard' case, when ei-

ther '$d_u > 0$' or '$d_u \neq 0$ & $\alpha \geq 0.5$', are

$$0 < \delta_u < 1 \tag{B.20}$$

$$\delta_u d_w K_c - d_u > 0 \tag{B.21}$$

$$d_w > \frac{(3+2\sqrt{2})(2d_u + \delta_u \alpha)}{2\delta_u}. \tag{B.22}$$

However, together with (B.20)-(B.21), when $d_u = 0$ & $0 \leq \alpha < 0.5$ we require,

$$d_w > \frac{(1+2\alpha)}{4(1-2\alpha)}. \tag{B.23}$$

These conditions delimit the region where pattern formation is possible and the two cases are referenced in parameter space plots through different shades of grey. In particular, the 'standard' case is denoted by the light grey region with the second case ($d_u = 0$ & $0 \leq \alpha < 0.5$) shown in dark grey (see Chapter 4: Fig. 4.1, 4.5, 4.8).

B.2 Linear Stability Analysis: Case Study II

We follow a similar framework for the nondimensionalised two species discrete model considering Schnakenberg type kinetics (see (4.48)-(4.49)):

$$\frac{du_j}{dt} = \beta + u_j \bar{u}_j w_j - u_j + d_u(u_{j+1} - 2u_j + u_{j-1}) \tag{B.24}$$

$$\frac{dw_j}{dt} = \rho - u_j \bar{u}_j w_j + d_w(w_{j+1} - 2w_j + w_{j-1}) \tag{B.25}$$

The homogeneous steady state is given by $(u_s, v_s) = (\beta + \rho, \frac{\rho}{(\beta+\rho)^2})$. Using the framework of Chapter 4 §4.2.1, we evaluate the partial derivatives of the reaction terms such that for nontrivial solutions we require,

$$\begin{vmatrix} \frac{\rho}{\beta+\rho} - 1 + \frac{\rho}{\beta+\rho}K_c - \lambda + d_u K_{diff} & (\beta+\rho)^2 \\ -\frac{2\rho}{(\beta+\rho)} - \frac{2\rho}{(\beta+\rho)}K_c & -(\beta+\rho)^2 - \lambda + d_w K_{diff} \end{vmatrix} = 0. \tag{B.26}$$

On expanding, this leads to a characteristic polynomial of the form

$$\lambda^2 + a_1(k)\lambda + a_0(k) = 0, \tag{B.27}$$

where

$$a_1(k) =(\beta+\rho)^2 - \frac{\rho}{(\beta+\rho)}K_c - \frac{\rho}{(\beta+\rho)} + 1 - (d_u+d_w)K_{diff}, \tag{B.28}$$

$$\begin{aligned} a_0(k) =& d_u d_w K_{diff}^2 + ((\frac{\rho}{(\beta+\rho)} - 1)d_w + \frac{\rho d_w}{(\beta+\rho)}K_c - d_u(\beta+\rho)^2)K_{diff} \\ &+\rho(\beta+\rho)K_c - (\frac{\rho}{(\beta+\rho)} - 1)(\beta+\rho)^2 + 2\rho(\beta+\rho), \end{aligned} \tag{B.29}$$

where $K_c = \alpha\cos(k) + (1-\alpha)$ and $K_{diff} = 2(\cos(k)-1)$. We omit the details of the calculation as it follow the same reasoning as that of the Gierer-Meinhardt type kinetics (see Appendix B.1).

The set of conditions for pattern formation in the 'standard' case, when either '$d_u > 0$' or '$d_u \neq 0$ & $\alpha \geq 0.5$', consist of

$$(\beta+\rho)^2 - \frac{2\rho}{(\beta+\rho)} + 1 > 0, \tag{B.30}$$

$$-\left(\frac{\rho}{(\beta+\rho)} - 1\right)(\beta+\rho)^2 + (\beta+\rho)\rho > 0 \tag{B.31}$$

$$\left(\frac{\rho}{(\beta+\rho)} - 1\right)d_w + \frac{\rho K_c d_w}{(\beta+\rho)} - d_u(\beta+\rho)^2 > 0, \tag{B.32}$$

$$d_w > \frac{(\rho\alpha + 3d_u\rho + d_u\beta + \sqrt{(\rho^2\alpha^2 + 6d_u\rho^2\alpha + 2d_u\beta\rho\alpha + 8d_u^2\rho^2 + 8d_u^2\beta\rho)})(\beta+\rho)^3}{(\beta^2+\rho^2-2\beta\rho)}. \tag{B.33}$$

However, together with (B.30)- (B.31), when $d_u = 0$ & $0 \leq \alpha < 0.5$ we require,

$$d_w > \frac{(\beta+\rho)^3}{(4(\rho-\beta-2\rho\alpha))} \tag{B.34}$$

The different regions are denoted through the shaded regions in parameter space plots. In particular, light and dark grey regions represent the 'standard' and '$d_u = 0$ & $0 \leq \alpha < 0.5$' cases respectively (see Chapter 4: Fig. 4.12).

B.3 Linear Stability Analysis: Full Three Species Model

We present the linear stability analysis for the three species model with discrete Gierer-Meinhardt type kinetics (see Chapter 3 §3.3.1):

$$\frac{du_j}{dt} = \frac{u_j \bar{v}_j}{w_j} - \delta_u u_j \tag{B.35}$$

$$\frac{dv_j}{dt} = \mu(u_j - v_j) + d_v(v_{j+1} - 2v_j + v_{j-1}) \tag{B.36}$$

$$\frac{dw_j}{dt} = u_j^2 - w_j + d_w(w_{j+1} - 2w_j + w_{j-1}) \tag{B.37}$$

The homogeneous steady state is given by $(u_s, v_s, w_s) = (\frac{1}{\delta_u}, u_s, u_s^2)$. Considering small perturbations to the steady state, expanding by the Taylor series and ignoring higher order terms we can obtain the linearised system. Looking for solutions of the form $\propto exp(\lambda t + ijk)$, a standard analysis shows non trivial solutions occur for

$$\begin{vmatrix} -\lambda & \delta_u K_c & -1 \\ \mu & -\mu - \lambda + d_v K_{diff} & 0 \\ \frac{2}{\delta_u} & 0 & -1 - \lambda + d_w K_{diff} \end{vmatrix} = 0 \tag{B.38}$$

Expanding the determinant, leads to a characteristic polynomial of the form,

$$\lambda^3 + a_2(k)\lambda^2 + a_1(k)\lambda + a_0(k) = 0 \tag{B.39}$$

where

$$a_2(k) = 1 + \mu - (d_v + d_w)K_{diff}(k), \tag{B.40}$$

$$a_1(k) = d_v d_w K_{diff}^2(k) - (d_v + d_w\mu)K_{diff}(k) + \mu + \frac{2}{\delta_u} - \delta_u \mu K_c, \tag{B.41}$$

$$a_0(k) = \left(-\frac{2d_v}{\delta_u} + \delta_u \mu d_w K_c(k)\right) K_{diff}(k) + \frac{2\mu}{\delta_u} - \delta_u \mu K_c(k). \tag{B.42}$$

As previously, $K_c(k) = \alpha\cos(k) + (1-\alpha)$ and $K_{diff}(k) = 2(\cos(k) - 1)$. Again we examine conditions under which the homogeneous steady state is $[i]$ stable to a homogeneous perturbation and $[ii]$ unstable to an inhomogeneous perturbation.

$[i]$ Stable to a homogeneous perturbation: In the absence of any spatial term $k = 0$

and therefore $K_c(0) = 1$, $K_{diff} = 0$. This leads to,

$$a_2 = 1 + \mu, \tag{B.43}$$

$$a_1 = \mu + \frac{2}{\delta_u} - \delta_u \mu, \tag{B.44}$$

$$a_0 = \frac{2\mu}{\delta_u} - \delta_u \mu, \tag{B.45}$$

Using the Routh-Hurwitz conditions, we find stability to homogeneous perturbations for

$$\mu > 0, \tag{B.46}$$

$$0 < \delta_u < \sqrt{2}, \tag{B.47}$$

$$(\mu + \frac{2}{\delta_u} - \delta_u \mu)(1 + \mu) - \frac{2\mu}{\delta_u} - \delta_u \mu > 0. \tag{B.48}$$

[*ii*] Unstable to an inhomogeneous perturbation: with spatially varying terms ($k \neq 0$) $K_c = \alpha \cos(k) + (1 - \alpha)$ and $K_{diff} = 2(\cos(k) - 1)$. Then, the coefficients of the characteristic polynomial are

$$a_2(k) = 1 + \mu - (d_v + d_w) K_{diff}(k), \tag{B.49}$$

$$a_1(k) = d_v d_w K_{diff}^2(k) - (d_v + d_w \mu) K_{diff}(k) + \mu + \frac{2}{\delta_u} - \delta_u \mu K_c, \tag{B.50}$$

$$a_0(k) = \left(-\frac{2 d_v}{\delta_u} + \delta_u \mu d_w K_c(k) \right) K_{diff}(k) + \frac{2\mu}{\delta_u} - \delta_u \mu K_c(k). \tag{B.51}$$

The homogeneous steady state becomes unstable if either $a_0(k) < 0$ or $a_1(k) a_2(k) - a_0(k) < 0$. From the following we note $a_2(k) > 0$, $a_1(k) > 0$:

$$a_2(k) = \overbrace{1 + \mu}^{>0 \text{ from (i)}} - \overbrace{(d_v + d_w) K_{diff}(k)}^{<0 \ (Kdiff \leq 0)} \tag{B.52}$$

$$a_1(k) = \underbrace{d_v d_w K_{diff}^2(k)}_{>0} - \underbrace{(d_v + d_w \mu) K_{diff}(k)}_{<0 \ (Kdiff \leq 0)} + \underbrace{\mu + \frac{2}{\delta_u} - \delta_u \mu K_c}_{>0} \tag{B.53}$$

Finding an explicit analytical result for the instability requirement given by $a_1 a_2 - a_0(k) < 0$ becomes difficult due to the complexity of the expression. Within the

parameter regimes explored and the resolution of the numerical method, we did not find any regimes for which have $a_0(k) > 0$ and $a_1a_2 - a_0(k) < 0$. Therefore, while we cannot definitively rule out instability via this route, our numerical investigation suggests it is an unlikely source of instability. From this, we predict that $a_1a_2 - a_0(k) > 0$ and the only way to instability is via $a_0(k) < 0$.

A necessary condition for $a_0(k) < 0$ is $-\frac{2d_v}{\delta_u} + \delta_u\mu d_w K_c(k) > 0$. However, we also require the minimum $a_0(K_{min}) < 0$:

$$\begin{aligned} a_0(K = \cos(k)) = 2\delta_u\mu\alpha d_w K^2 - (\delta_u\mu\alpha + \frac{4d_v}{\delta_u} - 2\delta_u\mu d_w + 4\delta_u\mu\alpha d_w)K \\ -\delta_u\mu(1-\alpha) - 2\delta_u\mu d_w(1-\alpha) + \frac{2\mu}{\delta_u} + \frac{4d_v}{\delta_u}, \end{aligned} \tag{B.54}$$

$$K_{min} = \frac{\delta_u\mu\alpha + \frac{4d_v}{\delta_u} - 2\delta_u\mu d_w + 4\delta_u\mu\alpha d_w}{4\delta_u\mu\alpha d_w}, \tag{B.55}$$

$$\begin{aligned} a_0(K_{min}) = -\frac{\delta_u\mu\alpha + \frac{4d_v}{\delta_u} - 2\delta_u\mu d_w + 4\delta_u\mu\alpha d_w}{8\delta_u\mu\alpha d_w} \\ -\delta_u\mu(1-\alpha) - 2\delta_u\mu d_w(1-\alpha) + \frac{2\mu}{\delta_u} + \frac{4d_v}{\delta_u}. \end{aligned} \tag{B.56}$$

Solving for d_w leads to the condition,

$$d_w > \frac{\left(-\frac{1}{2}\delta_u^2\mu\alpha + 2\mu\alpha + 2d_v + \sqrt{2\delta_u^2\mu^2\alpha^2 - 4\delta_u^2\mu\alpha d_v + 4\mu^2\alpha^2 + 8d_v\alpha\mu}\right)}{\delta_u^2\mu}. \tag{B.57}$$

However, this time the typical forms of $a_0(K)$ and the corresponding dispersion relations exhibit different behaviour that is purely dependent on α. In this three species system, both diffusivity cases follow similar behaviour to the one diffusible species reduced system, Fig. B.2. Therefore, when $0 \leq \alpha < 0.5$ we are required to consider $K_2 > -1$, leading to the condition

$$d_w > \frac{(\delta_u^2\mu - 2\mu - 2\delta_u^2\mu\alpha - 8d_v)}{\mu\delta_u^2(2\alpha - 1)}. \tag{B.58}$$

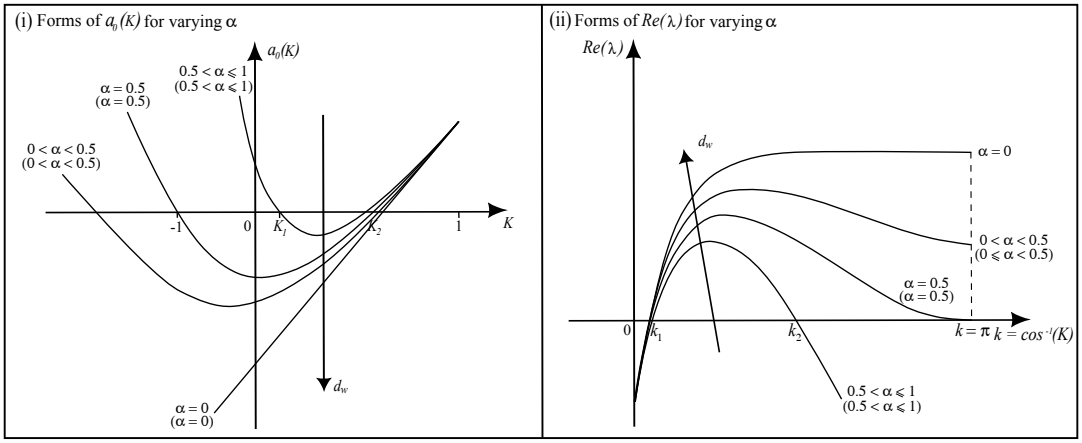

Figure B.2: Schematic illustrating the typical forms of $a_0(K)$ and $Re(\lambda)$ for different parameter regimes. In particular, the forms for a model with one diffusible species ($d_v = 0$) and two diffusible species ($d_v \neq 0$) are similar. However, the forms for the different parameter regimes of the two diffusible species model are referenced via the bracketed values.

We now have a set of conditions that, if satisfied, will lead to pattern formation:

$$\mu > 0, \tag{B.59}$$

$$0 < \delta_u < \sqrt{2}, \tag{B.60}$$

$$-\frac{2d_v}{\delta_u} + \delta_u \mu d_w K_c(k) > 0, \tag{B.61}$$

$$d_w > \frac{\left(-\frac{1}{2}\delta_u^2\mu\alpha + 2\mu\alpha + 2d_v + \sqrt{2\delta_u^2\mu^2\alpha^2 - 4\delta_u^2\mu\alpha d_v + 4\mu^2\alpha^2 + 8d_v\alpha\mu}\right)}{\delta_u^2\mu}. \tag{B.62}$$

The above conditions, (B.59)-(B.62), are applicable when $\alpha \geq 0.5$. However, together with (B.59)-(B.61), when $0 \leq \alpha < 0.5$ we require,

$$d_w > \frac{(\delta_u^2\mu + 2\mu + 2\delta_u^2\mu\alpha + 8d_v)}{4\mu\delta_u^2(1-2\alpha)}. \tag{B.63}$$

These conditions produce distinct regions of parameter space with different shades of grey denoting the different cases. In particular, the conditions that satisfy $\alpha \geq 0.5$ are given by the light grey region and $0 \leq \alpha < 0.5$ by the dark grey region (see Fig. 4.23).

Appendix C

Numerical Methods

C.1 Cell Differentiation

Due to the analytically intractable form, a numerically investigation was undertaken throughout the analysis of Chapter 2. Here we provide details of the numerical methods.

C.1.1 Parameter Space Analysis

To determine the regions of parameter space in §2.3.2, we used the in-built roots function in MATLAB to find the eigenvalues, λ, of the characteristic polynomials for the models (2.30)-(2.37). Over the discretised parameter domains, we determined whether any parameters exhibited the fundamental conditions for Turing type pattern formation: homogeneous steady state is stable to a homogeneous perturbation ($Re(\lambda(k = 0)) < 0$) whilst being unstable to inhomogeneous perturbations ($Re(\lambda(k \neq 0)) > 0$). A discretisation of the parameter regimes, in steps of 0.01, were considered for a range of k values ($\Delta k = 0.01$) and the outer values of the parameters points that included both of these conditions were plotted using MATLAB. The corresponding plots can be seen in Fig. 2.7 and Fig. 2.9(a).

The percentage increase plots illustrating the changes in the parameter spaces for increasing feedback parameter, γ, are shown in Fig. 2.8. By using the same discretisation, $\Delta = 0.01$, of the whole domain and parameter space points, the numerical areas of both could be found. Using this, comparitive data regarding the percentage area consumed by the parameter space was evaluated and plotted using MATLAB.

C.1.2 Numerical Simulations

- The one dimensional simulations given in §2.3.3: Fig. 2.12, 2.13, 2.14, 2.18(a) and 2.19 are plotted using the MATLAB in-built Partial Differential Equation (PDE) solver *pdepe*. This solves initial-boundary value problems for parabolic

and elliptic PDEs in one dimension by converting the PDEs into a set of Ordinary Differential Equations (ODEs) via the method of lines. The remaining set of ODEs are then solved using *ode*15*s* (see below). Here, we consider a default discretisation in space of $\Delta x = 0.1$ with relative and absolute tolerance levels at 10^{-6}. However, it should be noted that no difference in simulations is observed when investigating tolerance levels at 10^{-8}. In all simulations, we define the initial conditions to be a 2% random perturbation to the homogeneous steady state and boundary conditions as zero-flux.

- The two dimensional simulations given in §2.3.3: Fig. 2.15, 2.16, 2.17, 2.18(b), 2.20 and 2.21 are solved using an Alternating Direction Implicit (ADI) scheme and implemented using Fortran with a tridiagonal solver. In particular, the ADI scheme is a finite difference method that is split into two parts that implicitly solves the different models, (2.30)-(2.37), in one space dimension and then the other. Discretisations of $\Delta x = 0.1$ and $\Delta t = 0.001$ are given for space and time respectively. Furthermore, to be consistent with the one dimensional simulations the initial conditions are given as a 2% random perturbation to the homogeneous steady state with zero-flux imposed at the boundary. The output figures were produced using MATLAB.

C.2 Cell Signalling

The models in Chapter 4 (see §4.2) with different diffusion and signalling scenarios were numerically solved on both one and two dimensional domains. Here we give an brief overview of the numerical methods used:

- The one dimensional simulations given throughout Chapter 4 were solved using the MATLAB in-built ODE solver *ode*15*s*. This multi-step solver approximates the solution at time point $t + \Delta t$ by considering the solution at previous time points. As a result, it can adapt the time-step, Δt, according to changes in the solution. The spatial domains in simulations consist of 100 and 200 cells. The relative and absolute tolerance levels were given as 10^{-6} but, once again, levels at 10^{-8} appeared to not affect the solutions. Initial conditions were considered to be a 2% random pertutrbation to the homogeneous steady state and periodic boundary conditions were implemented.

- The two dimensional simulations considered square cells on a 200x200 grid and hexagonal cells on a 50x50 grid. Similarly to the one dimensional simulations, we used the in-built MATLAB solver *ode*15*s* with tolerance levels at 10^{-6}, initial conditions given by a 2% random perturbation to the steady state and boundary conditions being periodic.

- §4.7.1, Fig. 4.25(c): To determine the effect of increasing μ on the parameter space, we tracked the progressive differences between the $d_v = 0$ and $d_v \neq 0$ parameter space curves for increasing μ. We calculated the l_2-norm in both cases and found the difference between these for $\mu = 1, ..., 200$. From this, the l_2-norm tends to zero as μ is increased suggesting that for large μ the $d_v \neq 0$ tends to the $d_v = 0$ parameter space curve. Mathematically, this is represented by

$$\left(\left|\mathbf{x}_{(d_v=0)}\right|_2 - \left|\mathbf{x}_{(d_v\neq 0;\,\mu)}\right|_2\right) \to 0 \quad \text{as } \mu \to \infty;$$

where $\mathbf{x}$ is a vector with $\mathbf{x}_{(d_v=0)}$ and $\mathbf{x}_{(d_v\neq 0;\,\mu)}$ denoting the parameter space curves for $d_v = 0$ and $d_v \neq 0$ for increasing μ respectively.

Bibliography

[1] Aristotle. *On The Generation of Animals*. Translation by Arthur Platt: `http://ebooks.adelaide.edu.au/a/aristotle/generation/`.

[2] Murray J.D. *Mathematical Biology II: Spatial Models and Biomedical Applications*. Springer, third edition edition, 2002.

[3] Maini P.K., Painter K.J., and Chau H.N.P. Spatial pattern formation in chemical and biological systems. *Journal of the Chemical Society, Faraday Transactions*, 93(20):3601–3610, 1997.

[4] Murray J.D. *Mathematical Biology I: An Introduction*. Springer, third edition edition, 2002.

[5] Meinhardt H. Morphogenesis of lines and nets. *Differentiation*, 6(2):117–123, 1976.

[6] Nelson T. and Denglerb N. Leaf vascular pattern formation. *The Plant Cell*, 9:1121–1135, 1997.

[7] Polezhaev A.A., Pashkov R.A., Lobanov A.I., and Petrov I.B. Spatial patterns formed by chemotactic bacteria escherichia coli. *International Journal of Developmental Biology*, 50(2-3):309–314, 2006.

[8] C.H. Waddington. *Organisers and Genes*. Cambridge University Press.

[9] Turing A.M. The chemical basis of morphogenesis. *Philosophical Transactions of the The Royal Society of London B*, 237(641):37–72, 1952.

[10] Wolpert L. Positional information and the spatial pattern of cellular differentiation. *Journal of Theoretical Biology*, 25(1):1–47, 1969.

[11] Wall N.A. and Hogan B.L.M. Tgf-β related genes in development. *Current Opinion in Genetics and Development*, 4:293–320, 1994.

[12] Jung H.S., Francis-West P.H., Widelitz R.A., Jiang T.X., Ting-Berreth S.A., Tickle C., Wolpert L., and Chuong C.M. Local inhibitory action of bmps and

their relationships with activators in feather formation: Implications for periodic patterning. *Developmental Biology*, 196(1):11–23, 1998.

[13] Widelitz R.B., Jiang T.X., Noveen A., Chen C.W., and Chuong C.M. Fgf induces new feather buds from developing avian skin. *Journal of Investigative Dermatology*, 107(6):797–803, 1996.

[14] Schlake T. and Sick S. Canonical wnt signalling controls hair follicle spacing. *Cell Adhesion and Migration*, 1(3):149–51, 2007.

[15] Andl T., Reddy S.T., Gaddapara T., and Millar S.E. Wnt signals are required for the initiation of hair follicle development. *Developmental Cell*, 2(5):643–653, 2002.

[16] Drew C.F., Lin C.M., Jiang T.X., Blunt G., Mou C., Chuong C.M., and Headon D.J. The edar subfamily in feather placode formation. *Developmental Biology*, 305(1):232–245, 2007.

[17] Mou C., Jackson B., Schneider P., Overbeek P.A., and Headon D.J. Generation of the primary hair follicle pattern. *Proceedings of the National Academy of Sciences U S A.*, 103(24):9075–9080, 2006.

[18] Sick S., Reinker S., Trimmer J., and Schlake T. Wnt and dkk determine hair follicle spacing through a reaction-diffusion mechanism. *Science*, 314:1447, 2009.

[19] Lewis J. From signals to patterns: space, time, and mathematics in developmental biology. *Science*, 322:399–403, 2008.

[20] Edelstein-Keshet L. *Mathematical Models in Biology.* SIAM, 2005.

[21] Dillon R., Maini P.K., and Othmer H.G. Pattern formation in generalized turing systems i. steady-state patterns in systems with mixed boundary conditions. *Journal of Mathematical Biology*, 32:345–393, 1994.

[22] Gierer A. and Meinhardt H. A theory of biological pattern formation. *Kybernetic*, 12:30–39, 1972.

[23] Castets V.V., Dulos E., Boissonade J., and De Kepper P. Experimental evidence of a sustained standing turing-type nonequilibrium chemical pattern. *Physical Revier Letters*, 64(24):2953–2956, 1990.

[24] Kauffman S.A., Shymko R.M., and Trabert K. Control of sequential compartment formation in drosophila. *Science*, 199(4326):259–270, 1978.

[25] Bard J.B. A model for generating aspects of zebra and other mammalian coat patterns. *Journal of Theoretical Biology*, 93(2):363–385, 1981.

[26] Kondo S., Iwashita M., and Yamaguchi M. How animals get their skin patterns: fish pigment pattern as a live turing wave. *International Journal of Developmental Biology*, 53(5-6):851–856, 2009.

[27] Barrio R.A., Baker R.E., Vaughan B. Jr., Tribuzy K., de Carvalho M.R., Bassanezi R., and Maini P.K. Modeling the skin pattern of fishes. *Physical Review E*, 79(3):031908, 2009.

[28] Meinhardt H. and Klingler M. A model for pattern formation on the shells of molluscs. *Jounal of Theoretical Biology*, 126:63–89, 1987.

[29] Nagorcka B.N. and Mooney J.R. The role of a reaction-diffusion system in the formation of hair fibres. *Journal of Theoretical Biology*, 98:575–607, 1982.

[30] Nagorcka B.N. and Mooney J.R. The role of a reaction-diffusion system in the initiation of primary hair follicles. *Journal of Theoretical Biology*, 114:243–272, 1985.

[31] Nagorcka B.N. and Mooney J.R. Spatial patterns produced by a reaction-diffusion system in primary hair follicles. *Journal of Theoretical Biology*, 115:299–317, 1985.

[32] Painter K.J., Hunt G.S., Wells K. L., Johansson J. A., and Headon D. J. Towards an integrated experimental-theoretical approach for assessing the mechanistic basis of hair and feather morphogenesis. *The Royal Society Interface Focus*, 10.1098/rsfs.2011.0122, 2012.

[33] Maini P.K. and Solursh M. Cellular mechanisms of pattern formation in the developing limb. *International Review of Cytology*, 129:91–133, 1990.

[34] Othmer H.G., Painter K.J., Umulis D., and Xue C. The intersection of theory and application in elucidating pattern formation in developmental biology. *Mathematical Modelling of Natural Phenomena*, 4(4):3–82, 2009.

[35] Barrio R.A., Varea C., Aragón J.L., and Maini P.K. A two-dimensional numerical study of spatial pattern formation in interacting turing systems. *Bulletin of Mathematical Biology*, 61(3):483–505, 1999.

[36] Ermentrout B. Spots or stripes? nonlinear effects in bifurcation of reaction diffusion equations on the square. *Proceedings of the Royal Society A*, 434:413–417, 1991.

[37] Nagorcka B.N. and Mooney J.R. From stripes to spots: prepatterns which can be produced in the skin by a reaction-diffusion system. *IMA Journal of Mathematics Applied in Medicinal Biology*, 9(4):249–67, 1992.

[38] Edelstein-Keshet L. *Mathematical Models in Biology*. SIAM, 2005.

[39] Headon D.J. and Painter K.J. Stippling the skin: Generation of anatomical periodicity by reaction-diffusion mechanisms. *Mathematical Modelling of Natural Phenomena*, 4(4):10.1051/mmnp/20094403, 2009.

[40] Lengyel I. and Epstein I.R. Modelling of turing structures in the chloriteiodide-malonic acid-starch reaction system. *Science*, 251(4994):650–652, 1991.

[41] Thomas D. *Artificial enzyme membranes, transport, memory, and oscillatory phenomena In: Analysis and Control of Immobilized Enzyme Systems*. Springer, 1975.

[42] Prigogene I. and Lefever R. Symmetry breaking instabilities in dissipative systems. ii. *Journal of Chemical Physics*, 48(4):1665–1700, 1968.

[43] Schnakenberg J. Simple chemical-reaction systems with limit-cycle behaviour. *Journal of Theoretical Biology*, 81:389–400, 1979.

[44] Koch A.J. and Meinhardt H. Biological pattern formation: From basic mechanisms to complex structures. *Review of Modern Physics*, 66(4):1481–1507, 1994.

[45] Oster G.F., Murray J.D., and Harris A.K. Mechanical aspects of mesenchymal morphogenesis. *Journal of Embryology and Experimental Morphology*, 78:83–125, 1983.

[46] Keller E.F. and Segel L.A. Initiation of slime mold aggregation viewed as an instability. *Journal of Theoretical Biology*, 26(3):399–415, 1970.

[47] Hillen T. and Painter K.J. A user's guide to pde models for chemotaxis. *Journal of Mathematical Biology*, 58(1-2):183–217, 2009.

[48] Palsson E. and Othmer H.G. A model for individual and collective cell movement in dictyostelium discoideum. *Proceedings of the National Academy of Sciences USA.*, 97(19):10448–10453, 2000.

[49] Hofer T., Sherratt J.A., and Maini P.K. Dictyostelium discoideum: Cellular self-organization in an excitable biological medium. *Proceedings of the Royal Society B*, 259(1356):249–257, 1995.

[50] Painter K.J., Maini P.K., and Othmer H.G. Stripe formation in juvenile pomacanthus explained by a generalized turing mechanism with chemotaxis. *Proceedings of the National Academy of Sciences USA.*, 96(10):5549–5554, 1999.

[51] Murray J.D. and Myerscough M.R. Pigmentation pattern formation on snakes. *Journal of Theoretical Biology*, 149(3):339–360, 1991.

[52] Lin C.M., Jiang T.X., Baker R.E., Maini P.K., Widelitz R.B., and Chuong C.M. Spots and stripes: pleomorphic patterning of stem cells via p-erk-dependent cell chemotaxis shown by feather morphogenesis and mathematical simulation. *Developmental Biology*, 334(2):369–382, 2009.

[53] Vasiev B., Balter A., Chaplain M., Glazier J.A., and Weijer C.J. Modeling gastrulation in the chick embryo: formation of the primitive streak. *PLoS One*, 5(5):e10571, 2010.

[54] Murray J.D., Oster G.F., and Harris A.K. A mechanical model for mesenchymal morphogenesis. *Journal of Mathematical Biology*, 17:125–129, 1983.

[55] Olsen L., Sherratt J.A., and P.K. Maini. A mechanochemical model for adult dermal wound contraction and the permanence of the contracted tissue displacement profile. *Jornal of Theoretical Biology*, 117:113–128, 1995.

[56] Holmes M.J. and Sleeman B.D. A mathematical model of tumour angiogenesis incorporating cellular traction and viscoelastic effects. *Journal of Theoretical Biology*, 202(2):95–112, 2000.

[57] Graner F. and Glazier J.A. Simulation of biological cell sorting using a two dimensional extended potts model. *Physical Review Letters*, 69(13):2013–2016, 1992.

[58] Glazier J.A. and Graner F. Simulation of the differential adhesion driven rearrangement of biological cells. *Physical Review E*, 47(3):2128–2154, 1993.

[59] Deutsch A. and Dormann S. *Cellular Automaton Modeling of Biological Pattern Formation Characterization, Applications, and Analysis*. Springer, 2005.

[60] Gerisch A. and Painter K.J. *Mathematical modelling of cell adhesion and its applications to developmental biology and cancer invasion (pg* 319350*). In Chauviere A. & Preziosi L. (Editors), Cell and tissue mechanics*. Springer, 2010.

[61] Othmer H.G. and Scriven L.E. Instability and dynamic pattern in cellular networks. *Journal of Theoretical Biology*, 32(3):507–537, 1971.

[62] Alberts B., Bray D., Lewis J., Raff M., Roberts K., and Watson J.D. *Molecular Biology of the Cell*. Garland Publishing, Third Edition, 1994.

[63] Anklesaria P., Teixidó J., Laiho M., Pierce J.H., Greenberger J.S., and Massagué J. Cell-cell adhesion mediated by binding of membrane-anchored transforming growth factor alpha to epidermal growth factor receptors promotes cell proliferation. *Proceedings of the National Academy of Sciences U.S.A.*, 87(9):3289–3293, 1990.

[64] Massague J. and Pandiella A. Membrane-anchored growth factors. *Annual Review of Biochemistry*, 62:515–526, 1993.

[65] Collier J.R., Monk N.A., Maini P.K., and Lewis J.H. Pattern formation by lateral inhibition with feedback: a mathematical model of delta-notch intercellular signalling. *Journal of Theoretical Biology*, 183(4):429–46, 1996.

[66] Simpson P. Lateral inhibition and the development of the sensory bristles of the adult peripheral nervous system of drosophila. *Development*, 109:509–519, 1990.

[67] Owen M.R. and Sherratt J.A. Mathematical modelling of juxtacrine cell signalling. *Mathematical Biosciences*, 153:125–150, 1998.

[68] Owen M.R., Sherratt J.A., and Myers S.R. How far can a juxtacrine signal travel? *Proceedings of the Royal Society B*, 266:579–585, 1999.

[69] Owen M.R., Sherratt J.A., and Wearing H.J. Lateral induction by juxtacrine signaling is a new mechanism for pattern formation. *Developmental Biology*, 217:54–61, 2000.

[70] Wearing H.J., Owen M.R., and Sherratt J.A. Mathematical modelling of juxtacrine patterning. *Bulletin of Mathematical Biology*, 62:293–320, 2000.

[71] Webb S.D. and Owen M.R. Intra-membrane ligand diffusion and cell shape modulate juxtacrine patterning. *Journal of Theoretical Biology*, 230:99–117, 2004.

[72] Gilbert S.F. *Developmental Biology*. Sinauer Associates, Ninth Edition, 2010.

[73] Levy V., Lindon C., Harfe B.D., and Morgan B.A. Distinct stem cell populations regenerate the follicle and interfollicular epidermis. *Developmental Cell*, 9(6):855–861, 2005.

[74] Marshman E., Booth C., and Potten C.S. The intestinal epithelial stem cell. *Bioessays*, 24(1):91–98, 2002.

[75] Baker R.E., Gaffney E.A., and Maini P.K. Partial differential equations for self organization in cellular and developmental biology. *Nonlinearity*, 21(11):251–290, 2008.

[76] Jiang T.X., Jung H.S., Widelitz R.B., and Chuong C.M. Self-organization of periodic patterns by dissociated feather mesenchymal cells and the regulation of size, number and spacing of primordia. *Development*, 126(22):4997–5009, 1999.

[77] Maderspacher F. and Nüsslein-Volhard C. Formation of the adult pigment pattern in zebrafish requires leopard and obelix dependent cell interactions. *Development*, 130(15):3447–3457, 2003.

[78] Nakamasu A., Takahashi G., Kanbe A., and Kondo S. Interactions between zebrafish pigment cells responsible for the generation of turing patterns. *PNAS*, 106(21):8429–8434, 2009.

[79] Rauch E.M. and Millonas M.M. The role of trans-membrane signal transduction in turing-type cellular pattern formation. *Journal of Theoretical Biology*, 226:401–407, 2004.

[80] Wodarz A. and Huttner W.B. Asymmetric cell division during neurogenesis in drosophila and vertebrates. *Mechanisms of Development*, 120:1297–1309, 2003.

[81] Zhong W. Timing cell-fate determination during asymmetric cell divisions. *Current Opinion in Neurobiology*, 18(5):472–478, 2008.

[82] Knoblich J.A. Mechanisms of asymmetric stem cell division. *Cell*, 132(4):583–597, 2008.

[83] Taylor G., Lehrer S.M., Jensen J.P., Sun T.T., and Lavker M.R. Involvement of follicular stem cells in forming not only the follicle but also the epidermis. *Cell*, 102:451–461, 2000.

[84] Klika V., Baker R.E., Headon D., and Gaffney E.A. The influence of receptor-mediated interactions on reaction-diffusion mechanisms of cellular self-organisation. *Bulletin of Mathematical Biology*, 74(4):935–957, 2012.

[85] Miyazawa S., Okamoto M., and Kondo S. Blending of animal colour patterns by hybridization. *Nature Communications*, 1(66):10.1038/ncomms1071, 2010.

[86] Meinhardt H. Out-of-phase oscillations and traveling waves with unusual properties: the use of three-component systems in biology. *Physica D: Nonlinear Phenomena*, 199(1-2):264–277, 2004.

[87] Suzuki N., Hirata M., and Kondo S. Traveling stripes on the skin of a mutant mouse. *PNAS*, 100(17):9680–9685, 2003.

[88] Crampin E.J., Hackborn W.W., and Maini P.K. Pattern formation in reaction-diffusion models with nonuniform domain growth. *Bulletin of Mathematical Biology*, 64(4):747–769, 2002.

[89] Barrass I., Crampin E.J., and Maini P.K. Mode transitions in a model reaction-diffusion system driven by domain growth and noise. *Bull Math Biol.*, 68(5):981–995, 2006.

[90] Liu R.T., Liaw S.S., and Maini P.K. Two-stage turing model for generating pigment patterns on the leopard and the jaguar. *Physical Review E*, 74(1):011914, 2006.

[91] Haddon C., Smithers L., Schneider-Maunoury S., Coche T., Henrique D., and Lewis J. Multiple delta genes and lateral inhibition in zebrafish primary neurogenesis. *Development*, 125(3):359–370, 1998.

[92] Stroedicke M., Karberg S., and Korge G. Domina (dom), a new drosophila member of the fkh/wh gene family, affects morphogenesis and is a suppressor of position-effect variegation. *Mechanisms of Development*, 96:67–78, 2000.

[93] Cohen M., Baum B., and Miodownik M. The importance of structured noise in the generation of self-organizing tissue patterns through contact-mediated cellcell signalling. *Journal of the Royal Society Interface*, 8(59):787–98, 2010.

[94] Rawls J.F., Mellgren E.M., and Johnson S.L. How the zebrafish gets its stripes. *Developmental Biology*, 240:301–314, 2001.

[95] Morgan T.H. The theory of the gene. *The American Naturalist*, 51:513–544, 1917.

[96] Wharton K.A., Johansen K.M., Xu T., and Artavanis-Tsakonas S. Nucleotide sequence from the neurogenic locus notch implies a gene product that shares homology with proteins containing egf-like repeats. *Cell*, 43(3):567–581, 1985.

[97] Kidd S., Kelley M.R., and Young M.W. Sequence of the notch locus of drosophila melanogaster: relationship of the encoded protein to mammalian clotting and growth factors. *Molecular and Cellular Biology*, 6(9):3094–3108, 1986.

[98] Muskavitch M.A. Delta-notch signaling and drosophila cell fate choice. *Developmental Biology*, 166(2):415–430, 1994.

[99] Basson M.D. Mucosal healing and adaptation in the small intestine. *Current Opinion in General Surgery*, pages 138–46, 1994.

[100] Masood R., Kundra A., Zhu S., Xia G., Scalia P., and Smith D.L. Malignant mesothelioma growth inhibition by agents that target the vegf and vegf-c autocrine loops. *International Journal of Cancer*, 104(5):603–610, 2003.

[101] Moreira I.S., Fernandes P.A., and Ramos M.J. Vascular endothelial growth factor (vegf) inhibition–a critical review. *Anticancer Agents in Medicinal Chemistry*, 7(2):223–245, 2007.

[102] Kawano Y. and Kypta R. Secreted antagonists of the wnt signalling pathway. *Journal of Cell Science*, 116:2627–2634, 2003.

[103] zur Lage P. and Jarman A.P. Antagonism of egfr and notch signalling in the reiterative recruitment of drosophila adult chordotonal sense organ precursors. *Development*, 126(14):3149–57, 1992.

[104] Mattila P.K. and Lappalainen P. Filopodia: molecular architecture and cellular functions. *Nature Reviews Molecular Cell Biology*, 9(6):446–454, 2008.

[105] Qi H., Rand M.D., Wu X., Sestan N., Wang W., Rakic P., Xu T., and Artavanis-Tsakonas S. Processing of the notch ligand delta by the metalloprotease kuzbanian. *Science*, 283(5398):91–94, 1999.

[106] Thorne R.G., Hrabetov S., and Nicholson C. Diffusion of epidermal growth factor in rat brain extracellular space measured by integrative optical imaging. *Journal of Neurophysiology*, 92(6):3471–3481, 2004.

[107] Gompela N., Cubedoa N., Thisseb C., Thisseb B., Dambly-Chaudierea C., and Ghysen A. Pattern formation in the lateral line of zebrafish. *Mechanisms of Development*, 105(1-2):69–77, 2001.

[108] Mustonen T., Ilmonen M., Pummila M., Kangas A.T., Laurikkala J., Jaatinen R., Pispa J., Gaide O., Schneider P., Thesleff I., and Mikkola M.L. Ectodysplasin a1 promotes placodal cell fate during early morphogenesis of ectodermal appendages. *Development*, 131(20):4907–4919, 2004.

[109] Chitnis A.B. The role of notch in lateral inhibition and cell fate specification. *Molecular and Cellular Neuroscience*, 6(6):311–321, 1995.

[110] Doe C.Q. and Goodman C.S. Early events in insect neurogenesis. i. development and segmental differences in the pattern of neuronal precursor cells. *Developmental Biology*, 111(1):193–205, 1985.

[111] Doe C.Q. and Goodman C.S. Early events in insect neurogenesis. ii. the role of cell interactions and cell lineage in the determination of neuronal precursor cells. *Developmental Biology*, 111(1):206–219, 1985.

[112] Cho B. and Fischer J.A. Ral gtpase promotes asymmetric notch activation in the drosophila eye in response to frizzled/pcp signalling by repressing ligand-independent receptor activation. *Development*, 138(7):1349–1359, 2011.